ROTATIONAL ANALYSIS OF RHODIUM CARBIDE AND RHODIUM MONOXIDE IN THE GAS PHASE

by

Romey Frances Heuff
B.Sc. Mount Allison University 1984

A dissertation submitted in partial fulfillment of the requirement for the degree of
DOCTOR OF PHILOSOPHY
Department of Chemistry.

ABSTRACT

Supervisor: Dr. Walter Balfour

RhC: The spectrum of RhC between 400 – 500 nm contains two band systems labeled $C^2\Sigma^+ - X^2\Sigma^+$ and $B^2\Pi_i - X^2\Sigma^+$. Numerous perturbations exist due to strong mixing of the two excited states, which lie very close in energy. The C –X system is very strong and a time filtering technique was required to observe the weaker B – X bands. A de-perturbation analysis of the global homogeneous ($\Delta\Omega = 0$) and local heterogeneous ($\Delta\Omega = \pm 1$) interactions gave spectroscopic parameters in quantitative agreement with the observed spectrum. The extent of the Λ-doubling in the $B^2\Pi_i$ state and the spin-rotation splitting, γ, in the $C^2\Sigma^+$ state, suggests the involvement of remote perturbers.

RhO: Two forbidden transitions between 540 – 640 nm in the spectra of $Rh^{16}O$ and $Rh^{18}O$ have been identified as $[15.8]^2\Pi - X^4\Sigma^-$ and $[16.0]^2\Pi - X^4\Sigma^-$ in character. The assignment was confirmed by lifetime and intensity measurements. The ground state is intermediate between Hund's case (a) and (b) coupling, while both of the regular $^2\Pi$ states adhere to case (a) coupling, with somewhat irregular spin-orbit separations of ~300 cm^{-1}. The individual band profiles are extremely complex, containing 12 branches per sub-band. The central regions of each sub-band are severely congested. Hyperfine resolved spectra were required to identify unambiguously the branches and to determine the value of Ω for the upper states. In total, 16 sub-bands for $Rh^{16}O$ and 11 sub-bands for $Rh^{18}O$, all with $\upsilon'' = 0$, were rotationally analyzed (on a band-by-band basis). Λ-doubling in the excited states is quite variable and no correlation with respect to Ω can be made. Also, several excited states required separate parameters to describe their *e/f* rotational levels, suggesting a complex rotational environment.

TABLE OF CONTENTS

LIST OF TABLES

LIST OF FIGURES

Acknowledgements

I would like to extend my sincerest thank you to my supervisor, Dr. Walter J. Balfour for his patient and pleasant demeanor; without which, I would have surely been frightened off this path, long ago. The learning curve was steep, nay treacherous, after a thirteen years absence from academic pursuits. I have endeavored to feel proud of myself, succeeding finally, in the end.

I must thank Janice Snyder, nanny and surrogate mother to my four children, who have not seen a lot of me in the past seven years. They have not suffered greatly because of her sincere and loving devotion towards us. Acknowledgement of her contribution to this project and my life is given in the epigraph.

I must also thank my parents for setting such splendid examples of human potential and behaviour, throughout my life. We had trying times during my formidable years of youth, but the bonds of respect, trust and friendship have been welded solid with my maturity.

I would like to thank my friends for their support and laughter, which have carried me through the many trying times. Laughter is truly the best medicine!

Thanks are due to my sister, Darlene,, who convinced me to apply to grad school in the first place.

My children, Cara, Audrey-Marie, Raven and Adam require great thanks, although they do not realize it. I have been pretty cranky over the years, extremely stressed out from so many the demands. They remind me constantly what an opportunity being alive really is.

The past years have given me many opportunities to grow. It is time to enjoy being me...

April 20th 2004

To Jan...

It is you, not I

That will cherish this piece of work in the years to come.

I owe you my undying respect and friendship.

Your sincerity, your time and your effort,

Have not gone unnoticed,

Thank you so much!

Foreword

The abundance of rhodium in nature is very small, yet its catalytic properties, along with the platinum group metals - iridium, osmium, palladium, platinum and ruthenium– are outstanding. Naturally occurring platinum and platinum-rich alloys have been known for a long time and were originally named "platina," or little silver, by the Spaniards, who regarded platinum as an impurity in the silver they were mining. Rhodium was first discovered by William Hyde Wollaston, in 1803-4, in crude platinum ore obtained from the South America. Rhodium, (Greek *rhodon,* meaning "rose") was so named because of the predominance of atomic lines in the red region of the visible spectrum (1).

The platinum group metals are highlighted in yellow in the periodic table in figure (i). Although one might expect rhodium, Rh, to have a [Kr] $5s^2$ $4d^7$ ground state electronic configuration, it actually has a [Kr] $5s^1$ $4d^8$ electronic configuration. Iridium, Ir, directly below Rh, has the predicted [Xe] $6s^2$ $5d^7$ configuration, and cobalt, Co, directly above Rh, has the predicted [Ar] $4s^2$ $3d^7$ configuration. The energy levels of the $4d$ and $5s$ orbitals are very close, so close in fact that for rhodium they are reversed in order.

Atomic lines of metals are traditionally observed by burning salt solutions in an oxygen/acetylene flame and dispersing the emitted light. The atomic lines of rhodium were first published in 1901 by C. P. Snyder, who was able to arrange 476 Rh(I) lines into an array of 19 columns and 54 rows(2). This was years before regularities were found in many other atomic spectra and so he earns a place in spectroscopic history. Over

1000 Rh(I) lines have now been classified, with 950 of them between 198.784 and 861.523 nm, and atomic lines for Rh(II) and Rh(III) have also been published.

Periodic Table of the Elements

1 IA																	18
1																	2
H	2											13	14	15	16	17	He
1.008	IIA											IIIA	IVA	VA	VIA	VIIA	4.003
3	4											5	6	7	8	9	10
Li	Be											B	C	N	O	F	Ne
6.939	9.012											10.81	12.01	14.01	16.00	19.00	20.18
11	12											13	14	15	16	17	18
Na	Mg	3	4	5	6	7	8	9	10	11	12	Al	Si	P	S	Cl	Ar
22.99	24.31	IIIB	IVB	VB	VIB	VIIB		VIIIB		IB	IIB	26.98	28.09	30.97	32.06	35.45	39.95
19	20	21	22	23	24	25	26	27	28	29	30	31	32	33	34	35	36
K	Ca	Sc	Ti	V	Cr	Mn	Fe	Co	Ni	Cu	Zn	Ga	Ge	As	Se	Br	Kr
39.10	40.08	44.96	47.90	50.94	52.00	54.94	55.85	58.93	58.71	63.54	65.37	69.72	72.59	74.92	78.96	79.91	83.8
37	38	39	40	41	42	43	44	45	46	47	48	49	50	51	52	53	54
Rb	Sr	Y	Zr	Nb	Mo	Tc	Ru	Rh	Pd	Ag	Cd	In	Sn	Sb	Te	I	Xe
85.47	87.62	88.91	91.22	92.91	95.94	(98.91)	101.1	102.9	106.4	107.9	112.4	114.8	118.7	121.8	127.6	126.9	131.3
55	56	57	72	73	74	75	76	77	78	79	80	81	82	83	84	85	86
Cs	Ba	La*	Hf	Ta	W	Re	Os	Ir	Pt	Au	Hg	Tl	Pb	Bi	Po	At	Rn
132.9	137.3	138.9	178.5	180.9	183.9	186.2	190.2	192.2	195.1	197.0	200.6	204.4	207.2	209.0	(209)	(210)	(222)
87	88	89	104	105	106	(107)	(108)	(109)									
Fr	Ra	Ac*	Db	Jl	Rf	Bh	Hn	Mt									
(223)	226.0	227.0	(261)	(262)	(263)	(262)	(265)	(268)									

		58	59	60	61	62	63	64	65	66	67	68	69	70	71		
	La*	Ce	Pr	Nd	Pm	Sm	Eu	Gd	Tb	Dy	Ho	Er	Tm	Yb	Lu		
		140.0	140.9	144.2	(145)	150.4	152.0	157.3	158.9	162.5	164.9	167.3	168.9	173.0	175.0		
		90	91	92	93	94	95	96	97	98	99	100	101	102	103		
	Ac*	Th	Pa	U	Np	Pu	Am	Cm	Bk	Cf	Es	Fm	Md	No	Lr		
		232.0	231.0	238.0	237.1	(244)	241.1	247.1	(247)	251.1	(252)	257.1	258.1	(259)	(260)		

Figure (i) Periodic Table of the Elements, showing rhodium (Rh) with the other platinum group metals (highlighted in yellow), whose physical and chemical properties are similar. The electronic configuration of rhodium is given in the insert.

The industrial extraction of rhodium is complex, as the metal occurs in mixed ores, often with palladium, silver, platinum, and gold. Rhodium metal is inert and silvery white, with a lower density and higher boiling point than platinum. Electroplated rhodium is very hard and the most reflective of all the elements in the optical range and considered to be white in color. It is used for optical instruments and jewelry production. As an electrical contact material, rhodium has low electrical resistance, low and stable contact

resistance and is highly resistant to corrosion. Rhodium is used as an alloying agent to harden platinum and palladium, these alloys being used in furnace windings, bushings for glass fiber production, thermocouple elements, electrodes for aircraft spark plugs, and laboratory crucibles. World consumption of rhodium, however, is dominated by its use as an industrial catalyst.

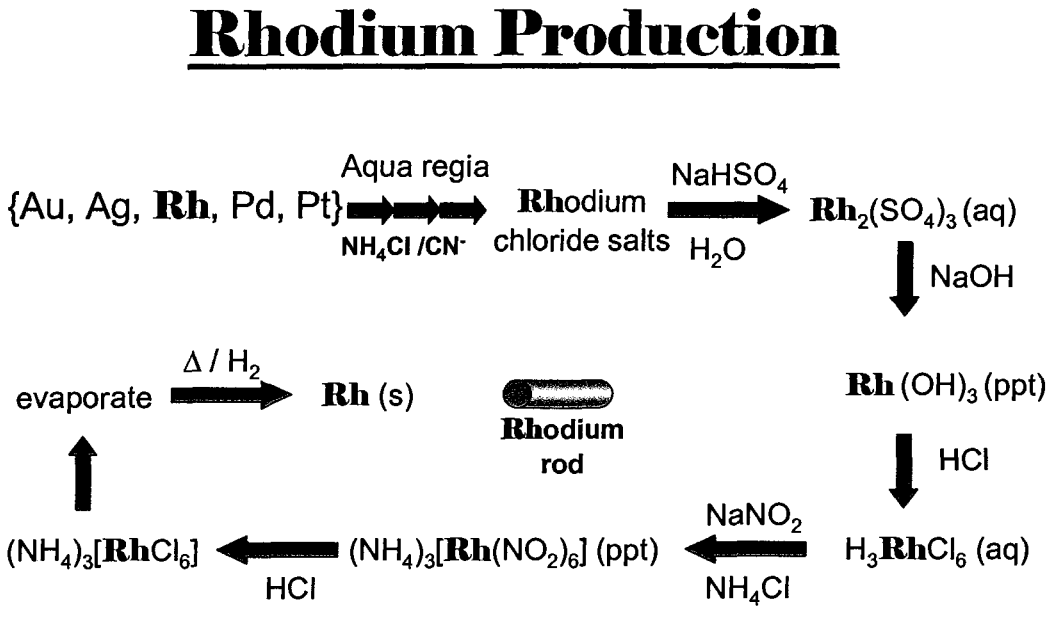

Figure (ii) Industrial extraction of rhodium metal from mixed ores is complex and expensive. Rhodium is very hard, making it difficult to shape. The small rod in the center is approximately 2cm long and 0.5 cm in diameter. A large portion of the $2000 cost is due to the fabrication of the rod itself as rhodium is very difficult to work with.

South Africa is the major source of rhodium, accounting for almost 60% of the world's supply. Russia is the second largest producer of rhodium, however, its sales, as with the other platinum group metals, are volatile and subject to political intervention, causing considerable fluctuations in the world market price. Another principal source of rhodium is the copper-nickel sulfide mining area of the Sudbury, Ontario region.

rhodium is the copper-nickel sulfide mining area of the Sudbury, Ontario region. Although the quantity at Sudbury is very small, < 0.1%, the large amount of nickel ore processed there, makes rhodium recovery cost effective, especially when the market price is high. Production of rhodium metal is a complex process and outlined in figure (ii).

Homogeneous catalysis by transition metal complexes plays an important role in industrial chemistry, being used in hydrogenation, isomerization, dimerization, hydroformylation and carbonylation reactions. Rhodium containing catalysts show enhanced catalytic activity relative to other platinum group metals in many instances. The square planar geometry of the $4d^8$ Rh(I) oxidation state essentially allows the substrate to enter the coordination sphere of the metal, thereby lowering the activation energy of the reaction (2) and is very useful for asymmetric synthesis, especially in the area of pharmaceuticals. Often, only one enantiomer of a particular compound is biologically active, and to obtain catalytic enantiomeric control of an important synthetic step is highly desirable.

Understanding the bonding at the transition metal (TM) center of these rhodium catalysts is of great value, both theoretically and experimentally. The diatomic gas phase studies of rhodium carbide (RhC) and rhodium oxide (RhO) presented in this dissertation are part of a series of rhodium–ligand complexes, that have been studied in our laboratory over the past decade. Information on both the ground state and low lying excited electronic states have been obtained from the Laser Induced Fluorescence (LIF) experiments described herein, and information such as bond strengths, bond lengths, dissociation limits and electronic configurations are helping in unraveling the mystery behind the catalytic properties of the platinum group metals.

The $5s^1 4d^8$ ground state electronic configuration of rhodium produces an inverted ^{4}F ground state, along with several doublet and quartet electronic states, many of which are energetically low lying. The atomic spectrum of rhodium is extremely dense in the red region and quite complex as a result. Depending upon the number of unpaired electrons, the spectral complexity of diatomic species involving rhodium can be quite overwhelming. Intersystem crossing between doublet and quartet series of terms is observed in the rhodium atomic spectrum (2), as well as in the spectrum of RhO analyzed in this dissertation. The large number of low lying electronic states in transition metal diatomic species, results in spectra that are severely perturbed and difficult to analyze in complete detail. The spectrum of RhC presented in Chapter 4 of this dissertation is a fine example of this complexity.

Chapter 1 presents the basic theory required to understand the development of the molecular energy level expression and subsequent analyses. Chapter 2 explains the experimental apparatus and details the type of information that can be obtained, as well as the limitations which may be encountered. Chapter 3 is a brief overview of the procedures and techniques used to transform the observed spectral data into meaningful tables of related information that are subsequently analyzed. Chapters 4 (RhC) and 5 (RhO) include all equations used in the rotational analysis as well as tables of molecular constants. Chapter 6 is a summary of the knowledge gained from this work in terms of molecular orbitals and bond orders is discussed with suggestions for future investigations.

Chapter 1

Introduction and Basic Concepts

1.1 Total Energy of a System

The absorption, emission or scattering of electromagnetic radiation from a suitably prepared sample produces spectra of specific wavelengths, which map the allowable transitions between atomic and/or molecular energy levels in that region. The energy levels themselves therefore, are not directly measured, but may be determined upon careful examination of the spectra, using quantum theory.

In both classical and quantum mechanics, the total energy of a system is given by the total Hamiltonian, H_0, which is the sum of the kinetic, T, and potential, V, energies. In classical mechanics observables are functions of position and momentum, while in quantum mechanics wave functions are used to describe the system and observables are predicted (expectation values), when operations are performed on the wave functions.

Classical mechanics $$E_{Total} = H_0 = T + V \qquad [1]$$

Quantum mechanics $$E_{Total}\Psi = \hat{H}_0\Psi = (\hat{T} + \hat{V})\Psi \qquad [2]$$

The simplest molecular model depicts a collection of nuclei and electrons, held together by Coulombic interactions, with the resulting potential

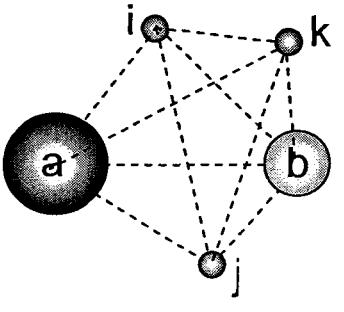

Figure 1.1 The simple molecular model depicts a collection of charged particles.

energy, $V(r,R)$, a function of electronic and nuclear coordinates only (figure 1.1). The total kinetic energy is the sum of the kinetic energies of all the particles. The Hamiltonian operator, excluding spin, for the total internal energy of such a system consisting of N nuclei and η electrons is given by (3)

$$\hat{H}_0 = \frac{1}{2m_e}\sum_{i=1}^{\eta}\hat{p}_{ei}^2 + \frac{1}{2}\sum_{j=1}^{N}\frac{\hat{p}_{nj}^2}{M_{nj}} + V(r,R) \qquad [3]$$

where $\hat{p}_e$ and $\hat{p}_n$ represent the linear momenta of electrons η (mass m_e) and nuclei N (mass M_n).

The potential energy is the sum of the nucleus-electron interactions, the nucleus-nucleus repulsions and the electron-electron interactions

$$V(r,R) = \sum_{A}^{N}\sum_{i}^{\eta}\frac{Z_A e^2}{\hat{r}_{Ai}} + \sum_{A}^{N}\sum_{B>A}^{N}\frac{Z_A Z_B e^2}{\hat{R}_{AB}} + \sum_{i}^{\eta}\sum_{j>i}^{\eta}\frac{e^2}{\hat{r}_{ij}} \qquad [4]$$

The nuclear charges are given by $Z_A e$ and $Z_B e$, while e is the charge of an electron. The momentum operator, in Cartesian coordinates is defined as

$$\hat{p} = \frac{-ih}{2\pi}\left(\frac{\partial}{\partial x} + \frac{\partial}{\partial y} + \frac{\partial}{\partial z}\right) \qquad [5]$$

In both classical and quantum physics, the total internal energy of the system is a constant (steady state condition) as long as no outside force acts upon the system. Classically, all energies are allowed, however in quantum mechanics, only certain energies satisfy the wave equation [6] leading to discrete energy levels within the system.

$$\hat{H}_0\Psi(x,y,z,t) = E_0\Psi(x,y,z,t) \qquad [6]$$

The wave function, $\Psi(x,y,z,t)$, is a function of both position and time for all the particles in the system. However, since the total internal energy operator $\hat{H}_0$ is

independent of time, the solutions of this eigenvalue problem represent the stationary states of the system and, for spectroscopic purposes, only the time independent version of the wave equation needs to be solved.

$$\hat{H}_0\Psi_k(r) = E_0\Psi_k(r) \qquad [7]$$

The solutions to [7], are a set of wave functions, $\{\Psi_i\}$, called eigenfunctions or state functions, and a corresponding set of eigenvalues $\{E_i\}$. The wave function $\Psi_k(r)$ has a set of quantum numbers, k, characterizing the system as well as a set of variables, (r).

1.2 Electronic States in Atoms and Diatomic Molecules

Schrödinger's equation can only be solved exactly for very simple (two body) systems, such as the hydrogen atom with one proton and one electron. For the hydrogen atom, the solution is most readily obtained using spherical polar coordinates and includes the factorization of the state function into two parts, a radial function, $R_{n\ell}(r)$, and an angular (spherical harmonic) wave function, $Y_{\ell m_\ell}(\theta,\phi)$.

$$\Psi_{n,l,m_l}(r,\theta,\phi) = R_{n\ell}(r)Y_{\ell m_\ell}(\theta,\phi) \qquad [8]$$

The state functions are time independent functions, the square of which, describes the probability density for the electron around the nucleus. The eigenfunctions are characterized by the quantum numbers n, ℓ and m_ℓ, where $n = 1,\ 2,\ 3...\ \ell = 0,\ 1,\ 2...n-1$ (labeled s, p, d,...) and $m_\ell = 0,\ \pm1,\ \pm2...\pm\ell$.

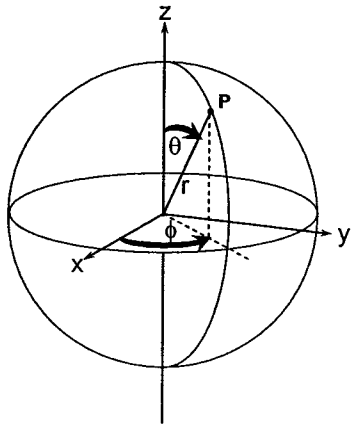

Figure 1.2 Polar coordinate system is convenient for wave calculations.

The electronic energy levels of the hydrogen atom are proportional to $\frac{1}{n^2}$, where n is referred to as the principal quantum number. The azimuthal quantum number, ℓ, is a function of n, and determines the number of nodes in the angular wave function. The number of nodes in the radial wave function is given by n-1. The orbital angular momentum is denoted by the magnetic orbital quantum number, m_ℓ, and is related to spatial orientation, where the $(2l+1)$ different values of m_ℓ are degenerate (same energy) in the absence of a magnetic field. The observed differences in energy of the orbitals with the same n and different l, the ns, np, nd,... of the hydrogen atom, are mainly due to interactions between the orbital angular momentum and electron spin.

The electron itself has an intrinsic angular momentum, denoted by the quantum number, $s = \frac{1}{2}$ and a spatial orientation (spin direction) given by $m_s = \pm\frac{1}{2}$ (also degenerate in the absence of a magnetic field). These quantum numbers (s, m_s) are needed to fully describe an electron in the potential field of a nucleus. Each atomic orbital designated by n, l, m_l can accommodate two electrons with opposing spins, $m_s = \pm\frac{1}{2}$ only, such that no two electrons may be described by exactly the same set of four quantum numbers n, l, m_l and m_s (Pauli Principle). A closed shell refers to completely filled orbital containing the maximum number of electrons possible. The occupancy for a closed shell with:

i) $l = 0$, or s orbital with $m_l = 0$ is one spin pair

ii) $l = 1$, or p orbital with $m_l = 0, \pm1$ is three spin pairs

iii) $l = 2$, or d orbital with $m_l = 0, \pm1, \pm2$ is five spin pairs

iv) $l = 3$, or f orbital with $m_l = 0, \pm1, \pm2, \pm3$ is seven spin pairs

The total angular momentum, for a multi-electron atom, can be approximated by the vectorial sum of the individual electronic orbital $\vec{L} = \sum_i \vec{l}_i$ and spin $\vec{S} = \sum_i \vec{s}_i$ angular momenta. These total angular momenta may couple to give the total electronic angular momentum for the atom of $J = L+S,\ L+S-1,...|L-S|$.

The electronic state of an atom is determined by the total angular momentum, J, and S. Electronic states are designated by the symbolic representation ${}^{2S+1}L_J$, where $2S+1$ is called the multiplicity of the state. The vector notation has been dropped for simplicity. A single electronic configuration (orbital occupancy) can result in more than one electronic state. As an example, the electronic configuration of carbon ${}^{12}_{6}C$ is $1s^2\,2s^2\,2p^2$. There are two unpaired electrons with $l_1 = l_2 = 1$, $m_{l_i} = 1,\ 0,\ -1$ and $m_{si} = \pm\frac{1}{2}$. If $m_{l_1} = m_{l_2}$ then $m_{s_1} \neq m_{s_2}$ since no two electrons can have all four quantum numbers the same (Pauli principle). Therefore, only three distinct electronic states are possible for carbon, one each of type ${}^1D_2$, ${}^3P_{2,1,0}$ and ${}^1S_0$. Hund's rule predicts the state with the highest multiplicity is the lowest in energy and the ground state for carbon is predicted to be ${}^3P_{2,\,1,\,0}$ being confirmed experimentally.

Molecular orbitals are labeled using n, m_l and m_s as in atoms and also by the projection of $\vec{l}$ on the inter-nuclear axis, $l_z = 0,\ 1,\ 2,\ \ldots$, denoted by $\lambda = 0,\ 1,\ 2,...$, and labeled $(\sigma,\ \pi,\ \delta,...)$. Filled molecular orbitals of the type:

i) $\lambda = 0$ or σ orbital with $m_l = 0$; contain one spin pair

ii) $\lambda = 1$ or π orbital with $m_l = \pm 1$; contain two spin pairs

iii) $\lambda = 2$ or δ orbital with $m_l = \pm 2$; contain two spin pairs.

As with atoms, within a single molecular electronic configuration, different electronic states exist, with different total angular momenta, depending upon the spin angular momentum, $\vec{m}_s$, and orbital angular momentum, $\vec{m}_l$, of the unpaired or valence electrons. These different electronic states have different symmetry properties and can have very different energies. Electronic states in diatomic molecules are classified in an analogous manner to atomic states (see figure 1.3) by the following criteria

1) The multiplicity defined as $2S+1$

2) The projection of $\vec{S}$ along the (inter-nuclear) z-axis, $S_z = \Sigma$

3) The projection of $\vec{L}$ along the z-axis, $L_z = \Lambda$

4) The projection of $\vec{J} = \vec{L} + \vec{S}$ along the z-axis, $J_z = \Omega = \Sigma + \Lambda$

Figure 1.3 Electronic states of diatomic molecule are labeled according to the angular momentum present and may be predicted using molecular orbital theory and/or experimentally determined from spectra.

$$^{2S+1}\Lambda_{\Omega}$$

The electronic state of an atom or molecule, describes the total angular momentum and electronic transitions represent changes in the state of an atom or molecule and not necessarily changes in electronic configuration.

1.3 The Zero Order Model of Diatomic Molecules

The zero-order model neglects the effects of electronic and nuclear spin, dealing only with the energies associated with the vibrational and rotation of the molecule. The true Hamiltonian, $\hat{H}_0$, is replaced by an approximate, "effective" Hamiltonian, $\hat{H}_{eff}$, which assumes the electronic, vibrational and rotational motions may be treated independent of each other and that the wave function, $\Psi(k)$, can be factored into an

electronic, $\Psi_{el}(h)$, a vibrational, $\Psi_{vib}(i)$ and a rotational, $\Psi_{rot}(j)$, wave function, each with its own set of quantum numbers.

$$\hat{H}_{eff} = \hat{H}_{el} + \hat{H}_{vib} + \hat{H}_{rot} \qquad [9]$$

and $$\Psi(k) = \Psi_{el}(h) \cdot \Psi_{vib}(i) \cdot \Psi_{rot}(j) \qquad [10]$$

thus $$E_{Total} = E_{el} + E_{vib} + E_{rot}. \qquad [11]$$

The separation of nuclear motion from the electronic motion is called the Born-Oppenheimer approximation and assumes that electronic rearrangement is orders of magnitude faster than nuclear rearrangement, so that in effect the position of the nuclei are parameters rather than variables in the electronic Hamiltonian. The nuclei, therefore, are considered to move under the influence of an average electronic potential (which is not an observable) and the potential energy of the system is a function of the inter-nuclear distance only.

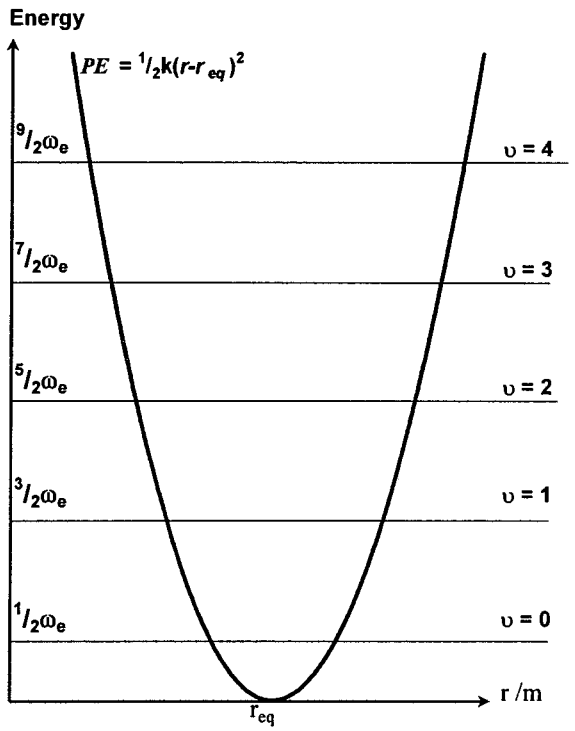

Figure 1.4 Harmonic oscillator model of the inter-nuclear potential of a diatomic molecule as a function of inter-nuclear distance. The quantized vibrational levels resulting from the quantum mechanical treatment are shown with ω_e in units of cm^{-1}.

By using the reduced mass of the molecule, the vibrational motion of a diatomic molecule may be transformed from two particles on a spring to that of a ball rolling on a

potential energy curve. The potential energy of this system is given by a Taylor series expansion. Considering only very small displacements from the equilibrium position, the potential energy reduces to

$$V(q) = V(0) + \left(\frac{1}{2}\frac{d^2V}{dq^2}\right)_0 q^2 + ... = V(0) + \frac{1}{2}kq^2 + ... \qquad [12]$$

where $q = (r - r_{eq})$ and k is the force constant or bond strength. Equation [12] defines a parabola and follows Hooke's law of harmonic motion which is written as

$$V(r - r_{eq}) = \tfrac{1}{2}k(r - r_{eq})^2 \qquad [13]$$

where *V(0)* has been defined as zero, *k* is the restoring force and as *k* increases the potential curve defined by [12,13] becomes steeper or more narrow. Along the potential curve, the kinetic energy is zero and the potential energy is at its maximum, while the total energy of the system is conserved. The potential energy at the equilibrium position reaches a minimum, is called the electronic energy of the molecule, and is zero for the ground electronic state only (figure 1.4).

The vibrational Hamiltonian for the harmonic oscillator now takes the form

$$\hat{H}(q)\Psi(q) = \frac{\hbar^2}{2\mu}\frac{d^2}{dq^2}\Psi(q) + \frac{1}{2}kq^2\Psi(q) = E(q)\Psi(q) \qquad [14]$$

where $q = (r\text{-}r_{eq})$. The eigenvalues of the harmonic oscillator are given by

$$E_\upsilon = \omega_e(\upsilon + \tfrac{1}{2}) = \frac{h\nu}{c}(\upsilon + \tfrac{1}{2}) \text{ in units of cm}^{-1} \qquad [15]$$

where $\upsilon = 0,\ 1,\ 2,\ 3...$ is the vibrational quantum number, and μ, is the reduced mass of the system. The frequency of the vibration is $\nu = \frac{1}{2\pi}\sqrt{\frac{k}{\mu}}$, and is the same as that

obtained classically. The eigenfunctions are symmetrical and even or odd, for even or odd values of υ.

The potential function of the harmonic oscillator model (figure 4.1) predicts a minimum potential energy at the equilibrium internuclear distance, $(r - r_{eq}) = 0$, which is a constant for any given electronic state and often called the Term value $V(0) = T$. For the ground electronic state, $T = 0$ by definition. However, molecules are in constant vibrational motion and the vibrational eigenvalues indicate the presence of residual zero-point vibrational energy $E_\upsilon = \frac{1}{2}\omega_e$ even, when $\upsilon = 0$.

The eigenfunctions of the harmonic oscillator contain maxima, minima and nodal points (the number of which is determined by the vibrational quantum number υ). The eigenfunctions also have finite amplitude outside the bounds of the potential function. With increasing vibrational quantum number, the portion of the eigenfunction outside the potential boundary decreases and the system approaches classical behaviour.

Molecular rotation is, to a first approximation, defined by the rigid rotor model of figure 1.5. The moment of inertia is zero about the inter-nuclear (z) axis, while the moment of inertia about the two perpendicular axes, (x and y) are equal, or otherwise indistinguishable, from each other. Using vector notation and spherical polar coordinates the rotational Hamiltonian may be solved. The rotational eigenfunctions are identical in form to the spherical harmonics found as solutions to the hydrogen atom and the eigenvalues of the rotational motion of the rigid rotor (where r_{eq} is constant) are

$$E(J) = BJ(J+1) \text{ in units of cm}^{-1} \text{ and where } J = 0, 1, 2, 3\ldots \qquad [16]$$

where $$B_v = \frac{h}{8\pi^2 c\mu r_v^2} \text{ (in cm}^{-1}\text{)} \qquad [17]$$

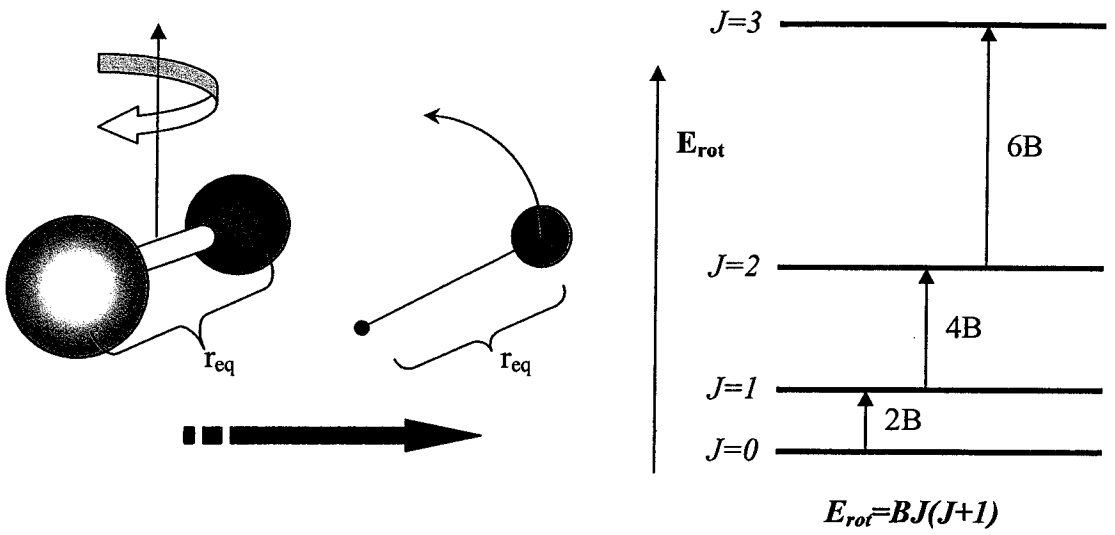

is

Figure 1.5 Eigenvalues of the rigid rotor are determined when the system is represented by a (reduced) mass point on a string of length r_{eq}.

the rotational constant, and smaller than the vibrational constant ω_e by two orders of magnitude.

The overall energy level expression for a diatomic molecule is therefore

$$E_{\upsilon,J} = V(0) + \omega_e(\upsilon + \tfrac{1}{2}) + B_\upsilon J(J+1) \qquad [18]$$

where the vibrational and rotational constants can be determined from the spectra and compared to theoretically calculated values. These classical movements have been used to model the internal motions of a diatomic molecule since their exact solutions to the wave equation are well known and serve as a basis for more complex treatments.

In most spectroscopic applications, however, the zero-order model is insufficient to describe fully the energy levels of a real molecule. Only at very low vibrational energies is the harmonic oscillator model adequate. The true vibrational motion of the nuclei is anharmonic; nuclei cannot superimpose themselves, nor can chemical bonds be defined at large or infinite internuclear distances. Since the molecule is always vibrating,

the inter-nuclear distance is not constant and the bond is not stiff as suggested by the rigid model. As well, at high rotational energies, the rotational levels suffer from centrifugal distortion due to bond stretching.

These effects are small, but noticeable, making molecular spectra more complex than suggested by equation [18]. Using perturbation theory, small first-order corrections are made to the zero-order energy levels, approximating better, the observed energy levels associated with the more realistic models of molecular motion.

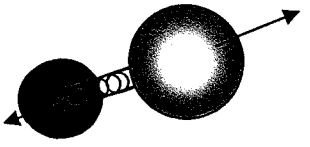

Figure 1.6 Non-rigid rotor model visualizes the chemical bond as being spring- like. The bond stretches at higher rotation and the rotational energy levels deviate from those predicted by the rigid rotor model.

1.4 Corrections to the Zero Order Model

The harmonic potential is not steep enough at the inner wall and too steep at the outer wall. Diatomic molecules behave more like anharmonic oscillators (figure 1.7) and a function that reflects the limitations of real chemical bonds is required. There are many such functions that have been proposed, however, the Morse function, with the form

$$V(r-r_e) = D_e(1-e^{-\beta(r-r_{eq})})^2 \text{ (in cm}^{-1}\text{)} \qquad [19]$$

is commonly used to represent the potential energy curve of an anharmonic oscillator. D_e is the maximum value of $V(r-r_{eq})$ as $r \to \infty$ or the dissociation energy referred to the potential minimum as in figure 1.7 and $\beta = \omega_e\sqrt{\frac{2\pi^2 c\mu}{D_e h}}$ (in units of cm^{-1}).

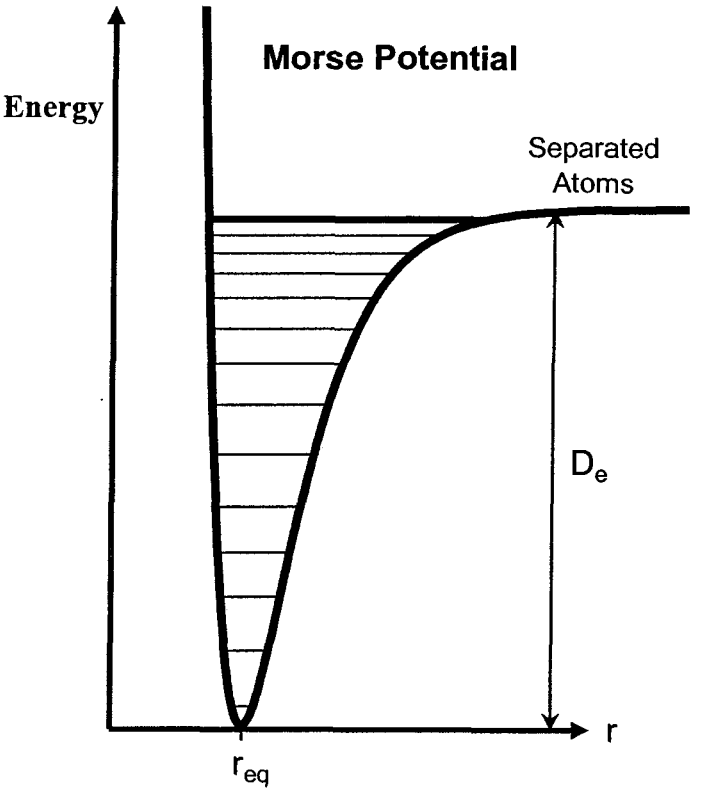

Figure 1.7 Morse function is a better approximation for the potential energy of a real molecule.

It is assumed that the perturbing operator $\hat{H}'$ is small compared to the original operator $\hat{H}_0$ so that the Hamiltonian for the system is of the form

$$\hat{H} = \hat{H}_0 + \alpha\hat{H}' + \alpha^2\hat{H}'' + \ldots \qquad [20]$$

where $\hat{H}_0$ has only discrete eigenvalues $\{E_i^0\}$ and eigenfunctions $\{\Psi_i^0\}$. Since the perturbation is small it will cause only slight changes in the total energy of the system

$$E_i = E_i^0 + \alpha E_i' + \alpha^2 E_i'' + \ldots \qquad [21]$$

and only slight modifications to the wave functions

$$\Psi_i = \Psi_i^0 + \alpha\Psi_i' + \alpha^2\Psi_i'' + ... \quad [22]$$

The vibrational energy levels of the anharmonic oscillator derived by applying perturbation theory to the harmonic oscillator model are

$$E_{vib} = \omega_e(\upsilon + \tfrac{1}{2}) - \omega_e x_e(\upsilon + \tfrac{1}{2})^2 + \omega_e y_e(\upsilon + \tfrac{1}{2})^3 ... \quad [23]$$

The first correction term $\omega_e x_e(\upsilon + \frac{1}{2})^2$ is adequate to describe the spectra described in this dissertation. It can be seen from [23] and figure 1.7 that the vibrational energy levels no longer increase in constant increments, but rather converge as the dissociation limit of the molecule is reached. The anharmonic oscillator model is usually a good approximation to the vibrational levels of a real molecular system. The wave functions, Ψ_υ, and the probability density functions, $(\Psi_\upsilon^*\Psi_\upsilon)^2$, of the anharmonic oscillator are more asymmetrical than those of the harmonic oscillator, increasing their magnitude on the shallow side of the potential curve compared to the steep side.

The rotational energy levels of the non-rigid rotor derived by applying perturbation theory to the rigid rotor are

$$E_{rot} = B_v J(J+1) - D_v[J(J+1)]^2 + H_v[J(J+1)]^3 ... \quad [24]$$

The first order correction $D_v[J(J+1)]^2$ is called the centrifugal distortion term and is only necessary if spectroscopic data include transitions to high J rotational levels.

1.5 Electronic Fine Structure

For atomic or molecular systems where there are one or more unpaired electrons, electron spin fine structure may be observed in the spectra and the operators for spin-orbit interactions, $\hat{H}_{SO}$, spin-rotation interactions, $\hat{H}_{SR}$, and spin-spin interactions may need to

be included in the total Hamiltonian. In the event where a nucleus may possess magnetic spin angular momentum such as ^{103}Rh (with $I = {}^1/_2$), hyperfine structure may be observed in the spectra (as in RhO) and the appropriate, $\hat{H}_{hf}$, operator must also be included The Hamiltonian for a diatomic molecule with spin angular momentum is, therefore,

$$\hat{H}_{eff} = \hat{H}_{el} + \hat{H}_{vib} + \hat{H}_{rot} + \hat{H}_{SO} + \hat{H}_{SR} + \hat{H}_{SS} + \hat{H}_{hf} \qquad [20]$$

where the operators are treated as perturbations to the rotational Hamiltonian.

Each operator can be represented by a matrix, **H,** where the matrix elements, H'_{ij}, are determined from

$$H'_{ij} = \int \Psi_i^0 * \hat{H}' \Psi_j^0 d\tau = \left\langle \Psi_i^0 \middle| \hat{H}' \middle| \Psi_j^0 \right\rangle \qquad [21]$$

The complete set of the eigenfunctions, $\{\Psi_i^0\}$, has been taken as a basis set $\Psi_i^0 = \sum_i c_i f_i$, or in Dirac notation), $\left|\Psi_i^0\right\rangle = \sum c_i \left| f_i \right\rangle$.

When rotation is involved in molecular spectroscopy, it is convenient to write the Hamiltonian operator in terms of angular momentum operators. Angular momentum operators obey the following commutation relation for their space-fixed Cartesian components $[\mathbf{A}_i, \mathbf{A}_j] = i\hbar\epsilon_{ijk}\mathbf{A}_k$, where $\epsilon_{ijk} = +1$, 0 or -1. Each of the components of **A** also commutes with $\mathbf{A}^2$ that is $[\mathbf{A}_i, \mathbf{A}^2] = 0$, where i = X, Y or Z (the space-fixed axes). The explicit functional forms of the eigenfunctions are not needed in order to determine the eigenvalues of the angular momentum operators. It is sufficient to represent them by the quantum numbers A and M_A for the operators $\mathbf{A}^2$ and $\mathbf{A}_z$ respectively, or in Dirac notation $\left|A, M_A\right\rangle$. The eigenvalues for these operators acting on these basis functions are:

$$\mathbf{A}^2 \left| A, M_A \right\rangle = \hbar A(A+1) \left| A, M_A \right\rangle \text{ and } \mathbf{A}_Z \left| A, M_A \right\rangle = \hbar M_A \left| A, M_A \right\rangle \qquad [22]$$

where $\hbar$ is Planck's constant divided by 2π. In general the quantum numbers are either integer or half-integer with M_A having $(2A+1)$ possible values A, A-1, A-2...-A for each value of A.

Angular momentum in molecules (listed in table 1.1) results from the electronic spin of the ith electron s_i and/or nuclear spin of nucleus A or B, I_A, I_B; electronic orbital angular momentum of the ith electron l_i as well as the rotation of the nuclear framework R and may couple due to magnetic interactions.

Table 1.1 Electronic angular momenta coupling options.

Total electronic orbital angular momentum	$\mathbf{L}$: $\mathbf{L} = \sum_i l_i$
Total electron spin	$\mathbf{S}$: $\mathbf{S} = \sum_i s_i$
Angular momentum of nuclear framework	$\mathbf{R}$: $\mathbf{R_z} = \mathbf{0}$
Total Angular momentum (no nuclear spin)	$\mathbf{J}$: $\mathbf{J} = \mathbf{R} + \mathbf{L} + \mathbf{S}$
Molecule fixed projection of $\mathbf{L_z}$	Λ : $\Lambda = 0, 1, 2, \ldots$ (Σ, Π, Δ, ...)
Molecule fixed projection of $\mathbf{S_z}$	Σ : Σ = integral or half integral
Molecule fixed projection of $\mathbf{J_z}$	Ω : $\Omega = \Lambda + \Sigma$
Total angular momentum (no nuclear or electronic spin)	$\mathbf{N}$: $\mathbf{N} = \mathbf{J} - \mathbf{S} = \mathbf{R} + \mathbf{L}$

Hund's case (a) coupling limit (figure 1.8 a) has strong coupling of $\vec{L}$ and $\vec{S}$ to the inter-nuclear axis, while Hund's case (b) limit has weak coupling to the inter-nuclear axis. The difference between the basis sets is primarily the presence or absence of spin-orbit coupling, and from the rotational structure of the spectra, electronic states can be designated as to which coupling case is most representative.

The total angular momentum (excluding nuclear spin) is represented by the vector $\vec{J}$ of length $[J(J+1)]^{1/2}\hbar$ units. The projection of $\vec{J}$ along the inter-nuclear axis (z), is quantized, $M_J\hbar$, so that different values of $M_J\hbar$ correspond to different spatial orientations of $\vec{J}$. In the absence of any electrical or magnetic interactions, the energy is independent of the orientation of the total angular momentum, $\vec{J}$, in space and there is a $(2J+1)$ degeneracy, corresponding to all allowed $M_J\hbar$ values.

There are only a few operators that commute with the exact Hamiltonian, **H**, however, many operators, especially angular momentum operators commute with parts of **H**. Each of Hund's coupling cases, represented pictorially in figure 1.8, corresponds to a different set of mutually commuting operators and requires a different partitioning of **H** into two parts so that $\mathbf{H^0}$ will commute with the appropriate set of angular momentum operators and be fully diagonal in the selected basis set (4).

$$\mathbf{H} = \mathbf{H^0_{(a)}} + \mathbf{H'_{(a)}} \quad |n, J, S, \Omega, \Lambda, \Sigma\rangle \qquad [23]$$

$$\mathbf{H} = \mathbf{H^0_{(b)}} + \mathbf{H'_{(b)}} \quad |n, J, S, N, \Omega, \Lambda\rangle \qquad [24]$$

For both cases (a) and (b), $\mathbf{H^0}$ includes $\mathbf{H_{el}}$ and only the diagonal parts of $\mathbf{H_{ROT}}$ where **H'** includes $\mathbf{H_{SO}}$, $\mathbf{H_{SR}}$ and $\mathbf{H_{SS}}$ and when required $\mathbf{H_{HF}}$.

Figure 1.8 Hund's case (a) and Hund's case (b) coupling cases for the angular momenta (excluding nuclear spin) present in a molecule with unpaired electrons. The good quantum numbers used to describe the basis sets are given in the Dirac "ket" notation. The n, refers to all other quantum numbers needed to completely specify the basis set.

Case (a)

$|n,J,S,\Omega,\Lambda,\Sigma\rangle$

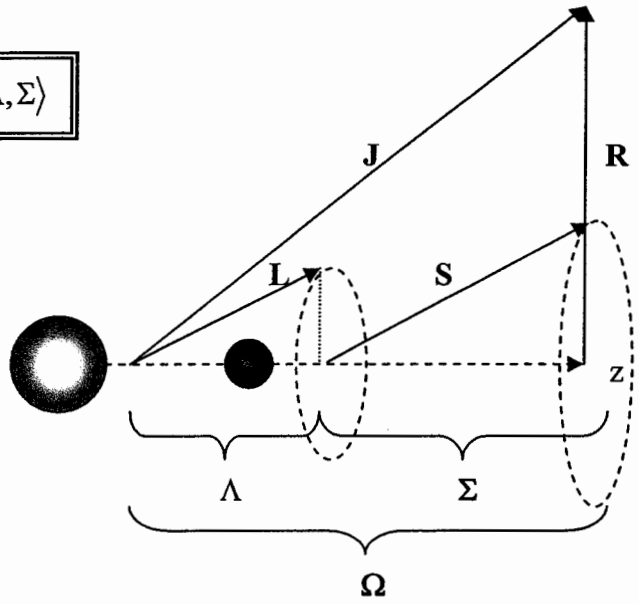

Case (b)

$|n,J,S,N,\Lambda\rangle$

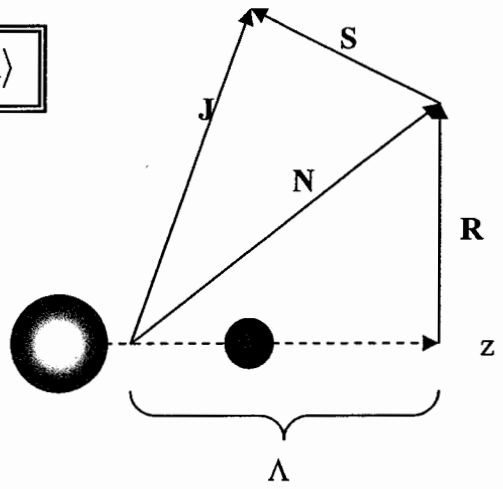

The case (a) basis is a good approximation when $\mathbf{H_{SO}} >> \mathbf{H_{SR}}$.

The spin-orbit Hamiltonian $\mathbf{H_{SO}} = \sum_i \hat{a}_i \, \mathbf{l}_i \cdot \mathbf{s}_i$ is a single electron operator meaning it is possible to relate observable spin-orbit matrix elements to one-electron orbital integrals, which are called molecular spin-orbit parameters. Using the case (a) basis set the diagonal matrix element of $\mathbf{H_{SO}} = A \, \Lambda \cdot \Sigma$ which implies that the fine structure levels are expected to be equally spaced.

The spin-rotation Hamiltonian is approximated as $\mathbf{H_{SR}} = \gamma \, \mathbf{R} \cdot \mathbf{S} = \gamma \, \mathbf{(N-L)} \cdot \mathbf{S}$ convenient for the case (a) basis or $\mathbf{H_{SR}} = \gamma \, \mathbf{N} \cdot \mathbf{S}$ convenient for the case (b) basis sets since $\mathbf{N} \cdot \mathbf{S}$ has only diagonal matrix elements in the case (b) basis. The observed value of γ cannot be directly compared to the calculated value since γ_{obs} is an effective constant that includes direct (or first order) contributions from $\mathbf{H_{SR}}$ and second-order effects from $\mathbf{H_{SO}}$ and $\mathbf{H_{Rot}}$ (5).

The rotational Hamiltonian is $\mathbf{H_{ROT}} = B_\upsilon \mathbf{R}^2$, where $\mathbf{R}^2 = (\mathbf{R_x}^2 + \mathbf{R_y}^2 + \mathbf{R_z}^2)$. Since $\mathbf{R_z} = 0$ by definition and $\mathbf{J} = \mathbf{R} + \mathbf{L} + \mathbf{S}$ the rotational Hamiltonian can be expressed as

$$\begin{aligned} \mathbf{H_{ROT}} &= B_\upsilon [(\mathbf{J_x} - \mathbf{L_x} - \mathbf{S_x})^2 + (\mathbf{J_y} - \mathbf{L_y} - \mathbf{S_y})^2] \\ &= B_\upsilon [(\mathbf{J}^2 - \mathbf{J_z}^2) + (\mathbf{L}^2 - \mathbf{L_z}^2) + (\mathbf{S}^2 - \mathbf{S_z}^2) \\ &+ (\mathbf{L}^+\mathbf{S}^- + \mathbf{L}^-\mathbf{S}^+) - (\mathbf{J}^+\mathbf{L}^- + \mathbf{J}^-\mathbf{L}^+) - (\mathbf{J}^+\mathbf{S}^- + \mathbf{J}^-\mathbf{S}^+)] \end{aligned} \qquad [25]$$

where B_υ is the rotational constant. The symbols $\mathbf{L}^\pm$ $\mathbf{S}^\pm$ and $\mathbf{J}^\pm$ refer to the molecule fixed raising and lowering operators defined by $\mathbf{A}^\pm = \mathbf{A_x} \pm i\mathbf{A_y}$ however, the $\mathbf{J}^\mp$ operator obeys anomalous commutation rules since it involves rotation of the molecule with respect to the space-fixed coordinates. The first three terms of [25] have diagonal matrix elements only and define the rotational energy of the basis function while the remaining three terms of [25] are those which couple the orbital, spin and total angular momenta.

For a 2-dimensional matrix in terms of the basis set $\{|f_1\rangle,|f_2\rangle\}$

$$H'_{ij} = \langle f_i|\hat{H}|f_j\rangle = \int f_i * \hat{H} f_j d\tau \qquad [26]$$

and the total Hamiltonian is written as the sum of a zero-order term and an interaction term $\mathbf{H} = \mathbf{H}^{(0)} + \mathbf{H}^{(1)}$ where

$$\mathbf{H} = \begin{pmatrix} E_1^0 & H'_{12} \\ H'_{21} & E_2^0 \end{pmatrix} \qquad [27]$$

$H'_{12} = H'_{21}$ and the solution of the secular equation

$$(E_1^0 - E)(E_2^0 - E) - V^2 = 0 \qquad [28]$$

leads to the eigenvalues

$$E_{1,2} = \frac{E_1^0 + E_2^0}{2} \pm \frac{((E_1^0 - E_2^0)^2 + 4H_{12}{}^2)^{1/2}}{2}. \qquad [29]$$

The new energies, (E_1, E_2), are the original energies, (E_1^0, E_2^0), ± a small correction factor, $\frac{H_{12}^2}{\Delta E}$, determined by the original separation ΔE of the energy levels and the strength of the perturbation matrix element, H_{12}; if the energy levels are accidentally, or nearly degenerate, the perturbation matrix element induces a separation or distinction between the levels and extra lines or structure may occur in the observed spectra (see figure 1.9).

Perturbation theory can be applied in a stepwise manner, making corrections for the most significant matrix elements, then for the second most significant ones, and so on. The selection rules applying to perturbations are given in section 4.5. As a result of the mixing, the eigenfunctions are "contaminated" and depending upon the magnitude of the mixing coefficient, may appear quite different, adopting characteristics of each other.

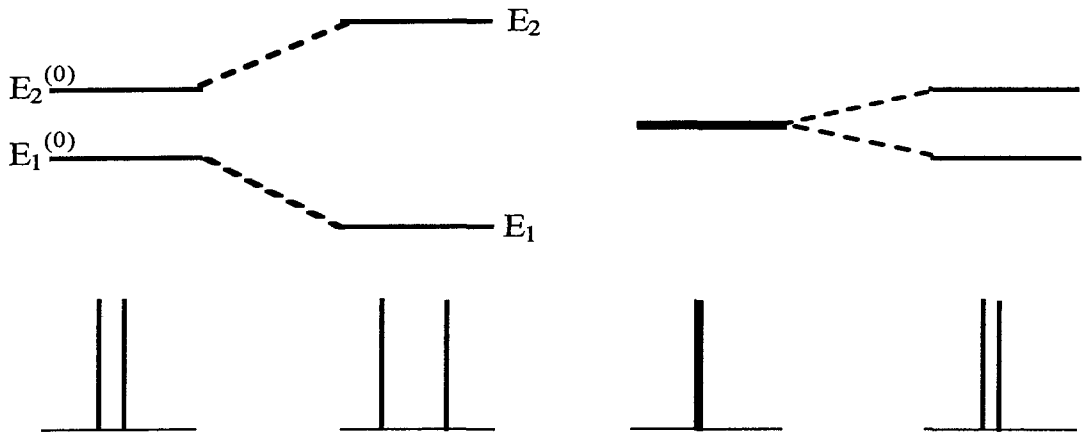

Figure 1.9 Interacting energy levels push away from each other. The strength of the perturbation operator dictates the strength of the interaction. On the right two accidentally degenerate energy levels have interacted strongly enough that two lines are resolved (observed) instead of one.

1.6 Hyperfine Interactions

Splitting of individual rotational lines may be observed in atomic and molecular spectra due to hyperfine coupling, the interaction of the nuclear magnetic dipole moment operator with i) the orbital angular momentum operator of each unpaired electron, ii) the spin angular momentum operator of each unpaired electron and/or iii) unpaired *s* electrons in an isotropic interaction (also called Fermi interaction).

To a first approximation, the nuclear spin angular momentum has its origin at the center of the nucleus. It can thus be expected that the strongest of the three coupling possibilities will be with unpaired *s* electrons, since only they have a non-zero probability of being located at the nucleus. Hyperfine structure of this nature is generally of the same magnitude in both atomic and molecular spectra. If splitting is observed in the molecular spectra, and the Fermi interaction is known for the atom, deductions can be made about

the electron spin distribution in the molecule (or at least the extent of *s* character of the electron).

Dunn (6,7) has described in detail the Hamiltonian operators for hyperfine interactions in case (b) diatomic molecules. If there is an appreciable amount of atomic *s* character to the wave function of an unpaired electron, the following term is expected to dominate

$$\mathbf{H_{HF}} = b\mathbf{I}\cdot\mathbf{S} \qquad [30]$$

where b is the Fermi contact (usually expressed in Hz or MHz). The nuclear spin angular momentum vector, $\vec{I}$, and the electronic spin angular momentum vector, $\vec{S}$, may also couple to the end-over-end rotational angular momentum of the molecule, as in Hund's cases. Thus different values of the total energy levels are expected, depending on which coupling scheme dominates. The nuclear spin, $\vec{I}$, may couple with the electronic spin, $\vec{S}$, to form a resultant, $\vec{G}$, which can then couple with end-over-end rotation as in case ($b_{\beta S}$) or, the nuclear spin couples with, $\vec{J}$, the rotational angular momentum including electron spin to form a resultant $\vec{F}$, as in case ($b_{\beta J}$) (figure 1.10)

A third type of coupling is also possible, case ($b_{\beta N}$). The nuclear spin couples directly to the molecular rotation, $\vec{N}$, forming a resultant, which then couples with the electronic spin to give the total angular momentum of the molecule. This type of coupling is not expected since the interaction of the small nuclear magnetic moment with the molecular fields should be considerably less (~1000x) than the coupling of the electronic moment and the molecular fields (8).

In case ($b_{\beta S}$) the diagonal part of the energy reduces to

$$W(b_{\beta S}) = \frac{b}{2}\left[G(G+1) - S(S+1) - I(I+1)\right]\mathbf{N}\cdot\mathbf{G} \qquad [31]$$

where $\mathbf{N}\cdot\mathbf{G} = \frac{1}{2}[F(F+1) - N(N+1) - G(G+1)]$ [32]

For case ($b_{\beta J}$) the diagonal part of the energy reduces to

$$W(b_{\beta J}) \cong \frac{b}{2}\frac{\left[J(J+1) - N(N+1) + S(S+1)\right]}{J(J+1)}\mathbf{I}\cdot\mathbf{J} \qquad [33]$$

where $\mathbf{I}\cdot\mathbf{J} = \frac{1}{2}[F(F+1) - I(I+1) - J(J+1)]$ [34]

The two types of coupling cases discussed are expected to produce different hyperfine structure in the spectra. For molecules exhibiting case ($b_{\beta S}$) coupling the hyperfine splitting should be independent of *J*, while for molecules with case ($b_{\beta J}$) coupling the hyperfine structure will be *J*-dependent.

Figure 1.10 Vector diagrams for the two most common types of hyperfine coupling.

Case ($b_{\beta S}$) hyperfine splitting is independent of the molecular rotation.

Case ($b_{\beta J}$) hyperfine splitting decreases with increasing molecular rotation.

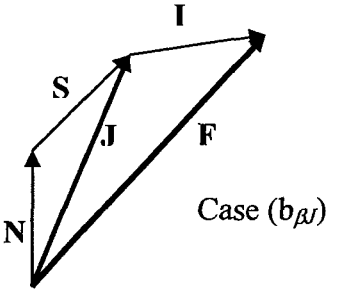

Case ($b_{\beta J}$)

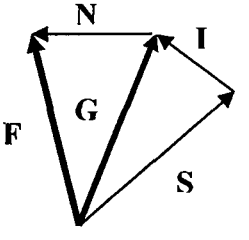

Case ($b_{\beta S}$)

1.7 Transition Energies and General Selection Rules

Transitions between electronic states generally occur in the visible / ultraviolet region of 300 - 800 nm (or 10 000 to 40 000 cm^{-1}) but transitions to low-lying electronic states may occur in the infrared region of the electromagnetic spectrum. The electronic transition (figure 1.11) contains both vibrational (band) and rotational (branch) structure. Vibrational progressions and sequences may occur corresponding to $\Delta\upsilon = 0,\ \pm1,\ \pm2...$ and rotational structure is present according to the rotational selection rules $\Delta J = 0,\ \pm1$. Since the rotational constant B_υ is a function of the vibrational level, a rotational analysis is often performed on a band-to-band basis depending upon the presence (or absence) of global perturbations.

For electronic transitions the general selections rules are (9):

$\Delta\upsilon = 0,\ \pm1,\ \pm2...$

$\Delta\Lambda = 0,\ \pm1$

$\Delta S = 0$

$\Delta\Sigma = 0$: for transitions between case (a) states only.

$\Delta\Omega = 0,\ \pm1$

$\Delta R = 0$: for transitions between case (b) states only.

and

$\Delta J = 0,\ \pm1$ (If $\Delta\Lambda = 0$ then $\Delta J \neq 0$: also $J = 0 \leftrightarrow J = 0$ is forbidden).

These are the general selection rules governing case (a) and case (b) coupling schemes for heterogeneous diatomic molecules.

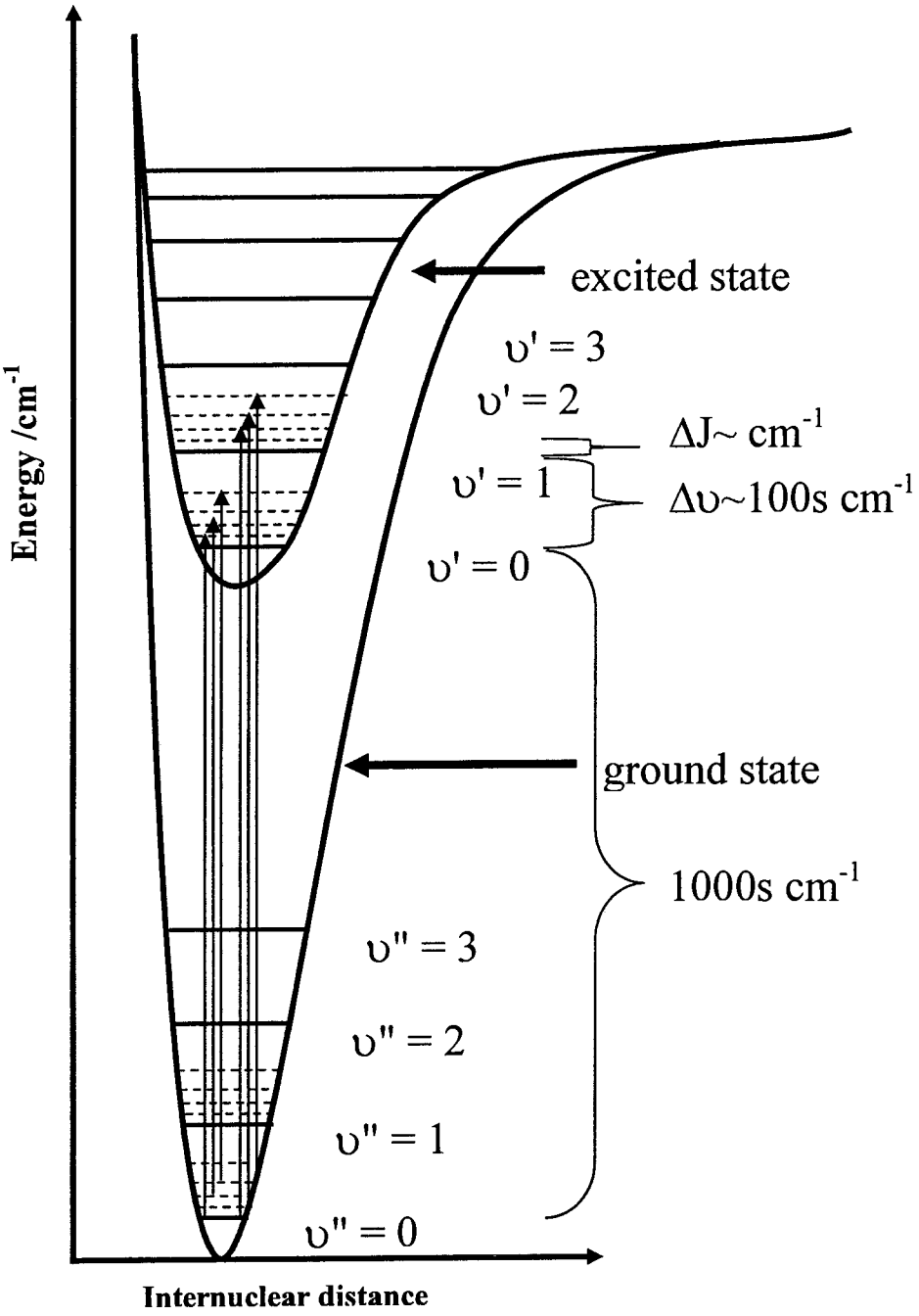

Figure 1.11 Electronic Transitions are accompanied by vibrational band and rotational branch structure. The approximate differences in energy are noted on the right.

Chapter 2

Experimental Details

2.1 Laser Induced Fluorescence

Laser induced fluorescence (LIF) experiments produce spectra which provide information pertaining to the internal quantized energy levels of a suitably prepared sample of identical target molecules. In our laboratory this was accomplished by scanning a tunable dye laser (probe) which perpendicularly intercepts the path of a jet-cooled molecular beam (produced by laser ablation of a metal rod in the presence of a pulsed gaseous mixture which expands into the vacuum chamber). If the energy of the probe laser radiation precisely matches the difference between two energy levels of the target molecules for which a transition is allowed to occur, then the molecules absorb that radiation. The experimental set-up is such that the generated sample of target molecules has had sufficient relaxation time for all of the molecules to be in their electronic and vibrational ground state before the probe laser intercepts them.

Once excited the molecules emit the excess energy as photons of the appropriate frequencies in order to relax. The induced fluorescence is detected by converting the photons to an electrical signal using a photomultiplier tube (PMT). The signal is displayed on a digital storage oscilloscope and recorded on a personal computer (PC). The advantage of this technique over conventional emission is that it offers significantly simplified spectra with little or no question as to the nature of the lower state involved in the observed transitions. Another possible mode of operation, utilizing the same principles, is dispersed fluorescence (DF) where a scanning monochromator is inserted

before the PMT and the wavelength of the dye laser is held constant. The signal recorded is a function of the relaxation emission wavelengths (see figure 2.1 b) and can give information on the vibrational levels of the ground state. This technique also provides the possibility of detecting low lying electronic states of appropriate symmetry.

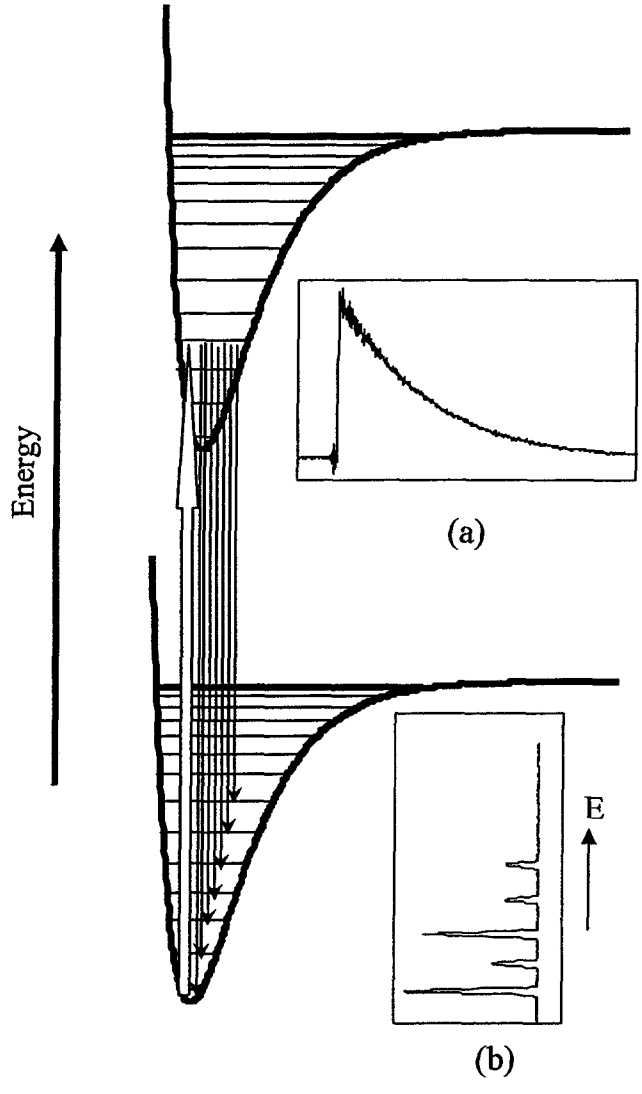

Figure 2.1 Laser induced fluorescence between two electronic states. The signal on the oscilloscope (a) is a resultant of all photons reaching the detector. A monochromator is used in dispersed fluorescence to resolve the signal into its constituent wavelengths to give the lower state vibrational levels (b).

2.2 Equipment and Apparatus

The electronic spectra and rotational analysis of two diatomic molecules are presented in this dissertation, rhodium carbide (RhC) and rhodium oxide (RhO). The RhC/RhO experiments were done in a (9 liter) vacuum chamber (10^{-5} Torr). An Edwards E2M8 mechanical pump was used as a roughing pump until a pressure of ~10^{-2} Torr was reached. Further evacuation of the chamber (figure 2.2) was performed by an Edwards Diffstack 160 diffusion pump backed by the Edwards E2M8. Pressure inside the chamber was monitored with a Granville-Phillips 270006 ion gauge. The background pressure was typically 10^{-6} Torr and increased by a factor of 10 to 100 with the valve operating.

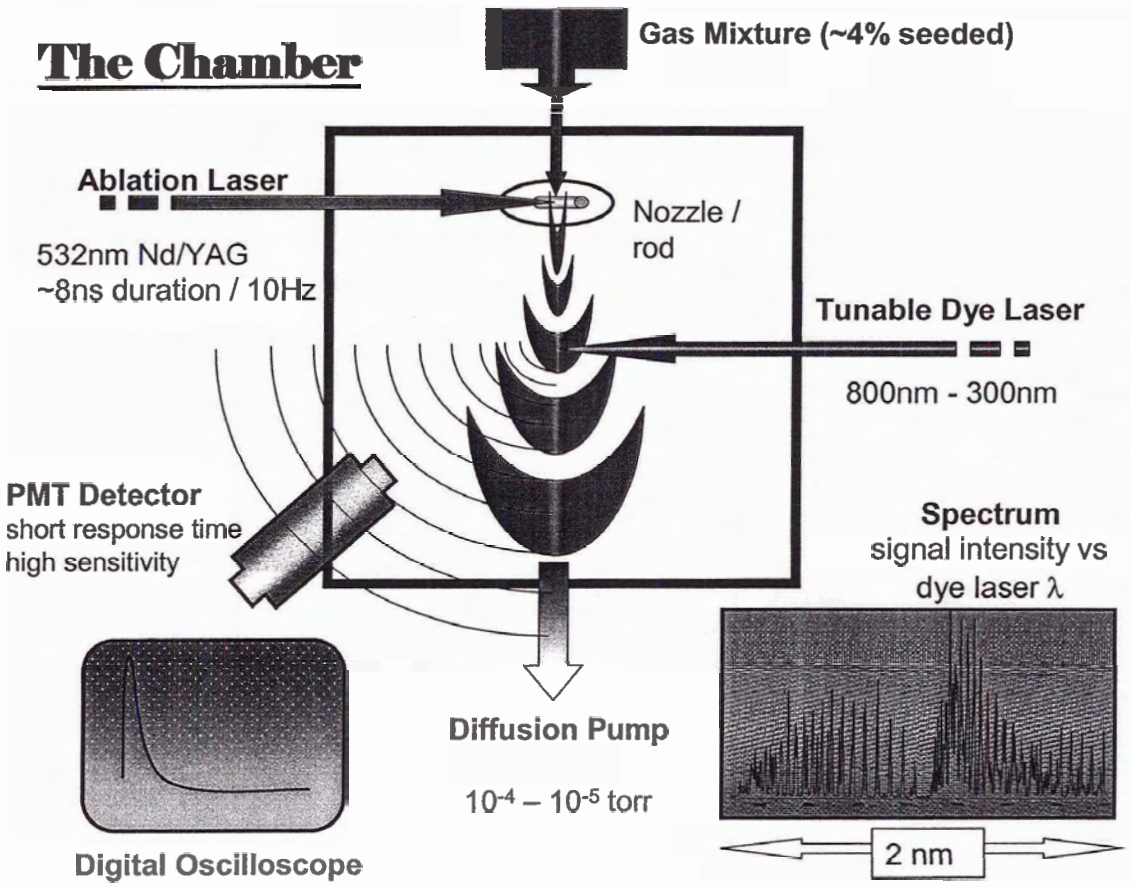

Figure 2.2 Schematic illustration of the LIF experiment illustrating its main features. The timing between the two laser pulses is determined manually by optimizing the signal. See text for more explicit details.

The gas mixtures were prepared in a 10 liter glass bulb using ultra pure (PraxAir, 99.9% or greater) grade reagents. Approximately 5% methane (RhC) or oxygen (RhO), was used with helium to a pressure of 1 - 2 atm. The gas entered the chamber through a 0.5 mm orifice by way of a piezoelectric disk and valve system (Physik Instrument, P286.20) which could be controlled in terms of pulse activation, width and delay. It was noted that increasing the pulse width of the gas beyond 350 μs did nothing to enhance the LIF signal. It was concluded that the amount of gas in the pulse then exceeds the amount of metal being ablated and therefore the pulse width was kept to a minimum. Since a higher background pressure reduces the degree of cooling during the expansion of the molecular beam the temperature in the observed spectra can be controlled by partially closing the plate valve between the chamber and the diffusion pump.

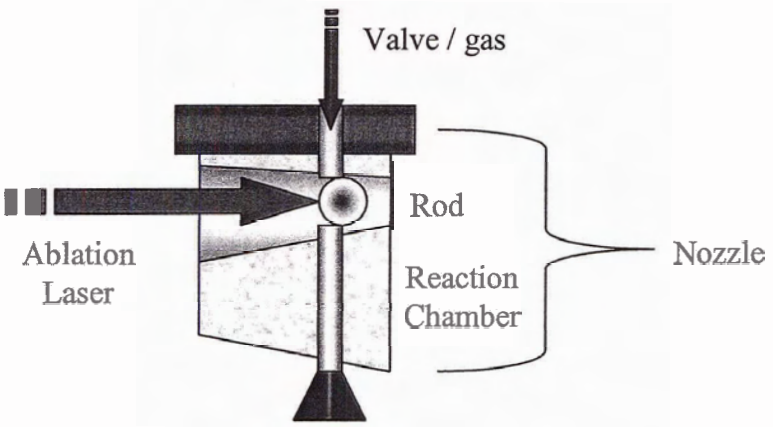

Figure 2.3 Schematic detail of the nozzle showing how the gas mixture, the rod and the ablation laser intercept each other. The molecules exiting the reaction chamber have relaxed to the ground electronic state.

The reaction between the metal plasma and the gas mixture is confined to an area referred to as the nozzle. The rotating rhodium rod (Goodfellow 99.9% purity) is 5 mm in diameter by 30 mm in length and perpendicularly situated 2.0 mm below the orifice of the entering gas mixture. The rod is 2.5 mm off-axis from the direction of the gas stream allowing for a relatively unimpeded gas flow around the rod and into the chamber (see figure 2.3). Two nozzles were used, which differ only in the length of the exit channel.

For RhO it was necessary to use the longer nozzle with a 25 mm channel to provide adequate residence/ reaction time between the plasma and the gas mixture. For RhC a 17 mm nozzle sufficed.

The second harmonic (532 nm) of a Continuum NY61 Nd:YAG laser (10 Hz) was used as the vaporization source (~200 mJ / pulse, 9 μs pulse width). A convex lens (focal length 50 cm) focused the laser beam onto the surface of the rhodium rod (bp:3970 K) while a stepping motor translated and rotated the rod to ensure a continuously fresh surface for ablation. The pulsing of the ablation laser and the opening of the piezoelectric valve (controlled by the PC) were timed to produce a maximum number of target molecules (as determined by monitoring the LIF signal produced downstream).

Table 2.1 Dyes used to obtain LIF and DF data with wavelength ranges and maxima as quoted by the manufacturer (Lumonics).

Dye	**Max /nm**	**Range /nm**	**Dye**	**Max /nm**	**Range /nm**
LDS750	718	699-743	C500	504	481-550
LDS698	692	659-732	C480	477	458-507
DCM	643	611-685	C460	459	443-485
R640	643	607-640	C450	452	436-457
KR620	596	594-641	C440	435	422-459
R610	600	588-632	EXA428	426	415-436
R590	574	563-597	EXA417	416	406-425
C540A	543	523-586	EXA411	411	402-419
C485	529	499-565	EXA404	404	396-413

A Lumonics HY600 Nd:YAG laser operating at 355 mm was used to pump the tunable Lumonics HD-300 dye laser with a dispersing element consisting of a 2400 grooves/mm grating. The wavelength and output energy of the dye laser is dependent upon the dye used (see table 2.1). The carefully timed probe laser perpendicularly intersects the molecular beam pulse, inducing fluorescence emission. The emission was collected by a lens (d = 5.0 cm, focal length = 7.5 cm) perpendicular to both the probe laser and the molecular beam and then imaged onto the entrance of a Jobin Yvon H20 monochromator. A Hamamatsu R1477 photomultiplier converted the photon intensity to an electrical signal which was channeled to a Tektronics 2440 digital oscilloscope.

The timing and pulse width of all events are crucial for detection and optimization of the LIF signal. The lasers must fire at the appropriate times to intersect the gas pulse at each stage of the experiment. The PC is equipped with a timing card (Advantech PCL-830) that triggers the flash lamps of both lasers, the piezoelectric valve, the photomultiplier and a digital delay generator (Princeton EG&G 9650) which supplies the delay, duration and magnitude of the triggers for the Q switches of both the ablation laser and the probe laser.

2.3 Recording Spectra

The fluorescence signal was measured in voltage as a function of the 1024 input channels of the scope. The time resolution of the channels was adjusted as required from 5 s down to 2 ns. The LIF signal decays with time and its profile was integrated (box car averaged) over a selected number of channels and data from many laser "shots" were collected and averaged (time averaged signal).

The LIF data were converted to an actual spectrum by plotting the time averaged signal for each wavelength of the tunable dye laser. Therefore, in part, the resolution of the LIF spectra obtained in our laboratory is pre-determined by the stepping function of the tunable dye laser (minimum step size 0.001 nm). To maximize the signal to noise ratio typically 10 laser "shots" were averaged before proceeding to the next wavelength.

The width of a scan was limited by the processing capacity of the computer data acquisition program and ranged from 10 nm for a global scan (step size 0.02 nm) to 2 nm for a moderate resolution scan (0.001 nm). For RhO certain key regions of the spectra were not resolved enough for a complete rotational analysis. This necessitated the recording of high resolution spectra which was performed by the Adam group, at the University of New Brunswick (UNB). The high resolution scans (obtained using a Coherent 699-29 ring laser) were 1 cm^{-1} wide with a step size of 0.0003 cm^{-1}covering a range of about 25 cm^{-1} in the central regions of the more prominent bands for $Rh^{16}O$.

To ensure reliability of the data and that the observed peaks were "real", scans were repeated several times for each region. Optogalvanic lines (OGE) from a Fe/Ne hollow cathode lamp (figure 2.4) were used to check the wavelength calibration of the dye laser for the moderate resolution spectra. The optogalvanic signals are not recorded simultaneously with the laser induced or dispersed fluorescence scans, and therefore are not considered to accurately calibrate the spectra. However, the maximum uncertainty in the transition wavelength was estimated to be around ±0.04 nm (10). Where ever possible, the Stockholm spectra were compared to the moderate resolution data for calibration purposes, since the rotational / vibrational data are much more accurately calibrated.

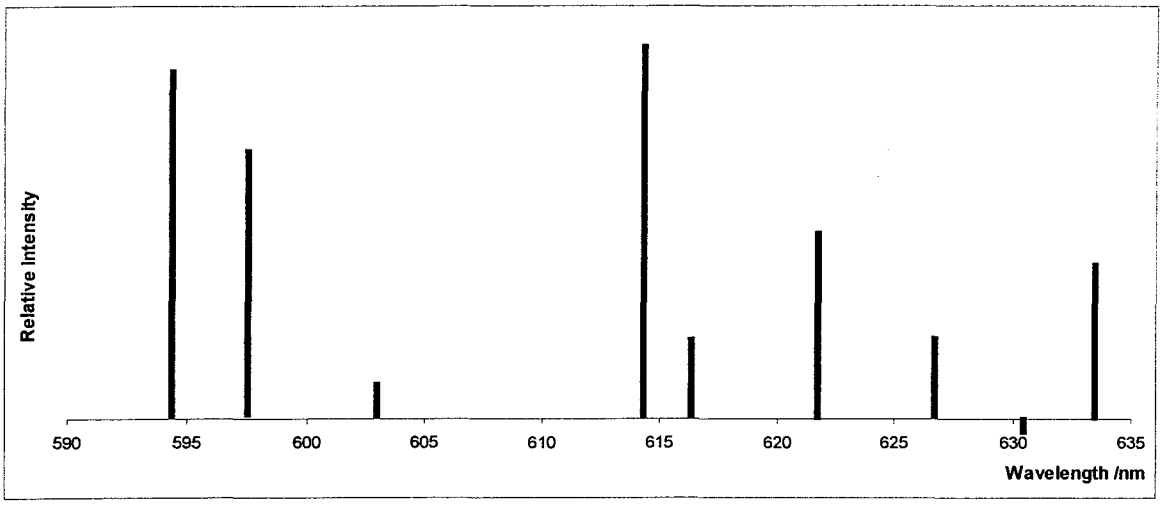

Figure 2.4 Schematic Representation of Opto-galvanic Fe/Ne lines in the range of the Rhodamine 610 dye curve.

For a typical dispersed fluorescence experiment, the signal from 20 shots were averaged and then stored as a function of the monochromator setting (0.5 nm step size). To improve resolution (at the expense of some signal intensity) entrance and/or exit slits on the monochromator were used to reduce the band pass. A 0.5 mm aperture yielded a band pass of ~20 cm^{-1}. Repeated scans indicated the precision of the band centers to be ±2 cm^{-1} and the uncertainty in the spectral intervals is estimated at ±15 cm^{-1} (10). The scan usually began about 20 to 30 nm to the blue of the excitation wavelength (allowing for the appearance of hot bands) and continued to the wavelength limit of the monochromator (~900 nm). The dispersed fluorescence spectrum at 517.998 nm is shown for RhC in figure 2.5. The x-axis shows the displacement of the peaks from the probe position and gives the vibrational spacing of the ground state vibrational energy levels.

Two peaks associated with relaxation to two vibrational levels of a low lying excited state are observed at higher wave numbers.

Calibration of the wavelength scale was checked with the aid of the second order peak associated with the excitation wavelength when present with absolute wavelengths determined by OGE signals.

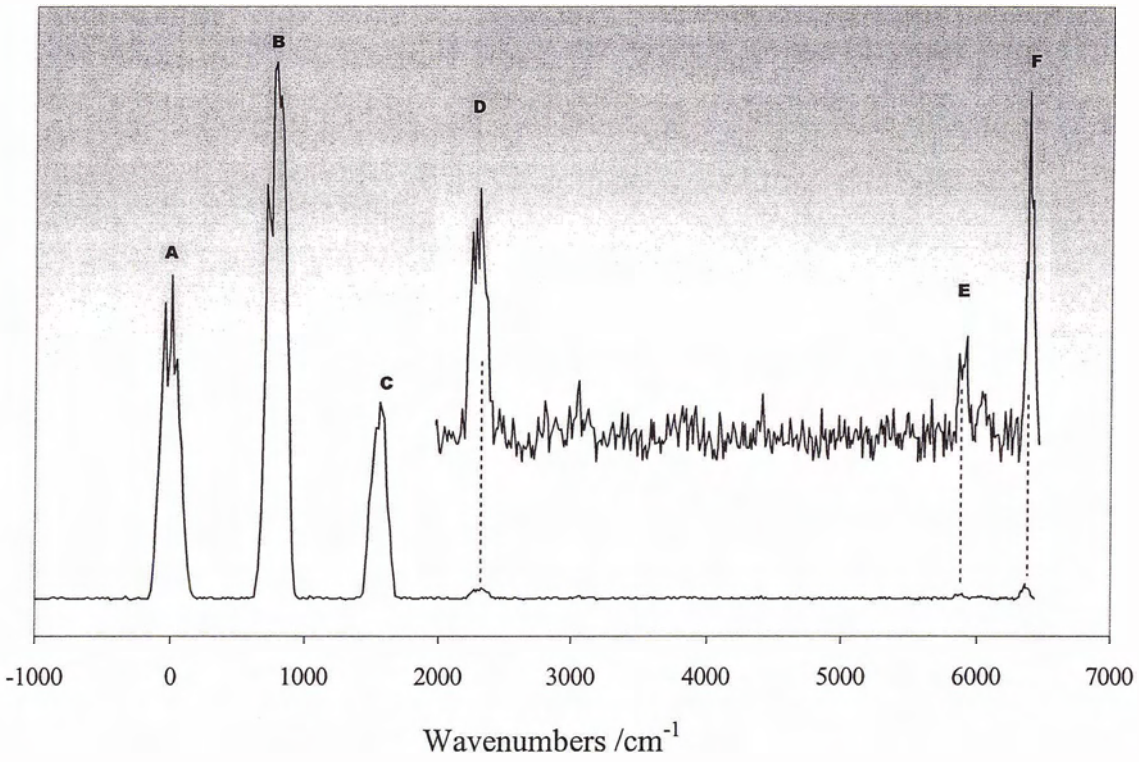

Figure 2.5 Dispersed fluorescence spectrum of $Rh^{16}O$ with excitation wavelength at 517.998 nm. The x-axis shows the displacement of the signal from the pump wavelength. The y-axis is signal intensity in arbitrary units.

Lifetime measurements of the excited states were determined from decay profiles. Typically 500 laser shots were averaged for a single decay profile (11). The decay function at a particular wavelength was corrected for background noise and fitted exponentially to give the measured fluorescence lifetime using.

$$signal = A\exp(-t/\tau_1) + B\exp(-t/\tau_2) \qquad [35]$$

where the A and B are the amplitude coefficients and τ_i are the lifetime(s) of the excited state(s) from which the observed signal originates. When only a single exponential is needed to fit the data the presence of a single state can be inferred.

Figure 2.6 shows a typical molecular decay profile and the background noise (the signal with the ablation laser off). After subtracting the background signal the decay can be fitted using [35] to give the radiative lifetime of the emitting state.

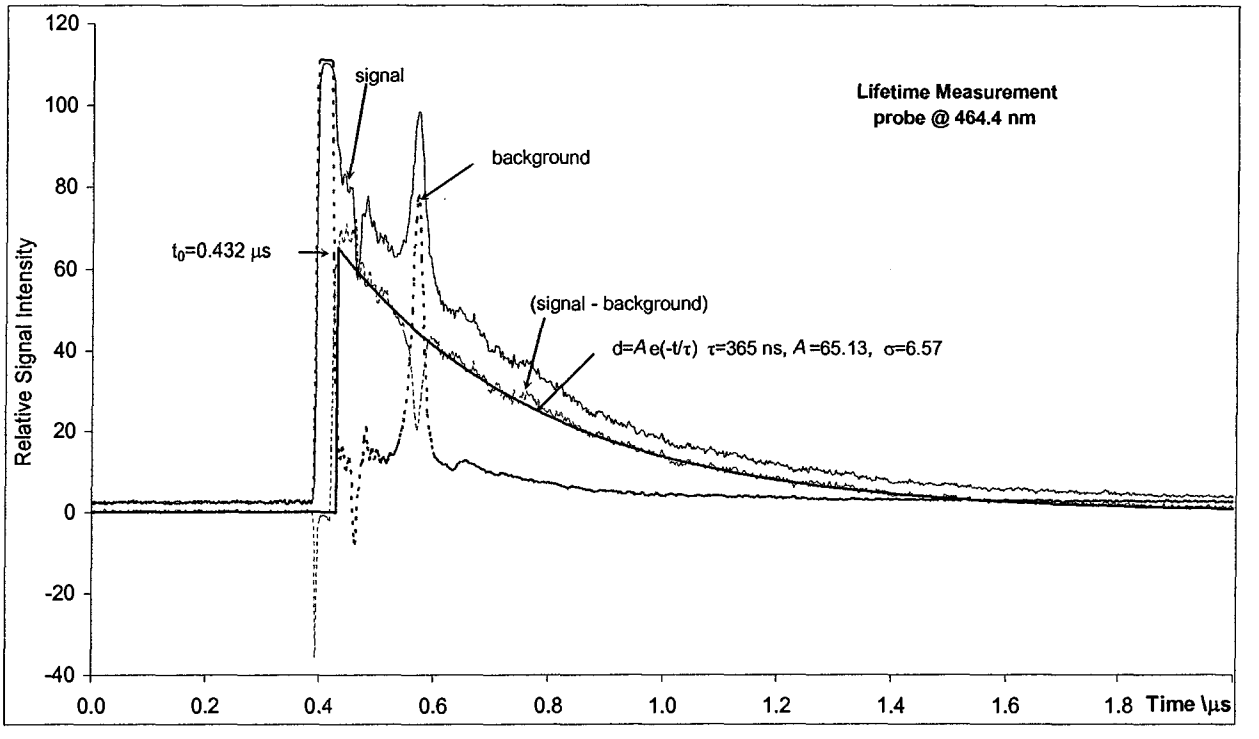

Figure 2.6 Typical data and analysis for a single fluorescence lifetime measurement with the tunable dye laser sitting at 464.4 nm Background noise was subtracted from the signal and t_0 was chosen so as not to include the initial very steep portion of the data. The molecule in this example is iron carbide (FeC).

Typically three to five decay profiles were recorded and fitted for different regions of the spectrum for a particular LIF vibrational band. A single profile was easily fitted to within ±5 ns however lifetime measurements from one wavelength to another within the same band system varied considerably more (11).

In some cases emission from more than one excited state contributes to the observed fluorescence signal and the LIF spectra obtained are overlapped and more complicated in structure and hence more difficult to decipher. Provided the excited states have different radiative lifetimes it is possible to separate the two signals by sampling only the initial or tail end portion of the fluorescence decay signal. This time-filtering technique was used to enhance the observation of very weak signals hidden underneath a strong system in RhC, essentially allowing for the discovery of a new band system.

2.4 Signal Intensity and Population Distributions

The overall intensity of LIF spectra is directly proportional to the number of emitting target molecules. This will depend upon the cross section and intensity of the beam, the density of states present (or the number of molecules in the initial state) as well as the efficiency of absorption as determined by the Einstein transition probability. Since the sample has been produced in a jet-cooled expansion, non-radiative relaxation, by means of collisions, are not competitive with the re-emission of photons, and the quantum efficiency of emission approaches unity.

Intensities of the vibrational bands, as well as the individual rotational lines, vary with the internal temperature of the molecules. The distribution of molecules over the different quantum states can be predicted using the *Maxwell-Boltzmann distribution law,* which takes into account the internal vibrational and rotational temperatures of the molecules, as well as any degeneracy which might exist within the states under consideration.

Classically the number of molecules dN_E that have a vibrational energy between E and $E + dE$ in cm^{-1} is

$$\frac{dN_E}{dE} = e^{-E/kT} \qquad [36]$$

where k is the Boltzmann constant ($k = 0.6952\ cm^{-1}$ per degree, when E is expressed in cm^{-1}) with no restrictions for the values of E. In quantum mechanics, however, only discrete energy levels are populated, and even at room temperature, the number of molecules in the higher vibrational levels fall off rather quickly (see figure 2.7). The number of molecules in the quantized vibrational level υ therefore, is given by

$$N_\upsilon = \frac{N}{Q_\upsilon} e^{-G_0(\upsilon)hc/kT} \qquad [37]$$

where N is the total number of molecules, and $G_0(\upsilon)hc$ is the energy difference between the vibrational levels expressed in cm^{-1}. $Q_\upsilon = 1 + e^{-G_0(1)hc/kT} + e^{-G_0(2)hc/kT} + \ldots$ and is the vibrational partition function where successive terms decrease very rapidly and are unimportant. Therefore for most practical purposes

$$N_\upsilon = Ne^{-G_0(\upsilon)hc/kT} \qquad [38]$$

The larger the vibrational energy gap between two levels, the less populated the higher vibrational level will be. As temperature increases the upper vibrational levels become more and more populated. For most molecules at room temperature (300 K), however, there is a large excess of molecules in the $\upsilon = 0$ state compared to those in the $\upsilon = 1$, and $\frac{N_0}{N_1} \approx 1$. Lower the internal molecular temperatures are produced when the plate valve between the vacuum chamber and the pump is wide open. The spectra therefore, are simplified, by lowering the pressure in the vacuum chamber.

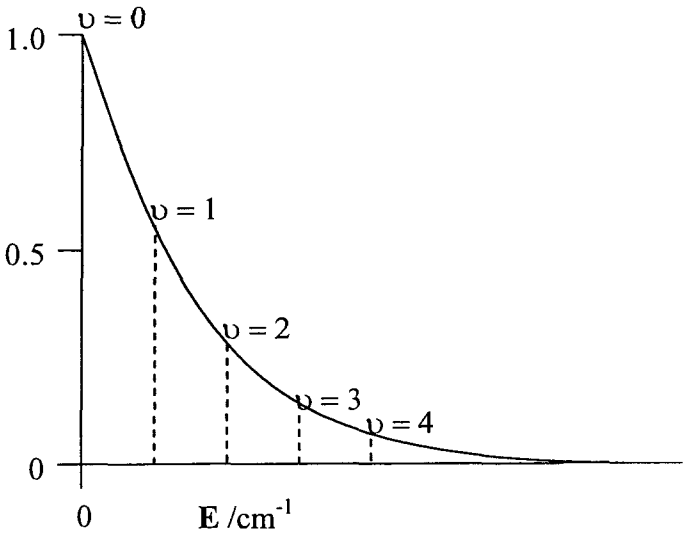

Figure 2.7 Vibrational population distributions. The classical vibrational distribution is given by the (solid line). The vibrational levels of a hypothetical molecule are indicated by the dashed lines. From the figure it can be seen that the population of higher vibrational levels diminishes rapidly. At room temperature most molecules have only the lowest vibrational energy level significantly populated.

The thermal distribution of the rotational levels is not quite so simple. The $(2J+1)$ degeneracy of each rotational level J adds a statistical weight to the calculation. For the rigid rotor model, $E_J = BJ(J+1)$, and for most practical cases the number of molecules in the rotational level J for the lowest vibrational level is

$$N_J \propto (2J+1)e^{-BJ(J+1)hc/kT} \qquad [39]$$

Since the factor $(2J+1)$ increases linearly with J the number of molecules in the different rotational levels goes through a maximum before decreasing (see figure 2.8). The maximum lies at

$$J_{max} = \sqrt{\frac{kT}{2Bhc}} - \frac{1}{2} \qquad [40]$$

The rotational energy levels spread further apart with higher values of the rotational constant B and the value of J_{max} decreases. To a first approximation for higher vibrational levels the rotational distribution is the same but the absolute population is considerably smaller corresponding to the decrease in the vibrational population. With increasing temperature higher rotational (as well as vibrational) levels become populated. As temperature increases a spreading effect can be seen in the rotational intensities of a vibrational band increasing the band width.

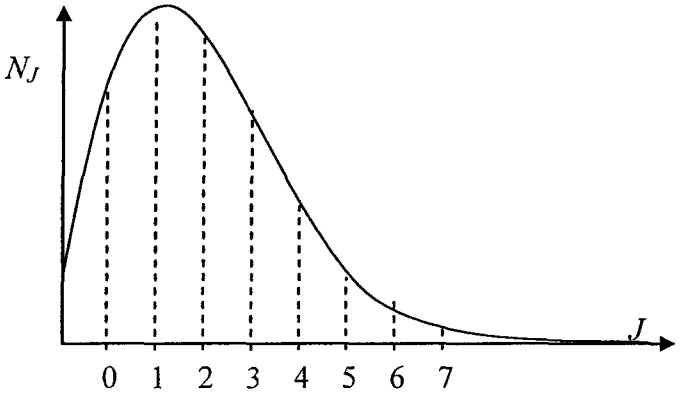

Figure 2.8 Classical (solid line) and quantum mechanical (dashed lines) thermal distributions of the rotational energy levels for a single vibrational level of a theoretical molecule.

The temperature of the spectra can be deduced if the B value (rotational constant) is known or vice versa from the separation $\Delta\nu_{PR^{max.}}$ of the maxima in the P and R branches (in cm^{-1}) from the relationship

$$\Delta\nu_{PR^{max.}} = \sqrt{8BkT/hc} \qquad [41]$$

The strength of the Q, P and R branches will differ depending on $\Delta\Lambda$ of the electronic transition. The general rules for singlet-singlet transitions are as follows:

$\Delta\Lambda = 0$ Q branch will be weak

$\Delta\Lambda = \pm 1$ Q branch will be strong

$\Delta\Lambda = +1$ R branch will be stronger than P branch

$\Delta\Lambda = -1$ P branch will be stronger than R branch

If states of higher multiplicity are involved then more branches may appear making the spectra even more complex making the above relationships difficult to use. Kovacs (12) has published analytical expressions of rotational line intensities for the different branches associated with many of the more complex transitions which may be used for simulating spectra.

The Boltzmann distribution does not always apply to emission spectra since they are not necessarily created under conditions of thermal equilibrium. The Stockholm emission plates used in the analysis of RhC and RhO were recorded under very different conditions, from the jet-cooled LIF spectra. The RhC emission spectrum was recorded using a King furnace (~800° C) under conditions of thermal equilibrium. The emission spectrum of RhO, however, was recorded using a hollow cathode lamp (~2000° C) (13). In the latter technique, many vibrational levels, as well as low lying electronic states, are populated. The emission spectra are more complex with many more lines present as can be seen in figures 2.9 and 2.10. The spectrum of RhO, obtained at very high temperatures, is very difficult to interpret. The high multiplicity and the uncertainty of the lower state, compounded with the sheer number of lines and overlapping rotational structure, are formidable problems to say the least.

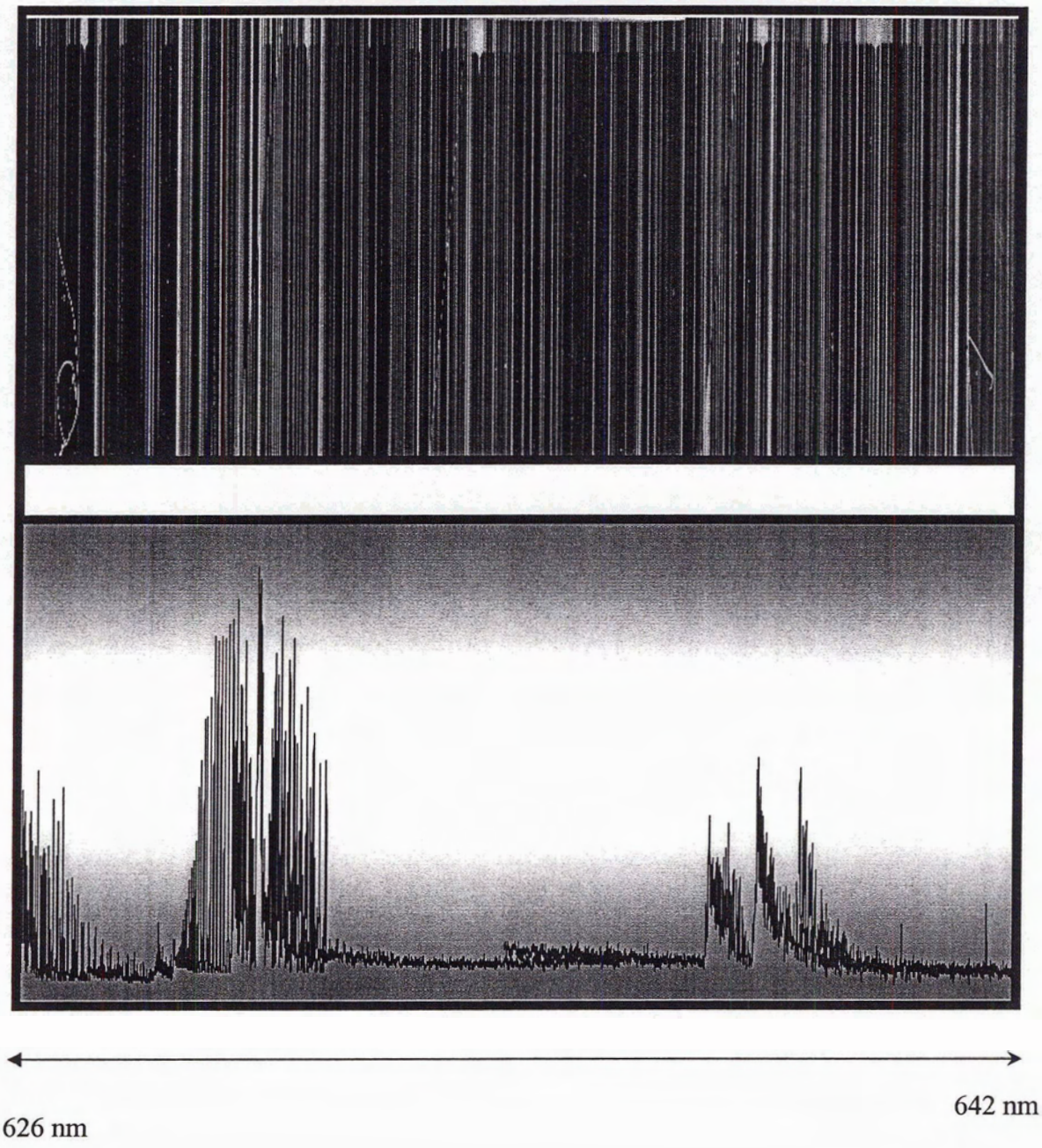

Figure 2.9 Stockholm emission spectra (top) and the LIF spectra (bottom) of $Rh^{16}0$ between 626 and 642 nm (left to right). Three band systems are apparent in the LIF. The lines in the emission plate are white and so congested that individual band systems are not readily discernable. The LIF spectrum shows nicely the presence of several band systems in this region of the spectrum.

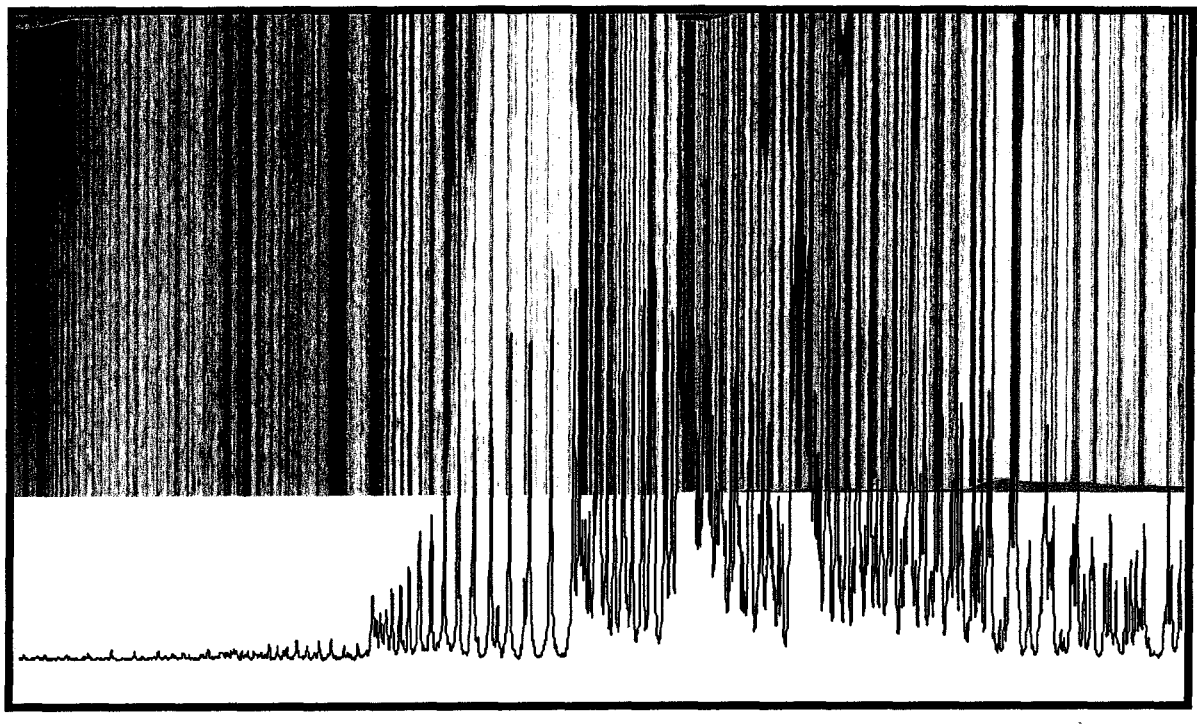

16 218 cm^{-1} 16 146 cm^{-1}

Figure 2.10 Stockholm plates (top) and the corresponding LIF (bottom) spectra of the 618 nm band of $Rh^{16}0$, between 16 218 and 16 146 cm^{-1}. Intensity of the spectra are in arbitrary units. The band head at the far left in the emission plate (dark lines this time) is very distinct. In the LIF spectrum, however, this feature is not even noticeable. This is due to the fact that much higher rotational levels are populated in the hollow cathode emission spectrum than in the LIF spectrum.

2.5 Peak Measurements

For RhC the transition data were simply run through an automatic peak picking program as the spectra were not congested. The LIF spectra were then shifted linearly to

match the accurately calibrated RhC emission lines of Lagerqvist and Scullman (14). For new bands not previously seen the OGE signals were used to calibrate the spectra.

The spectra of RhO on the other hand, were extremely congested and the automatic peak pick program was not used. The spectra of RhO were difficult to analyze and although emission spectra were available they were only partially calibrated and measured. The spectra of MoN (15,16), VO (17) and CrN (18) result from $^4\Pi - {}^4\Sigma$ transitions and were used as a reference, particularly the paper on VO by Merer and coworkers.

The vibrational-rotational bands in the RhO spectra contained many branches, some strong and some weak with many overlapping lines. As a result the LIF spectra were recorded several times over the same region to assess peak reproducibility. The emission spectra are difficult to interpret due to the increase in line density; however they were extremely helpful in calibrating the LIF data, and often weak lines or shoulder peaks in the LIF spectra corresponded to strong lines in the emission plates (figure 2.11).

The emission spectra, as well as the higher resolution spectra from UNB were calibrated using the well known lines of Fe and I_2 respectively, and therefore the absolute line positions are more accurate than the LIF spectra which use OGE data as a reference. As a result the LIF data were shifted linearly to match the lines in the emission data. The wave numbers (in units of cm^{-1}) of the LIF lines are reported to 2 decimal places, the emission lines to 3 decimal places and the UNB lines to 4 decimal places.

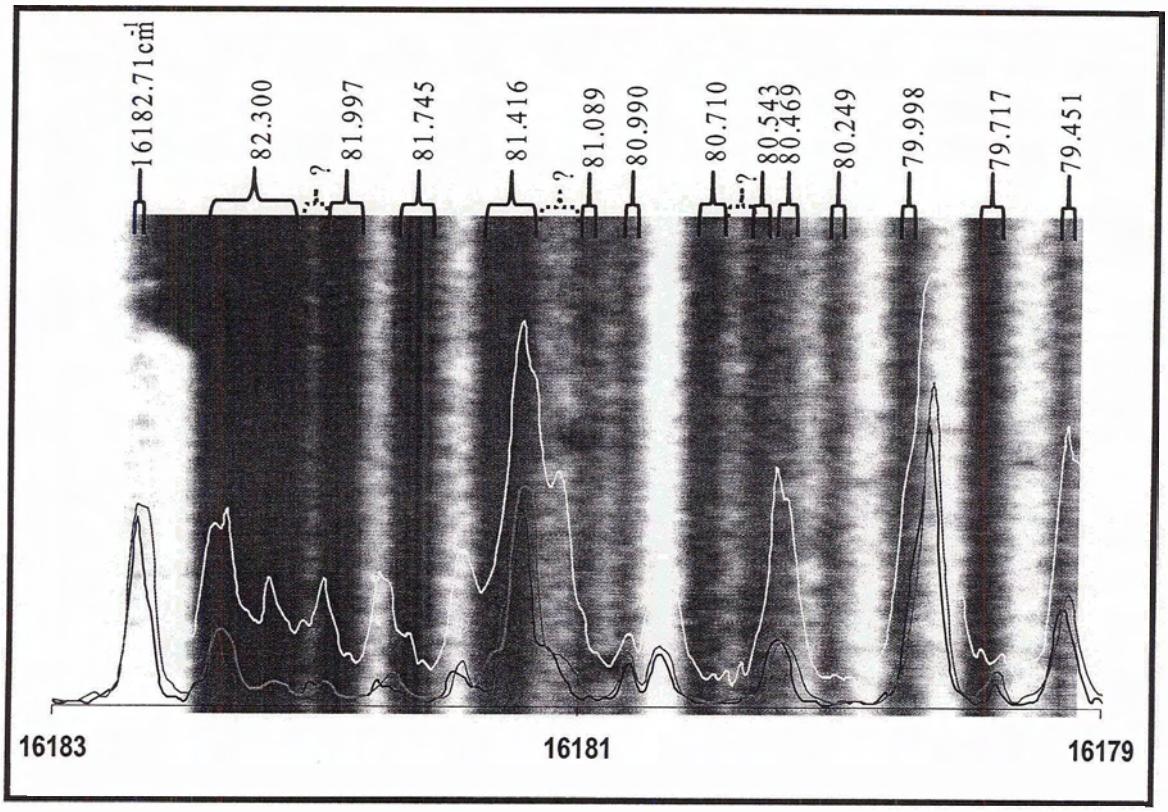

Figure 2.11 Close up of the branch head at 16182.3 cm^{-1} of the 618 nm band with intensity in arbitrary units. Line widths vary with signal intensity as well as the degree of overlap. The regions indicated by the dashed parentheses have not been measured but comparison with the LIF data indicates the presence of weak lines. The LIF spectra from several runs are shown as an indication of reproducibility.

Chapter 3

Spectral Analysis Methods

3.1 Vibrational Structure and Assignments

Vibrational bands are labeled according to υ', υ''; they appear as progressions, ($\Delta\upsilon = \pm 1,\ 2,\ 3,\ldots$), and series, ($\Delta\upsilon$ is constant), in the spectra (see figure 3.1). The vibrational energy level expressions of the harmonic and the anharmonic oscillators predict only slightly different vibrational band structure. If the molecule is sufficiently described by the harmonic oscillator, progressions are equally spaced. The anharmonic oscillator model predicts band separations that are not constant, but that decrease slightly with increasing υ. The energy of the 0,0 band is approximately equal to the energy difference between the two electronic states. More than one electronic transition may occur, increasing the complexity of the observed structure in the spectra.

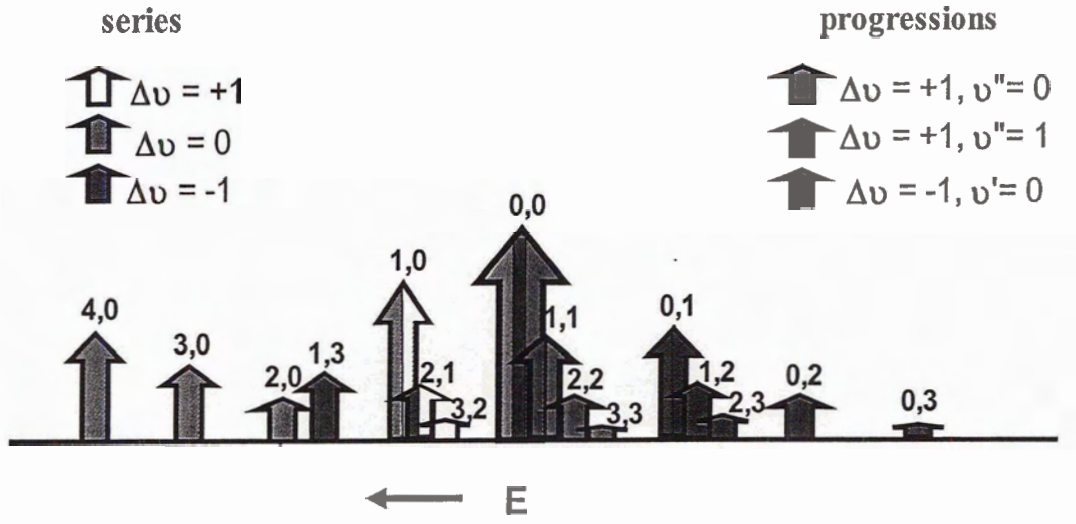

Figure 3.1 Hypothetical band structure of a single electronic transition. In this case ω_e for the ground state is larger than ω_e for the upper state. The 0,0 transition will be the most intense if the equilibrium bond length is similar in both upper and lower states.

Increasing the vacuum in the chamber, helps to reduce the number of bands present and/or the degree of spectral overlap, but this also reduces the amount of information available for the analysis (of course). Isotopic substitution is the primary means of assigning vibrational bands since the energy shift in a band's position is characteristic of $\Delta\upsilon$ and can be calculated.

The classical vibrational frequency of the harmonic oscillator is given by

$$\nu_{osc.} = \frac{1}{2\pi}\sqrt{\frac{k}{\mu}} \qquad [42]$$

The force constant k is determined by the electronic structure only and is independent of the different isotopic masses that might be used to modify the molecule. The vibrational frequency of the harmonic oscillator is given (in cm^{-1}) by $\omega_e = \frac{\nu_{osc.}}{c}$ and is inversely proportional to the square root of the reduced mass μ of the system. Assuming that all of the transitions originate from the $\upsilon''= 0$ level of the ground state, members of the $\upsilon,0$ progression will be separated in energy by

$$\Delta E_{vib.} = (\omega_e - \omega_e x_e)\upsilon - \omega_e x_e \upsilon^2 \qquad [43]$$

where ω_e, $\omega_e x_e$ and υ are those of the upper state. The heavier the isotopic molecule the smaller is the oscillation frequency. The vibrational spacing of progressions in the spectra of the heavier isotope will be smaller. To a very good approximation $\omega_e^i = \rho\omega_e$ and $\omega_e^i x_e^i = \rho^2 \omega_e x_e$ where ρ is the isotopic ratio given by (9)

$$\frac{\nu^i{}_{osc.}}{\nu_{osc.}} = \sqrt{\frac{\mu}{\mu^i}} = \rho \qquad [44]$$

As long as ρ is only slightly different than 1 the expected $\upsilon,0$ vibrational band shift is

$$shift / cm^{-1} = (1-\rho)\upsilon\Delta E_{vib.} \qquad [45]$$

where υ refers to the upper state vibrational level and $\Delta E_{vib.}$ is the same as equation 36. For all bands where $\Delta\upsilon \neq 0$ the isotope shift increases with $\Delta\upsilon$, with the (0,0) band expected to show little or no isotope shift (figure 3.2).

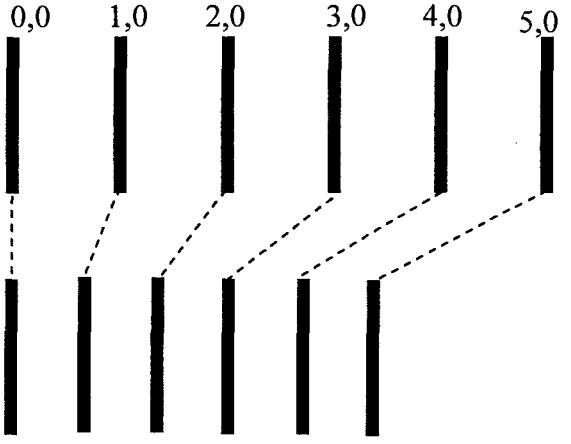

Figure 3.2 Schematic diagram of characteristic isotope shifts in the υ,0 progression. When the reduced mass is increased the vibrational spacing is reduced. Note that the shift in band positions increases with υ.

Rhodium has only one naturally occurring isotope. Oxygen and hydrogen however, both have more than one. LIF spectra were recorded for $Rh^{12}C$, $Rh^{13}C$, $Rh^{16}O$ and $Rh^{18}O$. The calculated values for ρ are

i) $$\sqrt{\frac{\mu(Rh^{12}C)}{\mu(Rh^{13}C)}} = \rho = 0.96483$$

ii) $$\sqrt{\frac{\mu(Rh^{16}O)}{\mu(Rh^{18}O)}} = \rho = 0.95059$$

The complete vibrational assignment may still be elusive even with isotope shift data. Sometimes individual band profiles and branch structure or a complete rotational analysis are required to finalize the vibrational assignments.

3.2 Rotational Structure and Branch Assignments

Since the rotational constant is a function of the reduced mass of the system, two isotopes will have different rotational energy levels ($B^i = \rho^2 B$) and hence

$$E^i{}_{rot.} = B^i J(J+1) = \rho^2 BJ(J+1) \qquad [46]$$

Since the rotational term is much smaller than the vibrational term, the rotational isotope shift is much smaller than the vibrational isotope shift. Due to the complex nature of the spectra under investigation and the fact that the absolute wavelength calibration of the LIF spectra was insufficiently accurate to permit the direct measurement of isotope shifts for rotational lines, isotopic mixtures were not used for rotational study of RhO and RhC.

The rotational branch structure of individual vibrational-rotational bands is a function of the general selection rules and the nature of the electronic states (multiplicity and angular momentum) involved in the observed transition. Band profiles can differ in the number of branches (and their relative intensities), the rotational line separations, the J values of the observed first lines and the appearance of fine or hyperfine structure.

In the spectrum, unperturbed rotational structure appears as a set of equally spaced lines with gradually increasing and /or decreasing intensity. All of the observed bands for RhC and RhO were red-degraded. This means that band heads (converging rotational lines) appeared in the R-branches to higher energy than the band origins indicating that $B' < B''$ or $r_{eq}^{'} > r_{eq}^{''}$. This is a clear indication of a decrease in bond order on going from the lower to the upper states and a change in electronic configuration can be inferred. The rotational lines in a band head are severely overlapped and difficult to determine. If the returning branch is observed, then fitting the branch to a polynomial will assist in the line location where combination differences are unavailable.

3.3 Combination Differences and the Rotational Analysis

The method of combination differences $\Delta_2 F(J)$ relates rotational lines that have either the upper $\Delta_2 F'(J)$ or lower $\Delta_2 F''(J)$ energy levels in common. The combination relations permit the separation of the upper and lower rotational levels from the observed transition lines. Combination differences therefore are consequentially very important, allowing the rotational constants of the upper and lower states to be evaluated independently. For relatively simple spectra where the R- and P- branches ($\Delta J = \pm 1$) are obvious, the combination differences for the ground and excited states are given by

$$\Delta_2 F''(J) = E''_{Rot.}(J+1) - E''_{Rot.}(J-1) = R(J-1) - P(J+1) \qquad [47]$$

$$\Delta_2 F'(J) = E'_{Rot.}(J+1) - E'_{Rot.}(J-1) = R(J) - P(J) \qquad [48]$$

for closed shell case (a) states. For case (b) states, J is simply replaced by N. Further combination differences arise in multiplet states and from Q branches if resolved.

The combination differences, once established, must agree for any band having either the upper or lower state in common, even if perturbations exist. Therefore, combination relations are a means of checking whether two bands have the same upper or lower state in common. Combination differences, therefore, can also be used to aid in the vibrational analysis as well as identifying ambiguous branches and/or lines and extending line assignments in difficult regions of the spectrum. The agreement of the observed combination difference relations is then a check on the correctness of the rotational assignments of lines and branches.

For RhO, there are two groups of 15 ground state combination differences relating rotational lines that start at different levels in the ground state but that end in either the

same *e* or *f* level in the excited state. In figure 3.3 the group of 15 rotational lines that end in the E(*f*), ($J = 2.5$) level are shown with shaded horizontal arrows. Only four of the thirty combination relations for a single excited state level, combine rotational lines starting from the same spin-rotational level in the ground state. These are depicted in figure 3.3 by the vertical white arrows.

After the combination differences of a particular band have been determined, the rotational energy levels for the upper and lower states can be calculated. An initial value for the rotational constants, B_υ and D_υ, are determined graphically by the relation

$$\Delta_2 F(J) = (4B_\upsilon - 6D_\upsilon)(J + \tfrac{1}{2}) - 8D_\upsilon (J + \tfrac{1}{2})^3 \qquad [49]$$

Since D_υ is on the order of $10^{-5} B_\upsilon$ the term $-6D_\upsilon$ can be neglected, simplifying the above relation to

$$\Delta_2 F(J) = 4B_\upsilon (J + \tfrac{1}{2}) - 8D_\upsilon (J + \tfrac{1}{2})^3 \qquad [50]$$

If all terms are divided by $4(J + \frac{1}{2})$ the left side of the resulting expression

$$\frac{\Delta_2 F(J)}{4(J + \frac{1}{2})} = B_\upsilon - 2D_\upsilon (J + \tfrac{1}{2})^2 \qquad [51]$$

can be plotted against $(J + \frac{1}{2})^2$ to give intercept B_υ and slope $-2D_\upsilon$. The method of least squares is then used to determine more precisely the values for the rotational constants by fitting the rotational energy levels, the observed transition lines or the combination differences.

The spectrum of RhC contained numerous and the spectrum of RhO was extremely complex. Therefore, in this dissertation all spectroscopic analysis employed Microsoft's Excel ® spreadsheet type graphic interface software exclusively instead of prewritten software packages for the rotational analysis.

Figure 3.3 The 15 ground state combination differences for RhO between transitions that end in the same J(e) upper state level. There are four combination differences indicated by white vertical arrows that return to the same spin-rotation component of the $X^4\Sigma$ state. These four are referred to as the traditional combination differences.

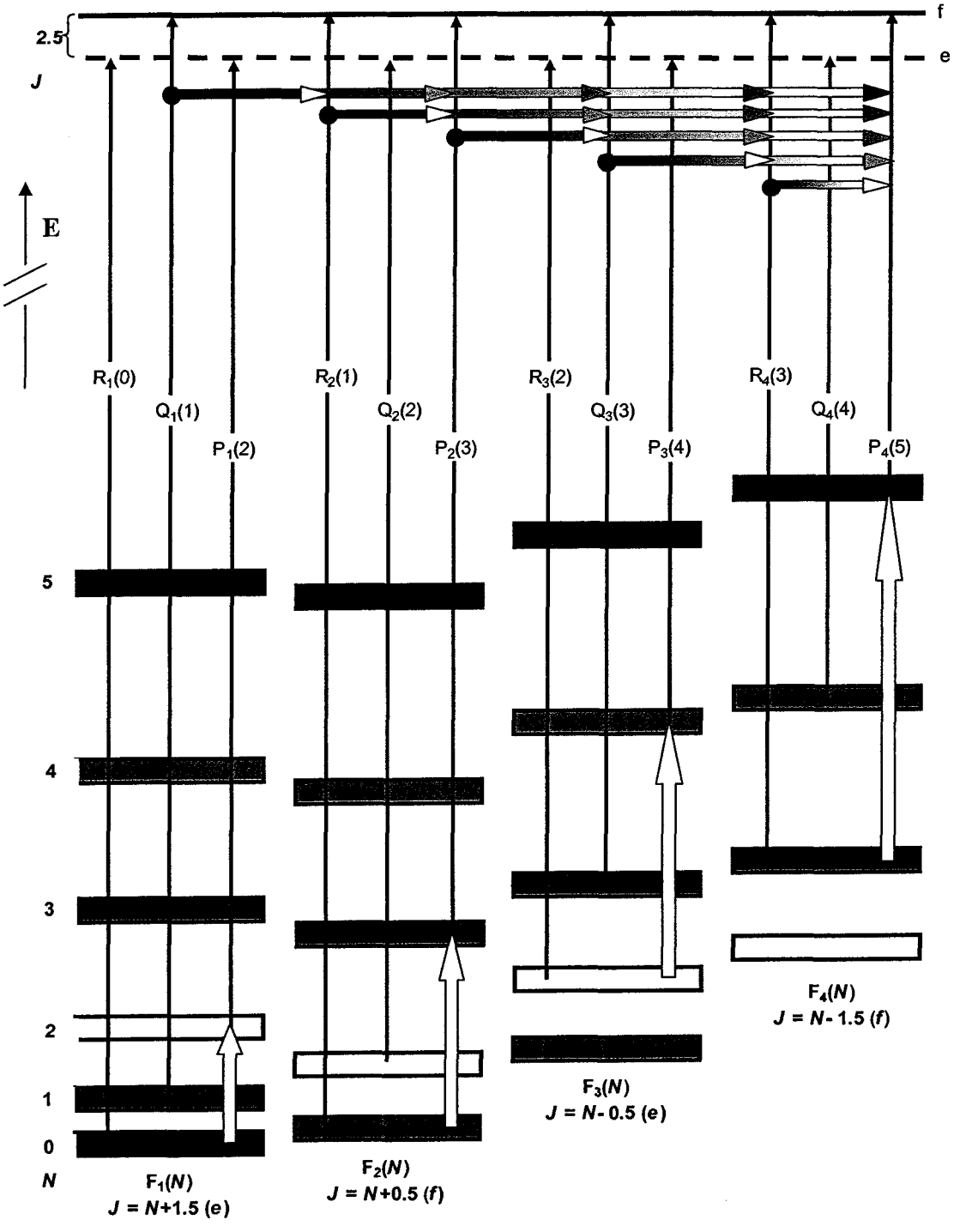

3.4 Molecular Energy Levels

The energy levels of the molecule are determined by solving the appropriate molecular Hamiltonian. For RhC and RhO unpaired valence electrons contribute to the total angular momentum requiring the complete molecular Hamiltonian

$$\mathbf{H} = \mathbf{H_{ROT}} + \mathbf{H_{SO}} + \mathbf{H_{SR}} + \mathbf{H_{SS}} + \mathbf{H_{HF}} \qquad [52]$$

which is defined in terms of angular momentum operators operating on the appropriate basis set defined by the good quantum numbers (and phase factors which describe the relative rotations of the molecule fixed and laboratory fixed frames of reference).

Diagonal matrix elements of the Hamiltonian operators define the eigenvalues of a particular set of quantum numbers and off diagonal matrix elements couple states with different L, S, Λ, Σ and Ω according to the selection rules for each operator. If hyperfine structure is not observed or is very small (as in the case of RhO) the hyperfine energies can be determined separately and matrix elements due to $\mathbf{H_{HF}}$ need not be included in the rotational Hamiltonian.

The diagonal parts of $\mathbf{H_{ROT}} = B\mathbf{R}^2$ for case (a) and case (b) coupling are

Case (a) $\lvert J,S,\Omega,\Lambda,\Sigma\rangle$	**Case (b)** $\lvert J,S,N,\Lambda\rangle$
$BJ(J+1)-D[J(J+1)]^2$	$BN(N+1)-D[N(N+1)]^2$

Off diagonal matrix elements of $\mathbf{H_{ROT}}$ are responsible for interactions between electronic states and are described in detail in section 4.5.

The effect of the diagonal part of $\mathbf{H_{SO}} = A\mathbf{L}\cdot\mathbf{S}$ on a case (a) situation is to separate the energies into groups of 2S+1 Ω sub-states all having the same rotational constant, and potential energy curve. The off diagonal part of $\mathbf{H_{SO}}$ leads to **S**-uncoupling, which at sufficiently high J will make case (a) cease to be a good approximation. The diagonal

part of $\mathbf{H_{SO}}$ in case (b) is noticeable only at low N levels for $\Lambda \neq 0$ states shifting the $J = N + S$ levels from the $J = N - S$ levels by the same amount making them approach case (a) behaviour. Off diagonal elements are responsible for interactions between electronic states.

The effect of the spin rotation operator $\mathbf{H_{SR}}$ is much smaller than $\mathbf{H_{SO}}$. $\mathbf{H_{SR}} = \gamma\, \mathbf{N}\cdot\mathbf{S}$ has only diagonal matrix elements in case (b) which removes the 2S+1 degeneracy of the each N level. $\mathbf{H_{SR}} = \gamma\, \mathbf{R}\cdot\mathbf{S}$ for case (a) and is negligible compared to $\mathbf{H_{SO}}$.

$\mathbf{H_{SS}} = 2/3\lambda(3S_z^2 - \mathbf{S}^2)$ for $\Delta\Lambda = 0$ is strictly zero for doublets and is only important for triplet or higher multiplicity states. The subtle effect of λ and more prominent effect of γ can be seen below (figure 3.4) on the reduced energy levels of a $^4\Sigma$ state.

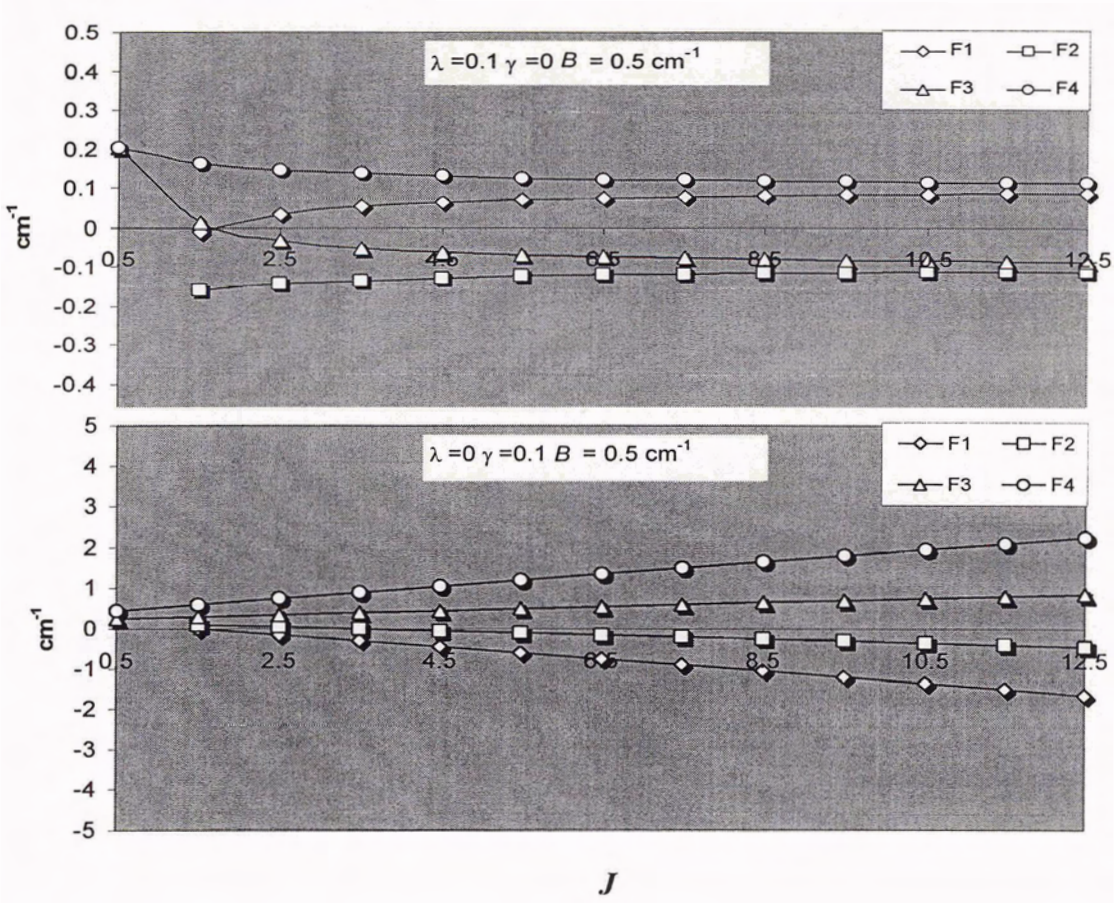

Figure 3.4 Reduced energy levels of a $^4\Sigma$ case (a) limit above and case (b) limit below. F_1 has J=N+1.5, F_2 has J=N + 0.5, F_3 has J=N - 0.5 and F_4 has J=N - 1.5.

Chapter 4

Perturbation Analysis of Rhodium Carbide

4.1 Historical Background

RhC was among the first transition metal carbide molecules to be spectroscopically identified and characterized in the gas phase. In 1966, the journal Arkiv för Fysik, published an article by Lagerqvist and Scullman entitled the "Rotational analysis of the spectrum of RhC in the 4000 - 5000 Å region" (14). Thirteen bands were present in this region forming two band systems (labeled B - X and C - X) both belonging to rhodium carbide. Just previous to this report another system consisting of 26 bands and labeled A – X had been observed in the near-infrared and reported (but not analyzed) by the same group (19). Lagerqvist and Scullman proceeded to rotationally analyze two bands of the B – X system and eight bands of the C – X system; both systems were determined to be $^2\Sigma^+ - X\ ^2\Sigma^+$ in character.

The B and C excited states lie very close in energy perturbing each other strongly over a large range of rotational energy levels and for several vibrational levels. Another "unseen" state, labeled D, with $^2\Sigma^-$ symmetry (opposite to that of the C state) was deduced by the existence of a relatively weak local perturbation, which occurs in several vibrational levels of the C state, producing only a few extra lines in the spectra.

Lagerqvist and Scullman were able to identify only the 0,0 band of the B – X system noting that the regions where further B- vibrational levels were expected to be found were however, tremendously rich in lines. This observation was surprising due to the fact the 0,0 transitions for both the B – X and C – X systems were very intense and

that many bands had been observed for the C- X system (irregularly spaced but approximately 850 cm^{-1} apart). Also surprising was the fact that the two 0,0 bands are only 168 cm^{-1} apart, since configuration interactions should push these two electronic states further away.

The spin-rotation constant (γ = 1.03 cm^{-1}) reported for the B state was unusual being almost exactly twice the rotational constant (0.5067 cm^{-1}) for that state. The spin-rotation constant for the B state was also two orders of magnitude and opposite in sign to γ = -0.03 cm^{-1} for the C state and γ = -0.06 cm^{-1} for the ground state.

Lagerqvist and Scullman's analysis remained essentially undisputed until recent LIF spectra of rhodium carbide were recorded at the University of Victoria in the mid 1990s. A renewed interest into the electronic structure of RhC led to a literature investigation revealing the above interesting anomalies. The original spectra had been obtained under conditions of thermal equilibrium employing a King furnace as the absorption tube; conditions were hot and the spectra were dense with rotational lines. The much colder LIF spectra contained well resolved low *J* rotational lines, providing a nice complement to the Stockholm data where many of these lines were not observed. Matrix studies of RhC in neon by Brom *et al.* (20) showed evidence for two electronic systems between 420 and 460 nm in addition to the C – X system. Their ESR measurements of the ground state indicated strong coupling with an unknown excited state of $^2\Pi_i$ symmetry.

Upon careful examination of Lagerqvist and Scullman's paper, it was speculated that perhaps a mistake had been made in the analysis, and that a least squares fitting program recently designed for spectroscopic applications would be more successful in

deriving the constants for the C state than the traditional graphing techniques used by Lagerqvist and Scullman. The standard deviation obtained however, was unacceptably large indicating that the energy levels of the C state were not obeying the standard energy relations. It was decided that Lagerqvist and Scullman's results needed to be systematically reproduced in order to examine their methodology more closely before any conclusions could be drawn. The two $^2\Sigma^+$- $X^2\Sigma^+$ transitions were studied in detail and this work is presented in the next two sections.

4.2 Analysis of the Ground State

The electronic states of RhC can be predicted from the ground states of the separated atoms by assuming that **LS** coupling holds true from the atoms to the molecule (7). The ground state of rhodium [...$4d^8$ $5s^1$] is ^{4}F and the ground state of carbon [...$2s^2$ $2p^2$] is ^{3}P. Together thirty-six states are possible with values for Λ of [Σ^+(2), Σ^-, Π(3), Δ(3), Φ(2) and Γ] and multiplicities of 2,4 and 6. *Ab initio* calculations (21) predict a $^2\Sigma^+$ ground state with a low lying $^2\Pi$ state nearby confirming what was observed experimentally by Lagerqvist and Scullman who however, could only speculate at what electronic configurations might lead to the observations.

The C – X and B – X bands of RhC observed by Lagerqvist and Scullman were all red degraded and contained doublet-type structure consisting of two P- and two R-type branches of about equal intensity. The lack of a Q-branch suggests that $\Delta\Lambda = 0$ and the lower state of the band systems was assumed to be the ground state since the spectra were obtained in absorption. The energy spacing between the first lines of the R- and P-branches from each spin-rotation component was $\approx 2B$, expected for $\Omega = {}^1/_2$ - $\Omega = {}^1/_2$

transitions. It was therefore concluded that both band systems belonged to $^2\Sigma^+ - ^2\Sigma^+$ transitions.

$^2\Sigma^+$ states belong to Hund's case (b) since $\Lambda = 0$, and the one unpaired electron with angular momentum $m_s = \pm\frac{1}{2}$ may couple to the rotation of the molecule to produce fine structure in the spectrum. These spin-rotational levels are designated F_1 and F_2 with $J = (N + \frac{1}{2})$ and $J = (N - \frac{1}{2})$ respectively. If the spin-rotation constant, γ, is negative then the F_1 levels are lower in energy than the F_2 levels (as in figure 4.1). The + sign on the state symbol $^2\Sigma^+$ indicates that the rotational eigenfunction of the levels with even values of N remains unaltered by a reflection of all particles (including the nuclei) at the origin (inversion) while the eigenfunctions for rotational levels with odd N change sign (see figure 4.2).

The rotational term values of a $^2\Sigma^+$ state are given by (9)

$$F_1(N) = T_\upsilon + B_\upsilon N(N+1) - D_\upsilon[N(N+1)]^2 + \tfrac{1}{2}\gamma_\upsilon N, \text{ for } J = N + \tfrac{1}{2} \qquad [53]$$

$$F_2(N) = T_\upsilon + B_\upsilon N(N+1) - D_\upsilon[N(N+1)]^2 - \tfrac{1}{2}\gamma_\upsilon(N+1), \text{ for } J = N - \tfrac{1}{2} \qquad [54]$$

where the vibrational dependences of the rotational parameters are given by

$$B_\upsilon = B_e - \alpha_e(\upsilon + \tfrac{1}{2}) \qquad [55]$$

$$D_\upsilon = D_e + \beta_e(\upsilon + \tfrac{1}{2}) \qquad [56]$$

$$\gamma_\upsilon = \gamma_e - \chi_e(\upsilon + \tfrac{1}{2}) \qquad [57]$$

α_e, β_e and χ_e are the vibrational-rotational coupling constants and the term value, T_υ, encompasses both the electronic and vibrational energies.

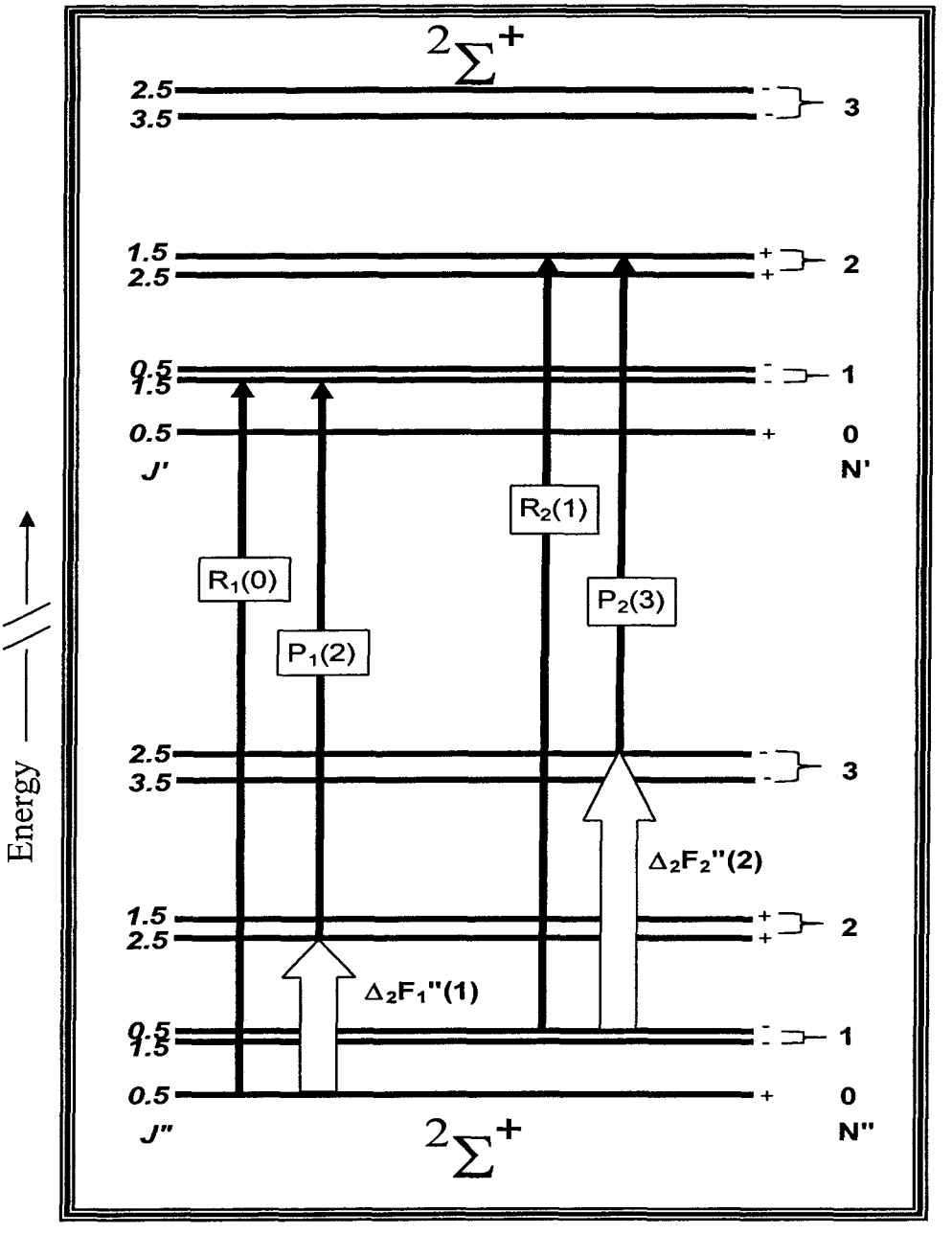

Figure 4.2 Energy level diagram of a $^2\Sigma^+$ - $^2\Sigma^+$ transition. Four branches only are expected. The value of N for the rotational lines is given in parenthesis. Solid arrows are the transition lines used to calculate the ground state combination differences (block arrows). The spin-rotation constant γ is negative for both the upper and lower states so that the F_2 levels lie higher in energy than the F_1 levels, as is the case for the ground state of RhC.

If the upper state is also a $^2\Sigma^+$ state, then the selection rules $\Delta N = \pm 1$ and $+ \leftrightarrow -$ apply. Only four branches are expected to appear in the spectra, one R- and one P- branch from each of the two spin components (F_1 and F_2) of the lower state (see figure 4.2). The selection rule $\Delta J = 0, \pm 1$ is a general selection rule producing weak satellite branches with $\Delta J \neq \Delta N$. The intensities of these satellite branches decrease rapidly with N; none were observed.

Theoretically, the rotational lines, which have the F_1 rotational levels in common, should be slightly more intense, especially at low J. Branch intensities, however, were so similar it was impossible for Lagerqvist and Scullman to tell which pair originated from which spin component, especially since low J rotational lines had not been observed. Examination of the A –X band system, which turned out to be a $^2\Pi_i - {}^2\Sigma^+$ transition, (figure 4.3 shows an energy level diagram for such a transition), settled this matter. The F_1 levels were lower in energy than the F_2 levels in the ground state, indicating that the sign of γ is negative (19).

The LIF spectra contain the low J data missing from the Stockholm plates. The two data sets were combined and the ground state rotational constants determined in the traditional graphical manner, using combination differences $\Delta_2 F(N)$. The left side of

$$\frac{\Delta_2 F''_{ave}(N)}{4(N+\frac{1}{2})} = B_\upsilon - 2D_\upsilon (N+\tfrac{1}{2})^2 \qquad [58]$$

plotted against $(N+\frac{1}{2})^2$ give a straight line with intercept B_υ and slope equal to $-2D_\upsilon$. Ground state combination differences, using data from the C-X(0,0) band, plotted against $(N+\frac{1}{2})^2$ appear in figure 4.4 for both the $F_1$and F_2 levels separately as well as for their

average $(F_1+F_2)/2$. A straight line is obtained for the average plot validating the use of relationship [58] for determining the rotational constants of an unperturbed state.

The spin coupling constant γ can be obtained from the differences between the combination differences by plotting the differences against *N*. The relationship,

$$\Delta_2 F_1''(N) - \Delta_2 F_2''(N) = 2\gamma_\upsilon \qquad [59]$$

should give a horizontal line graph, of intercept equal to $2\gamma_\upsilon$ (see figure 4.5).

Using data from all of the bands analyzed, Lagerqvist and Scullman, determined values for B_e (0.6027 cm^{-1}) and α_e (0.00396 cm^{-1}). Approximate values only were obtained for D_e (0.78×10^{-6} cm^{-1}) and β_e (0.01×10^{-6} cm^{-1}). The graphically determined rotational constants and those derived using equation [55] are shown in table 4.1. The agreement is quite good. The vibrational dependence of γ_υ was within the calculated standard deviation and is not readily observed. No perturbations were found for the ground state (as expected); a plot of the residuals observed (calculated from combination differences) minus calculated (theoretical) energy levels is shown in figure 4.6 for the C-X (0,0) band system.

Table 4.1 Rotational Constants for the ground state of RhC in cm^{-1}(14).

$\omega_e = 1049.87 \quad \omega_e x_e = 4.93_7 \quad \gamma = -0.065 \quad B_\upsilon = 0.6027 - 0.00396(\upsilon + \frac{1}{2})$

υ	B_{obs}	B_{calc}	$D_{obs}/10^{-6}$
0	0.6007	0.6007	0.79_5
1	0.5967	0.5968	0.79_5
2	0.5928	0.5928	0.80_8
3	0.5889	0.5888	0.83

Attempts to characterize the B and C states, using graphing techniques, were inconclusive and provided only qualitative information due to the numerous perturbations that were present. The lack of bands involving the B state was noted by Lagerqvist and Scullman, prompting our search via LIF spectroscopy for new bands, including higher vibrational levels of the elusive state.

Spin-orbit splitting in $^2\Pi$ states is much larger the spin-rotation splitting in $^2\Sigma$ states, by several orders of magnitude. Each sub-band of a $^2\Pi - {}^2\Sigma$ transition, consists of six branches of about equal intensity. The J numbering of the first rotational lines is different for each of the sub-bands. Since $J = \Omega, \Omega+1, \Omega+2\ldots$for the case (a) $^2\Pi$ state and $J = N+{}^1/_2$ and $J = N-{}^1/_2$ for the F_1 and F_2 spin-rotational levels of the $^2\Sigma$ state. The N numbering for the Q and P lines differ between the two sub-bands as shown in figure 4.3.

Each of the rotational levels of the $^2\Pi$ state is doubly degenerate due to $\pm\Lambda$ which may be removed by mixing with nearby $^2\Sigma$ states (Λ-type doubling). For states with case (a) coupling the splitting of the rotational lines with $\pm\Lambda$ is different for the different spin-orbit components. For $^2\Pi$ case (a) states the Λ-type doubling for the $^2\Pi_{1/2}$ component varies linearly with J, whereas for the $^2\Pi_{3/2}$ component it varies with the third power of J and is very small for low J compared to that of the $^2\Pi_{1/2}$ state. The energy level diagram for a $^2\Pi_{inv}$ case (a) – $X^2\Sigma^+$ would be identical to the $^2\Pi_{reg}$ case (a) – $X^2\Sigma^+$ of figure 4.3, except that theF_1 levels of the $^2\Pi_{inv}$ would be higher than the F_2 levels. This is the case for the $A^2\Pi_{inv}$ - $X^2\Sigma^+$ system of RhC.

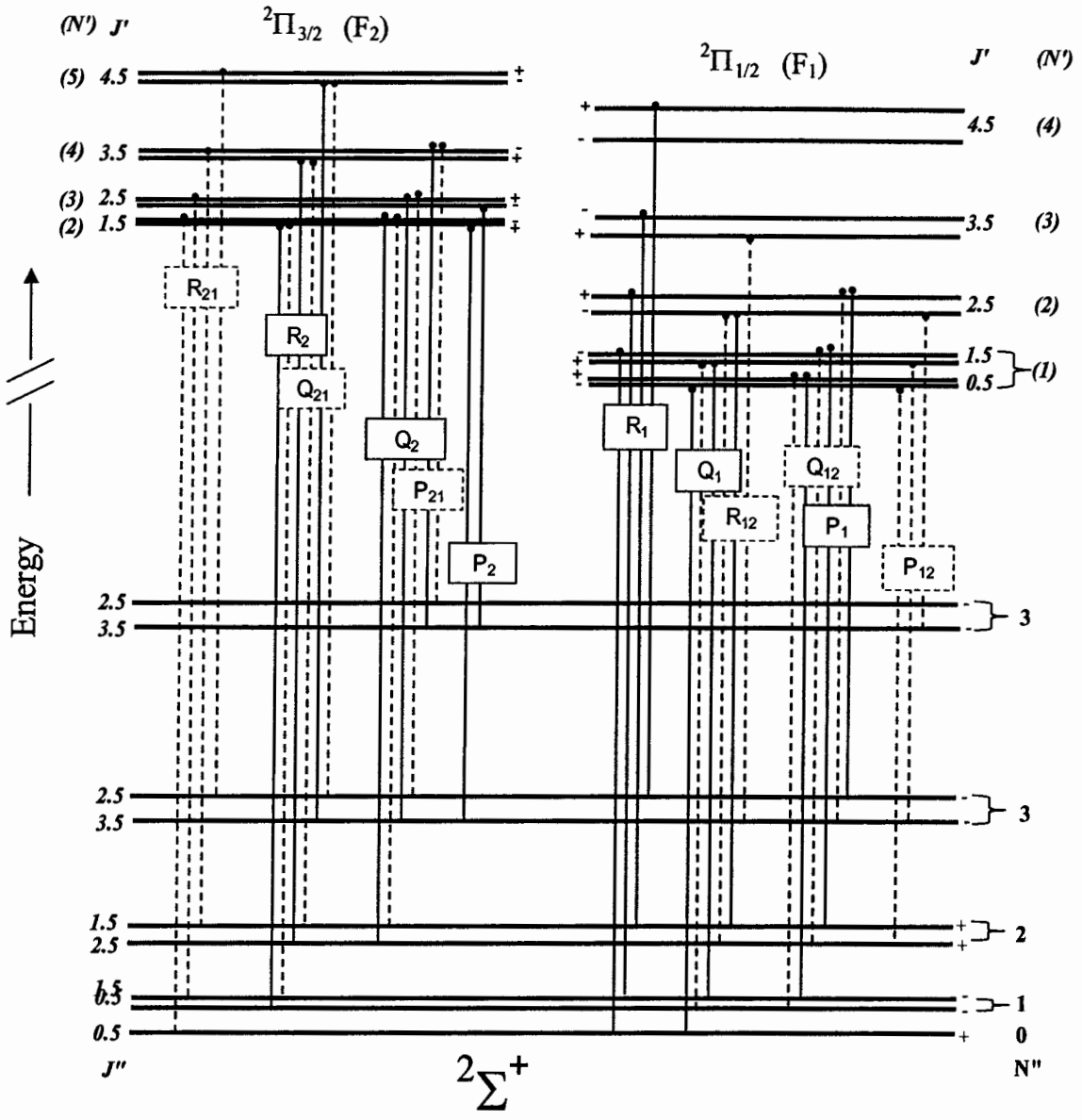

Figure 4.3 Energy level diagram and rotational lines of a $^2\Pi_{reg}$ case (a) – $X\,^2\Sigma^+$ transition. Usually the spin-orbit splitting is larger and the spin-rotation splitting much smaller than shown here.

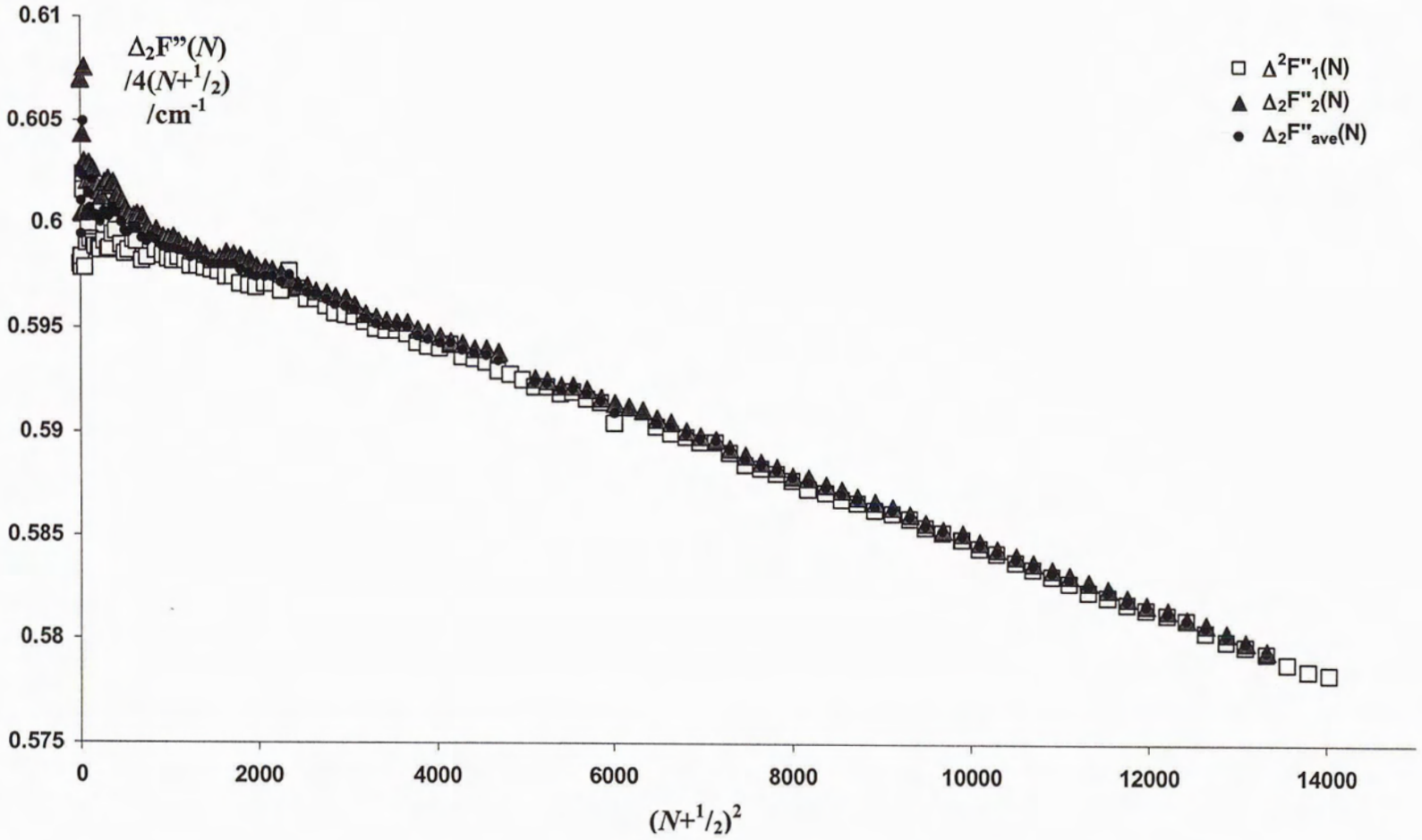

Figure 4.4 Ground state combination differences (cm^{-1}) plotted against $(N+1/2)^2$ for the determination of B_0 using the C – X (0,0) transition lines. The plot of the average combination differences produces a straight line of slope $-2D_0$.

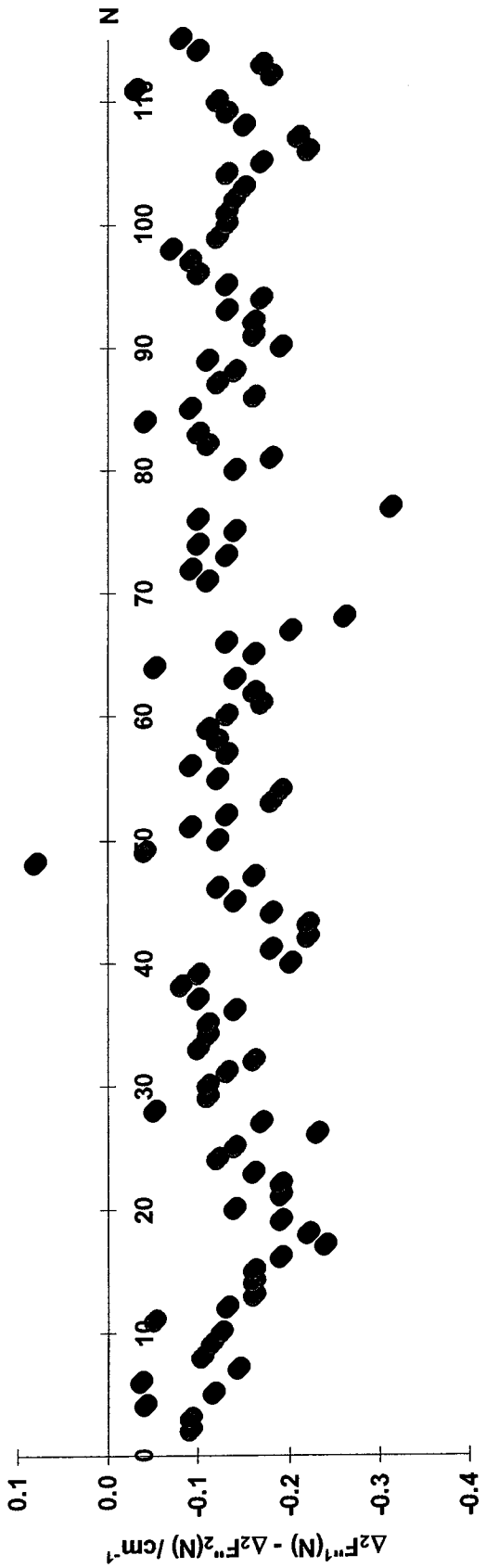

Figure 4.5 Determination of the spin-rotation coupling constant γ for the ground state using combination differences from the $C - X$ (0,0) transition.

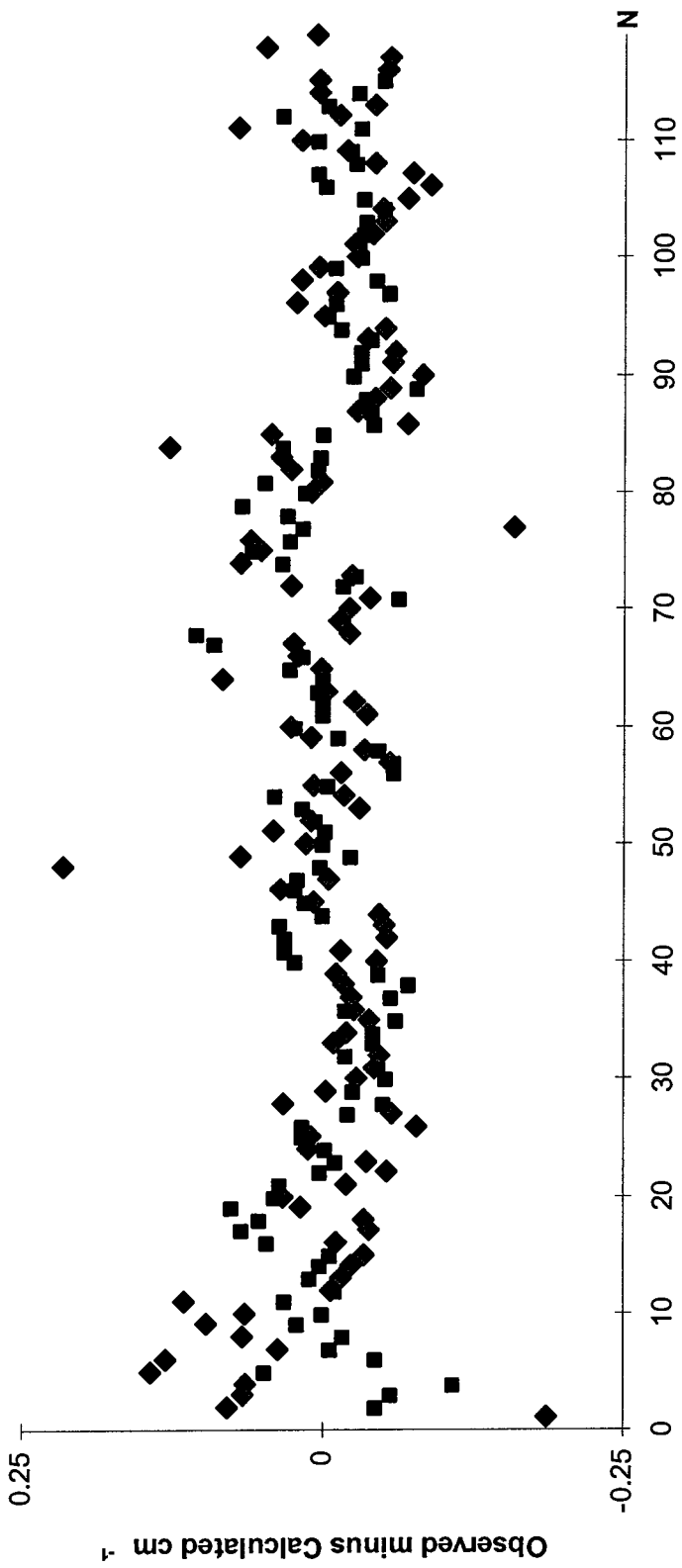

Figure 4.6 Observed minus calculated rotational term values for the ground state of $Rh^{12}C$, using data from the C-X (0,0) transition. The diamonds are the F_1 levels and the squares are the F_2 levels.

4.3 Analysis of the Excited States

Neither the B ($\upsilon = 0$) nor the C ($\upsilon = 0$) plots for B_υ produced the expected straight line plots for the determination of B_0 and D_0. However, Lagerqvist and Scullman noted that when their respective combination differences were added together and then divided by $8(N + \frac{1}{2})$ a straight line up to a certain N value was produced (figure 4.8), indicating that the two states perturb each other only and are not being perturbed by other states. Around N=100 the F_2 levels and then, slightly later, the F_1 levels of the C states start to fall below their predicted values. This may be due to interactions with higher vibrational levels of the B state.

Values for the spin-rotation constant γ for the upper states could only be approximated since the results of plotting equation [59] did not give the expected straight lines for any of the vibrational levels of the C or B state. Figure 4.7 is a prime example.

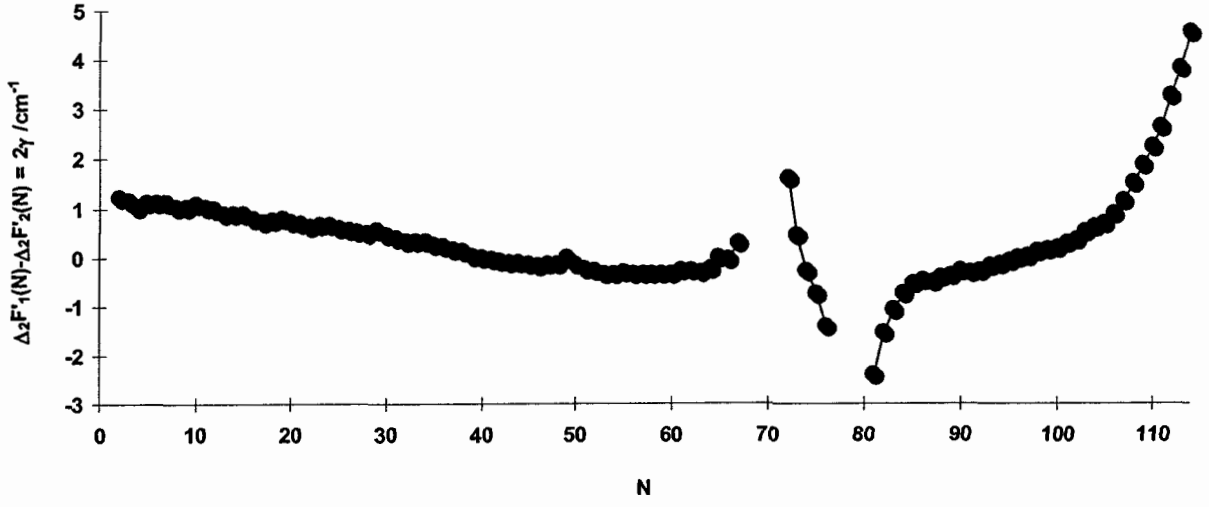

Figure 4.7 Determination of γ for the $\upsilon = 0$ level of the $C^2\Sigma^+$ state. The result is supposed to produce a horizontal line of height 2γ.

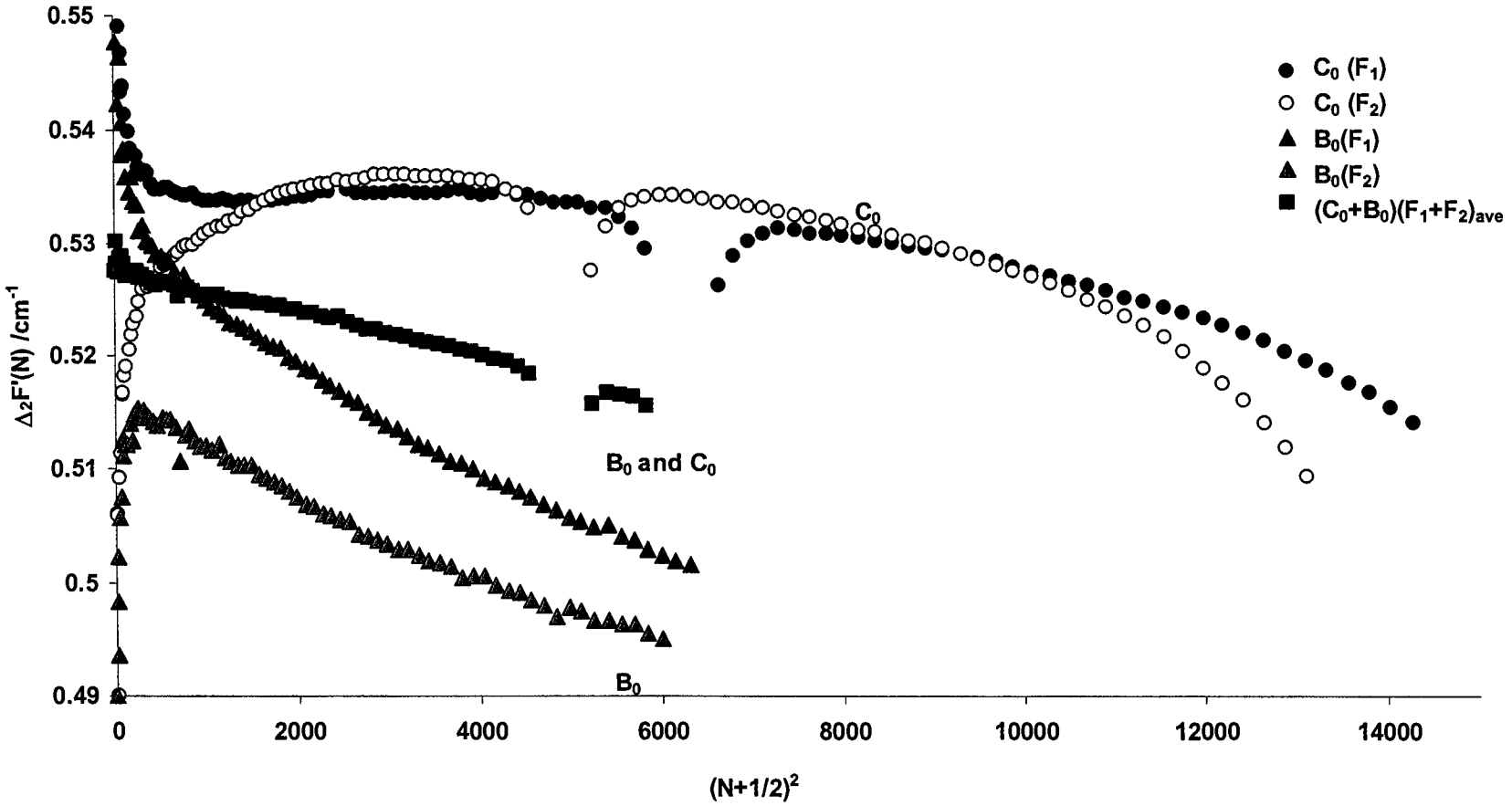

Figure 4.8 Determination of B_0 and D_0 for the B and C states of RhC using the traditional graphing techniques. The two vibrational levels appear to be interacting only with each other as evidenced by the relatively well behaved line produced by the average of their combination differences.

4.4 New Bands Discovered

An *ab initio* calculation (22) published during the reinvestigation of RhC predicted a $^2\Pi$ state and not a $^2\Sigma$ state in the immediate vicinity of the $C^2\Sigma^+$ state. This, along with the anomalies of the analysis mentioned previously, led to a closer look at the LIF spectra. The B – X system was suspected of being $^2\Pi_{1/2}$ - $X^2\Sigma^+$ in character and not the original $^2\Sigma^+$- $^2\Sigma^+$assignment. Dispersed fluorescence spectra and lifetimes were recorded for all of the bands observed by Lagerqvist and Scullman (table 4.3). The upper vibrational levels of the C state had much shorter lifetimes than the $\upsilon = 0$ level, and the $\upsilon = 0$ lifetime of the B state was even longer. Considering that these two states are heavily mixed, this indicated that the B - X system is associated with small oscillator strength and that the B state has a much longer radiative lifetime. This prompted the use of a time-delay in the data collection to find weak transitions to several more vibrational levels of the B state that were hidden under the strong signals of the C – X system. Very weak bands belonging to what appeared to be a $^2\Pi_{3/2}$ - $X^2\Sigma^+$ system (see figure 4.9) were also observed, and confirmed during the rotational analysis.

In all, 36 bands were recorded between 400-530 nm, all shaded to the red (table 4.2). The $Rh^{13}C$ spectra were also recorded, and three (0,0) bands were identified (centered at 465.9, 469.6 and 477.3 nm). Besides the three electronic transition systems for rhodium carbide, bands belonging to RhN, C_2 and C_3 were weakly present in the spectra. In a neon matrix, the C-X (and B-X) bands are about 350 cm^{-1} higher in energy than the gas phase counterparts. All of the additional features reported by Brom, Graham and Weltner (20) may be identified as $^2\Pi_i - X^2\Sigma^+$ transitions, with the exception of their band at 448.7 nm which has no LIF counterpart.

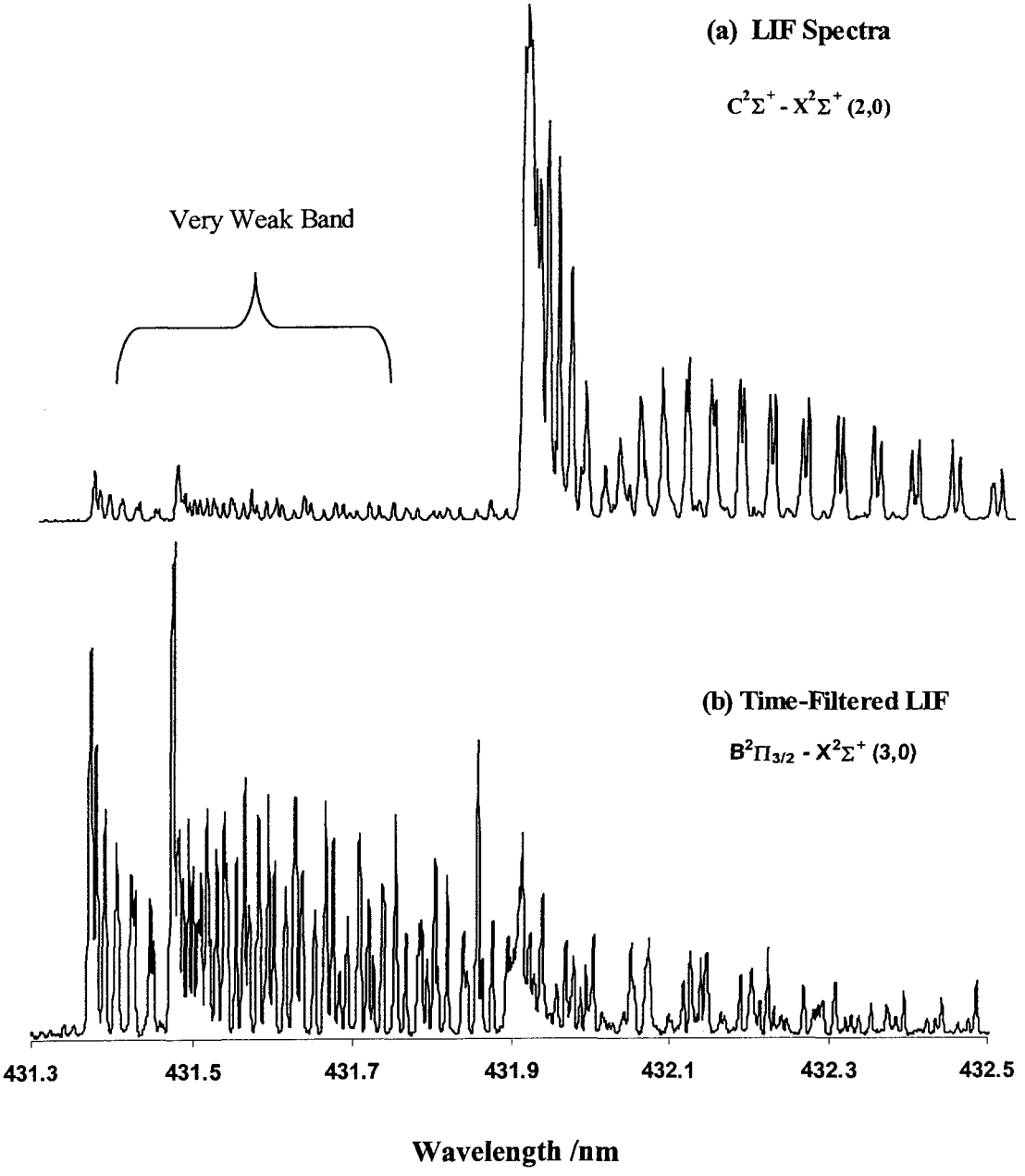

Figure 4.9 RhC spectra recorded using different time windows. Spectrum (a) was collected using $0 \leq t \leq 50$ ns and is dominated by the $C^2\Sigma^+ - X^2\Sigma^+$ (2,0) transition with band head at ~431.9 nm. The weak band to shorter wavelengths belongs to the $B^2\Pi_{3/2} - X^2\Sigma^+$ (3,0) transition. Spectrum (b) was collected using $100 \leq t \leq 800$ ns effectively eliminating the $C - X$ signal. The spectrum in figure 4.11 has only four branches looking like a $^2\Sigma^+ - ^2\Sigma^+$ transition.

Table 4.2 Band heads[a] in the 400 – 500 nm region for $Rh^{12}C$ and $Rh^{13}C$.

$Rh^{12}C$			$Rh^{13}C$		
λ /nm	ν_{vac} /cm^{-1}	Assignment	λ /nm	ν_{vac} /cm^{-1}	$\Delta\upsilon$ /cm^{-1}
528.92	18901	$C^2\Sigma^+$ - X (3,5)	526.32	18995	-94
524.66	19055	$C^2\Sigma^+$ - X (2,4)	522.27	19142	-87
520.63	19202	$C^2\Sigma^+$ - X (1,3)	518.64	19276	-74
520.07	19222	$B^2\Pi_{1/2}$ - X (0,2)	518.12	19295	-73
515.59	19390	$C^2\Sigma^+$ - X (0,2)	513.61	19465	-75
498.24	20065	$C^2\Sigma^+$ - X (2,3)	496.94	20118	-53
494.37[b]	20222	$C^2\Sigma^+$ - X (1,2)	493.32	20265	-43
493.65[b]	20252	$B^2\Pi_{1/2}$ - X (0,1)	492.62	20294	-42
489.58[b]	20420	$C^2\Sigma^+$ - X (0,1)	488.68	20458	-38
478.11[b]	20910	$C^2\Sigma^+$ - X (3,3)			
477.33	20944	$B^2\Pi_{3/2}$ - X (0,0)			
474.50	21069	$B^2\Pi_{1/2}$ - X (1,1)			
474.15	21085	$C^2\Sigma^+$ - X (2,2)			
469.55[b]	21291	$B^2\Pi_{1/2}$ - X (0,0)	469.58	21290	+1
465.87[b]	21459	$C^2\Sigma^+$ - X (0,0)	465.80	21462	+3
460.51	21709	$B^2\Pi_{3/2}$ - X (1,0)	461.03	21684	+25
455.87	21930	$C^2\Sigma^+$ - X (3,2)	456.39	21905	+25
452.34	22107	$B^2\Pi_{1/2}$ - X (1,0)			
452.08[b]	22114	$C^2\Sigma^+$ - X (2,1)	452.45	22096	+18
448.49[b]	22291	$C^2\Sigma^+$ - X (1,0)	449.04	22263	+28
445.47	22442	$B^2\Pi_{3/2}$ - X (2,0)	446.36	22397	+45
443.49	22542	$B^2\Pi_{1/2}$ - X (3,1)			
439.91	22726	$C^2\Sigma^+$ - X (4,2)			
437.4	22856	$B^2\Pi_{1/2}$ - X (2,0)			
435.44	22959	$C^2\Sigma^+$ - X (3,1)	436.24	22917	+42
431.77[b]	23154	$C^2\Sigma^+$ - X (2,0)	432.73	23103	+51
431.25	23182	$B^2\Pi_{3/2}$ - X (3,0)			
429.71	23265	$B^2\Pi_{1/2}$ - X (4,1)			
425.23	23510	$C^2\Sigma^+$ - X (5,2)			
423.86	23586	$B^2\Pi_{1/2}$ - X (3,0)			
420.80	23758	$C^2\Sigma^+$ - X (4,1)			
418.14	23909	$B^2\Pi_{3/2}$ - X (4,0)			
416.57[b]	23999	$C^2\Sigma^+$ - X (3,0)			
411.32	24305	$B^2\Pi_{1/2}$ - X (4,0)			
407.39	24540	$C^2\Sigma^+$ - X (5,1)			
403.17	24796	$C^2\Sigma^+$ - X (4,0)			

[a] Includes bands observed by Lagerqvist and Scullman
[b] The head to shortest wavelength

The $B^2\Pi_{1/2}$ - $X^2\Sigma^+$ bands have only four instead of the expected six branches. There are two R- and two P- branches evident, however, the two Q-branches are missing due to efficient mixing of the $B^2\Pi_{1/2}$ state with the nearby $C^2\Sigma^+$ state, causing these

bands to appear more like $^2\Sigma - ^2\Sigma$ bands. The $B^2\Pi_{1/2} - X^2\Sigma^+$ (0,0) transition with its missing Q-branches is shown in figure 4.11. The $B^2\Pi_{3/2} - X^2\Sigma^+$ bands, however, have all six of the expected branches (two each of type R-, P- and Q-). The spectrum of the $B^2\Pi_{3/2} - X^2\Sigma^+$ (3,0) transition is shown in figure 4.9 for comparison. The rotational analysis of the new bands proceeded without difficulty (23). The $B^2\Pi$ is inverted, meaning that the $^2\Pi_{3/2}$ spin-orbit component is lower in energy than the $^2\Pi_{1/2}$ spin-orbit component. The spin-orbit coupling constant of the $B^2\Pi_i$ state is $A = -430\,cm^{-1}$, effectively separating the two spin-orbit components into two sub-states (typical of Hund's case (a) coupling). They are, however, collectively labeled as a $B^2\Pi$ state.

The $A^2\Pi$ state was determined by Kaving and Scullman (19) to be regular, with $A = 776\,cm^{-1}$. The A-X band system occurs in the infrared and was not observed in the LIF experiments due to wavelength limitations of the dye laser. Transitions to this state were observed, however, in the dispersed fluorescence experiments .(see figure 4.12) where relaxation of the excited state to many vibrational levels of the ground state as well as transitions to states of appropriate symmetry and within the range of the monochromator may be observed.

The energies of the vibrational levels due to the $^2\Pi_{3/2}$ progression are very close to the vibrational origins of Lagerqvist and Scullman's D state; the fact they do indeed belong to the D state was confirmed during the rotational and de-perturbation analysis. Rh12C transition lines appear in appendix I. Since the LIF spectra have been previously published (9) they have not been reproduced again here. The Stockholm plates were not available to scan and therefore no image of them is available here.

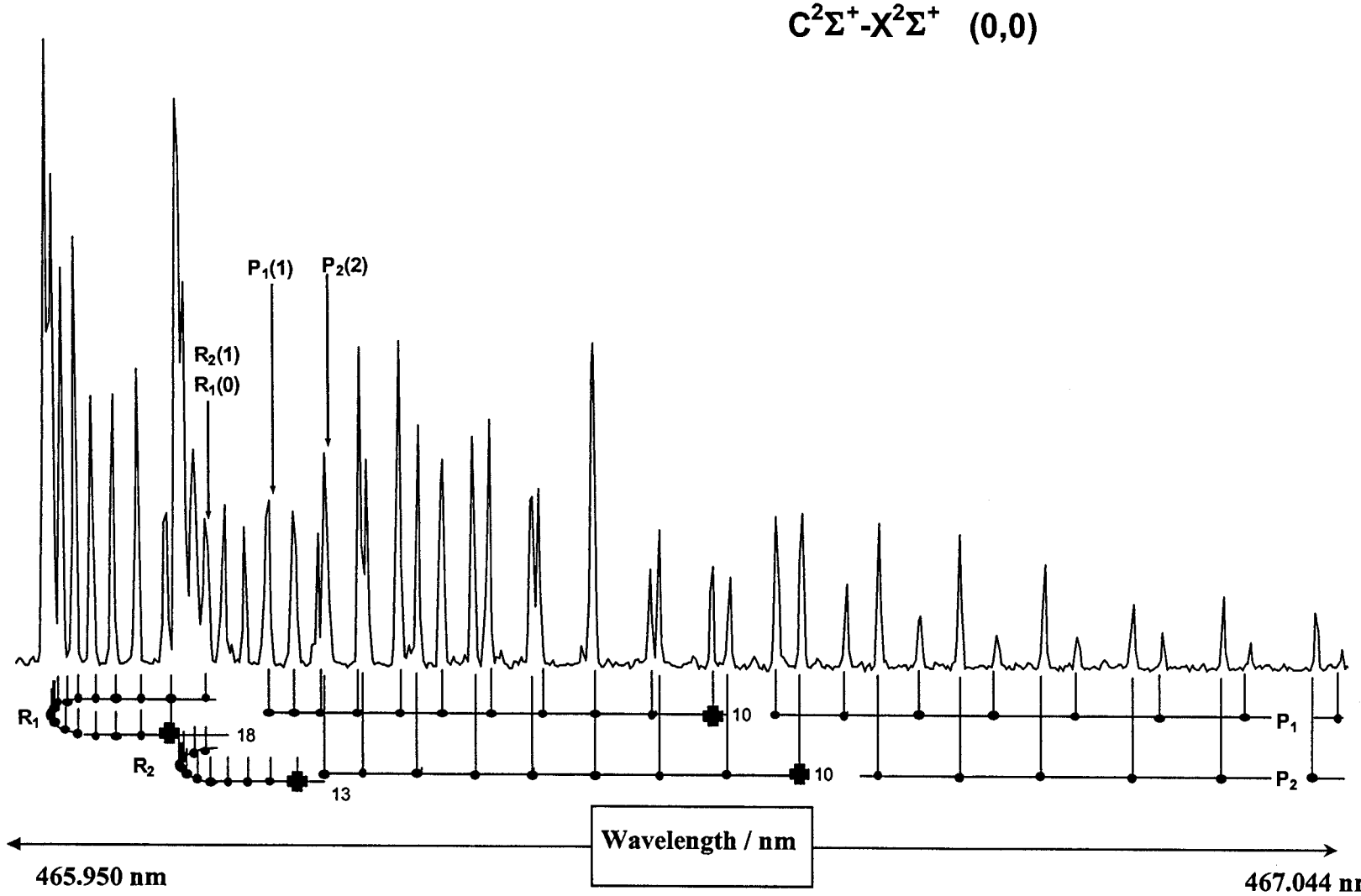

Figure 4.10 Rotational analysis of the $C^2\Sigma^+$ - $X^2\Sigma^+$ (0,0) system centered at 465.87 nm. There are four branches two R- forming heads at high energy and two P- type branches that tail to the red Transition lines are numbered according to N since the ground state is case (b) and shown for the lines marked by a cross in the figure. First lines are indicated with an arrow.

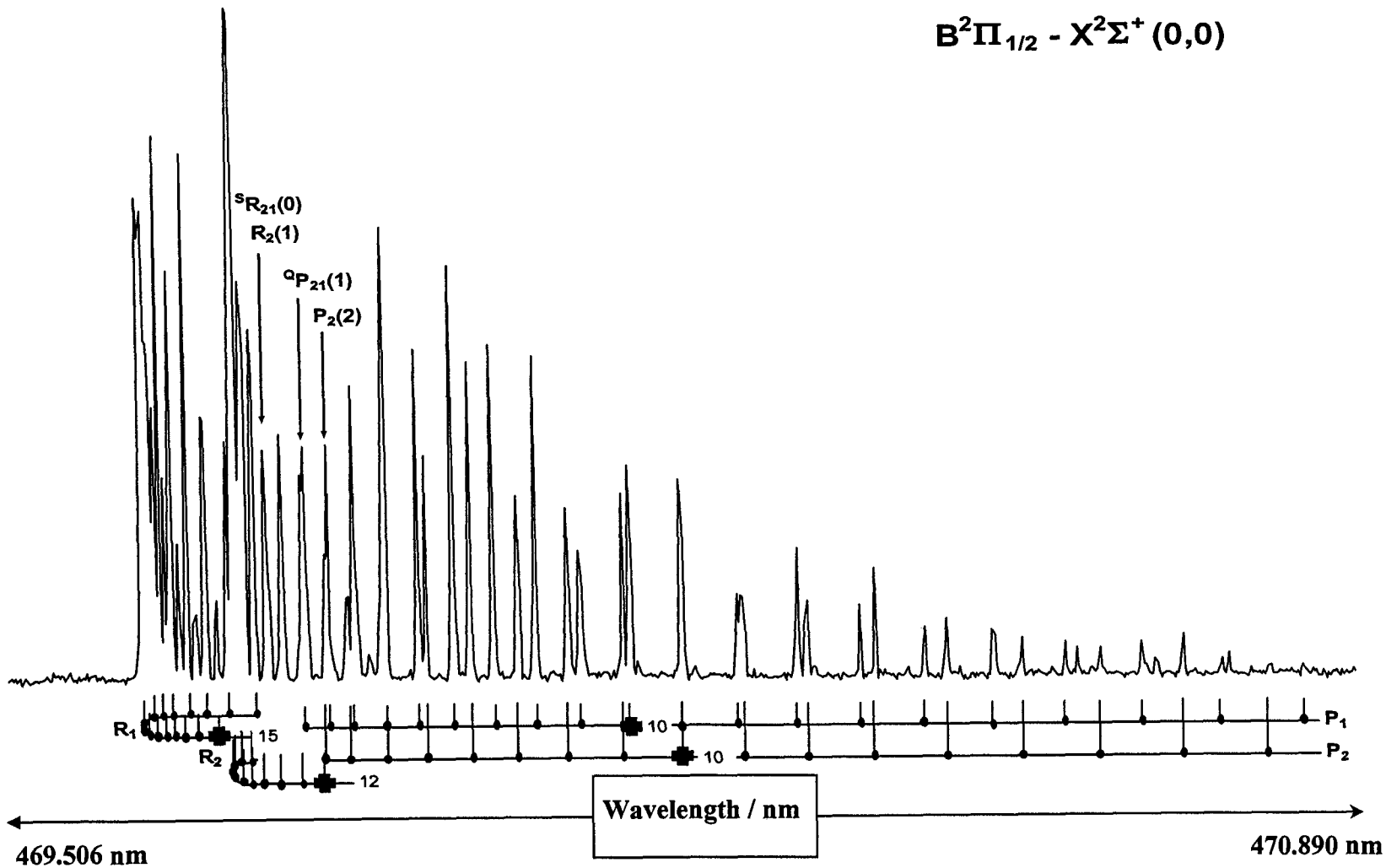

Figure 4.11 Rotational analysis of the $B^2\Pi_{1/2} - X^2\Sigma^+ (0,0)$ system centered at 469.55 nm. The N numbering is indicated by the crosses along the bottom and first lines by arrows at the top.

Table 4.3 Lifetimes for the B and C vibrational levels observed by Lagerqvist and Scullman.

Level	Band measured / nm	Lifetime / ±5 ns
$B^2\Pi_{1/2}$ $\upsilon = 0$	469.55	100
$C^2\Sigma^+$ $\upsilon = 0$	465.87	80
$C^2\Sigma^+$ $\upsilon = 1$	448.49	50
$C^2\Sigma^+$ $\upsilon = 2$	431.77	50
$C^2\Sigma^+$ $\upsilon = 3$	416.57	50

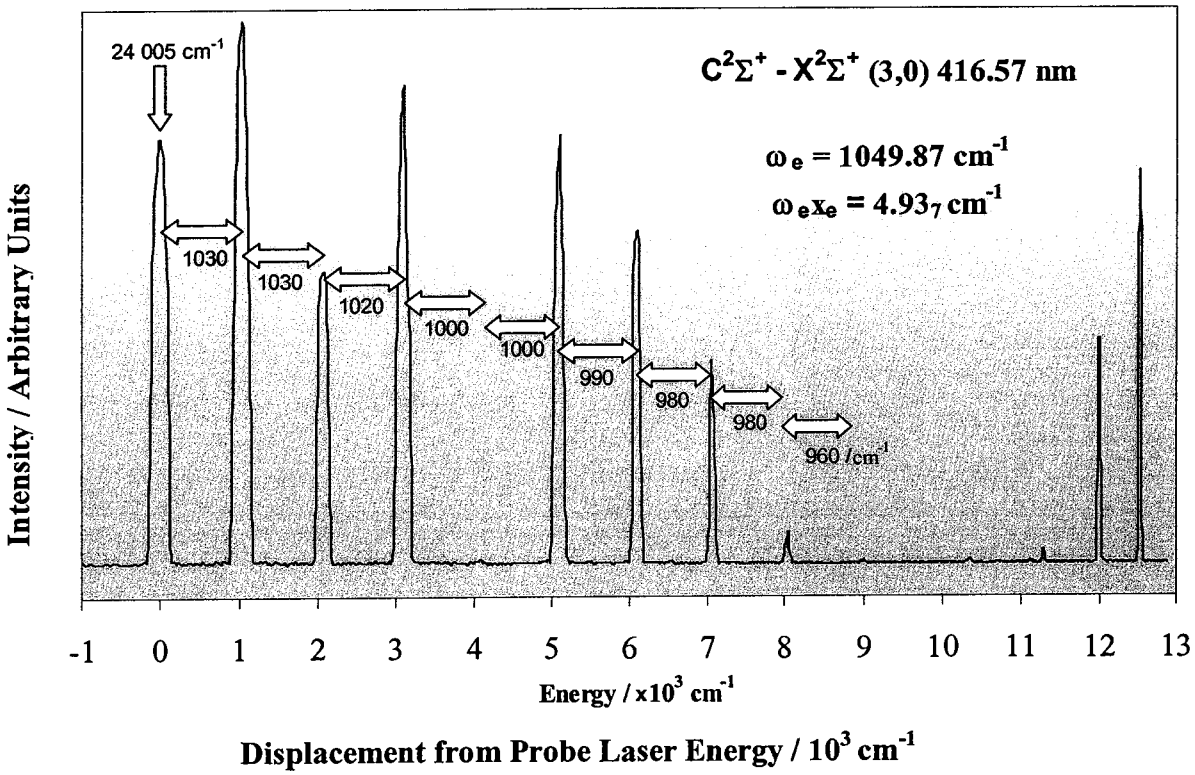

Figure 4.12 Dispersed fluorescence spectrum of the $C^2\Sigma^+ - X^2\Sigma^+$ (3,0) system with the pump laser at 416.57 nm (24 005 cm^{-1}. The ground state vibrational energy level spacing are noted (block arrows in cm^{-1}), and at the far right transitions to the $A^2\Pi_{inv}$ state can be seen.

4.5 Perturbation Analysis

The effects of terms neglected in the molecular Hamiltonian, that couple the zero-order functions associated with different electronic states, are taken into account in a perturbation analysis. These are the off diagonal matrix elements of the rotational Hamiltonian, $\mathbf{H_{ROT}}$, which couple the orbital, spin and total angular momentum.

Perturbations are classified with respect to the quantum number Ω. Homogeneous spin-electron perturbations occur between basis functions of the same Ω and S, but different Λ and/or Σ. In this type of perturbation, the interaction matrix element does not depend on *J*, the rotational quantum number. Heterogeneous perturbations have *J*-dependent interaction matrix elements and obey the selection rule $\Delta\Omega = \pm 1$ (***S***- and ***L***-uncoupling are heterogeneous perturbations).

Perturbations correspond to an interaction between two levels and the selection rules common to all perturbations are

i) $\Delta J = 0$ (the total angular momentum of the molecule remains well defined)

ii) $e \leftrightarrow e, f \leftrightarrow f$ where (e/f) labels refer to rotational eigenfunctions with total parity $(\pm 1)(-1)^J$ for molecules with an even number of electrons and $(\pm 1)(-1)^{J-1/2}$ for molecules with an odd number of electrons (5). The total parity alternates with *N* (or *J*) for Σ (or Π) states whereas the (*e*/*f*) patterns are invariant and thus more convenient as a labeling system (see energy level diagrams in figures 4.2 and 4.3).

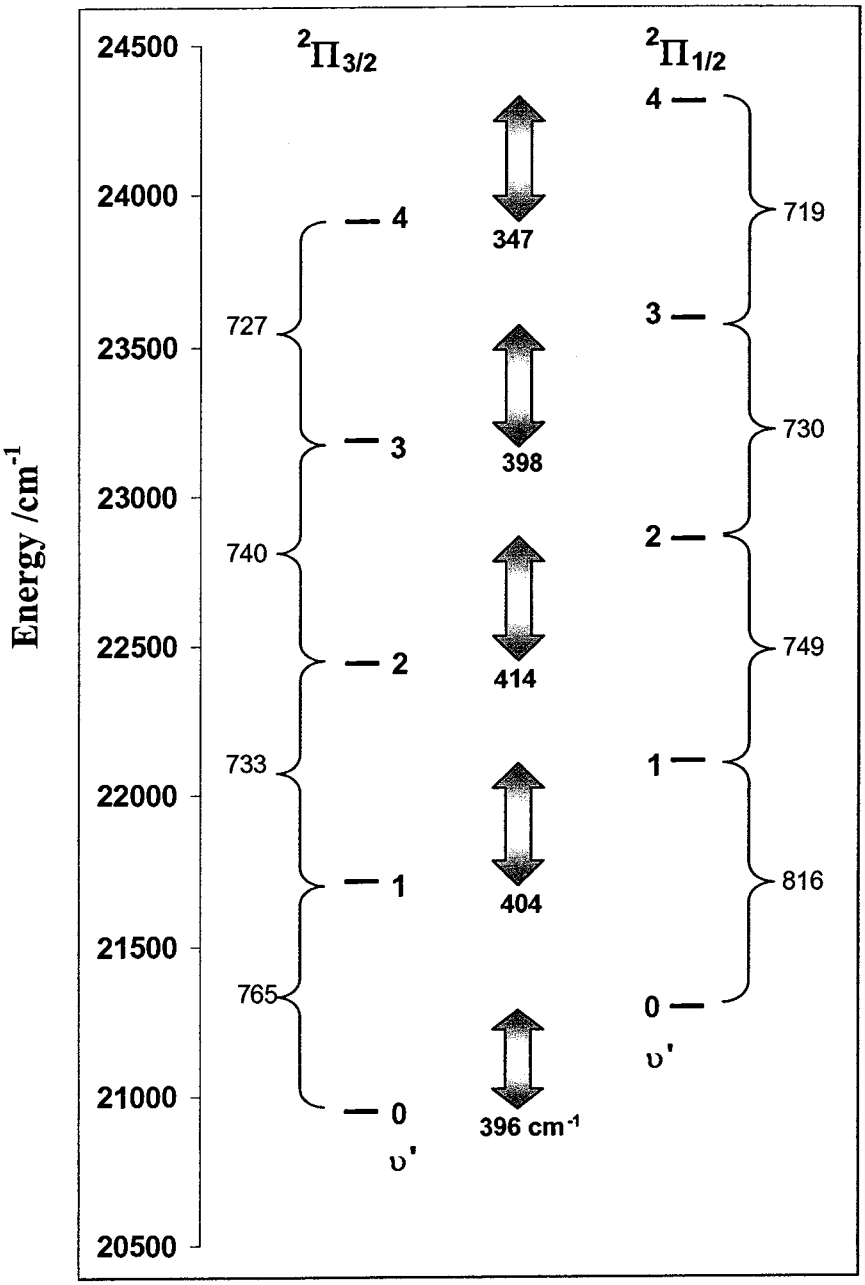

Figure 4.13 Spin-orbit splitting and vibrational spacing in the $B^2\Pi$ state.

The purpose of a perturbation analysis is not to obtain highly precise molecular constants, but to obtain a good fit of the observed spectral lines. The quality of the fit establishes the credibility of the model which includes the mechanism of the perturbation and the values of the perturbation parameters.

In RhC, the $^2\Pi_{1/2}$ and $^2\Pi_{3/2}$ states are perturbed by the $C^2\Sigma^+$ state in different ways. The vibrational band origins can not be fitted to equation [18] nor the rotational constants to equation [55], especially for the $B^2\Pi_{1/2}$ sub-state (figure 4.13). There is also a strong vibrational dependence of the observed Λ-doubling and the calculated lifetimes (24) (see table 4.3). In reality, a vibrational level of the $B^2\Pi_{1/2}$ state is probably mixed with many vibrational levels of the $C^2\Sigma^+$ state, and *vice versa. S*ince, no high *J* data were observed for the $^2\Pi$ bands, recorded using LIF, a complete de-perturbation analysis was not possible.

The perturbation analysis of the $B^2\Pi$ - $C^2\Sigma^+$ interaction was, therefore, divided into two parts, based on the relative strengths of the two types of interactions: the $B^2\Pi_{1/2}$ $(\upsilon = 0)$ - $C^2\Sigma^+$ $(\upsilon = 0)$ homogeneous interaction, which is considerably stronger than the much weaker $^2\Pi_{3/2}$ $(\upsilon = 1)$ - $^2\Sigma^+$ $(\upsilon = 0)$ heterogeneous interaction. This simplified the analysis into four 2x2 matrices, which could be solved algebraically. The diagonal matrix elements of (table 4.4), define the unperturbed E^0 energies of the $^2\Pi_{1/2}$, $^2\Pi_{3/2}$ and $^2\Sigma^+$ states, while, the off-diagonal matrix elements are responsible for mixing the states and are, therefore, responsible for the observed perturbations. The matrix elements of Table 4.4 are essentially those of Table 2.9 of reference (5).

Hund's case (a) was used to define the zero order functions $|nJS\Omega\Lambda\Sigma\rangle$ of the electronic states since the case (a) basis is easier to use; there are no intermediate angular

momenta (N, J_a) and there is a maximum number of molecule fixed z-components $(\Lambda\Sigma\Omega)$ enabling the matrix elements of $\mathbf{H_{SO}}$ and $\mathbf{H_{ROT}}$ to be evaluated using elementary raising and lowering operator techniques. The case (a) rotational energy levels (in units of cm^{-1}) of the 2S+1 Ω multiplet sub-states where $|\Lambda| - S \leq \Omega \leq |\Lambda| + S$ are given by

$$E_{rot}(\upsilon, J) = B_\upsilon[J(J+1) - \Omega^2 + S(S+1) - \Sigma^2] \qquad [60]$$

For this expression to be a good approximation to that of a real molecule, the effect of the **S**-uncoupling operator within the multiplet state, must be much smaller than the energy separation between the multiplet components resulting from the diagonal matrix elements of $\mathbf{H_{SO}}$, the spin-orbit operator. The reasoning for this is that the matrix elements of the ***S***-uncoupling operator

$$B\mathbf{J}\cdot\mathbf{S} = B/2\ [\mathbf{J}^2 + \mathbf{S}^2 - \mathbf{N}^2] \qquad [61]$$

are proportional to *J*, so that at sufficiently high *J*, case (a) ceases to be as good an approximation as case (b). The splitting due to spin-orbit coupling, must be larger than any splitting due to **S**-uncoupling around the *J* levels involved in the perturbation analysis. This is indeed the case for rhodium carbide, where the multiplets of the $B^2\Pi$ state are separated by $A \sim -430\ cm^{-1}$, and any effects due to the **S**-uncoupling operator are not seen below $J = 100$ ($BJ \sim 50\ cm^{-1}$), well within the area of the perturbation analysis. It is necessary to assume the two sub-states $^2\Pi_{1/2}$ and $^2\Pi_{3/2}$ have identical potential curves, and thus have the same vibrational wave functions.

The case (a) expression for the rotational energies of a $^2\Sigma^+$ using state equation [60] corresponds to $\Omega = \Sigma = \pm\frac{1}{2}$ and the following degenerate energy levels result:

$$E_\Sigma(\upsilon, J) = T_\Sigma^\upsilon + B_\upsilon[J(J+1) - \tfrac{1}{2}^2 + \tfrac{1}{2}(\tfrac{1}{2}+1) - \tfrac{1}{2}^2] = T_\Sigma^\upsilon + B_\upsilon(J+\tfrac{1}{2})^2 \qquad [62]$$

The **S**-uncoupling operator completely mixes levels with the same *J*, resulting in *e/f* symmetry components that differ in energy by $\mp B_\upsilon (J + \frac{1}{2})$. Substituting, $N = J \mp \frac{1}{2}$ for the F_1 and F_2 levels respectively, this gives the zero-order case (b) energy levels

$$E(^2\Sigma^+_{e/f}) = T^\Sigma_\upsilon + B[N(N+1)] \qquad [63]$$

The energy levels of [63] are degenerate with the same *N*, but the *e*, (F_1), and *f*, (F_2), levels, of the same *J* level, are separated by 2*B*(*J*+1). Interaction of the $^2\Sigma^+$ state with a $^2\Pi$ state will remove the *e/f* degeneracy of the same *N*, giving rise to spin-rotation splitting in the $^2\Sigma^+$ state. The de-perturbed energy levels actually used in table 4.4, however, incorporate first-order spin-rotation splitting due to $\mathbf{H_{SR}} = \mathbf{N}\cdot\mathbf{S}$, which has only diagonal matrix elements in the case (b) basis, separating the e/f levels by $\gamma\ (N + {}^1/_2)$, or by $\gamma\ (J + {}^1/_2)$, in the case (a) basis. The $^2\Sigma^+$ unperturbed levels written in case (b) basis, corresponding to the case (a) form, found in table 4.4 are

$$T_\Sigma + B_\Sigma N(N+1) - D_\upsilon[N(N+1)]^2 + \tfrac{1}{2}\gamma(N) \text{ for } (e) \text{ levels}$$

$$T_\Sigma + B_\Sigma N(N+1) - D_\upsilon[N(N+1)]^2 \text{ and } -\tfrac{1}{2}\gamma(N+1) \text{ for } (f) \text{ levels} \qquad [64]$$

If the potential curves of the $^2\Sigma^+$ state and the $^2\Pi$ states are identical and the electronic configurations are σ^1 and π^1 then the interaction matrix elements that will mix them can be determined. There are two types of $\Delta\Omega = 0$ interactions and one $\Delta\Omega = +1$ between the $^2\Sigma^+$ and the $^2\Pi_{1/2}$ states;

i) Spin-orbit interaction

$$\left\langle \Lambda = 1, \Sigma = -\tfrac{1}{2}, \Omega = \tfrac{1}{2}, \upsilon_\Pi \middle| \mathbf{H_{SO}} \middle| \Lambda = 0, \Sigma = \tfrac{1}{2}, \Omega = \tfrac{1}{2}, \upsilon_\Sigma \right\rangle = \frac{a^+}{2}\left\langle \upsilon_\Pi \middle| \upsilon_\Sigma \right\rangle \qquad [65]$$

where $a^+ = \left\langle \pi \middle| \hat{a}\, \mathbf{l}^+ \middle| \sigma \right\rangle$ and $\left\langle \upsilon_\Pi \middle| \upsilon_\Sigma \right\rangle = \delta_{\upsilon\Pi,\upsilon\Sigma}$

These interactions account for the rest of the off-diagonal matrix elements in table 4.4. The spin orbit parameter $a^+/2\langle 0|0\rangle = \left\langle {}^2\Pi_{1/2\upsilon=0} \left| (al^+s^-)/2 \right| {}^2\Sigma^+{}_{\upsilon=0} \right\rangle$ for the $^2\Pi_{1/2}$ - $^2\Sigma^+$ interaction is essentially half the energy difference between the two interacting levels (or η =83.3 cm^{-1} from Lagerqvist and Scullman's work).

To eliminate correlations between parameters in the global de-perturbation analysis, combination differences based on the sums of the energies, of the observed *e* and *f* levels of the two states were used, since their difference relates mainly to the unperturbed $^2\Sigma^+$ levels according to.

$$E_{sum}(f) - E_{sum}(e) = E^0\Sigma(f) - E^0\Sigma(e) + E^0\Pi(f) - E^0\Pi(e)$$

$$= (2B_\Sigma - \gamma + p)(J+\tfrac{1}{2}) - 4D_\Sigma (J+\tfrac{1}{2})^3 \qquad [69]$$

The adjustable parameters and results of the least squares fitting procedure of these combination differences (in units of cm^{-1}) are given below in table 4.5. These are the low *J* parameters only ($J \le 40.5$) since the local $^2\Pi_{3/2}$ $(\upsilon+1)$ - $C^2\Sigma^+$ (υ) perturbations occur at $J \ge 50$ and were treated separately. The residuals of 160 rotational levels ($J < 40.5$) were used to determine the parameters with σ = 0.0343 cm^{-1} (see figure 4.15).

Figure 4.14 is a summary of the interacting $B^2\Pi - C^2\Sigma^+$ levels. The homogeneous $^2\Pi_{1/2}$ (υ=0) – $^2\Sigma^+$ (υ=0) interaction is shown with a dark solid arrow. The heterogeneous interactions between the $^2\Pi_{3/2}$ (υ+1) – $^2\Sigma^+$ (υ) levels are indicated by dotted or broken arrows.

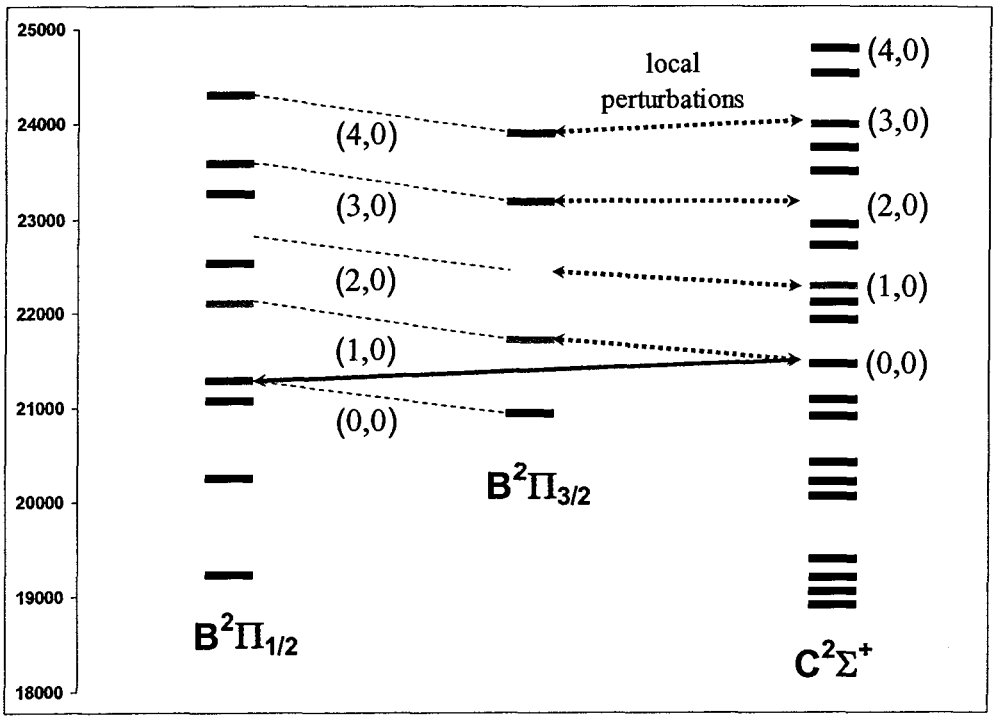

Figure 4.14 Summary of the interacting $B\,^2\Pi - C\,^2\Sigma^+$ levels (units of cm^{-1}).

Table 4.5 Results of the homogeneous $B\,^2\Pi_{1/2} - C\,^2\Sigma^+$ perturbation (units of cm^{-1})

Parameter	Result	Error Bar(σ +25%)
i) B_Σ Rotational constant for $^2\Sigma^+(\upsilon = 0)$	0.54842	0.00006
ii) D_Σ Centrifugal distortion for $^2\Sigma^+(\upsilon = 0)$	9.5×10^{-7}	0.5×10^{-7}
iii) T_Σ Term Value for $^2\Sigma^+(\upsilon = 0)$	21375.70	0.05
iv) B_Π Rotational constant for $^2\Pi_{1/2}(\upsilon = 0)$	0.50632	0.00006
v) D_Π Centrifugal distortion for $^2\Pi_{1/2}(\upsilon = 0)$	8.3×10^{-7}	0.5×10^{-7}
vi) T_Π Term Value for $^2\Pi_{1/2}(\upsilon = 0)$	21360.94	0.05
vii) γ Spin-rotation for $^2\Sigma^+(\upsilon = 0)$	-0.007	0.004
viii) $a^+/2\langle 0|0\rangle + b_1 B_{\upsilon\Pi,\upsilon\Sigma}$	83.32	0.03
ix) $b_2 B_{\upsilon\Pi,\upsilon\Sigma}$	-0.0419	0.0009

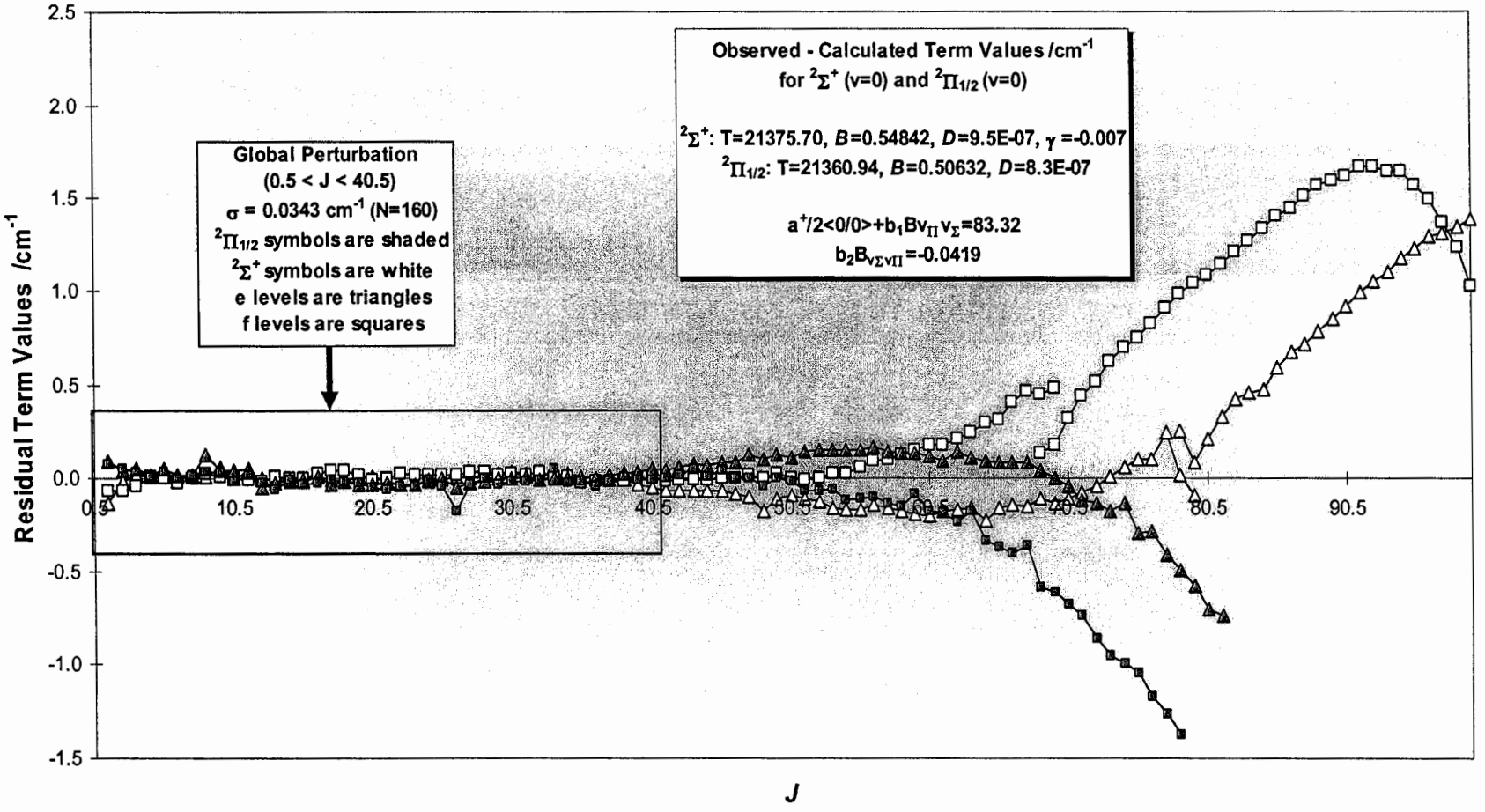

Figure 4.15 Residuals for the (homogeneous) perturbation analysis involving the $B^2\Pi_{1/2}$ ($\upsilon = 0$) and the $C^2\Sigma^+$ ($\upsilon = 0$) states.

The local perturbations for several vibrational levels of the C state were treated next on an individual basis. The rotational constants for the $^2\Sigma^+$ ($\upsilon = 0$) level is different from that obtained previously since only the rotational levels $60.5 < J < 90.5$ were evaluated (table 4.6). It can be seen in figure 4.14 that at very high J the fit deteriorates due to **L**- and **S**- uncoupling which has become comparable to the spin-orbit coupling. The parameters obtained in the fit are only effective parameters, and mixing of the two states with other electronic states (remote perturbers) is expected to influence the results.

Table 4.6 De-perturbed rotational parameters for the $C^2\Sigma^+ = (\upsilon)$ and $B^2\Pi_{3/2}$ $(\upsilon+1)$ levels (in units of cm^{-1})

Parameters for the $C^2\Sigma^+$ state

υ	T_υ	±	B_υ	±	$D_\upsilon(\pm)/\times10^{-7}$	γ	±
0	21375.0	0.1	0.5487	0.0001	9.5 (.6)	-0.065	0.002
1	22284.5	0.1	0.5408	0.0003	8.4 (.8)	0.013	0.003
2	23149.2	0.1	0.5357	0.0001	6.5 (.9)	-0.027	0.006

Parameters for the $B^2\Pi_{3/2}$ state

υ	T_υ	±	B_υ	±	$D_\upsilon(\pm)/\times10^{-7}$	$b_2 B_{\upsilon_\Pi \upsilon_\Sigma}$	±
1	21696.1	0.28	0.4958	0.0001	9.0 (.5)	0.0912	0.002
2	22445.3	0.44	0.4892	0.0002	5.6 (.4)	0.0909	0.003
3	23177.3	0.48	0.4865	0.0006	4.8 (.7)	0.0808	0.008

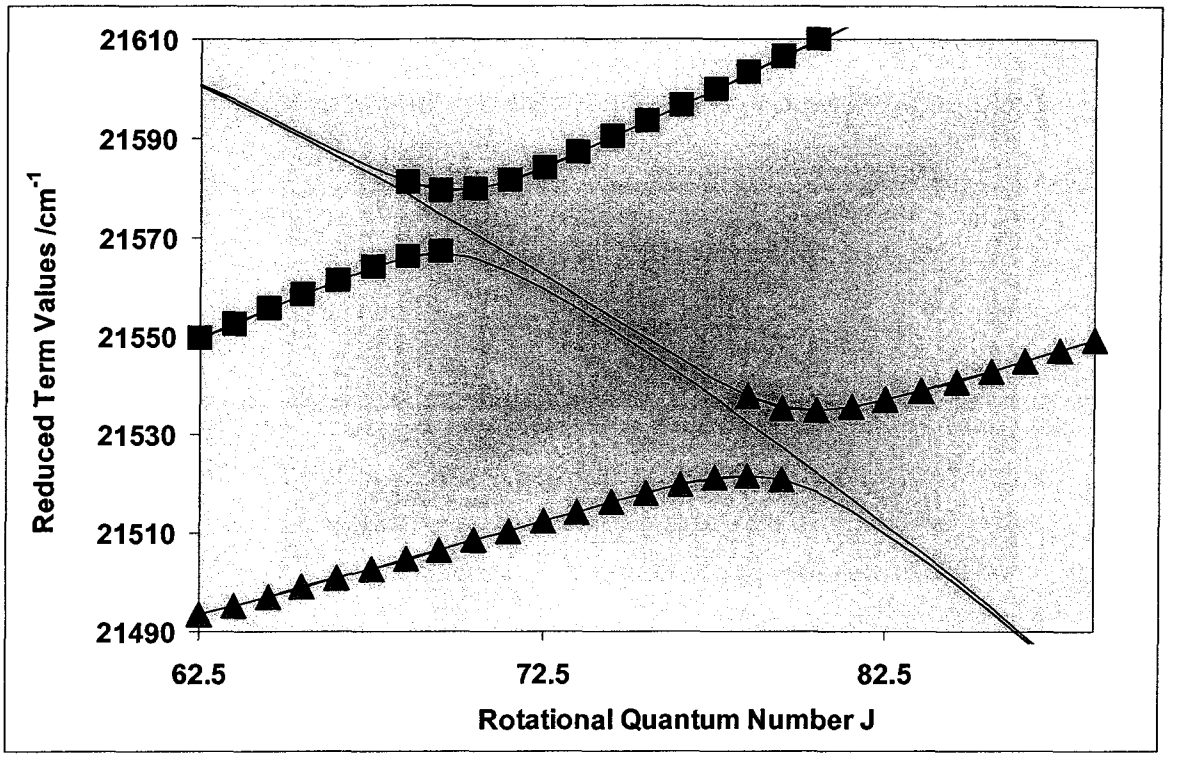

Figure 4.16 Observed (colored markers) and calculated (lines)reduced rotational energy levels for the $^2\Sigma^+$ ($\upsilon = 0$) and $^2\Pi_{3/2}$ ($\upsilon = 1$) states. The e levels are triangles and the f levels are squares. All energies have been reduced by $B_{ave}J(J+1)$ for clarity. Only calculated levels for the $^2\Pi_{3/2}$ state appear in this figure since there are no high J data in the region of the local perturbation due to the rotational coolness of the LIF spectra.

The reduced observed and calculated energy levels of the $C^2\Sigma^+$ ($\upsilon = 0$) state around the area of the perturbation are plotted in figure 4.16. The fit involves only the few J shown ($\sigma = 0.07$ cm^{-1}) and is well within experimental uncertainty, confirming the nature of the pairwise perturbations. The new parameters for the $C^2\Sigma^+$ ($\upsilon = 0$) state affect the previous global de-perturbation as seen by the residuals in figure 4.17 where the parameters have been optimized for the local perturbation. The residuals for the $B^2\Pi_{3/2}$ ($\upsilon = 1$) state are offset by about 5 cm^{-1} due to calibration differences between the LIF and Stockholm spectra and since no $B^2\Pi_{3/2}$ ($\upsilon = 1$) levels were observed in the regions of the

local perturbations only $C^2\Sigma^+$ ($\upsilon = 0$) levels were used for the fitting. The residuals for the $B^2\Pi_{3/2}$ ($\upsilon = 1$) system also reflect the fact that the molecular constants were forced to calculate high J levels at the perturbation location of $J = 68.5$ (f levels) and $J = 78.5$ (e levels) in the $C^2\Sigma^+$ ($\upsilon = 0$) state. Since the residuals for the $B^2\Pi_{12}$ ($\upsilon = 0$) state suffered considerably from this approach, a concerted fitting was done minimizing the residuals for the $C^2\Sigma^+$ ($\upsilon = 0$), $B^2\Pi_{1/2}$ ($\upsilon = 0$) and $B^2\Pi_{3/2}$ ($\upsilon = 1$) levels Spectroscopic constants produced from this effort are listed in table 4.7 with the residuals plotted in figure 4.18.

Table 4.7 Results of the concerted analysis (in units of cm^{-1})

	$B^2\Pi_{1/2}$ (v=0)	$B^2\Pi_{3/2}$ (v=1)	$C^2\Sigma^+$ (v=0)
T=	21362.02	21696.13	21374.65
B=	0.5059	0.4958	0.5487
D /10^{-7}=	8.2	9.0	9.5
p=	-0.007		---
γ=	---	---	-0.013

Interaction Parameters	
$a^+/2<0/0>+b_1Bv_\Pi v_\Sigma$=	83.49
(global) $b_2Bv_\Pi v_\Sigma$=	-0.040
(local) $b_2Bv_\Pi v_\Sigma$=	0.091
T_Σ-$T_{\Pi 1/2}$=	14.76
$[T_{\Sigma+}T_{\Pi 1/2}]/2$=	21368.24

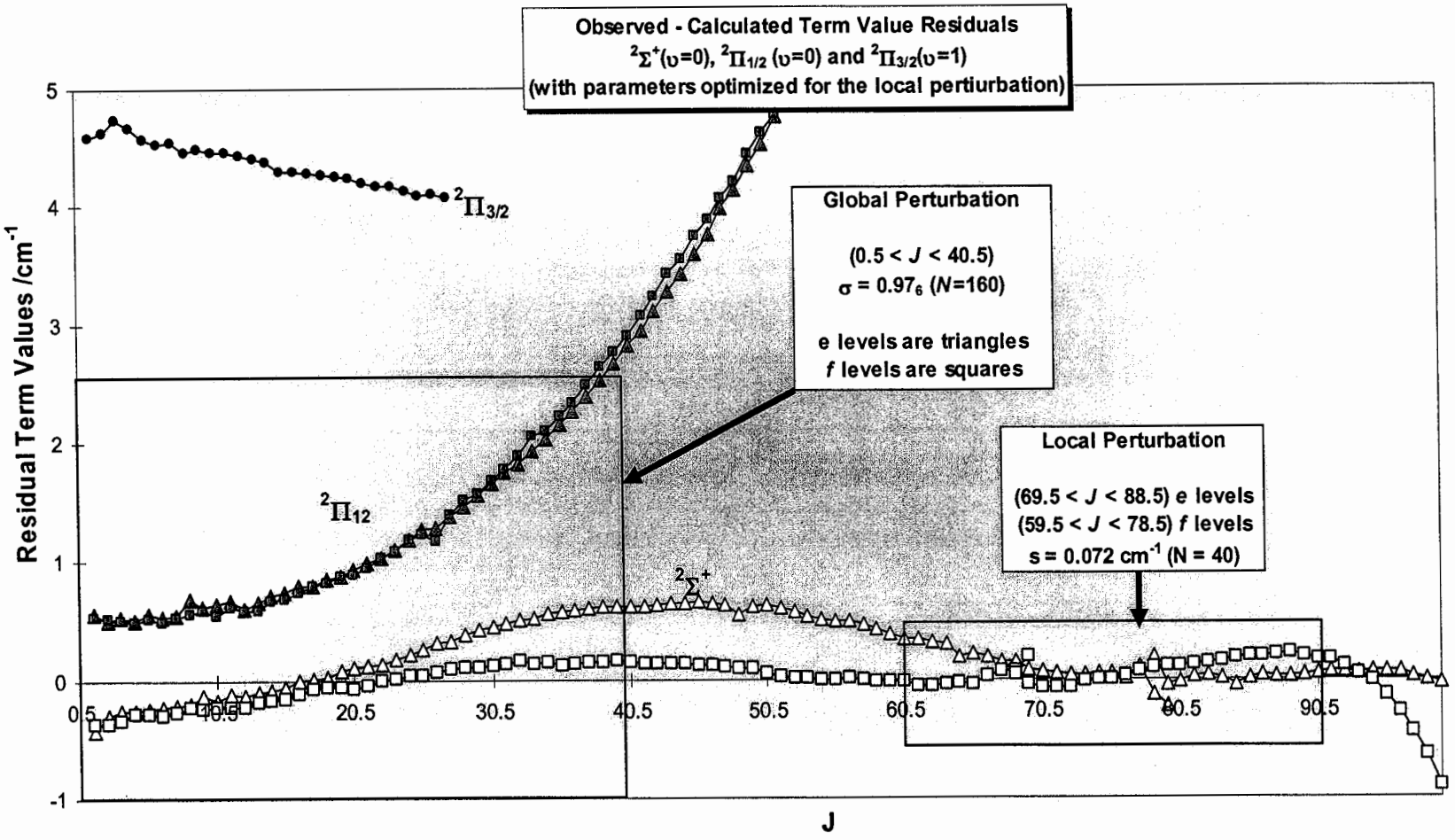

Figure 4.17 Observed minus calculated residuals of the $^2\Pi_{1/2}(\upsilon = 0)$, $^2\Sigma^+(\upsilon = 0)$ and $^2\Pi_{3/2}(\upsilon = 1)$ rotational energy levels.

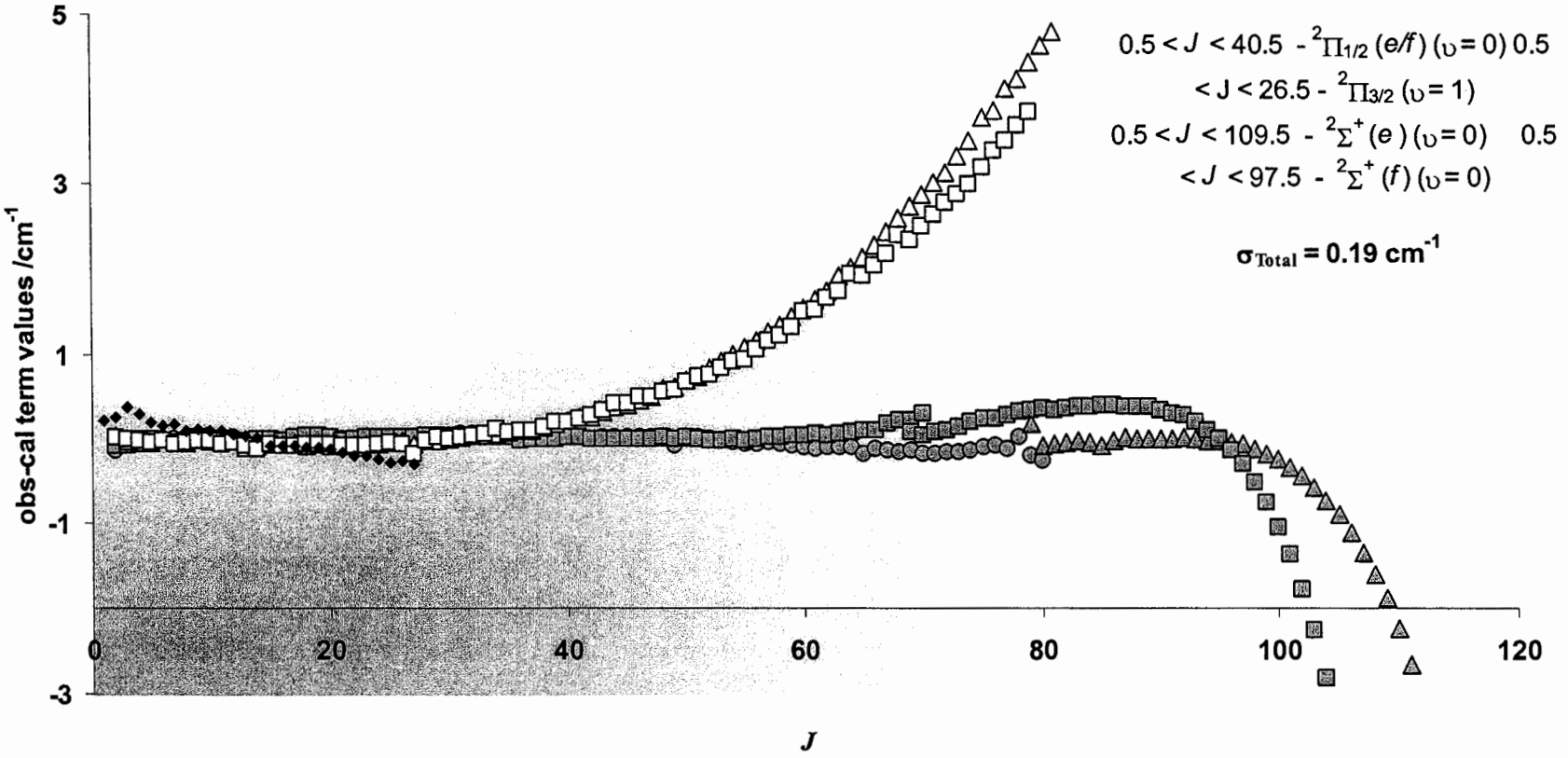

Figure 4.18 Observed minus calculated residuals of the $^2\Pi_{1/2}$ ($\upsilon = 0$) and $^2\Sigma^+$ ($\upsilon = 0$) levels following a concerted analysis. The triangles are e levels, the squares are f levels. The $^2\Pi_{1/2}$ levels are white and the $^2\Sigma^+$ levels are shaded. The $^2\Pi_{3/2}$ ($\upsilon = 1$) residuals are small black diamonds. The energy levels used and standard deviation of the residuals are noted above.

The residuals for $J < 40.5$ of the $B^2\Pi_{1/2}$ ($\upsilon = 0$) energy levels, along with $J < 26.5$ for the $B^2\Pi_{3/2}$ ($\upsilon = 1$) levels and $J < 109.5$ (*e*) and $J < 97.5$ (*f*) for the $C^2\Sigma^+$ ($\upsilon = 0$) levels, were minimized in the final concerted fit shown in figure 4.17, where a total of 228 rotational levels, from all three states were fitted to a standard deviation of 0.014 cm^{-1}, well within experimental uncertainty. The $B^2\Pi_{3/2}$ ($\upsilon = 1$) energy levels have been linearly shifted to match the calibrated spectra of Lagerqvist and Scullman in figure 4.17. However, a noticeable trend in the residuals still occurs since for the $B^2\Pi_{3/2}$ ($\upsilon = 1$) rotational levels. Only values to $J = 26.5$ were observed in the LIF, yet the rotational constants were forced to predict energy levels at the locations of the observed local perturbations in the $C^2\Sigma^+$ ($\upsilon = 0$) state. These were observed at 24 840 cm^{-1} for the $J =$ 78.5 (*e*) levels, and at 24 100 cm^{-1} for the $J = 68.5$ (*f*) levels.

The *B* values for the $B^2\Pi_{1/2}$ ($\upsilon = 0$) and $C^2\Sigma^+$ ($\upsilon = 0$) states, obtained from the concerted analysis, are slightly lower than the values obtained from the global analysis (including Lagerqvist and Scullman's value of 0.5479 cm^{-1} for the $C^2\Sigma^+$ ($\upsilon = 0$) state). There is also a slight increase in the values of the spin-rotation (γ) and Λ-doubling (p) parameters as well (tables 4.5 and 4.7). The rotational constants are expected to change from one focus to another (in terms of the fitting procedure) and all of the constants obtained are still only effective parameters at best.

There are many examples in the literature of interacting $^2\Pi$ and $^2\Sigma^+$ states, including CaH (24) and CN (5, 9, 12). The perturbations in RhC are numerous as well as complex but the observed transition lines have been predicted to within experimental uncertainty. The interactions parameters, used in table 4.4, turned out to be of similar

magnitude explaining why a concerted fitting procedure produced a better fit of the spectroscopic data than treating the perturbations separately.

4.6 Molecular Orbital Considerations

Recent *ab initio* calculations (22) indicate that a high density of $^2\Pi$ and $^2\Sigma$ states exist for RhC; the predicted single electronic configurations of the states observed are

i) $2\delta^4\ 12\sigma^1\ (X^2\Sigma^+)$

ii) $2\delta^4\ 12\sigma^0 6\pi^1\ (A^2\Pi_{regular})$ labeled B in ref (22)

iii) $2\delta^3\ 12\sigma^1\ 6\pi^1\ (B^2\Pi_{inverted})$ labeled D in ref (22)

iv) $2\delta^4\ 12\sigma^0\ 13\sigma^1\ (C^2\Sigma^+)$ labeled E in ref (22)

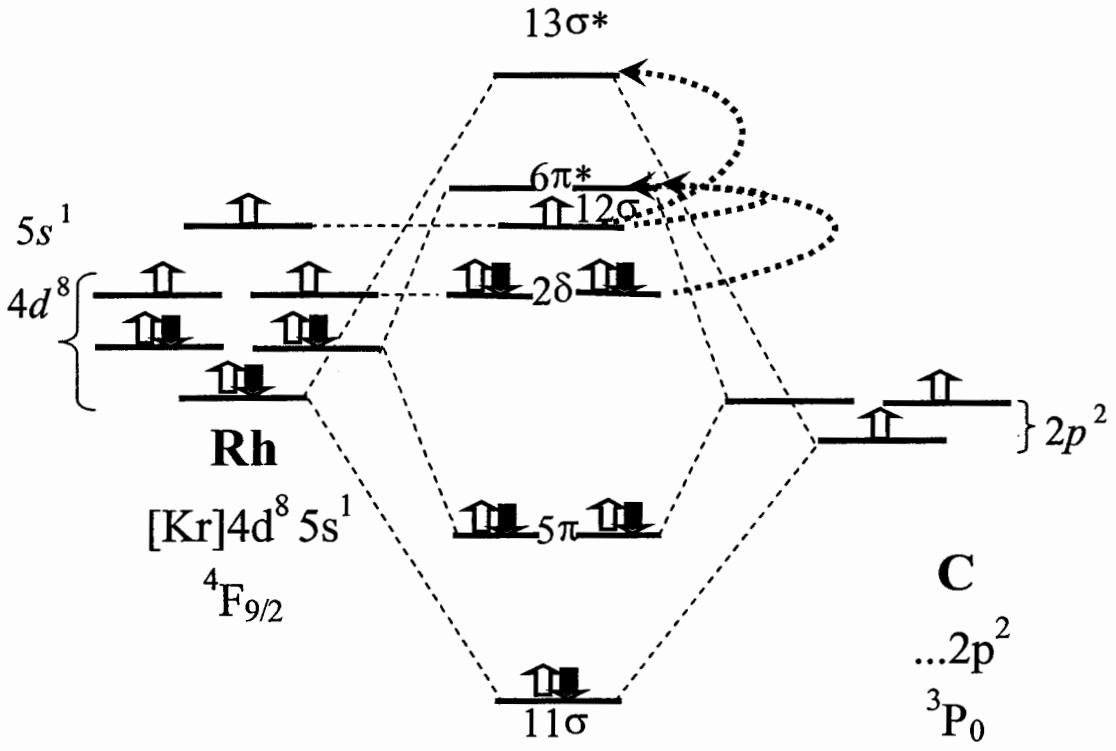

Figure 4.19 Qualitative molecular orbital diagram for RhC constructed using ionization potentials. The one electron transitions responsible for the observed spectra are given by the green, red and blue dotted arrows.

The molecular orbital diagram of figure 4.18 was built using ionization potentials for the atoms. The 5*s* (12σ) and 4*d* (2δ) orbitals are considered to be metal - centered and essentially non-bonding. The relative positions of these orbitals compared to the ligand based 11σ, 13σ, 5π and 6π orbitals change with the different ligand donors, and although the observed transitions are depicted schematically in figure 4.19, the energy of the 6π* and 13σ* orbitals are not known: the energy of an electronic state cannot be related easily to a simple MO diagram.

The spin-orbit splitting of the $A^2\Pi_{reg}$ state obtained by Kaving and Scullman (19) is $A = 775.82$ cm^{-1} implying that the one electron spin-orbit parameter $a_\pi = 775.82$ cm^{-1}. The $B^2\Pi_i$ state on the other hand has 5 valence electrons to consider, requiring a more complex wave function to describe this electronic state. Also, this electronic configuration yields two possible $^2\Pi$ states complicating matters further. The spin-orbit constant for the $A^2\Pi_{reg}$ and $B^2\Pi_i$ states can be related to the one electron parameter via $A = -a_\Pi$ and $A = (a_\pi - 4a_\delta)/3$ where a_δ is calculated to be 1253 cm^{-1}(5). This gives $A = -1412$ cm^{-1} for the $B^2\Pi_i$ state and $A = -776$ cm^{-1} for the $A^2\Pi_{reg}$ state.

The observed spin-orbit splitting of the $B^2\Pi_i$ state is irregular, but approximately 430 cm^{-1} and not close to either of the two limits (-776 and -1412 cm^{-1}). This is an indication that second-order mixing involving remote states must be involved, since there is no direct one-electron spin-orbit matrix element between these two configurations. This is a reasonable assumption since there are many electronic states calculated to be within 10 000 cm^{-1} of the two states (22) and the atomic spin-orbit parameter is large (1253 cm^{-1}). A mixing coefficient of 0.1 expected from perturbation theory would yield the observed a^+ constant (23).

Bonding in the ground state of RhC is just slightly under 3rd order as determined by simple MO diagram of figure 4.18 and also calculated theoretically. The δ electrons are essentially considered to be non-bonding. The bond order decreases in all of the proposed excited states with a corresponding increase in bond length (table 4.8).

Table 4.8 Bond lengths for the observed electronic states of RhC.

State /Configuration		B_0/cm^{-1}	Bond Length /nm
$X^2\Sigma^+$	$2\delta^4\ 12\sigma^1$	0.6007	0.1616
$A^2\Pi_{reg}$	$2\delta^4\ 12\sigma^0 6\pi^1$	0.57024[b]	0.16587
$B^2\Pi_{inv}$	$2\delta^3\ 12\sigma^1\ 6\pi^1$	0.5025[a]	0.1767
$C^2\Sigma^+$	$2\delta^4\ 12\sigma^0\ 13\sigma^1$	0.5479	0.1692

[a] Average value of B_0 from $^2\Pi_{1/2}$ and $^2\Pi_{3/2}$ ($\upsilon = 0$) levels.
[b] Ref (17)

Many transition metal carbides have been spectroscopically analyzed. The ground state bond length (0.1614 nm) of RhC is very similar to CoC (0.1612 nm) and slightly shorter than IrC (0.1683 nm) (11). An increase in the M-C bond length is expected as the metal increases in size going down the periodic table. The bond length of RuC (0.1608 nm) is very similar to RhC, however there is a noticeable increase to PdC (0.1712 nm) (11) explainable by an electron entering the $6\pi^*$ or $13\sigma^*$ orbitals.

The perturbations between the $B^2\Pi$ and $C^2\Sigma^+$ have been accounted for in the de-perturbation analysis but the fit is far from perfect. The de-perturbed term values for the $B^2\Pi_{1/2}$ and $C^2\Sigma^+$ states predict a difference in term values of only ~15 cm^{-1} (figure 4.20).

Heavy mixing of many vibrational levels of the two states with each other (and most probably with other remote perturbers) complicated the de-perturbation analysis beyond further completion.

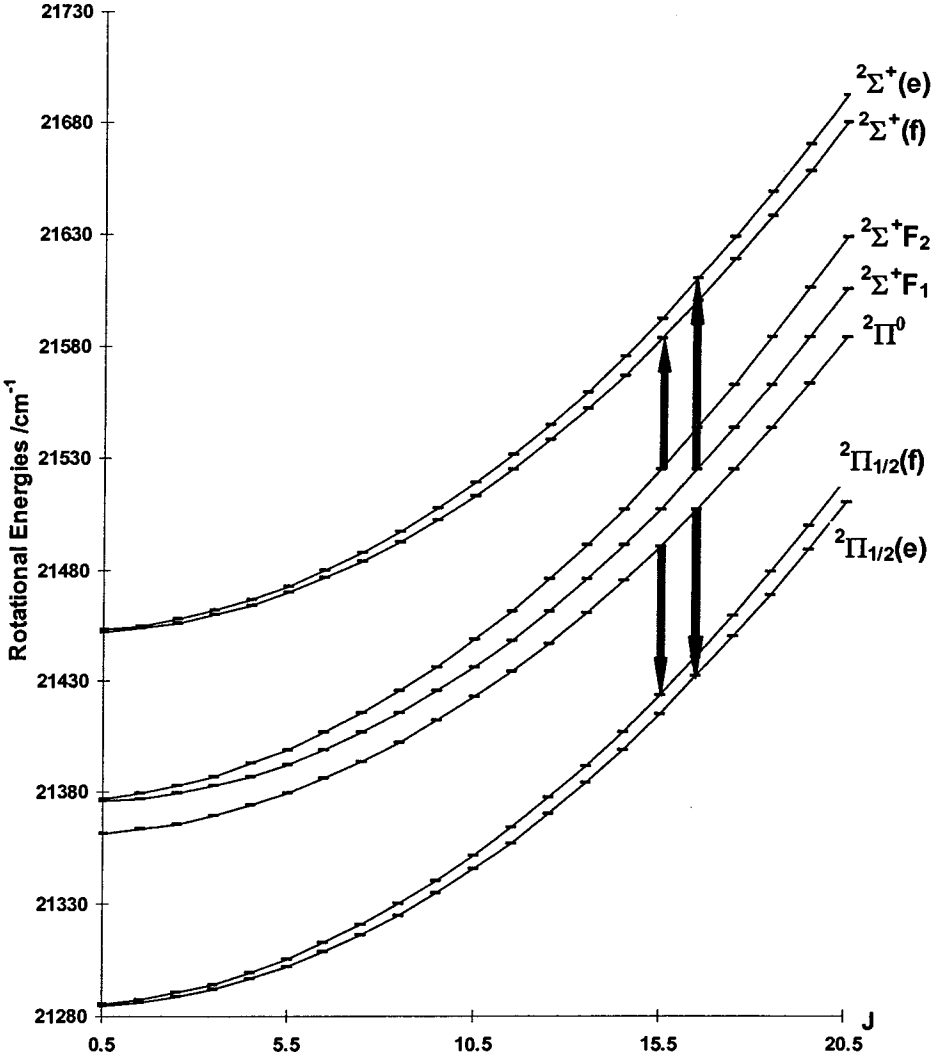

Figure 4.20 Perturbed and unperturbed low J rotational energy levels of the $^2\Sigma^+$ ($\upsilon = 0$) and $^2\Pi_{1/2}$ ($\upsilon = 0$) states. The strength of the perturbation matrix elements is indicated by the green and pink arrows. Note that for the same J, the F_1 levels have been pushed up further than the F_2 levels and their order has been reversed. It can easily be seen in this diagram that this perturbation is independent of J confirming its homogeneous nature. The de-perturbed $^2\Sigma^+$ levels still show signs of first-order spin-rotation effects and are already split into e/f levels by $\gamma(J+^1/_2)$.

Chapter 5

Rotational Analysis of Rhodium Monoxide

5.1 Historical Background and Literature Review

The emission spectrum of rhodium monoxide (RhO) was first observed and recorded in the 1960s in Stockholm, Sweden in the laboratory of Rosemary Scullman using a hollow cathode coated with a rhodium foil bent into a cylinder (13). Although some band heads and rotational structure were evident, the plates were over-crowded with lines and no interpretation of the spectrum was forthcoming. The plates were copied and brought to Victoria in the hopes that one day the data would be profitably revisited. Several sections of the emission spectrum (~16 nm in width) are shown in figure 5.1.

In the meantime, laser technology and molecular beam techniques advanced. LIF spectra of RhO recorded in1995-97 by coworkers and myself, were less congested and a rotational analysis looked much more promising. A small section of the emission spectrum (~50 cm^{-1}) near 618 nm is shown overlaid with the corresponding section of the LIF spectrum in figure 5.2. A number of published studies on RhO, as well as *ab initio* calculations had appeared in the literature by the time our investigation of RhO began.

Raziunas and co-workers reported observing the spectrum of RhO along with other platinum-group monoxides (26). They used ~3g of powdered rhodium metal in a hollow silver anode with a silver rod as a cathode, and a gas mixture of 10-30% by volume O_2 in argon. They reported red-degraded band heads at 17 011, 16 219, 16 199, 16 054, 15 954, 15 690, 15 236 and 15 170 cm^{-1}.

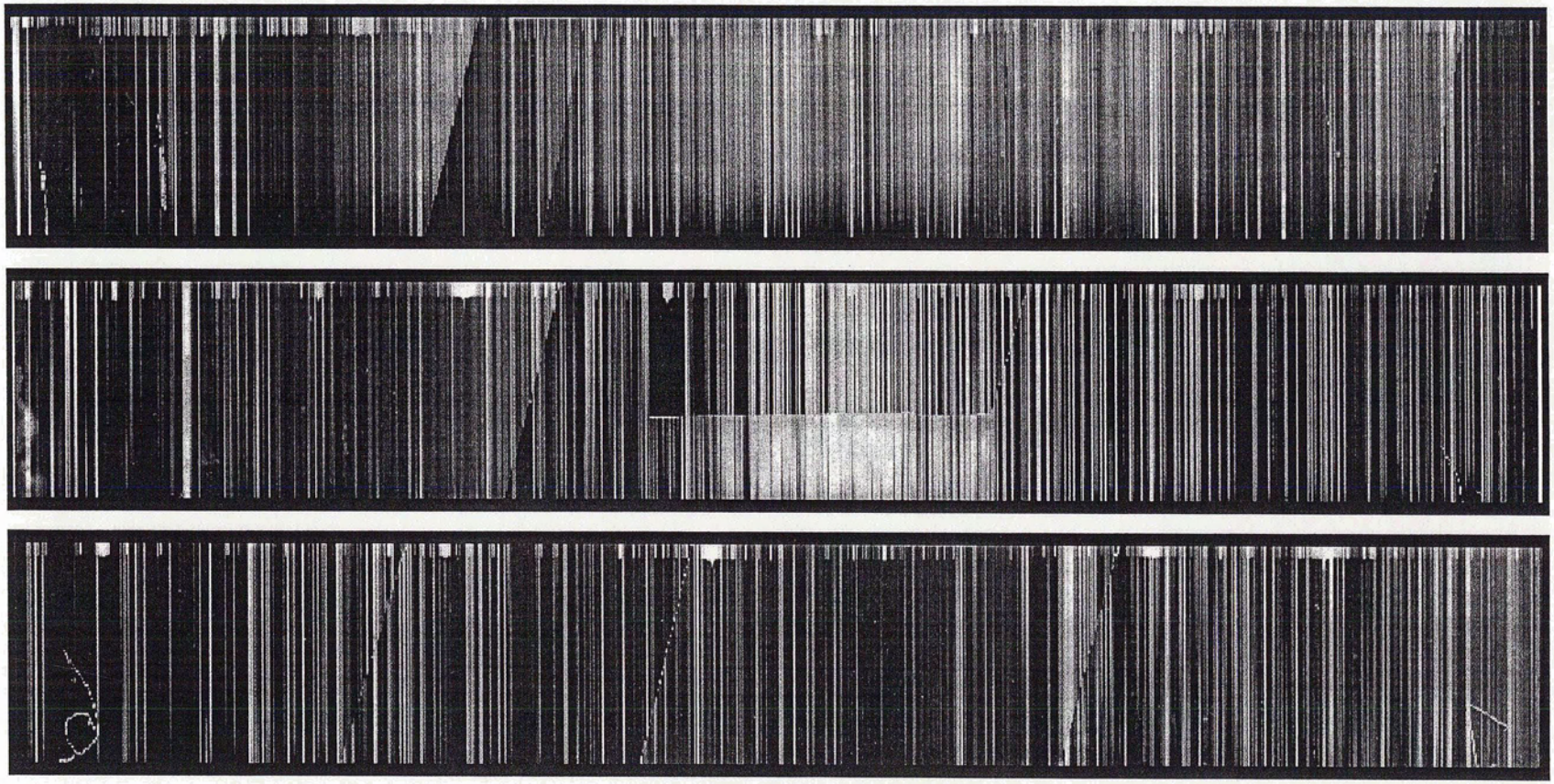

Figure 5.1 Sample of the Stockholm emission plates. Many hundreds of rotational lines appear in each of the segments - too congested for a successful rotational analysis. The emission lines are white in this reproduction. Each line is an image of the slit used to record the spectrum. The short calibration lines seen across the top of each plate, were recorded with a much shorter slit. The top plate covers the range from ~355 - 368 nm, the middle plate covers the range from ~616 - 624 nm and the bottom plate covers the range from ~625 - 642 nm.

Figure 5.2 The LIF spectra of the central region of the band near 618 nm overlaid onto the same region of the emission spectrum (lines are dark). There are still hundreds of rotational lines, many of them unresolved however the band structure is much more discernable and more information was available for an analysis.

Mains and White (26) used Gaussian86 and Gaussian88 to try 24 different basis sets (unsuccessfully) to completely describe the first dozen electronic energy levels of the Rh atom. Their calculations for RhO predicted the ground state to be $^4\Sigma^-$. They also calculated a stretching frequency for the Rh-O bond of 519 cm^{-1} and dissociation energy of 35 580 cm^{-1}.

Siegbahn (27) used different computational methods to investigate 4*d* transition metal oxides and carbenes. His calculations also predicted a $^4\Sigma^-$ electronic ground state for RhO with a bond length of 0.174 nm and dissociation energy 26 700 cm^{-1}.

Thermodynamic data were used by Chen and Armentrout (28) to estimate the RhO dissociation energy D_0 as 33 800 cm^{-1}.

A vibrationally resolved photoelectron spectrum of the RhO^- anion was observed by Li and Wang (29) covering the range to 3.4eV. Since the observed electron affinity for RhO is 1.58eV only electronic states below (3.4 – 1.58eV) or ~14 700 cm^{-1} were observed. The spectrum gave an indication that the neutral species has low-lying states at approximately 1600, 3800, 5700, and 8100 cm^{-1} relative to the ground state, which was assumed by them to be $X^4\Sigma^-_{3/2}$. They assigned these low-lying states respectively to be $X^4\Sigma^-_{1/2}$, $A^2\Sigma^-$, $B^2\Pi_{3/2}$, and $B^2\Pi_{1/2}$ states. The photoelectron spectrum also suggested vibrational frequencies in the $X^4\Sigma^-_{3/2}$ and $B^2\Pi_{3/2}$ states of 730 ± 80 and 800 ± 90 cm^{-1}, respectively. They also observed two weak peaks at 6700 and 9033 cm^{-1} above the ground state which they did not assign.

The infrared spectra of RhO and other $Rh(O_2)_n$ species were reported by Citra and Andrews (30) using laser ablation and FTIR in a solid argon matrix. They found a value of 799.0 cm^{-1} for the vibrational frequency of $Rh^{16}O$ and 759.8 cm^{-1} for $Rh^{18}O$. They also

carried out density functional theory calculations on $Rh^{16}O$ using the Gaussian94 program, which predicted the vibrational frequency to be 838.3 cm^{-1}, and the electronic symmetry of the RhO molecular ground state to be $^4\Sigma^-$ with a bond length of 1.739Å.

To summarize the data available, the ground state of RhO appears to be $^4\Sigma^-$ (three unpaired electrons, no electronic orbital angular momentum $\Lambda = 0$) with a bond length of 0.174 nm, vibrational frequency $\omega_e \cong 800\,cm^{-1}$ and dissociation energy $D_0 \cong 30\ 000\,cm^{-1}$.

Only two types of transitions are expected from the ground state according to the selection rules $\Delta\Lambda = 0, \pm 1$ and $\Delta S = 0$: $^4\Sigma - {}^4\Sigma$ and $^4\Pi - {}^4\Sigma$. Since these are high multiplicity transitions we can expect the spectra to be complex with many branches (some weak and some strong). A $^4\Sigma - {}^4\Sigma$ transition would be expected to be extremely dense (18 branches) with only one 0,0 band since the two $^4\Sigma$ states would essentially follow case (b) coupling (15). A transition to a $^4\Pi$ case (a) state, with a relatively large spin-orbit parameter, would appear as a set of four sub-bands each containing 12 branches (48 in all) and four 0,0 bands would be observed in the spectra.

5.2 Appearance of the Spectra

The hollow cathode emission plate data were never published. The density of lines is such that there was no way to tell from the plates what type (or how many) transitions had been recorded (see figure 5.1). Hundreds and hundreds of lines appear with many of these lines overlapped. Several band heads and some rotational branch structure are obvious but the bands themselves are severely overlapped and no vibrational structure could be discerned.

$...\pi^2\ \sigma^1$

$s_1 = s_2 = s_3 = {}^1/_2,\ m_s = \pm{}^1/_2$

$l_1 = 1,\ m_l = 1, 0, -1$

$l_2 = 1,\ m_l = 1, 0, -1$

$l_3 = 0,\ m_l = 0$

$\Sigma = M_S = \pm{}^3/_2, \pm{}^1/_2$

$\Lambda = M_L = 2, 0, -2$

$^2\Delta,\ ^4\Sigma^-,\ ^2\Sigma^-,\ ^2\Sigma^+$

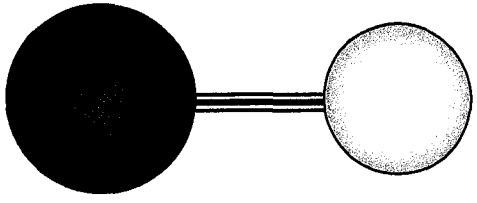

$^4\Sigma^-$

$M_S = \pm{}^3/_2, \pm{}^1/_2$

$M_L = 0$

Figure 5.3 Determination of the term symbol for the ground state of RhO from the $...\pi^2\ \sigma^1$ valence electrons determined by a simple molecular orbital diagram. The Pauli Principle together with Hund's Rule predicts the $^4\Sigma^-$ to be the ground state where the orbital angular momenta of the two π electrons are ±1; therefore they cancel each other as denoted by the opposing arrows.

In the less congested low energy region of the spectrum, some bands could be discerned centered near 638, 630, 626 and 618 nm. These bands were measured using the Fe/Ne reference lines recorded adjacent to the molecular spectrum. Figure 5.2 shows a small ~50 cm^{-1} section of the dense central region of the 618 nm band where several band heads are obvious. Although several branches could be picked out it was generally not possible to follow a branch unambiguously from the periphery in towards the dense central region, where line congestion and overlapping were severe. Line widths of approximately 0.04 to 0.09 cm^{-1} were estimated using lines which appeared to be completely resolved (not overlapped) and showed moderate intensity

Jet cooled spectra of $Rh^{16}O$, with resolution similar to the spectroscopic plates, were recorded between 700 and 380 nm, over several years, at first by coworkers and then later by me. The best spectrum of each of the bands analyzed appears in appendix III. In contrast to the emission plates the LIF spectra are rotationally much cooler and individual rotational-vibrational bands were readily discerned. Optogalvanic signals generated by a Fe/Ne hollow cathode were used to verify band positions to within 0.01nm. The energy region from 550 to 380 nm is very dense, containing at least 25 bands, many of them overlapped. Between 550 and 640 nm 14 red degraded bands were well resolved however, no vibrational patterns were obvious. Each band spans ~ 2 nm in width and contains at least 150 or more rotational lines. Intensity profiles and branch structures of individual bands show several strong red-degraded band heads plus an intense unresolved Q-type structure in the central region. Many branches appear to low energy of the central region with some strong structural features evident at the band periphery. The band centers were still congested with many unresolved rotational lines.

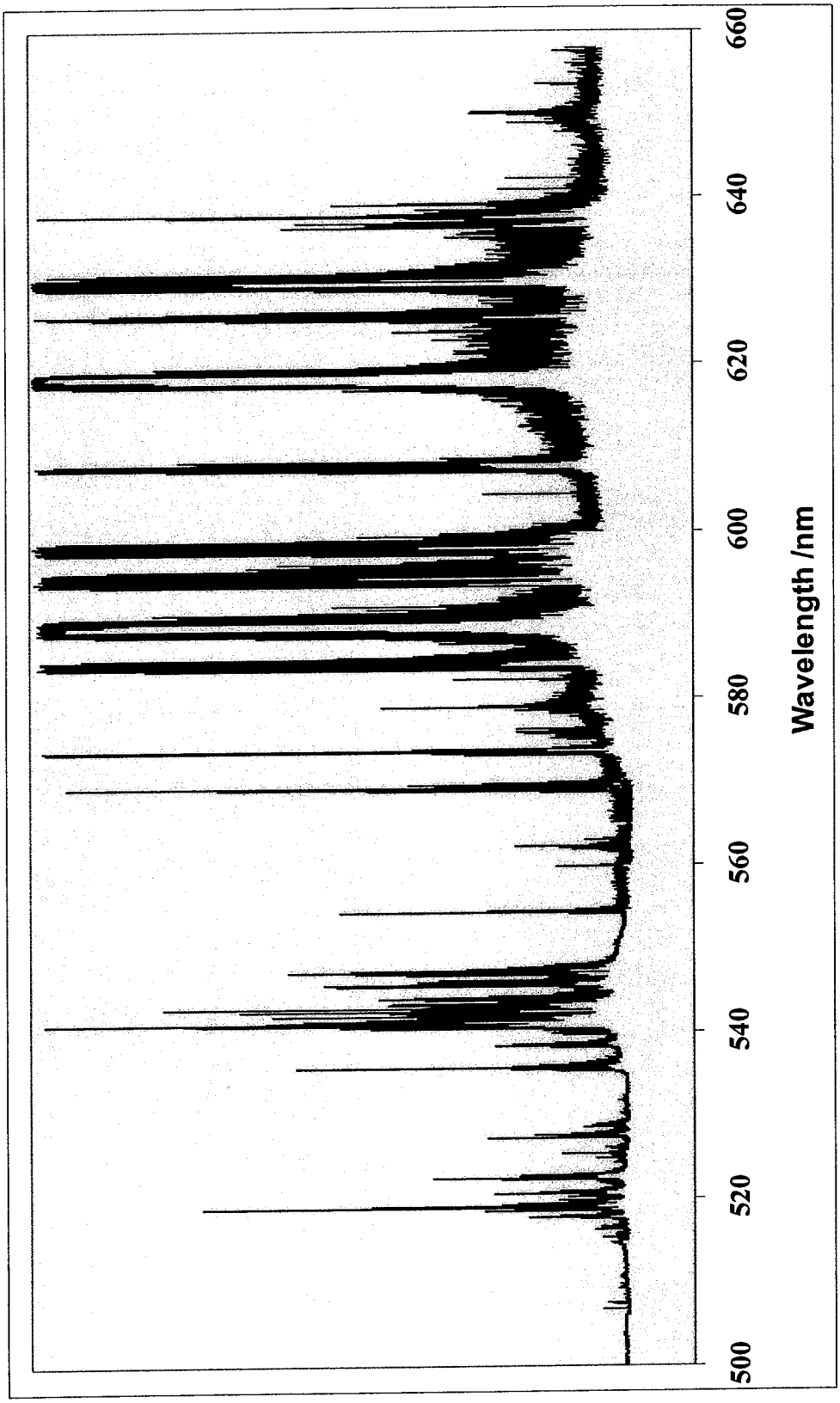

Figure 5.4 LIF spectrum between 500 and 660 nm. There are ~30 bands however the vibrational patterns are still not immediately obvious. The wavelength scale is given in nm, and the intensity is in arbitrary units.

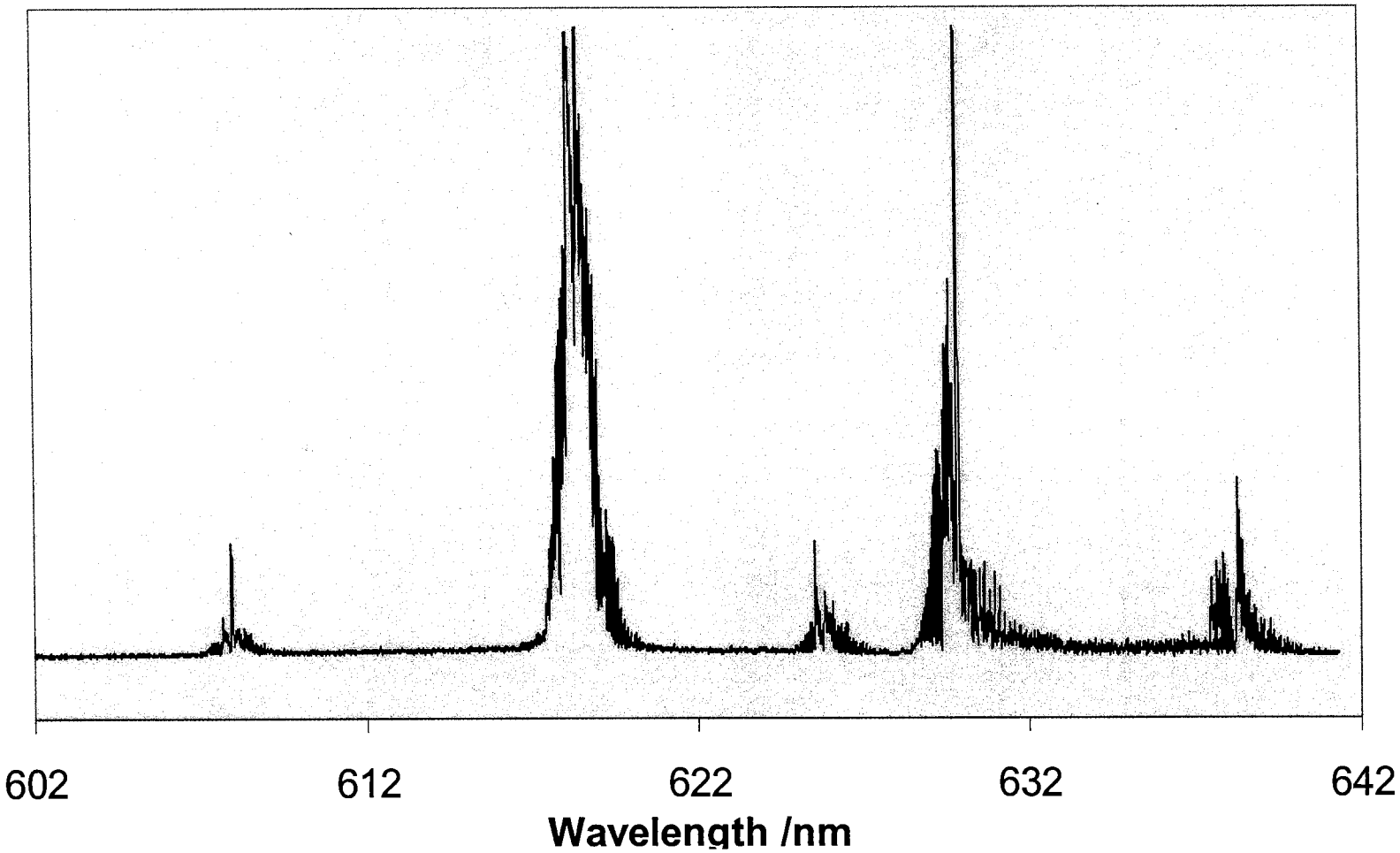

Figure 5.5 Close up of the LIF spectrum between 602 and 642 nm. The $Rh^{18}O$ spectra indicate that the bands centered at 618.3, 625.7, 629.9 and 638.2 nm are 0,0 bands. The weak band at 607.9 nm belongs to a 1,0 transition. The intensity alternation (arbitrary units) between the four 0,0 bands is obvious in this diagram.

There are several features of the LIF spectra, which are irregular, in addition to the lack of obvious vibrational structure. The bands at 629.9 and 618.3 nm are more intense (figure 5.5) and have a much longer radiative lifetime than the bands at 638.2 and 625.7 nm. Dispersed fluorescence spectra were obtained for all of the resolved bands in the $Rh^{16}O$ spectrum, for the purpose of a ground state vibrational analysis. Decay curves were recorded for excited state lifetime determinations. $^{18}O_2$ was used to record $Rh^{18}O$ spectra (these appear in appendix III), confirming the carrier of the initial spectrum to be $Rh^{16}O$ and the presence of four 0,0 bands (minimal isotope shift), as expected for a $^4\Pi - ^4\Sigma$ transition. Since the supply of $^{18}O_2$ was limited, many of these scans were done at low resolution (a rotational analysis of $Rh^{18}O$ was not a high priority). These spectra are much noisier than the $Rh^{16}O$ spectra nevertheless a few of the bands have been rotationally analyzed for completeness.

In a few cases a branch in the LIF data could be matched to an observable branch in the Stockholm emission plates, and the LIF data extended. This "splicing" procedure was only possible for some of the more obvious branches in the emission plates, due to the fact, that there are many more lines on the emission plates than in the LIF spectra and line intensities do not correlate well between the data sets. Figure 5.7, shows two high energy band heads, centered at 15 916 cm^{-1} and 15 877 cm^{-1}. The returning branch from the very strong head on the far left, is only visible on the emission plate, and some lines that are prominent in the LIF spectrum, are barely visible on the emission plate. The LIF were recorded under jet-cooled conditions, whereas the emission spectra were recorded using a hollow cathode; this, coupled with the fact, that the LIF spectra are not well calibrated proved matching the spectra, more difficult than anticipated.

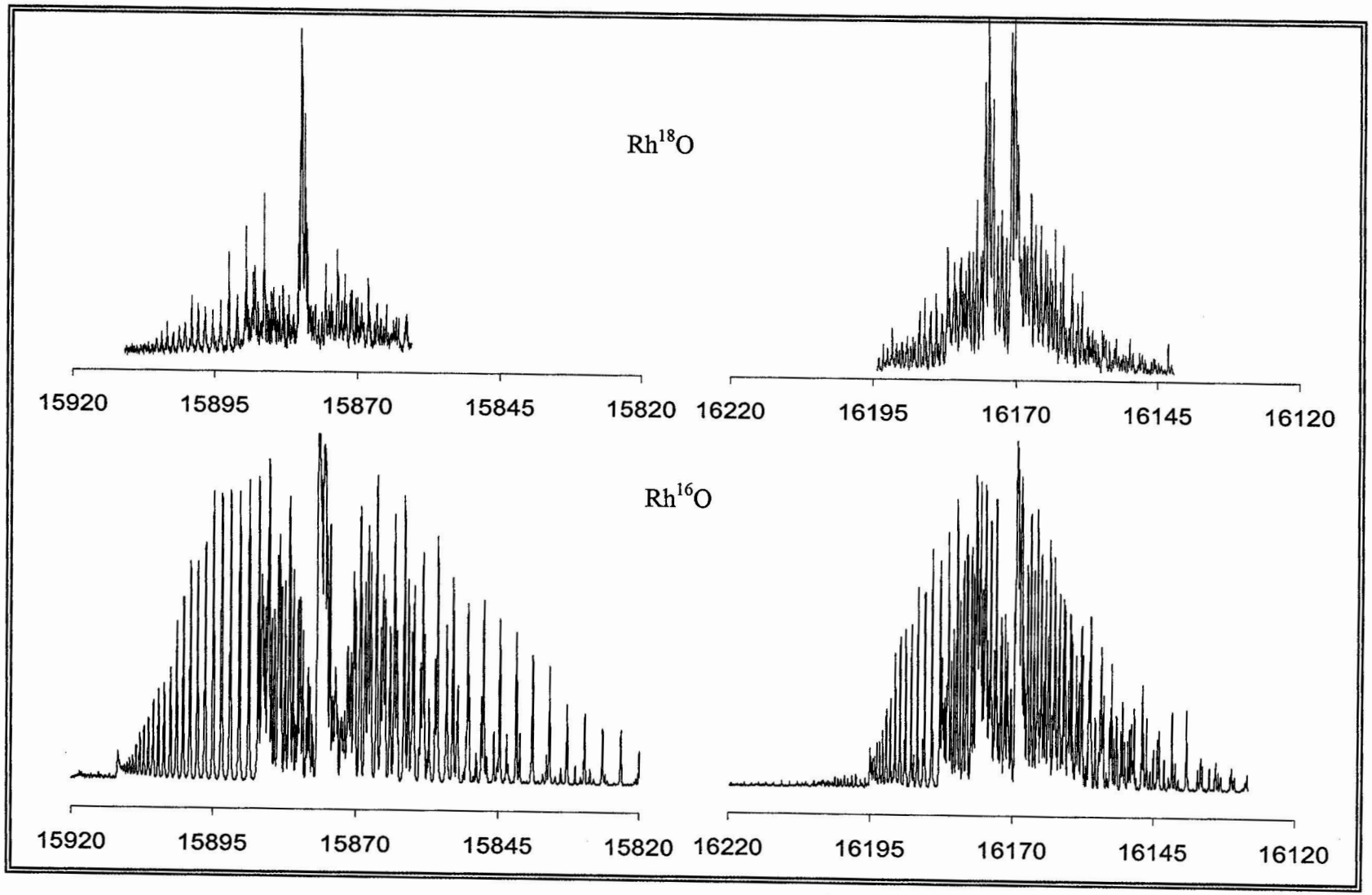

Figure 5.6 The 629.9 nm band (left) and the 618.3 nm band (right). The $Rh^{18}O$ spectra appear above for comparison.

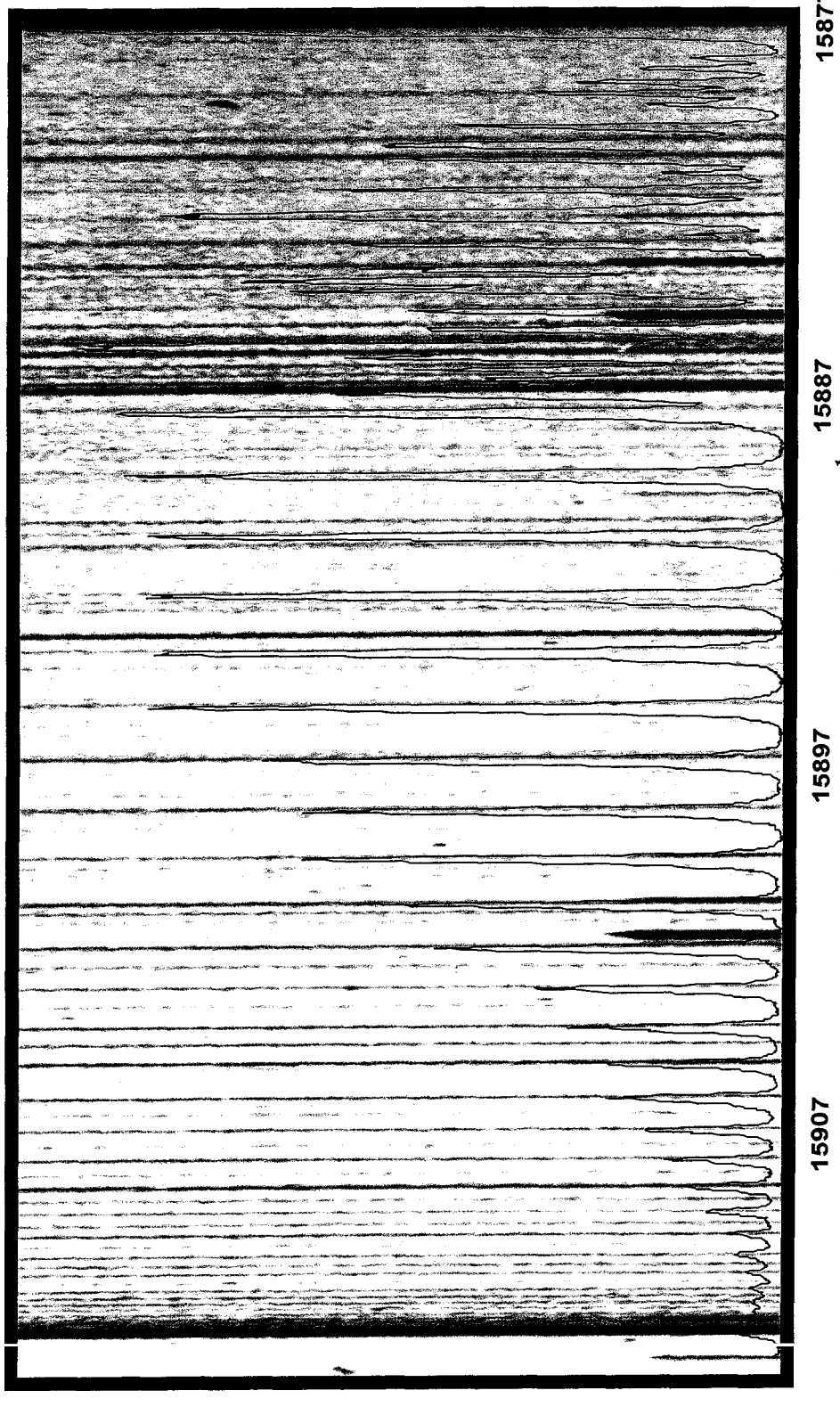

Figure 5.7 Two band heads are evident in this region of the629.9 nm band, however more lines are apparent emission spectrum.

The spectra of the transition from the ground state to the various spin-orbit sub-bands of the $^4\Pi_\Omega$ state, ($\Omega = {}^1/_2, {}^1/_2, {}^3/_2$ and ${}^5/_2$), are only expected to differ in branch intensities and the J or N numbering of the first rotational lines. By comparing the observed spectrum to the simulated spectrum of a $^4\Pi_\Omega$-$^4\Sigma^-$ transition, generated using a computer program (see Appendix II) many branches were identified and labeled.

Although branch intensities did not match exactly for any of the spectra, the transitions were still suspected of being $^4\Pi$ - $^4\Sigma^-$ in nature. Still missing, however, was the observation of key rotational lines, necessary for the conclusive identification of the four individual spin-orbit components of the excited state. This led to collaboration with the Adam group in New Brunswick where very high resolution spectra (100 MHz or 0.003 cm^{-1} resolution) of the central unresolved regions of the five prominent bands between 640 and 606 nm were recorded under very cold rotational conditions. The dense regions of the spectra were completely resolved, and first rotational lines were clearly visible in all of the spectra recorded, so that the value of Ω in each upper state could be determined.

High resolution scans, covering a 1 cm^{-1} range, were combined into a single spectrum, of about 25 cm^{-1} width, for each of the bands recorded (with spectral range limited by signal intensity). Each high resolution composite spectrum contains approximately 100 lines, with no band heads observed, due to the cold rotational temperatures.

Within a specific 1 cm^{-1} segment, the measured separation between a set of peaks, was reproducible to about ± 0.003 cm^{-1}. For peaks from different segments, error limits were two to three times larger, and therefore the experimental uncertainty is ~0.009 cm^{-1}.

Hyperfine splitting due to the ^{103}Rh nucleus ($I = {}^1/_2$) was observed in the spectra. Some branches were split into well resolved doublets (some of which coalesced into single features at higher J) while in other branches, only sharp single peaks were observed even for very low J, helping to identify the branches.

In all cases where doublets were observed, the peak to higher energy was consistently more intense. Hyperfine splitting, when observed, was generally $< 0.01 cm^{-1}$. No rotational perturbations were evident in these spectra which contained data for $J < 15$ and appear in appendix IV.

Thus, the rotational analysis of the electronic transition spectrum of $Rh^{16}O$ presented here is based on three generations of data spanning a period of four decades.

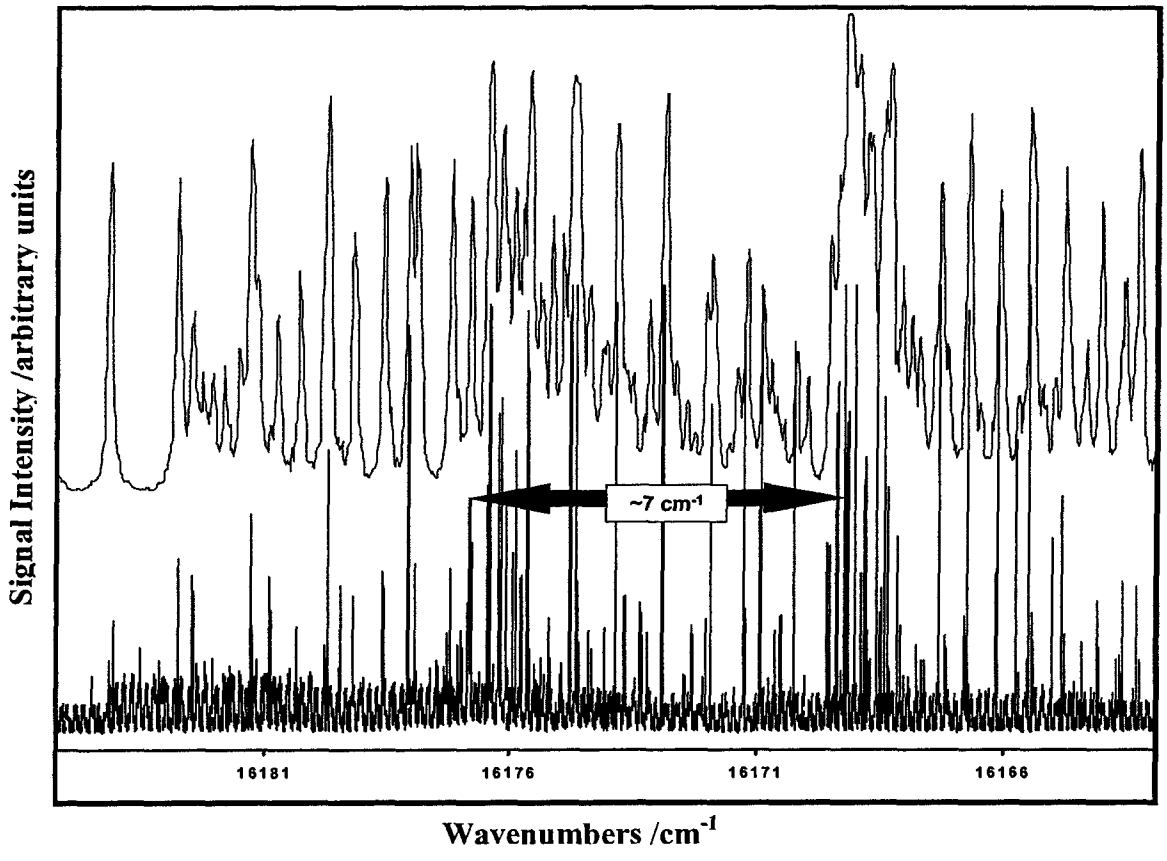

Figure 5.8 Central region of the 618.3 nm band from 16161 to 16186 cm^{-1}. The underlying UNB high resolution spectrum is completely resolved and the presence of a weak band (with a head at ~16177 cm^{-1}) was clearly visible.

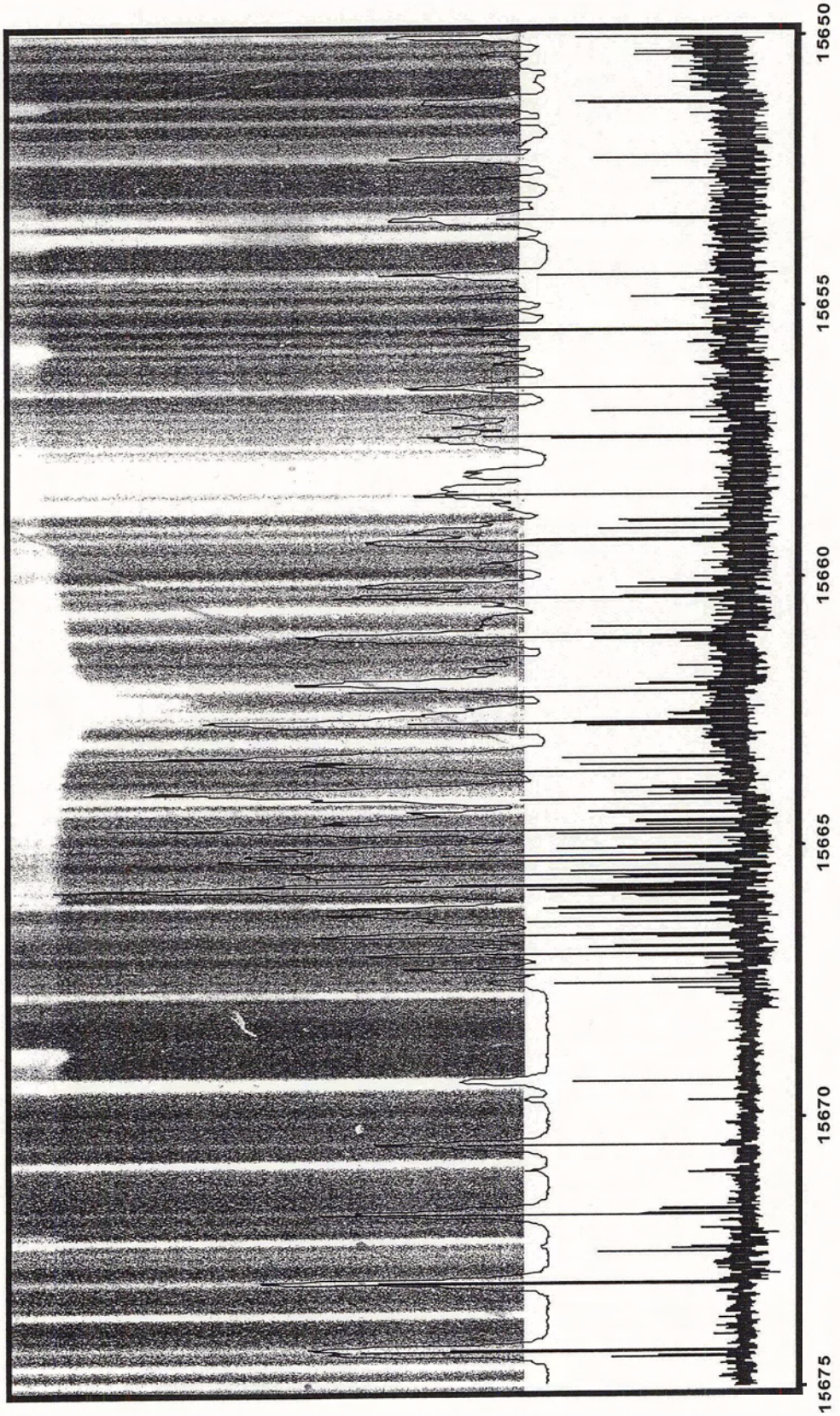

Figure 5.9 The central 25 cm^{-1} portion of the 638.2 nm band of $Rh^{16}O$ spanning over forty years of research are overlaid to show how the spectra correlate. The lines in the emission spectrum are light in this reproduction.

5.3 Preliminary Analysis

A number of observations can be made with respect to the data. The $Rh^{18}O$ spectrum between 555 to 640 nm revealed four bands with negligible isotopic shifts- characteristic of transitions with $\Delta\upsilon = 0$. The four (0, 0) bands centered at 638.2, 629.9, 625.7 and 618.3 nm are also relatively intense compared to other observed bands. The 14 resolved bands between 550 and 640 nm are complex with at least 9 and up to 12 branches identified with a dense Q-type center structure indicative of $\Delta\Lambda = \pm 1$(7). All of these observations led us to assume the spectra of $Rh^{16}O$ did indeed belong to a $^4\Pi - {}^4\Sigma^-$ transition (see figure 5.10). In such a transition four sub bands (twelve branches each) are anticipated making 48 branches in total: a P-, Q- and R- branch from each of the four spin-rotation components of the $^4\Sigma^-$ ground state (labeled F_1, F_2, F_3 and F_4) to each of the four spin-orbit components ($\Omega = {}^1/_2, {}^1/_2, {}^3/_2$ and ${}^5/_2$) of the $^4\Pi_\Omega$ excited state.

In a $^4\Pi - {}^4\Sigma^-$ transition, branches are designated by ΔN and ΔJ as well as the spin-rotation level of the ground state and the spin-orbit level of the excited state. The usual designation for a branch is R, Q or P with $\Delta J = +1, 0$, or -1. The "form" of the branch is written as a superscript to the left where u, t, s, r, q, p, o, n or m indicates $\Delta N = +4, +3, +2, +1, 0, -1, -2, -3$ or -4. Two numerical subscripts are used, one to indicate whether the branch terminates in one of the four F_1, F_2, F_3 or F_4 components of the $^4\Pi$ excited state, and one to indicate the spin-rotation component F_1, F_2, F_3 or F_4 of the $^4\Sigma^-$ ground state. For example, a Q- branch from the F_2 level in the ground state, going to the F_4 level of a $^4\Pi_{reg}$ excited state, would have $\Delta N = 2$, and be designated as ${}^sQ_{42}(N)$. The numbering of the rotational lines refers to the value of N in the ground state.

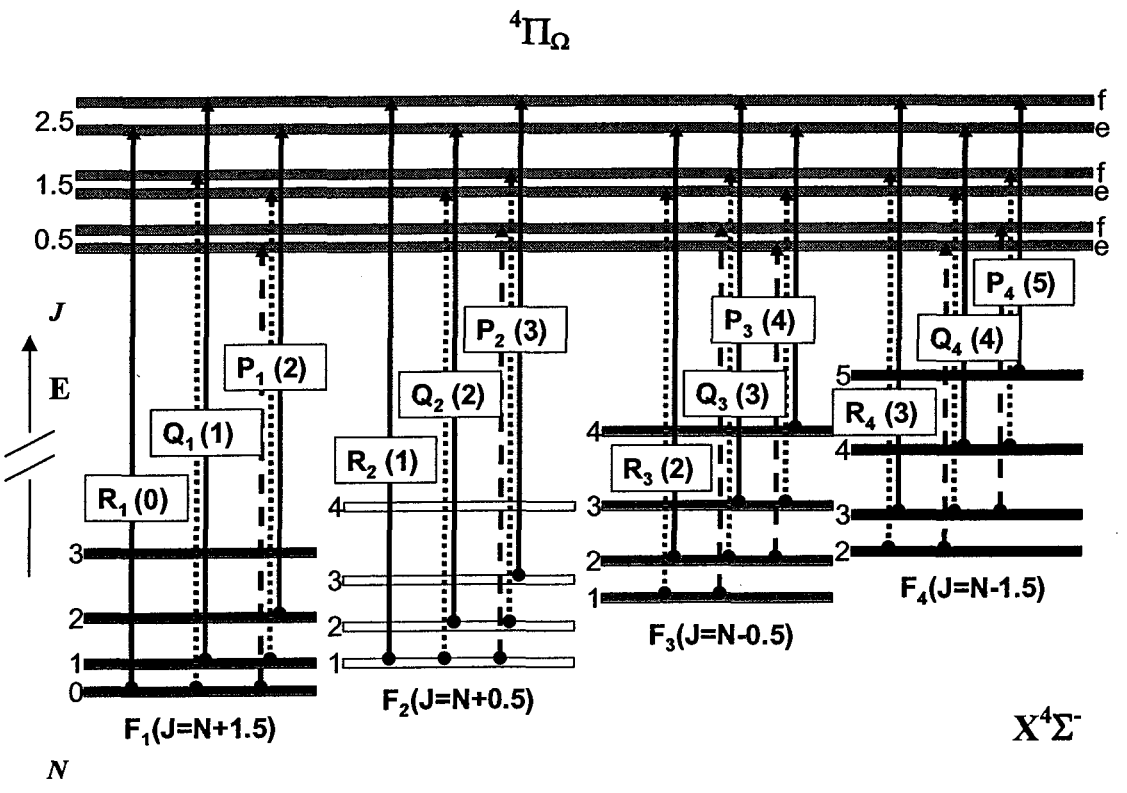

Figure 5.10 Energy level diagram of a $^4\Pi_\Omega$ - $^4\Sigma^-$ transition. Lines are labeled according to (N). The12 solid lines indicate the first lines expected in the $^4\Pi_{5/2}$ - $^4\Sigma^-$ sub-band; dashed and dotted lines (not labeled) are respectively the expected first rotational lines for the sub-band with $\Omega = {}^3/_2$ and the two sub-bands with $\Omega = {}^1/_2$ ($J = \Omega, \Omega+1, \Omega+2...$).

During the initial stages of the analysis a reduced version of this branch nomenclature was adopted since both subscript and superscript require prior knowledge of Ω for the excited state. The branches therefore, were simply labeled as R_i-, Q_i- or P_i- with a numerical subscript of 1, 2, 3 or 4 indicating the spin-rotation level of origin in the ground state. For example R_1- indicated $\Delta J = +1$ and the branch originated in the F_1 spin-rotation component of the ground state.

By comparing the observed spectra to simulated spectra, preliminary "ballpark" estimates of molecular constants were deduced. A reasonable guess could be made for the rotational constants B, based on the bond lengths of similar molecules (11), with the added assumption that $B' < B''$ since the observed band heads are red degraded (9). From the compact nature of the bands, the value of λ, the spin-spin parameter was assumed to be small however, it was much more difficult to predict from the spectra.

The parameters were adjusted, until a simulated spectrum was produced, similar in character to one of the observed bands. It was the 629.9 nm band that the simulation appeared to resemble (see figure 5.11). Different spectra were obtained, using small / large and positive / negative values for λ_0 and γ_0 in attempts to simulate some of the other bands. However, none were successful. Agreement between line positions (especially at high J) and line intensities calculated by Kovács (12) for a $^4\Pi$ case (a) – $^4\Sigma$ case (b) transition were never deemed completely satisfactory. Nonetheless, the simulated spectra were invaluable during the preliminary stages of the analysis, providing clues as to the type of branch structure to expect.

Once the general branch structure of the band was determined, individual rotational lines were sought after. This no longer required a simulated spectrum. At this point, line positions were compared directly. Spectroscopic constants were determined using least squares fitting of the residuals between the observed and calculated combination differences and/or rotational term values.

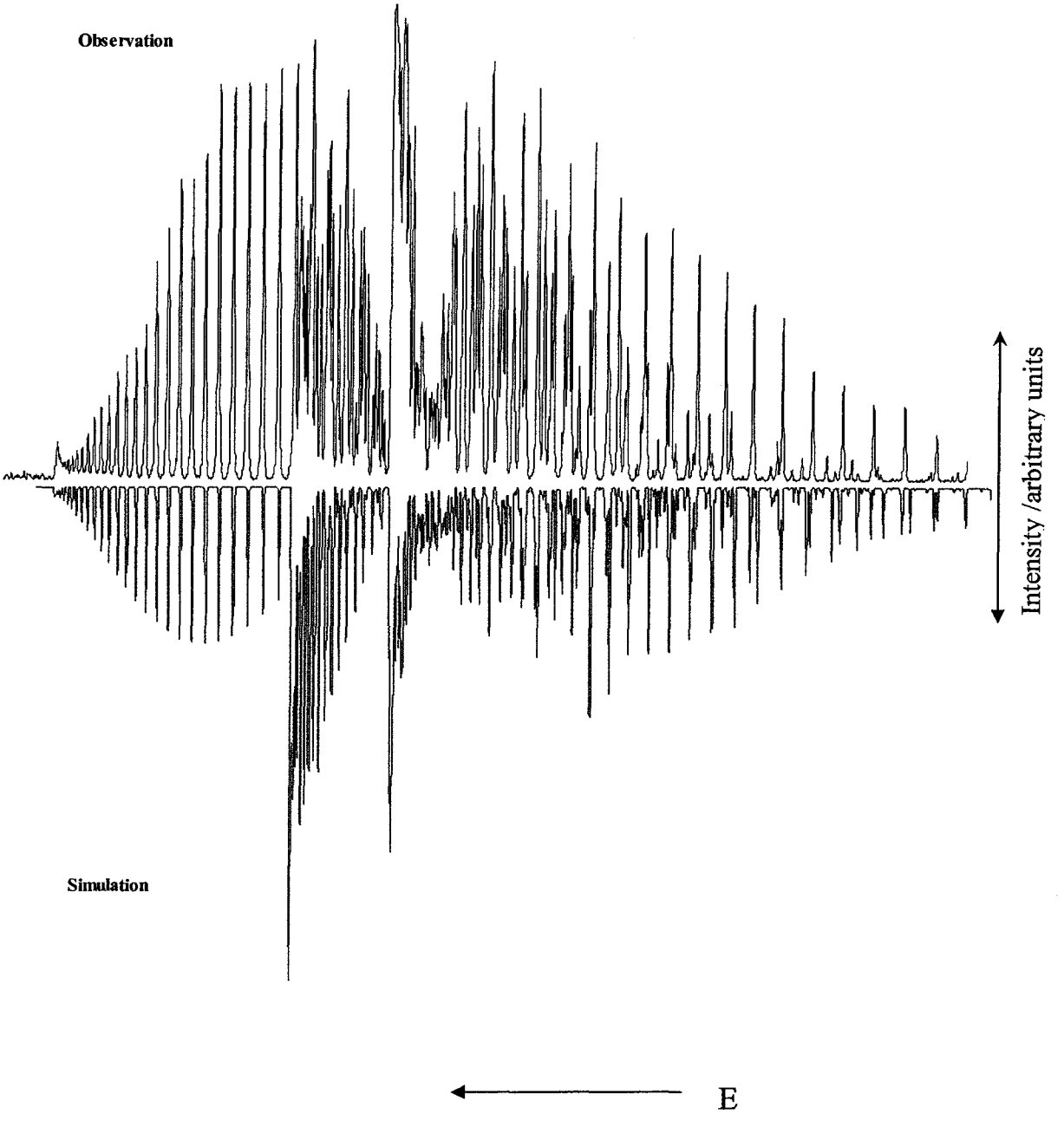

Figure 5.11 Simulations were used very early on in the LIF analysis. Attempts to match one of the observed spectra first resulted in success for the 629.9 nm band. From this simulation (T = 100 K) the branches were tentatively identified. Branches in other bands were then similarly picked out and a rotational analysis was underway.

Branches were initially assigned by comparison of observed to simulated spectra. Simulated spectra that were in reasonable agreement with the observed spectra always had the R_1-, Q_1- and R_2- branches forming red degraded heads, on the higher energy side of the band center. With the exception of the F_1 and F_2 rotational levels at low J, the transition lines indicate that the energy levels of the ground state follow the expected pattern for case (b) behavior. That is, for a given value of N, the energy levels of the spin rotation components are close in energy and follow the order $F_4 > F_3 > F_2 > F_1$.The energies of the branches always follow the order $R_i > Q_i > P_i$. For $J < 10$ the F_1 and F_2 rotational levels are very close and actually reversed in order. Above $J = 10$ however, they follow the case (b) order given above.

In the LIF spectra, the R_1- and R_2- heads are strong features; however the head formed by the Q_1- branch is typically not observed since it is a very weak branch. From the simulations it was noted that the three branches from the F_2 level originate near the band origin, sometimes forming one or more heads degraded to the blue and /or red, within the region of the dense Q-structure. The R_3- and Q_3- branches start just to lower energy of the band origin, often forming a red degraded band head within a few J, and are also part of the strong central Q-type structure. The P_3-, R_4-, Q_4- and P_4- branches begin lower in energy than the band origin and do not form heads. The R_1- and P_4- branches have a noticeably wide ~5B line spacing, making these branches easier to identify. In most of the bands, the R- and P- branches from any given spin-rotational level of the $^4\Sigma^-$ ground state were more intense than the corresponding Q- branch.

Branches are indicated for the 629.9 nm band according to spin-rotation level (F_1, F_2, F_3, and F_4) and type (R-, Q- or P-) by color and pattern respectively in Figure 5.12.

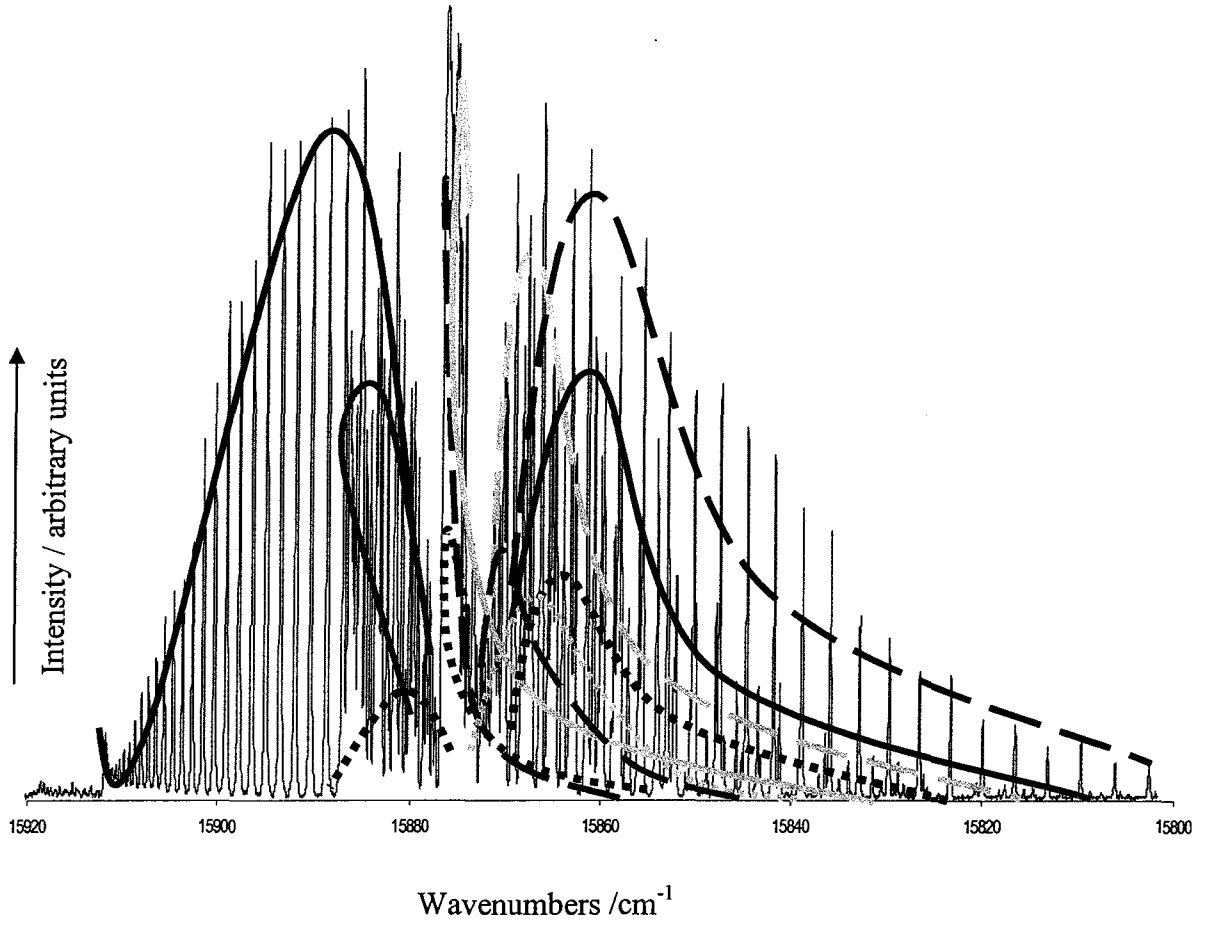

Figure 5.12 Branch structure for the 629.9 nm band as predicted by the simulation model. The branches are classified in two ways: branches originating from the F_1, F_2, F_3 and F_4 spin-rotation components of the ground state are colored blue, green, yellow and red respectively, and R-, Q- and P- branches are indicated by solid, dotted and dashed lines respectively.

Ground state combination difference relations were calculated, along with upper state term values, and using spread sheet graphics and least squares fitting, preliminary spectroscopic constants, for both lower and upper states were determined, for the 16 prominent $Rh^{16}O$ bands above 530 nm. Not all 12 branches were identified in each band, due to insufficient line intensity, and those branches that were identified, were limited to $J < 15$. In addition to these limitations, many lines from the band periphery relate to

unresolved lines in the congested central regions, further reducing the number of combination differences available for the least squares fitting. The 618.3 and the 629.9 nm bands, however, were considerably more intense than all of the other bands, containing substantially more measurable rotational lines ($J > 40$). The rotational analysis, therefore, was initially focused upon the data from these two bands.

Combination differences are traditionally used to determine the ground state parameters since they are considered to be more accurate. The theoretical energy levels of a $^4\Sigma^-$ state case (a) basis were determined using the matrix elements of Merer (17) summarized in table 5.1 Matrix elements of $\mathbf{H_{ROT}}$, $\mathbf{H_{SR}}$ and $\mathbf{H_{SS}}$ have been included. Combination differences were calculated from the theoretical energy levels and compared to the observed combination differences determined from the transition lines.

Table 5.1 Matrix elements for the rotational levels of a $^4\Sigma^-$ state.

	$\Sigma^-_{3/2}\lvert(e/f);J\rangle$	$\Sigma^-_{1/2}\lvert(e/f);J\rangle$
$\Sigma^-_{3/2}\lvert(e/f);J\rangle$	$Bx - D(x^2+3x)$ $+2\lambda - 1.5\gamma - 3\gamma_D x$	$-\sqrt{3x}[B - 0.5\gamma - 0.5\gamma_D\{x+7\mp(2J+1)\}$ $-2D\{(x+2)\mp(J+0.5)\}]$
$\Sigma^-_{1/2}\lvert(e/f);J\rangle$	symmetric	$B(x+4) - D[(x+4)^2+7x+4]$ $-2\lambda - 3.5\gamma - \gamma_D(7x+16)$ $\mp 2[B - 0.5\gamma - 0.5\gamma_D(x+11) - 2D(x+4)](J+0.5)$

Upper and lower signs give the e (F_1 and F_3) and f (F_2 and F_4) levels, respectively. F_1, F_2, F_3 and F_4 components have $J = N + 1.5$, $J = N + 0.5$, $J = N - 0.5$ and $J = N - 1.5$, respectively.

The upper state rotational levels were determined from the observed transition lines and the calculated ground state energy levels. Six values are obtained for each of the *e/f* levels, then averaged before comparison to the expected line positions determined by

$$E\{^{2S+1}\Pi_\Omega(e/f)\} = T_\Omega + B_\Omega[S(S+1)-\Sigma^2-\Omega^2]+B_\Omega J(J+1)-D_\Omega[J(J+1)]^2$$
$$\pm 0.5p_\Omega(J+\tfrac{1}{2})\mp 0.5p_{\Omega J}(J+\tfrac{1}{2})^3 \qquad [70]$$

[70] is a simplified expression for the rotational levels of a case (a) multiplet sub-band used because irregular spin-orbit coupling was observed. The $^4\Pi$ energy levels are therefore approximated on a band-to-band basis using [70] with effective parameters only.

The standard deviation of each excited state term value was kept within experimental uncertainty. An unacceptable standard deviation, for an upper state rotational level, was usually an indication of a typo or a miss-assigned line. There is one exception, the 577.8 nm band, which suffers from a local perturbation. The preliminary results are not given since the analysis was incomplete and the high resolution data had not been obtained from UNB at this point.

At this point, most of the branches had been identified satisfactorily and the preliminary analysis yielded reasonable initial values for both ground and excited state parameters (not yet reported). However, without the observation of "first" rotational lines, needed to determine the value of Ω for each of the assumed spin-orbit components of the $^4\Pi$ excited state, the analysis was incomplete. High resolution spectra, which completely resolved the congested central regions of the bands, were required. These were gratefully obtained from the Adam group, at the University of New Brunswick. The five most prominent low energy bands were recorded, at sufficiently high resolution that

hyperfine structure was observed in the spectra. The hyperfine transition lines are tabulated in appendix VII.

5.4 Hyperfine Structural Details

The nuclear spin quantum number I for ^{16}O is 0, whereas for ^{103}Rh it is $^1/_2$. Therefore in order for hyperfine interactions to occur in the $Rh^{16}O$ molecule there must be some electron spin density at the rhodium nucleus. This requires that at least one of the three unpaired electrons in the RhO molecule has some atomic *s*-character. If hyperfine structure is resolved in the spectra, each rotational line will be split into doublets, since $I = {}^1/_2$. For every value of J, two values of F result; $F_1 = J + {}^1/_2$ and $F_2 = J - {}^1/_2$, with each level $(2F+1)$ fold degenerate and therefore unequally populated. The unequal peak heights of the hyperfine doublets should be more pronounced at low J.

The proposed electronic configuration for the RhO ground state is $\ldots 2\delta^4 12\sigma^1 6\pi^2$. The singularly occupied 12σ orbital is basically Rh ($5s$) in character and essentially non-bonding, and the doubly occupied 6π orbital weakly anti-bonding in character and composed mainly of the Rh ($4d$) and O ($2p$) orbitals. Therefore, only one of the three unpaired electrons in the ground state has any atomic *s*-type character. It is, therefore, possible to observe hyperfine splitting in the molecular spectra, provided that the magnitude of the coupling constant, b, is large enough.

Hund's case (b) behavior is expected for the $^4\Sigma^-$ ground state, since there is no orbital angular momentum available to couple to the inter-nuclear axis. Since the width of the observed hyperfine doublets decreases with J, we concluded that the hyperfine coupling must follow case ($b_{\beta J}$) (see section 1.7). The observed doublet splitting is not

resolved for all of the branches in the high resolution spectra, leading to the conclusion that the hyperfine interaction must arise from the ground state electronic configuration only, otherwise it would be observed in all of the branches (since there are only *e* and *f* levels in each spin-orbit component of the $^4\Pi$ state). The center region of the 638.2 nm band in figure 5.13 displays many of the features just mentioned about the observed hyperfine splitting.

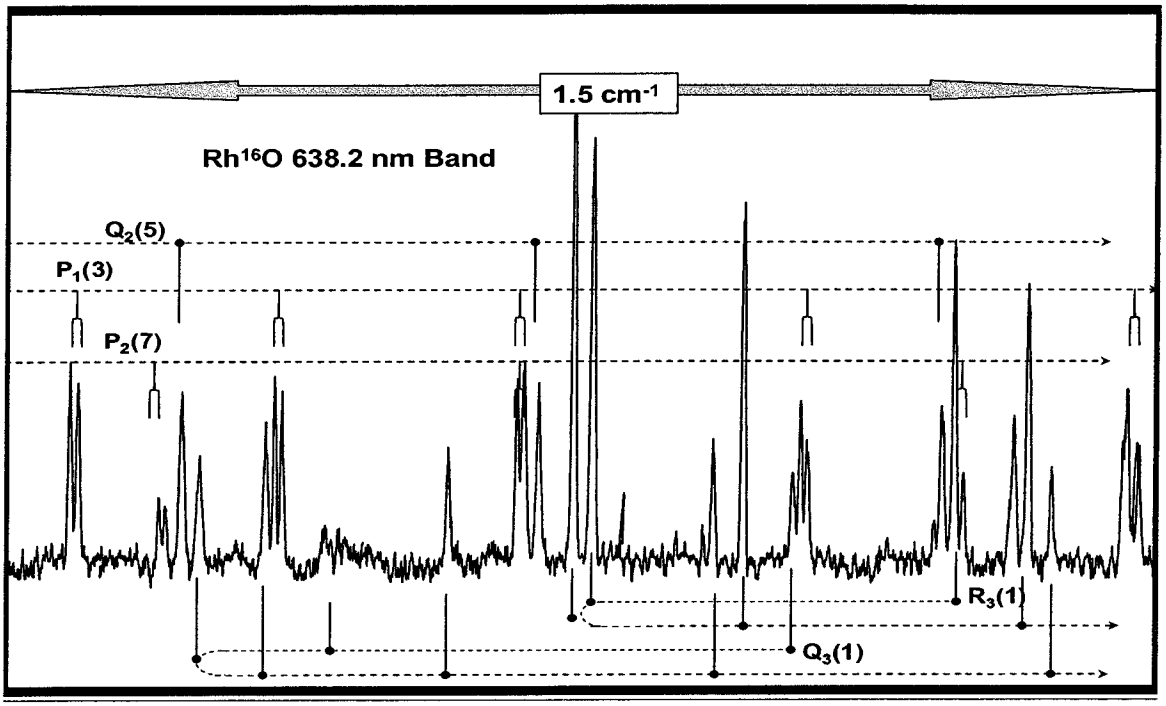

Figure 5.13 High resolution spectra showing the hyperfine doublets in the center region of the 638.2 nm band.

Dunn has derived expressions (6) for the hyperfine splitting of a $^4\Sigma^-$ case ($b_{\beta J}$) state, with all three unpaired electrons of *s*-type character. Since, only one of three electrons is expected to have *s*-type character in the RhO molecule, his expressions have been multiplied by a factor of $^1/_3$, before using them to determine the magnitude of the Fermi contact coupling parameter, *b*.

$$\Delta W(F_1) = I[(N+2)/(N+3/2)] \cdot b \quad [71]$$

$$\Delta W(F_2) = 1/3\, I(N+1)(N+9/2)/[(N+1/2)(N+3/2)] \cdot b \quad [72]$$

$$\Delta W(F_3) = -1/3\, I[N(N-7/2)/[(N+1/2)(N-1/2)] \cdot b \quad [73]$$

$$\Delta W(F_4) = -I[(N-1)/(N-1/2)] \cdot b \quad [74]$$

The hyperfine splitting determined from these expressions is expected to decrease with increasing N, and the observed splitting from the various branches should follow the order $F_1 > F_4 > F_2 > F_3$. Figure 5.14 shows the splitting of the $^4\Sigma^-$ energy levels due to spin-rotation and hyperfine interactions.

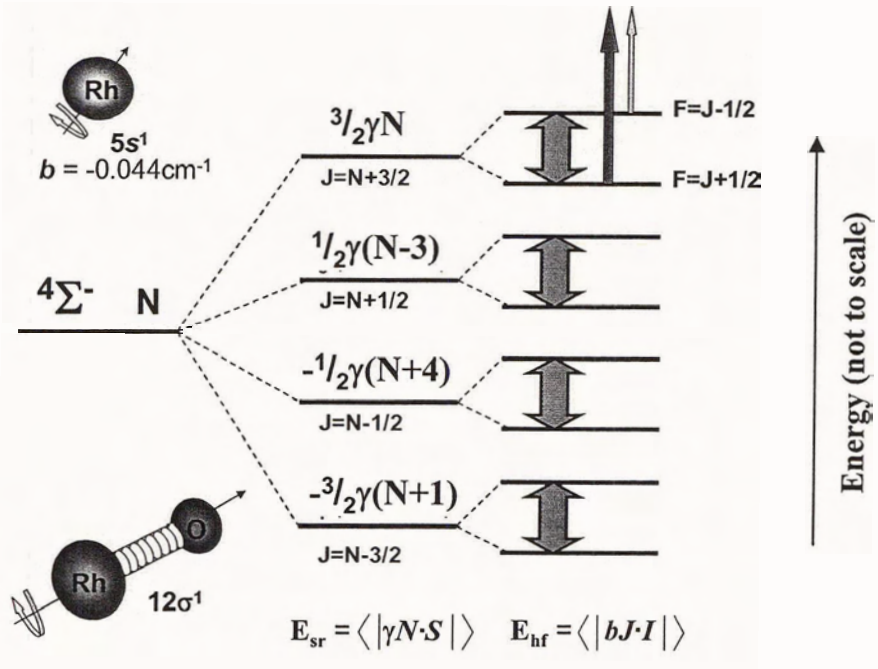

Figure 5.14 Schematic representation of electronic fine and hyperfine. The hyperfine doublet separations are indicated by the purple arrows. The green and yellow arrows indicate the statistical weights (due to degeneracy) of the two hyperfine levels.

The hyperfine splitting made identification of the branches unambiguous; observed values for $\Delta W(F_1)$ equation [73] for all of the high resolution spectra are given in figure 5.15 and the $\Delta W(F_i)$ averaged over all the available hyperfine data are given in figure 5.16. Branches originating from the F_3 spin-rotation component contained sharp single peaks only (the doublets are unresolved). The doublets observed in branches originating from the F_2 spin-rotation component coalesced quickly ($J < 10$), and lines in branches from the F_1 and F_4 levels remained wide doublets over the entire recorded regions of the spectra ($J = 15$). Hyperfine splitting in the spectra also decreases with increasing molecular rotation as was expected for case ($b_{\beta J}$) coupling and thus confirming the original supposition.

The observed ground state splitting (averaged over all of the recorded bands) for the level $N = 5$ is summarized in figure 5.17. A least squares fitting of 288 hyperfine observations to Dunn's expressions gave a value for the Fermi contact parameter $|b| = 0.0203 \pm 0.0021$ cm^{-1}. The relative intensities of the peaks in the doublets were always such that the higher energy component was the more intense; this confirms on statistical grounds that b is negative. The value for b is about 50% less than that estimated for a Rh 5*s* electron in the atom where (a_{iso}) = -1229 MHz (or -0.044 cm^{-1}) (35). This is in good agreement with the *ab initio* prediction of Siegbahn (27), where the Rh 5*s* character in the molecular ground state is calculated to be 39%.

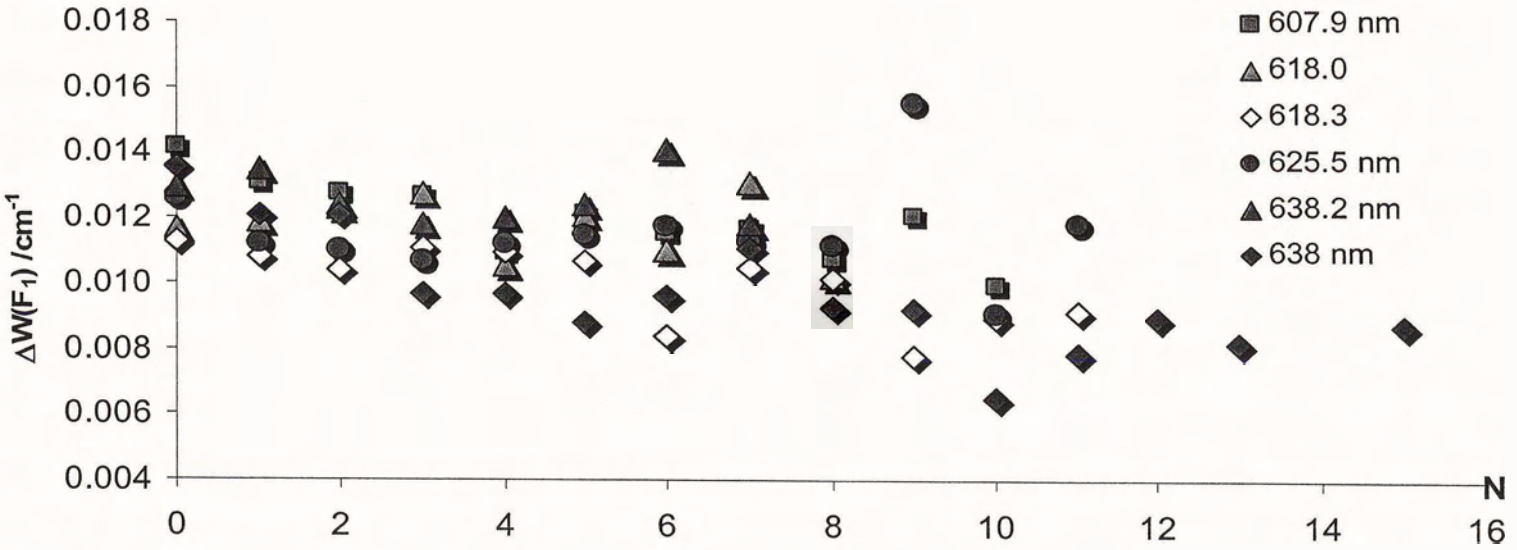

Figure 5.15 Observed hyperfine splitting for the F_1 level plotted individually for each of the bands recorded under high resolution. Each point on the chart is the average width for all peaks originating from that rotational level. All of the data is plotted giving an indication of the size of the data set and the low J limit of the data.

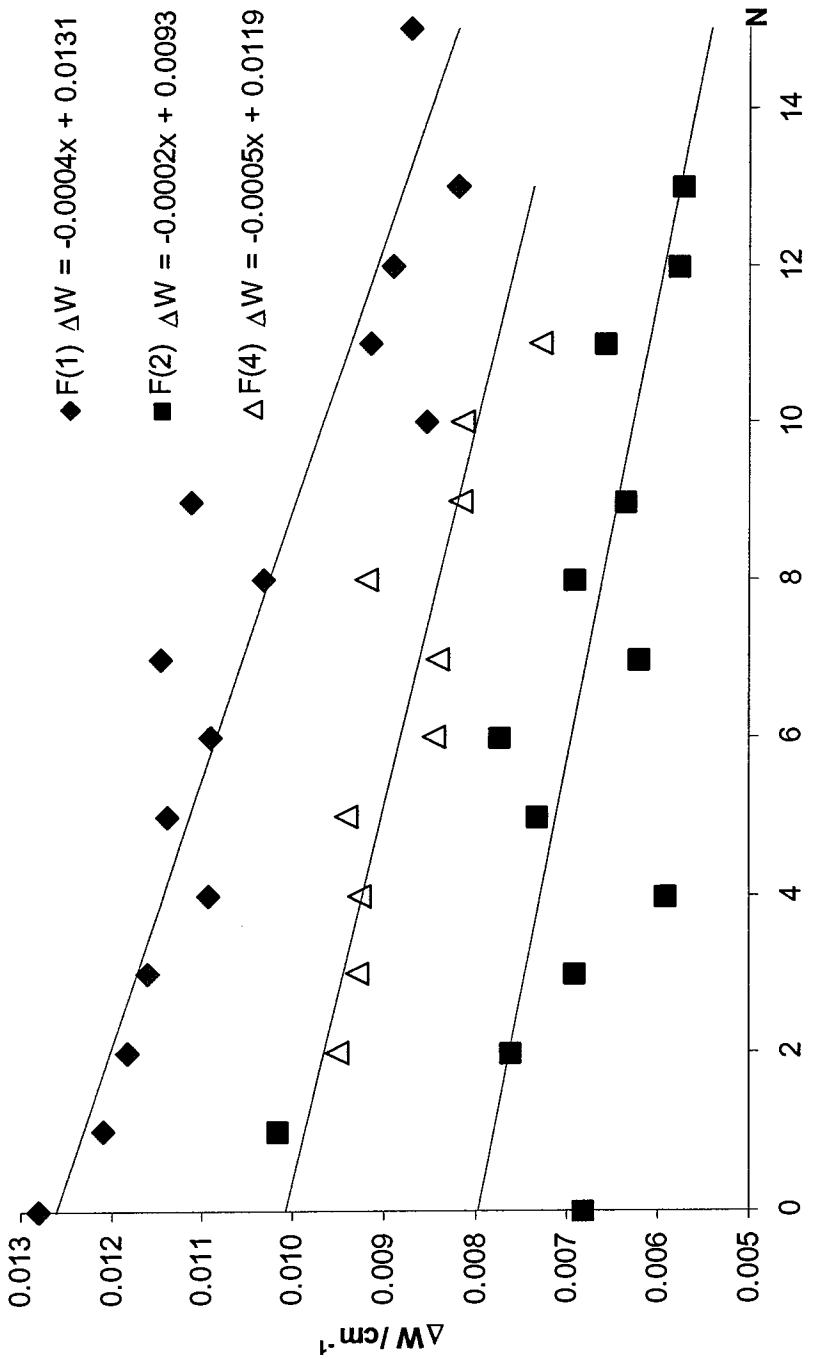

Figure 5.16 Observed hyperfine splitting grouped according to the spin-rotational level of the ground state that the transition originates from. Hyperfine data from all five bands are averaged into each point on the chart.

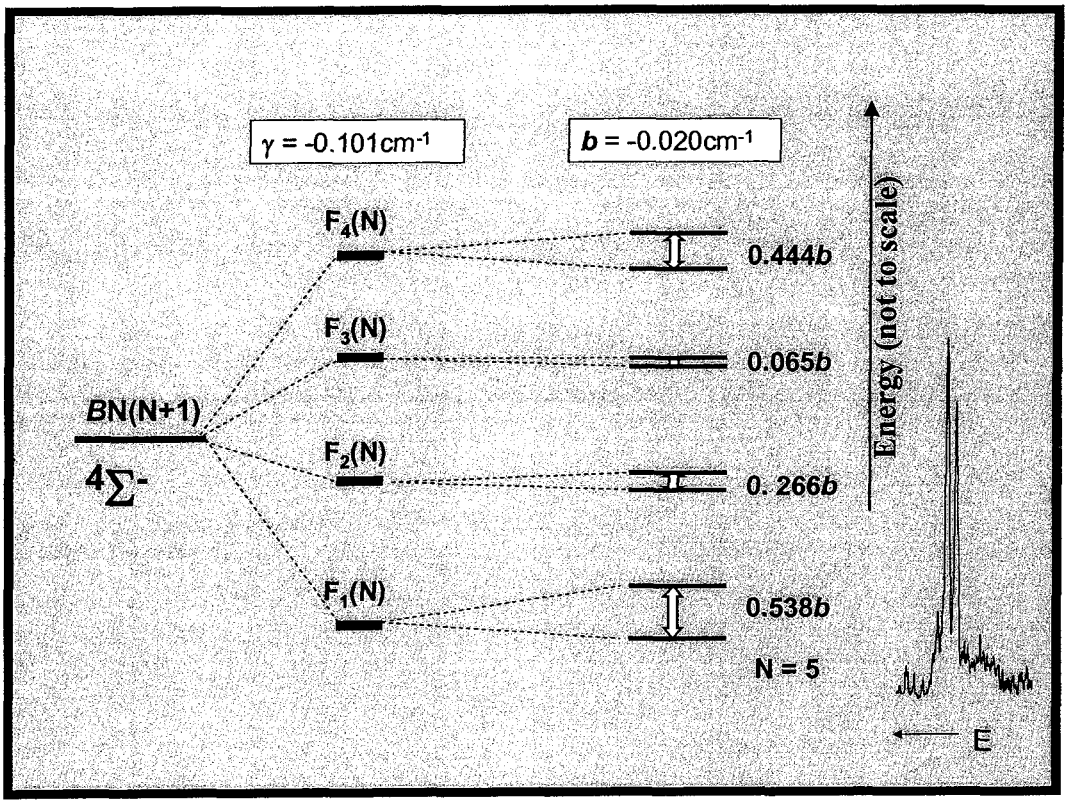

Figure 5.17 Summary of the observed fine and hyperfine structure for RhO (N = 5). The spectral insert shows a typical doublet with the high energy peak more intense as expected for a negative value of b. The spin-rotational levels are inverted since γ is also negative.

5.5 Complete Rotational Analysis of $Rh^{16}O$

There are 30 possible ground state combination difference relations for a $^4\Pi - {}^4\Sigma^-$ transition; these are split into two groups of 15, for transitions to either an *e* or *f* level, in the upper state (see table 5.2). Hyperfine doublet line positions were averaged, to give a single rotational line, before determining the combination differences, since hyperfine

matrix elements were not included in the $^4\Sigma^-$ rotational matrix (table 5.1). Ground state combination differences, from all the high resolution bands, were limited to low *J*. The least squares fitting, for the ground state, was done in a concerted fashion, using all of the available high resolution data, with residuals minimized using the least number of parameters possible. The parameters B_0, λ_0 and γ_0 were determined, with no centrifugal distortion coefficient needed to characterize the ground state using the high-resolution, low *J* data. A total of 543 lines (averaged) in the high-resolution spectra, combined to give 865 ground state combination differences. The concerted least-squares fitting, gave the following values, for the rotational parameters, in units of cm^{-1}, of

$$B_0 = 0.41320(12) \qquad \lambda_0 = -0.5733(16) \qquad \gamma_0 = -0.10276(30)$$

The overall standard deviation was 0.00079 cm^{-1} and the confidence limits shown in parentheses indicate what increase in the constant is required to increase the overall standard deviation by 15%. These numbers are approximate, since the negative values of the error bars do not necessarily produce identical behavior. The residuals show no obvious trends and the overall standard deviation (~0.0079 cm^{-1}) is well within the experimental uncertainty (which is estimated at 0.009 cm^{-1}).

The combination relations from every possible set of transition lines were determined and checked to help determine if lines were improperly assigned. All 30 combination differences were used to fit the ground state constants. A detailed drawing of the energy levels and resulting combination relations of table 5.3 is given in figure 3.3. Transition lines for the $Rh^{16}O$ LIF spectra appear in appendix V, and term values are given in appendix VI.

Table 5.2 Combination differences for the $^4\Pi_\Omega - {}^4\Sigma$ transitions. The column on the left, are those depicted in figure 3.3 (p.51) using shaded arrows.

Ground State Combination Differences for transitions from a $^{2S+1}\Lambda_\Omega$ Multiplet to a $^4\Sigma^-$ ground state	
from *J'(e)*	from *J'(f)*
$R_1(N\text{-}1)\text{-}P_1(N\text{+}1)$	$Q_1(N)\text{-}R_2(N)$
$R_1(N\text{-}1)\text{-}Q_2(N\text{+}1)$	$Q_1(N\text{-}1)\text{-}P_2(N\text{+}1)$
$R_1(N\text{-}1)\text{-}R_3(N\text{+}1)$	$Q_1(N\text{-}1)\text{-}Q_3(N\text{+}1)$
$R_1(N\text{-}2)\text{-}P_3(N\text{+}2)$	$Q_1(N\text{-}1)\text{-}R_4(N\text{+}1)$
$R_1(N\text{-}2)\text{-}Q_4(N\text{+}2)$	$Q_1(N\text{-}2)\text{-}P_4(N\text{+}2)$
$P_1(N)\text{-}Q_2(N)$	$R_2(N\text{-}1)\text{-}P_2(N\text{+}1)$
$P_1(N)\text{-}R_3(N)$	$R_2(N\text{-}1)\text{-}Q_3(N\text{+}1)$
$P_1(N\text{-}1)\text{-}P_3(N\text{+}1)$	$R_2(N\text{-}1)\text{-}R_4(N\text{+}1)$
$P_1(N\text{-}1)\text{-}Q_4(N\text{+}1)$	$R_2(N\text{-}2)\text{-}P_4(N\text{+}2)$
$Q_2(N)\text{-}R_3(N)$	$P_2(N)\text{-}Q_3(N)$
$Q_2(N\text{-}1)\text{-}P_3(N\text{+}1)$	$P_2(N)\text{-}R_4(N)$
$Q_2(N\text{-}1)\text{-}Q_4(N\text{+}1)$	$P_2(N\text{-}1)\text{-}P_4(N\text{+}1)$
$R_3(N\text{-}1)\text{-}P_3(N\text{+}1)$	$Q_3(N)\text{-}R_4(N)$
$R_3(N\text{-}1)\text{-}Q_4(N\text{+}1)$	$Q_3(N\text{-}1)\text{-}P_4(N\text{+}1)$
$P_3(N)\text{-}Q_4(N)$	$R_4(N\text{-}1)\text{-}P_4(N\text{+}1)$

The $^4\Sigma^-$ ground state energy levels, well characterized by the rotational analysis of the high resolution data, are intermediate between coupling cases (a) and (b) for low molecular rotation. Both the quantum numbers N as well as J are required for labeling the rotational lines, however, depending on whether N (case b) or J (case a) is being referenced, the ground state energy level description can look quite different.

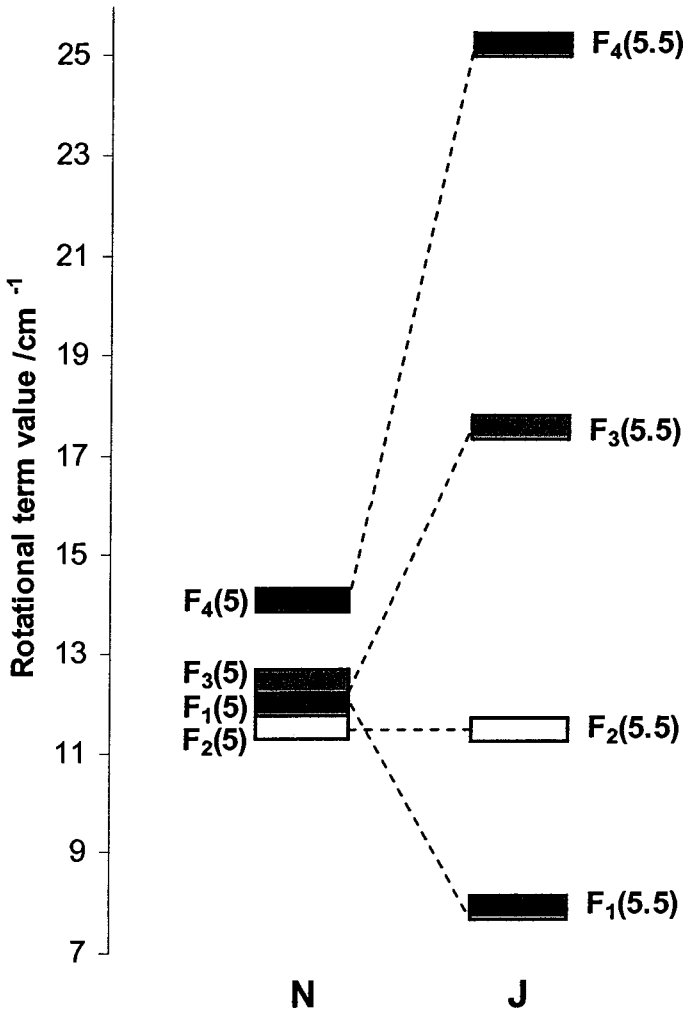

Figure 5.18 Rotational term levels (drawn to scale) for the $^4\Sigma$ ground state for the levels N = 5 (left) using case (b) labels and on the right J = 5.5 using case (a) labels. The rotational structure appears quite different depending upon the labeling system used.

If the ground state energy levels are plotted with respect to *N*, the spin rotational levels form a relatively tight group, compared to the *BN(N+1)* spacing, and the order of the F_1 and F_2 levels are reversed below $J = 10$. In contrast, the energy levels appear

dispersed, when related by J, and follow $F_4 > F_3 > F_2 > F_1$ ordering exclusively. This is illustrated in figure 5.18 for $N = 5$ or $J = 5.5$, where the energy levels are reversed for the F_1 and F_2 spin-rotation components.

The high resolution and moderate resolution data (including data from the emission plates), were combined and re-analyzed, using over 4000 ground state combination differences, ($J \leq 45$) and fitted using only 4 parameters, B_υ, D_υ, λ and γ, with a standard deviation of 0.0731 cm^{-1}. The results are summarized below in table 5.3. The residuals for the 638.2 nm band of $Rh^{16}O$, are shown in figure 5.19, as an example of a typical fit.

Table 5.3 Rotational constants for the $X^4\Sigma^-$ state of $Rh^{16}O$ using all 16 LIF bands.

$B_0 = 0.4130(10)$	$D_0 = 1.25(4)\cdot 10^{-7}$	$\lambda_0 = -0.58(3)$	$\gamma_0 = -0.103(3)$

(The error bars shown in parenthesis represent the change needed in the last significant figure(s) of the parameter to increase the standard deviation by 15%).

These parameters are slightly different, than those obtained by the high resolution analysis alone, due to the quality of the LIF spectra. Only the 629.7 and 618.3 nm bands contain rotational lines for $N > 50$, and only for the R_1 and P_4 branches (which do not share a common upper level and hence do not contribute to the ground state analysis).

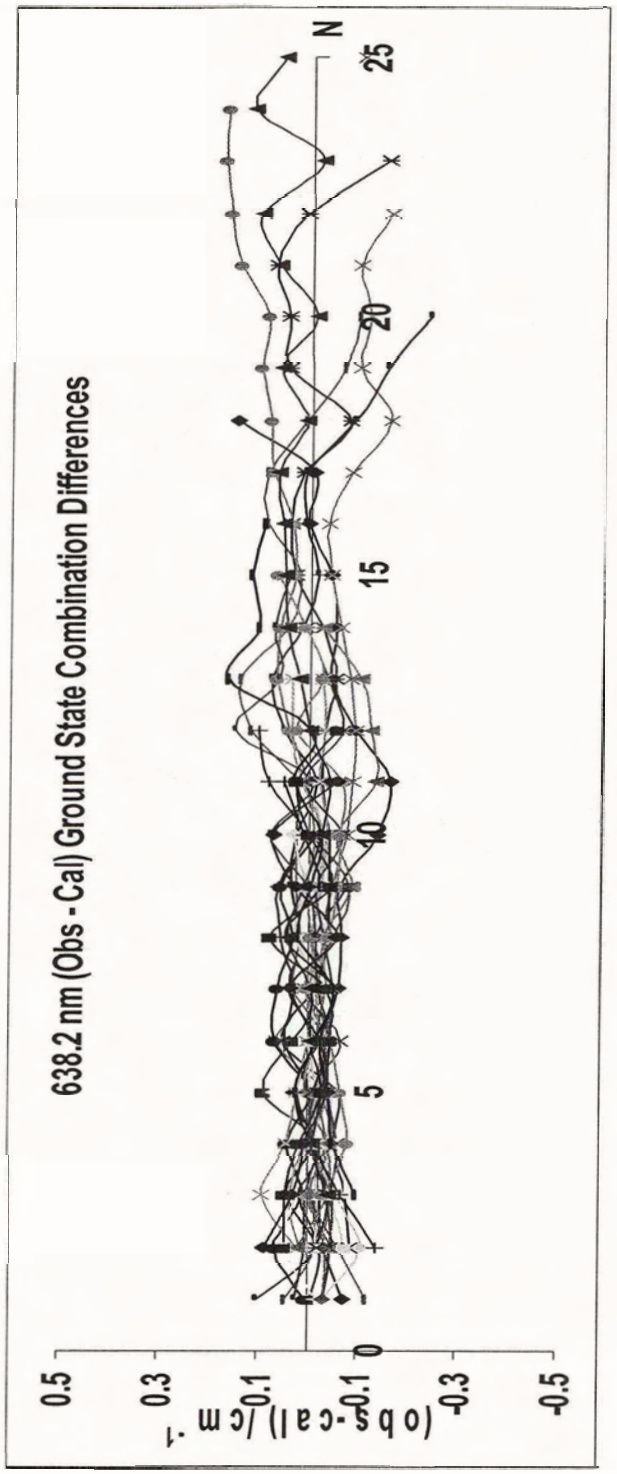

Figure 5.19 Observed minus calculated ground state combination differences for the 638.2 nm band of $Rh^{16}O$. This fit is typical of most of the bands analyzed. All of the possible 30 different combination difference residuals are plotted.

The observed $X^4\Sigma^-$ energy levels of $Rh^{16}O$ follow neither case (a) nor (b) exactly, however, the value for λ is sufficiently small, that case (b) is a better description of the ground state coupling (figure 5.20).

5.6 Characterization of the Excited Levels

The value for Ω in the upper state also determines the expected first rotational lines since $J = \Omega, \Omega+1 \ldots$ for Hund's case (a) coupling cases. The first rotational lines observed in the hyperfine spectra indicated that for the 638.2, 629.9, 625.9 and the 618.3 nm bands, $\Omega = {}^1/_2, {}^1/_2, {}^3/_2$ and ${}^3/_2$ respectively. No spin-orbit component with $\Omega = {}^5/_2$ was present in the four (0,0) bands as was expected for a $^4\Pi - {}^4\Sigma^-$ transition, leading us to re-evaluate this initial assignment. The values for Ω obtained from the observed first rotational lines suggested that two $^2\Pi - {}^4\Sigma^-$ transitions rather than one $^4\Pi - {}^4\Sigma^-$ transition were present in the spectra (figure 5.22). The 638.2 and 625.9 nm bands belong to one transition labeled $[15.8]^2\Pi_\Omega - {}^4\Sigma^-$ and the 629.9 and 618.3 nm belong to a second transition labeled $[16.0]^2\Pi_\Omega - {}^4\Sigma^-$. The labels used to differentiate the two transitions are merely their respective band origins reduced by 10^3 cm^{-1}. A rotational energy level diagram for a $^2\Pi - {}^4\Sigma^-$ transition with expected branches and first rotational lines is given in figure 5.21.

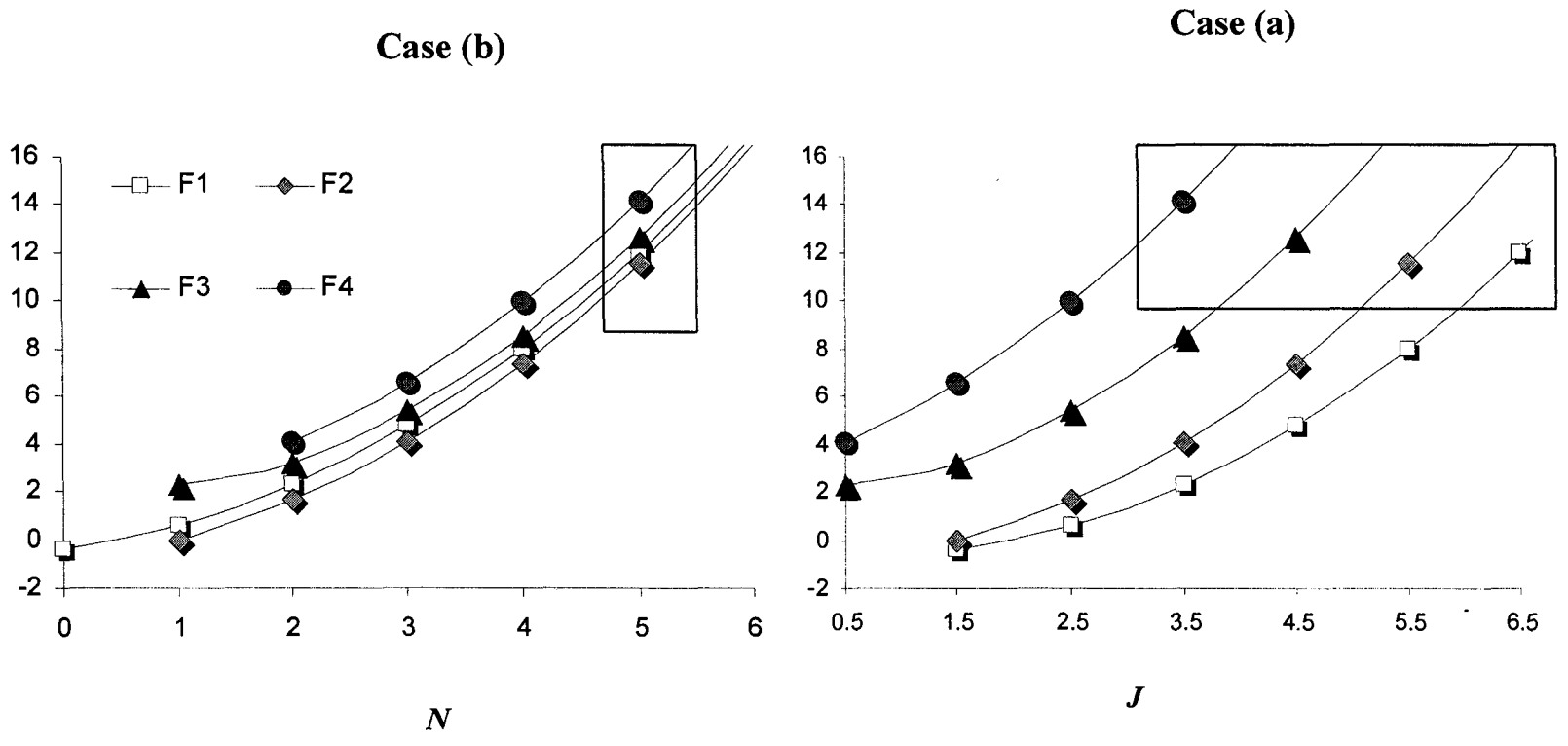

Figure 5.20 First few rotational term values (cm^{-1}) for the ground state using both case (b) and case (a) label systems. J=N+1.5, J=N+0.5, J=N-0.5 and J=N-1.5 for the F_1, F_2, F_3 and F_4 levels respectively. The same data points appear in the squares to emphasize the difference between labels since each is drawn around. The y axes represent the rotational energy levels of the ground state in wavenumbers / cm^{-1}.

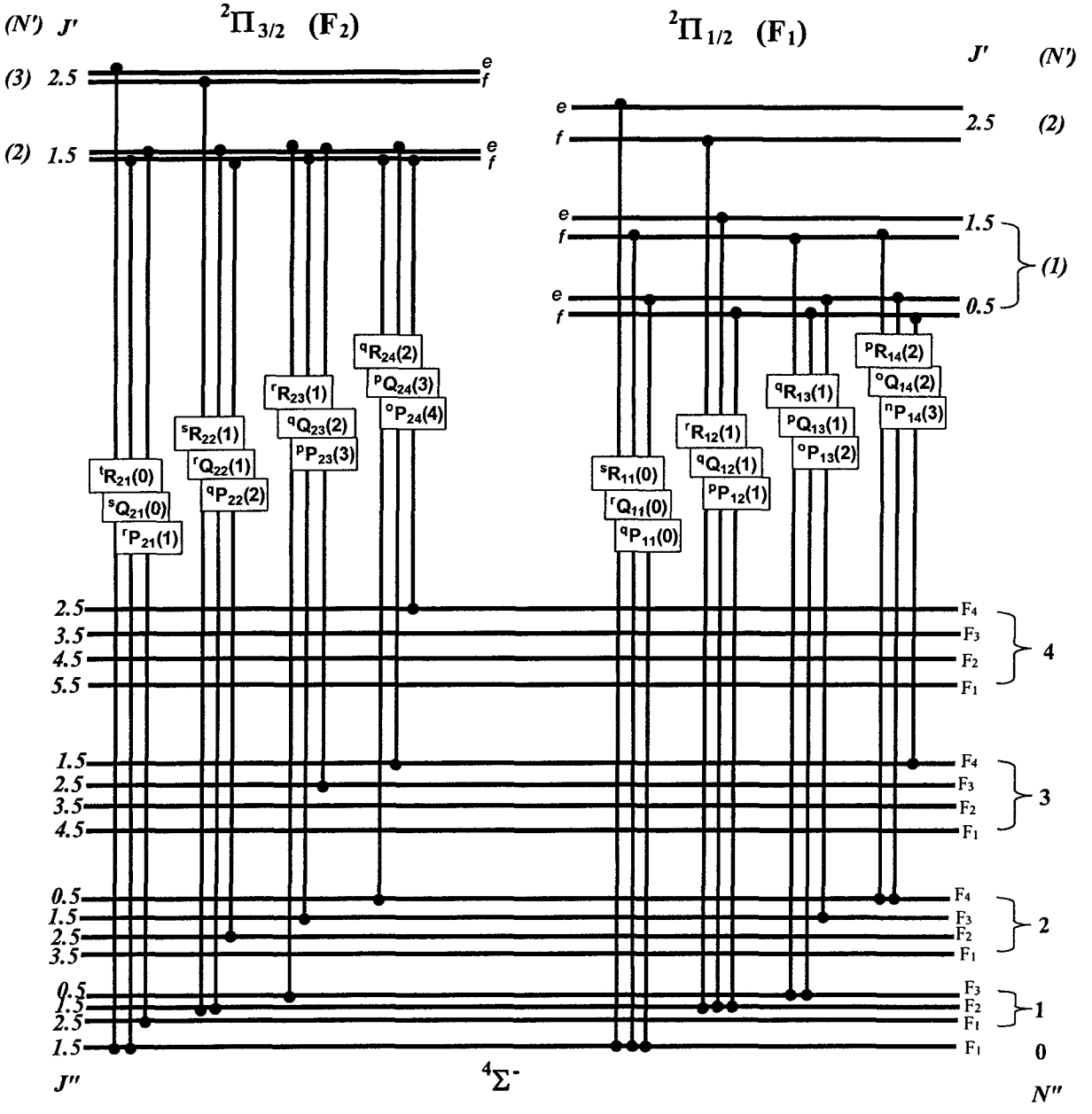

Figure 5.21 Energy level diagram for a $^2\Pi - ^4\Sigma^-$ transition. The branches are labeled using both ΔJ and ΔN. The value for N of the expected first rotational lines are indicated in parenthesis. The energy levels are not drawn to scale as the difference between the upper and lower state is 1000s of cm^{-1}, while the difference between rotational levels is only a few cm^{-1} at most.

The difference between these assignments is extremely subtle; essentially nothing changes in the rotational analysis except the explicit branch labels (which were not being used anyway) and the interpretation of the spin-orbit coupling irregularity (see figure 5.22 below). Supporting evidence for this assignment is found in the decay profiles and the relative intensities of the LIF signals for the four (0,0) bands (figure 5.5). The signal intensity is considerably weaker for the two bands at 638.2 and 625.9 nm than for the two bands at 629.9 and 618.3 nm. Also the calculated lifetimes are longer (1600 and 1000 ns) for the weaker bands compared to 900 and 500 ns for the stronger bands (31).The two $^2\Pi$ states are regular Hund's case (a) with spin-orbit splitting of roughly 300 cm^{-1} for each.

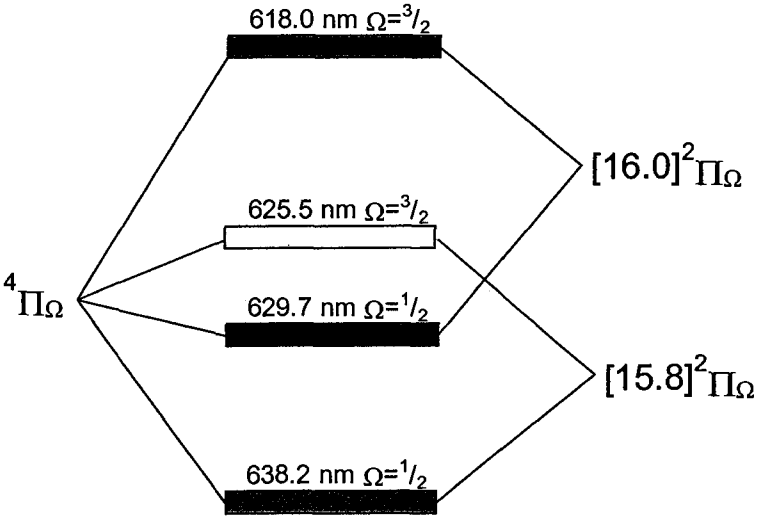

Figure 5.22 Reassignment of the four 0,0 bands of $Rh^{16}O$ to reflect the fact that two spin-forbidden transitions of type $^2\Pi - ^4\Sigma^-$ have been observed instead of one $^4\Pi - ^4\Sigma^-$ transition. The observed energy levels have been drawn to scale.

Doublet-quartet intersystem crossing for transition metal containing species has been reported for GeH (32), NbO (33) as well as for the rhodium atom itself (2). Relativistic effects leading to intersystem crossing between potential curves may cause the observed phosphorescent emission.

The reassignment of the upper states did not affect the rotational analysis of the bands since they had been analyzed individually (a decision made because of the irregularity and relatively large magnitude of the splitting of the spin-orbit splitting). The rotational constants determined are therefore the same whether the upper state is a $^2\Pi$ or a $^4\Pi$ state. Excited state energy levels (determined using transition line data and ground state energy levels calculated using the spectroscopic constants of table 5.3) were fitted. using least squares fitting to the $^{2S+1}\Pi_\Omega$ energy level expression of formulae [70].

Table 5.4 Results of the rotational analysis of the high resolution data (in units of cm^{-1}).

Band / nm	$^2\Pi_{1/2}$ **638.3**	$^2\Pi_{1/2}$ **629.9**	$^2\Pi_{3/2}$ **625.9**	$^2\Pi_{3/2}$ **618.0 main**	$^2\Pi_{1/2}$ **618.0 minor**	$^2\Pi_{1/2}$ **607.9**
T_Ω	15666.933(6)	15874.078(6)	15975.971(4)	16167.480(9)	16176.538(6)	16445.459(4)
B_v	0.377825(10)	0.38270(4)	0.36832(10)	0.38302(3)	0.39324(14)	0.36877(7)
$10^5 D$	0.05(2)	---	---	1.15(6)	---	---
p_Ω	-0.8917(10)	0.0976(13)	---	---	-0.6394(18)	0.0496(13)
$10^5 p_{\Omega,J}$	-5.7(7)	---	---	76(2)	-80(4)	---
std dev	0.0075	0.0062	0.0065	0.0100	0.0085	0.0074
r / nm	0.1795	0.1784	0.1818	0.1783	1.78E-10	1.82E-10
τ / ns	1600	900	1000	500	---	1700
# of lines	116	71	89	97	68	77

Sixteen bands of $Rh^{16}O$ (spectra appear in Appendix III) were spectroscopically characterized, all with the $\upsilon = 0$ ground state energy level in common. Parameters were kept to a desired minimum during the analysis, and only introduced if a visible decrease (>15%) in the overall standard deviation resulted. Results are given in table 5.5 of the analysis done on a band to band basis. In some cases (the upper states of the LIF bands at 618.3, 573.5, 553.3, 546.1 and 544.6 nm), a separate set of rotational constants was required for the *e* and *f* levels, indicating that perturbations are present at higher *J*. The need to characterize the *e* and *f* levels separately did not manifest, during the analysis of the high resolution data, (most probably due to the low *J* limit of this data set).

A local perturbation in the LIF spectra of the band at 588.7 is obvious around $J = 15$ (figure 5.23) producing a much larger standard deviation ($\sigma = 1.58$ cm^{-1}) for the excited state energy residuals than for any other band (σ_{Ave} ~0.07 cm^{-1}). The LIF data was limited to about $J < 25$, except in the 618.3 and 629.7 nm bands where some branches could be extended using the Stockholm data. The high *J* data were harder to fit however due to **L** and **S** uncoupling not uncommon at higher rotational frequencies.

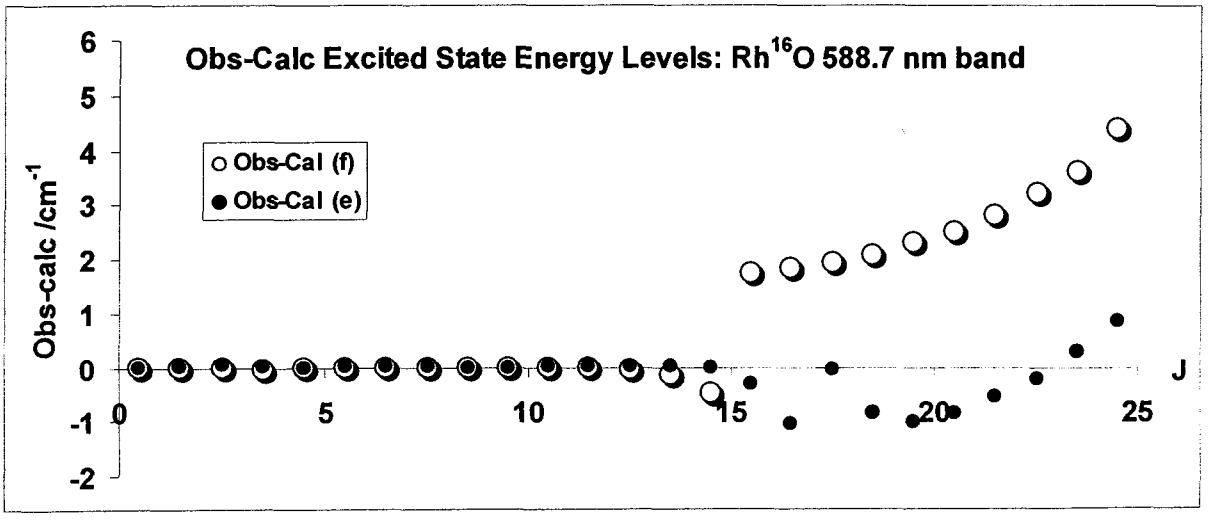

Figure 5.23 Perturbation in the 588.7 nm band of $Rh^{16}O$

Table 5.5 Results of the rotational analysis of the LIF data done band by band (units cm^{-1}).

υ',υ'' band position	0,0			
	638.2 nm	**629.7 nm**	**625.5 nm**	**618.3 nm**
Ω	$^1I_2$	$^3I_2$	$^1I_2$	$^3I_2$
ground state				
B"	**0.41257**	**0.41323**	**0.41202**	**0.41305**
D"		2.88E-07		
λ	-0.59	-0.58	-0.58	-0.58
γ	-0.103	-0.102	-0.103	-0.102
# of $\Delta_2F''_i(N)$	541	577	435	531
σ	0.059	0.070	0.057	0.054
upper state				(e) (f)
B'	**0.37700**	**0.38252**	**0.36699**	**0.36983** **0.38602**
D'				
p_Ω	-0.891	0.100	0.001	0.194 -0.017
$p_{\Omega J}$	-7.88E-05	4.64E-05	6.47E-06	
H		1.0E-11		
(T_Ω+C)	**15666.95**	**15874.07**	**15975.99**	**16167.27** **16167.40**
# of transition lines	255	352	204	293
# of (e/f) Levels	49	121	46	69
σ	0.025	0.039	0.036	0.047

υ',υ'' band position	1,0			
	607.9 nm	**598.1nm**	**594.3 nm**	**588.7 nm***
Ω	$^1I_2$	$^3I_2$	$^1I_2$	$^3I_2$
ground state				
B"	**0.41255**	**0.41353**	**0.41344**	**0.41388**
D"				
λ	-0.58	-0.59	-0.58	-0.58
γ	-0.103	-0.103	-0.100	-0.103
# of $\Delta_2F''_i(N)$	439	174	416	398
σ	0.056	0.053	0.082	0.049
upper state				
B'	**0.36831**	**0.38434**	**0.37958**	**0.39577**
D'				9.41E-06
p_Ω	0.051	-0.797	-0.697	
$p_{\Omega J}$	2.46E-07	-3.63E-05	5.90E-05	
H				
(T_Ω+C)	**16445.45**	**16715.20**	**16819.81**	**16977.83**
# of transition lines	201	107	202	207
# of (e/f) Levels	42	31	44	55
σ	0.026	0.020	0.047	1.580

** This band is perturbed above J = 15 resulting in a much higher standard deviation for the excited state energy levels.*

Table 5.5 continued...

υ',υ'' band position	2,0				
	584.1 nm	573.5 nm		569.3 nm	561.9 nm
Ω	$^1I_2$	$^3I_2$		$^1I_2$	$^3I_2$
ground state					
B''	**0.41564**	**0.41141**		**0.41415**	**0.41406**
D''	1.83E-06				
λ	-0.58	-0.57		-0.58	-0.58
γ	-0.101	-0.100		-0.104	-0.102
# of $\Delta_2F''_i(N)$	434	386		403	482
σ	0.071	0.088		0.077	0.069
upper state		(e)	(f)		
B'	**0.36839**	**0.34979**	**0.30483**	**0.38373**	**0.39107**
D'		1.60E-05	9.10E-05	3.91E-06	2.84E-06
p_Ω	0.127	-0.692	-0.916	-1.100	
$p_{\Omega J}$	-4.65E-05	-3.04E-03	8.35E-03	5.04E-04	
H		-2.5E-08			
(T_Ω+C)	**17116.99**	**17434.91**	**17432.08**	**17560.84**	**17780.27**
# of transition lines	217	183		211	235
# of (e/f) Levels	54	39		46	48
σ	0.051	0.045		0.072	0.041

υ',υ'' band position	3,0						
	553.3 nm		546.1 nm		544.6 nm		539.8nm
Ω	$^1I_2$		$^1I_2$		$^3I_2$		$^3I_2$
ground state							
B''	**0.41256**		**0.41226**		**0.41179**		**0.41289**
D''	1.00E-07						
λ	-0.59		-0.58		-0.57		-0.58
γ	-0.101		-0.103		-0.108		-0.102
# of $\Delta_2F''_i(N)$	323		372		323		246
σ	0.079		0.089		0.071		0.088
upper state	(e)	(f)	(e)	(f)	(e)	(f)	
B'	**0.36159**	**0.36477**	**0.35010**	**0.41626**	**0.32079**	**0.32600**	**0.37015**
D'							
p_Ω	-1.068	-0.315	-0.081	0.050	-0.012	-0.918	0.162
$p_{\Omega J}$	-2.91E-04	1.51E-04	-7.16E-04	-2.76E-03	-4.46E-03	1.72E-03	2.06E-04
H							
(T_Ω+C)	**18061.61**	**18061.52**	**18268.66**	**18268.10**	**18356.78**	**18356.51**	**18569.23**
# of transition lines	173		185		158		118
# of (e/f) Levels	46		39		33		28
σ	0.056		0.055		0.050		0.076

** These bands are obviously perturbed as can be seen by the difference in the rotational constants obtained for the e/f levels.*

Fortrat parabolas in figure 5.24, plot the observed transition lines (in units of cm^{-1}) against the quantum number used to label the lines (*N*, in the case of the $X^4\Sigma^-$ ground state).The branch structure for the bands at 629.7 nm and 618.0/618.3 nm, are revealed in figure 5.24. Close inspection of the branch structure in all the bands analyzed reveals subtle differences between the relative positions of the first rotational lines, due to the extent and sign of the lambda doubling in the excited state.

Two Λ-doubling terms, p_Ω and $p_{\Omega J}$, have been included in the energy level expression of equation [70] to "empirically" characterize the upper state Λ-doubling, which was suspected of being complex and due to multiple interactions. Λ-doubling results from second-order perturbations between electronic states with $\Delta\Omega = 0, \pm 1$. The strongest interactions are those for which Λ and Ω change by the same amount, and so the strongest perturbations are between states with $\Delta\Lambda = \pm 1$ (5).

The observed Λ-doublings (*f-e* levels), for the first three vibrational levels of the two $^2\Pi$ states are plotted in figure 5.25. Typically, for $^2\Pi$ states, the spin-orbit component with $\Omega = {}^1/_2$ has much larger Λ-doubling, than the component with $\Omega = {}^3/_2$ (7). However, most of the bands analyzed show negligible Λ-doubling, and only four bands, those at 638.2 nm ($\Omega = {}^1/_2$), 598.1 nm ($\Omega = {}^1/_2$), 594.3 nm ($\Omega = {}^3/_2$) and 569.3 nm and ($\Omega = {}^3/_2$), show large, positive Λ-doubling. There is no correlation of the Λ-doubling with Ω, nor with the bands that required separate rotational constants for the *e/f* levels.

The Y axes for both graphs are transition lines in wave numbers /cm^{-1}.

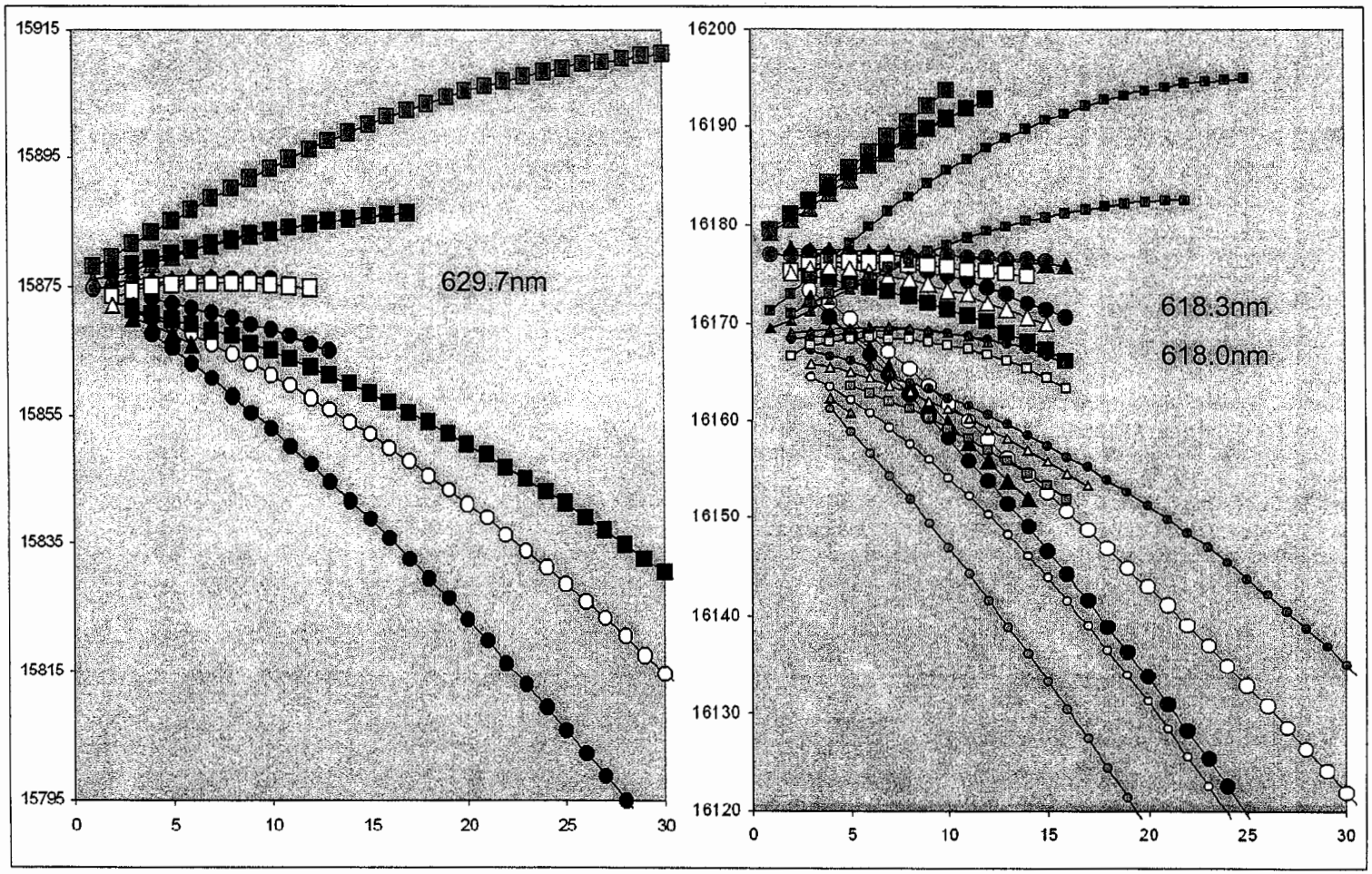

Rotational assignment N

Figure 5.24 Fortrat parabolas showing transition lines (y-axis, in units of cm^{-1}) against N, the rotational quantum number used to label them. Shown here are the transition lines for the 629.7, 618.0 and 618.3

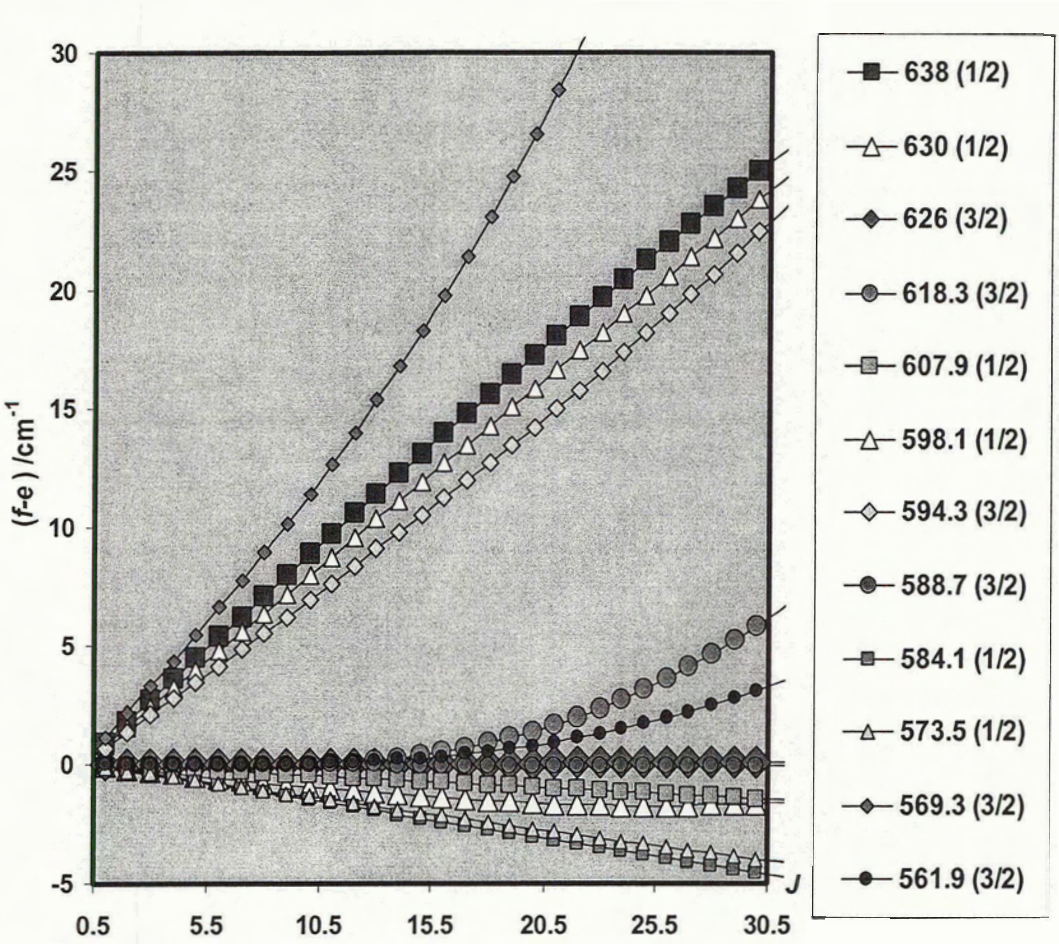

Figure 5.25 Λ-doubling (f-e) in the upper states of the $Rh^{16}O$ bands may be grouped into two types: small (positive/negative) and large (positive). Values for Ω are given in parenthesis.

Since only three branches, the R_1, R_2 and Q_1, appear in the higher energy region of the bands, they were among the first branches identified and labeled. The effect of Λ-doubling in these branches was, therefore, most noticeable. The relative positions of the $R_1(N)$ the $R_2(N+1)$ and the $Q_1(N+1)$ lines, vary depending upon the sign and relative magnitude of the lambda doubling, compared to the spin rotation-splitting in the ground state. Figure 5.26 shows the effect of the different relative values.

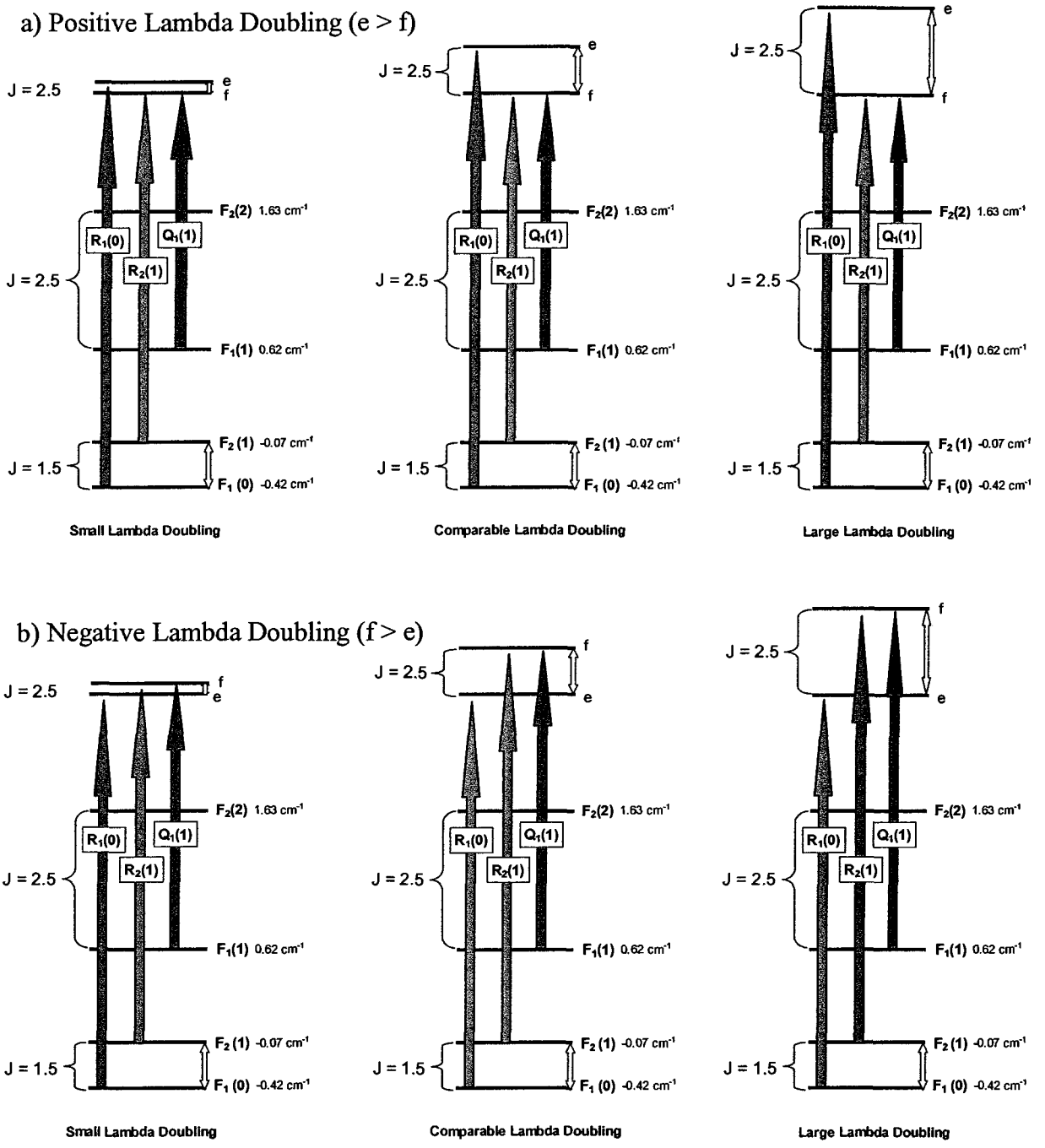

Figure 5.26 Different signs and relative magnitudes of the lambda doubling in the upper state compared to the negative spin-rotational splitting in the ground state (which is constant) creates different effects in the spectra. If the sign of the lambda doubling is positive as in the three examples of a) the e levels lie above the f levels and the $R_1(N)$ lines appears at higher energy than the $R_2(N+1)$ lines followed by the $Q_1(N+1)$lines for any magnitude of the relative splitting (yellow arrow). If the sign of the lambda doubling is negative as in b) a variety of possibilities occur depending upon the relative magnitudes of the splitting in the two states. When the lambda doubling is smaller than the spin rotation-splitting $R_1(N)$ lines appear at higher energy than $R_2(N+1)$ lines. The reverse is true if the lambda doubling is large compared to the spin rotational splitting.

The congested central region and heavily populated lower energy region of each band were deciphered almost exclusively by predicting their positions from the observed R_1 and R_2 branches, using the calculated ground state energies (34). From predicted line positions, observed peaks were found and labeled accordingly. Depending on the size and magnitude of the Λ-doubling, however, branches were often overlaid and peaks were broad or overlapped with considerable shoulder structure (see figures 5.27 and 5.28).

The lack of regularity in the Λ-doubling of the vibrational bands was not surprising. Even though the bands can be fitted to effective rotational constants, the fit does not take into account the multitude of second order (or higher) interactions between the two $^2\Pi$ states and/or the high density of doublet and quartet, Σ and Π states, calculated to be in the area of the observed transitions, especially at higher *J*. Since the vibrational progressions are irregular for the upper states and the transitions do not obey general selection rule $\Delta S = 0$, the nature of the perturbing state(s) is undetermined.

Irregularity in both the spin-orbit splitting as well as the vibrational spacing of the two band systems is noticeable in table 5.6. Considering the complexity of the spectra of $Rh^{16}O$ and the number of bands analyzed, the extent and results of the rotational analysis is already very good, encountering very few real difficulties. The analysis of the $Rh^{18}O$ bands can therefore be considered "cream on top" verifying the results already presented. The $Rh^{18}O$ spectra appear in appendix III, the transition lines in appendix V and the term values in appendix VI.

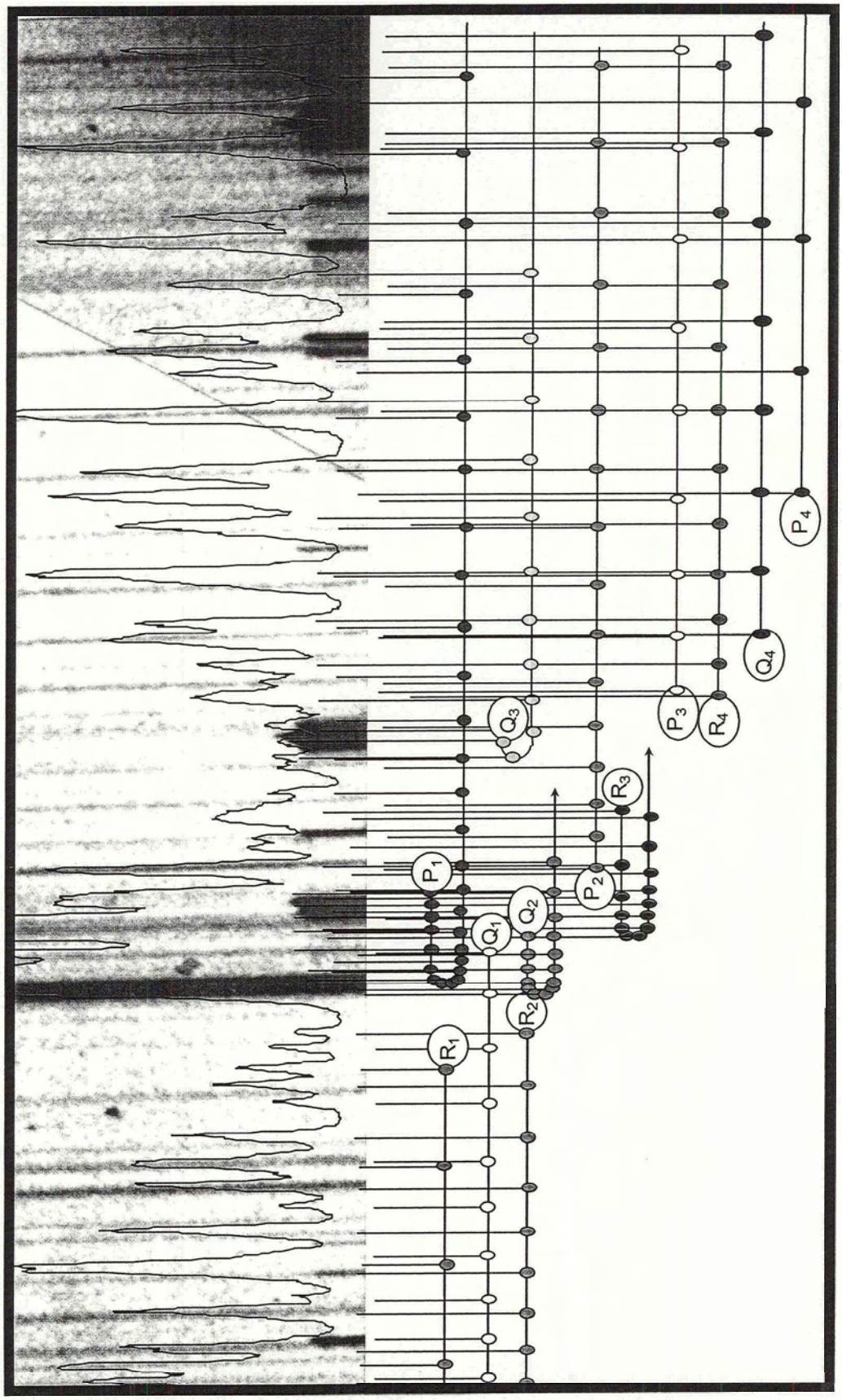

Figure 5.27 Center region of the 629.9 nm band where all 12 branches appear and are labeled using the abbreviated format.

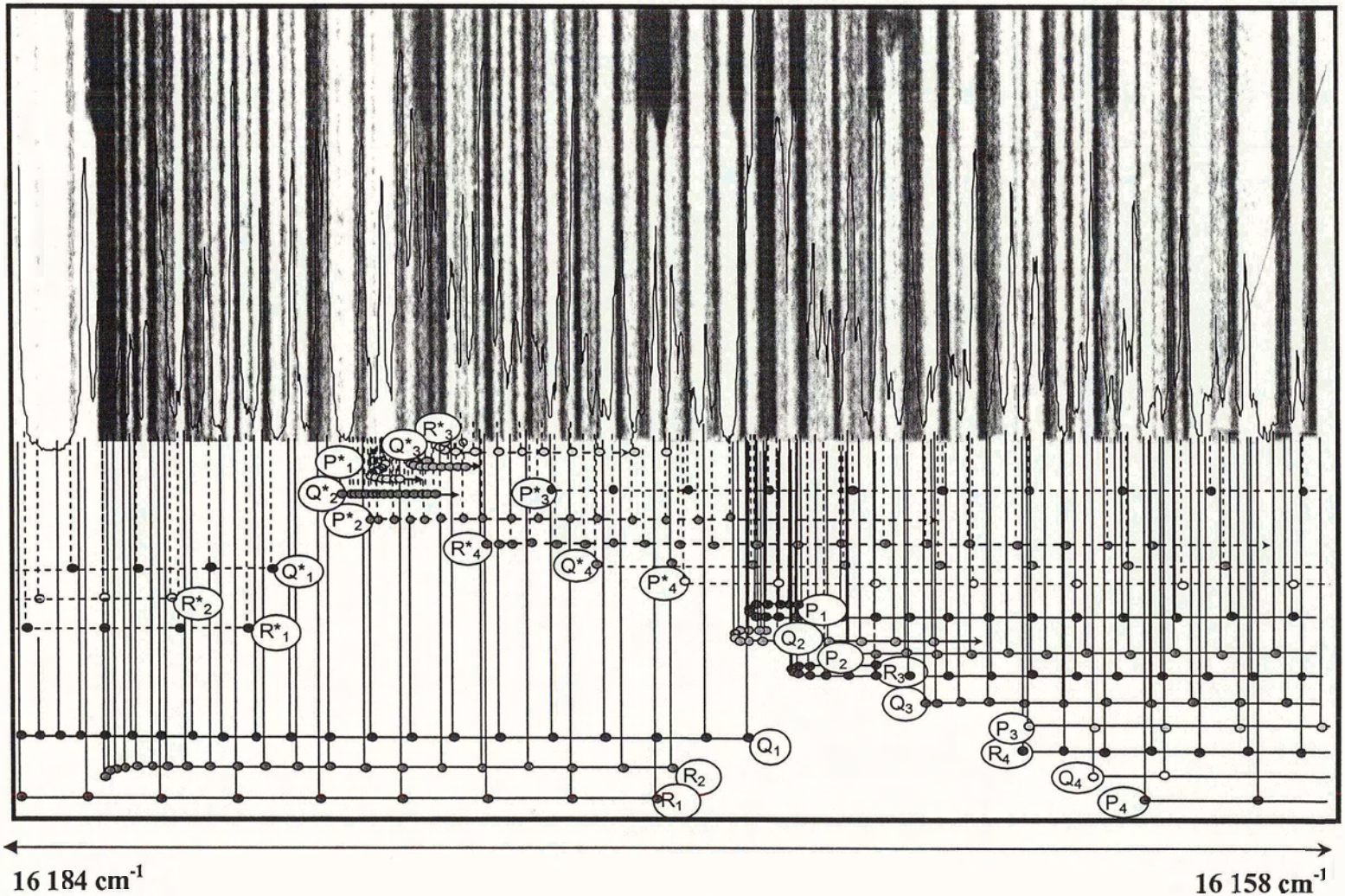

Figure 5.28 Center regions of the 618.3 (solid lines) /618.0 (dashed lines) nm bands showing the 24 labeled branches.

5.7 Rotational Analysis of the $Rh^{18}O$ Spectra

A detailed rotational analysis of the isotope-substituted molecule was not part of the initial investigation, when the spectra were being recorded. However, since many of the spectra were sufficiently resolved, it was decided that a least squares fitting would be performed, on a band-to-band basis, once the branches had been picked out and the rotational lines established. The relationship between the ground state rotational constants of $Rh^{18}O$ and $Rh^{16}O$ is given by the isotopic relation

$$B_0(Rh^{18}O) = \rho^2_{RhO} * B_0(Rh^{16}O) \qquad [75]$$

where $\rho^2_{RhO} = 0.9036$. $B_0(Rh^{16}O) = 0.4135$ cm^{-1} predicting a value of 0.3736 cm^{-1} for B_0 in the ground state, which agrees well with the observed value of 0.3712 cm^{-1}.

The observed band profiles of the $Rh^{18}O$ bands were expected to be similar to the $Rh^{16}O$ bands, since ΔB is only slightly altered. Line positions were predicted for the ground state of $Rh^{18}O$, using combination difference relations, calculated using the predicted B_0 value, with the other the rotational parameters kept constant. The spectra for $Rh^{18}O$, however, are weaker and not as well resolved as the $Rh^{16}O$ spectra. In many of the bands not all twelve branches were located. Spectroscopic parameters were determined for 11 bands with the results given in table 5.7.

A concerted rotational analysis involving over 1500 combination differences (σ = 0.095 cm^{-1}) yielded the following ground state parameters (in units of cm^{-1})

$$B_0 = 0.3712 \qquad \lambda_0 = -0.563 \qquad \gamma_0 = -0.1025$$

The values for λ_0 and γ_0 are very similar to those for $Rh^{16}O$ as expected.

Table 5.6 Band assignments for both the $Rh^{16}O$ and $Rh^{18}O$ spectra.

$Rh^{16}O$ Vibrational Assignments

	[15.8]$^2\Pi_\Omega$ - $^4\Sigma^-$		[16.0]$^2\Pi_\Omega$ - $^4\Sigma^-$		
υ',υ''	/nm	/cm^{-1}	/nm	/cm^{-1}	
0,0	638.2	15668	629.7	15877	**Ω = 1/2**
	625.5	15978	618.3	16170	**Ω = 3/2**
1,0	607.9	16447	598.1	16720	**Ω = 1/2**
	594.3	16827	588.7	16986	**Ω = 3/2**
2,0	584.1	17120	573.5	17438	**Ω = 1/2**
	569.3	17565	561.9	17797	**Ω = 3/2**
3,0	553.3	18074	546.1	18312	**Ω = 1/2**
	544.6	18362	539.8	18526	**Ω = 3/2**

$Rh^{18}O$ Vibrational Assignments

	[15.8]$^2\Pi_\Omega$ - $^4\Sigma^-$			[16.0]$^2\Pi_\Omega$ - $^4\Sigma^-$			
υ',υ''	/nm	/cm^{-1}	shift	/nm	/cm^{-1}	shift	
0,0	638.2	15668	-	629.7	15877	-	**Ω = 1/2**
	625.5	15978	-	618.3	16170	-	**Ω = 3/2**
1,0	608.9	16427	20	599.4	16684	36	**Ω = 1/2**
	595.7	16788	39	590.0	16948	38	**Ω = 3/2**
2,0	586.1	17062	58	575.1	17389	49	**Ω = 1/2**
	571.6	17495	70	564.3	17721	76	**Ω = 3/2**

Table 5.7 Rotational analysis results for the $Rh^{18}O$ bands analyzed (in units of cm^{-1})

υ',υ''	0,0			
band position	638.2 nm	629.7 nm	625.5 nm	618.3 nm
Ω	$^1I_2$	$^3I_2$	$^1I_2$	$^3I_2$
ground state				
B''	**0.37141**	**0.37043**	**0.37198**	**0.37033**
D''				
λ	-0.57	-0.56	-0.56	-0.58
γ	-0.107	-0.111	-0.098	-0.102
# of $\Delta_2F''_i(N)$	157	186	108	80
σ	0.100	0.076	0.107	0.089
upper state				
B'	**0.33843**	**0.34191**	**0.33653**	(e) **0.33256**
D'				
p_Ω	-0.777	0.066	0.153	0.028
$p_{\Omega,J}$	3.35E-04	4.00E-05	1.86E-03	2.01E-03
H			7.0E-08	
$(T_\Omega+C)$	**15674.15**	**15878.08**	**15950.71**	**16168.58**
# of transition lines	86	103	62	61
# of (e/f) Levels	20	35	21	26
σ	0.051	0.038	0.061	0.099

υ',υ''	1,0			
band position	608.9 nm	599.4nm	595.7 nm	590.0 nm
Ω	$^1I_2$	$^3I_2$	$^1I_2$	$^3I_2$
ground state				
B''	**0.37310**	**0.37028**	**0.37075**	**0.37149**
D''				
λ	-0.57	-0.57	-0.54	-0.55
γ	-0.098	-0.111	-0.098	-0.102
# of $\Delta_2F''_i(N)$	138	182	383	284
σ	0.076	0.081	0.079	0.047
upper state				
B'	**0.33293**	**0.34243**	**0.33926**	**0.35485**
D'				
p_Ω	0.052	-0.721	-0.529	0.002
$p_{\Omega,J}$			4.73E-05	4.98E-05
H				
$(T_\Omega+C)$	**16421.54**	**16682.38**	**16786.37**	**16945.42**
# of transition lines	105	112	184	144
# of (e/f) Levels	29	33	41	37
σ	0.023	0.042	0.034	0.023

Table 5.7 continued...

υ',υ'' band position	2,0		
	586.1 nm	**571.6 nm**	**564.3 nm**
Ω	$^1I_2$	$^1I_2$	$^3I_2$
ground state			
B"	**0.36846**	**0.37116**	**0.37016**
D"			
λ	-0.58	-0.55	-0.58
γ	-0.112	-0.104	-0.107
# of $\Delta_2F''_i(N)$	76	33	49
σ	0.061	0.042	0.070
upper state			
B'	**0.32507**	**0.31226**	**0.34626**
D'			
p_Ω	0.107	-0.343	0.173
$p_{\Omega,J}$	-2.55E-05	-8.31E-04	1.03E-03
H			
(T_Ω+C)	**17060.65**	**17493.92**	**17711.66**
# of transition lines	66	46	51
# of (e/f) Levels	30	19	24
σ	0.042	0.078	0.065

The 575.1 nm band was not rotationally analyzed due to the poor quality of the spectrum.

The results in table 5.7 are effective parameters only, describing the observables on a band–to–band basis. The vibrational spacing is irregular as with $Rh^{16}O$, and the Λ-doubling is also irregular, but consistent with the results of the $Rh^{16}O$ band. None of the $Rh^{18}O$ excited states required separate rotational constants for the *e/f* levels, in contrast to many of the $Rh^{16}O$ bands. This is probably due to the fact that only low *J* data were available for the $Rh^{18}O$ analysis. This is analogous to the analysis of the high resolution data, which also did not need separate rotational parameters for the e/f levels. The Λ-doubling for the $Rh^{18}O$ bands analyzed are given in figure 5.29. Similar type doublings exist for the comparative bands of the two isotopomers. The term values for the upper states of $Rh^{16}O$ and $Rh^{18}O$ are plotted in figures 5.30 and 5.31.

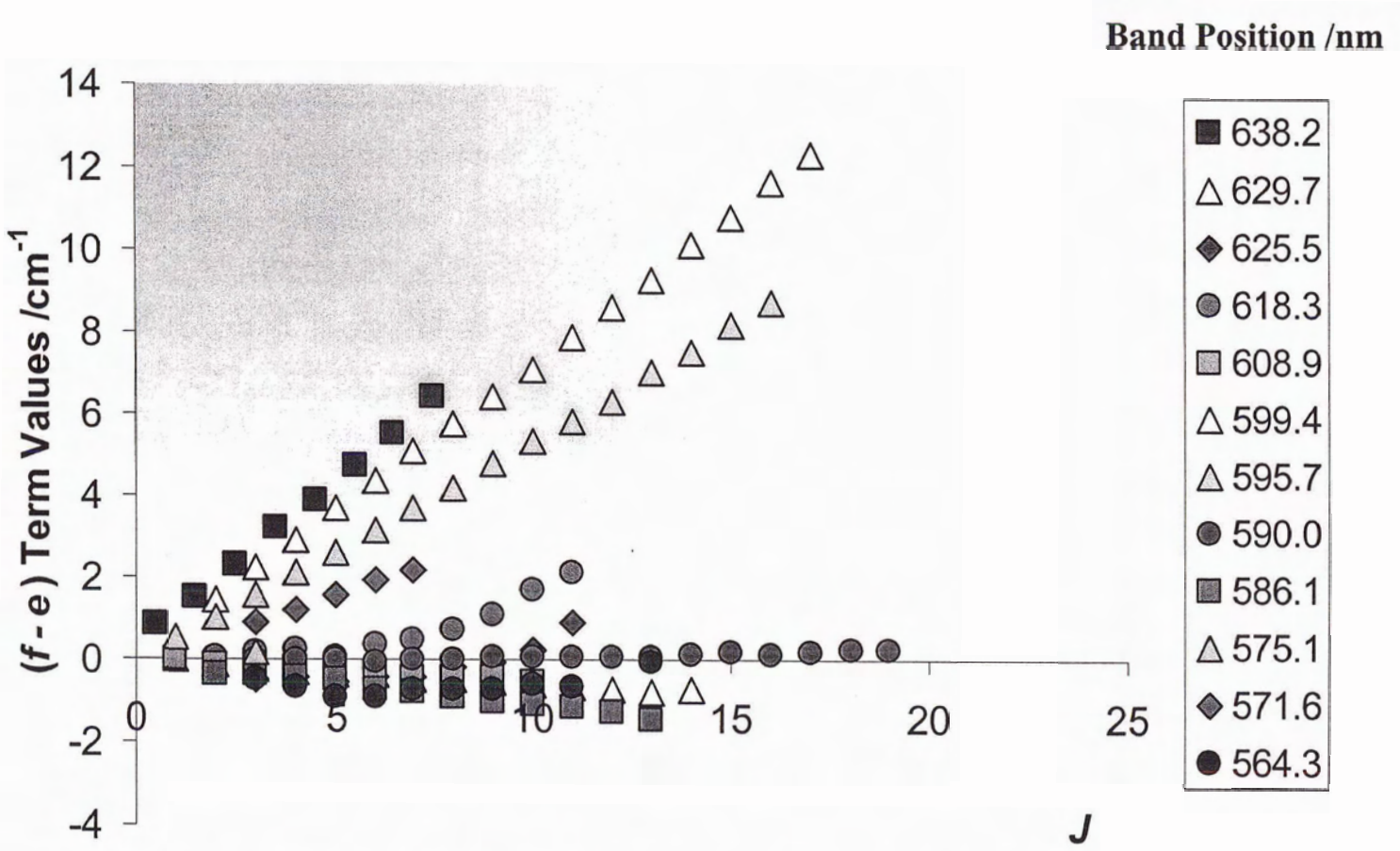

Figure 5.29 Λ-doubling in the analyzed $Rh^{18}O$ bands. The same bands in the $Rh^{16}O$ spectra show the large positive Λ-doubling (compare to figure 5.25).

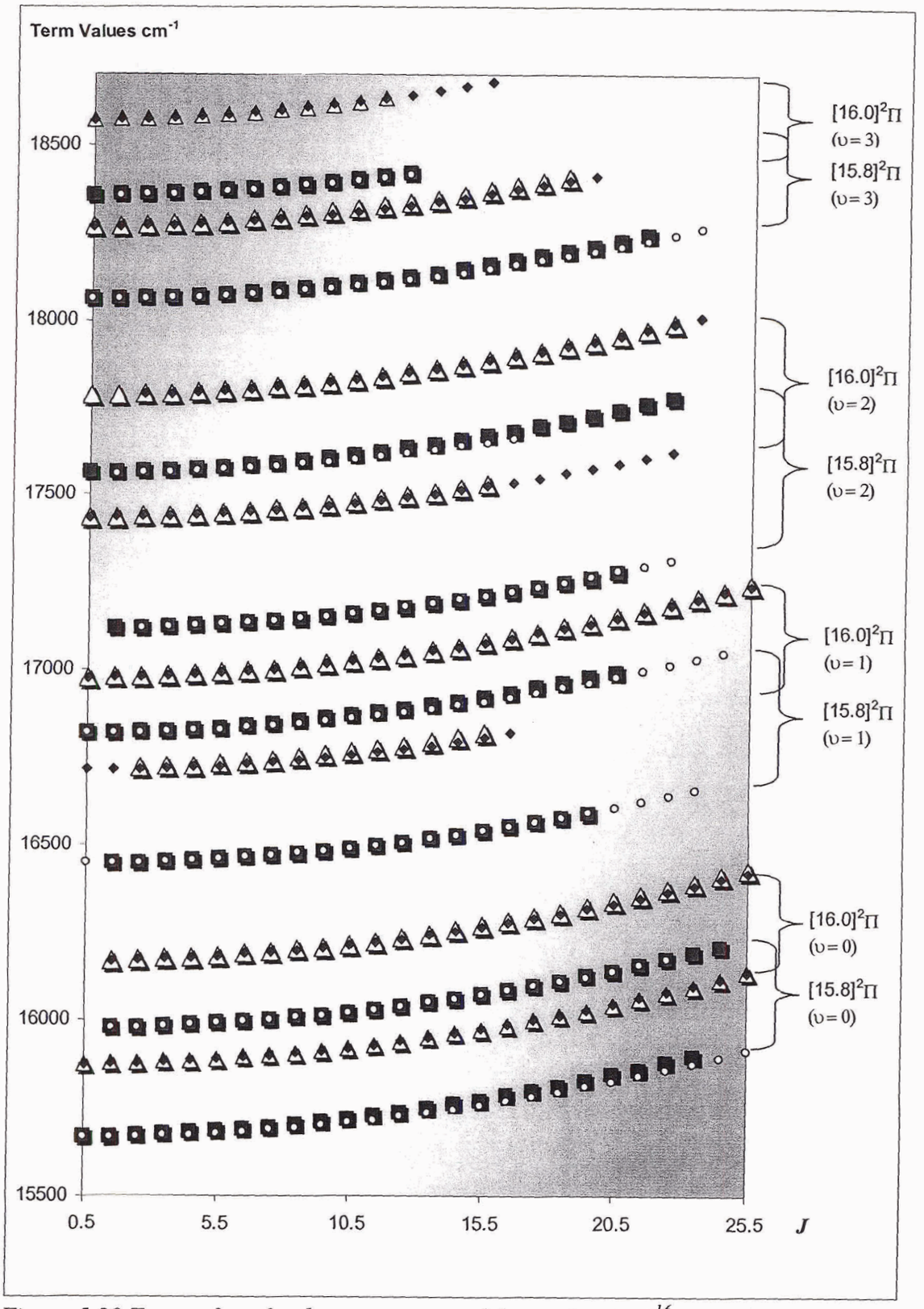

Figure 5.30 Term values for the upper states of the analyzed $Rh^{16}O$ bands. The [16.0] bands have e levels (small blue diamonds) and f levels (large white triangles). The [15.8] bands have e levels (small white circles) and f levels (large red squares).

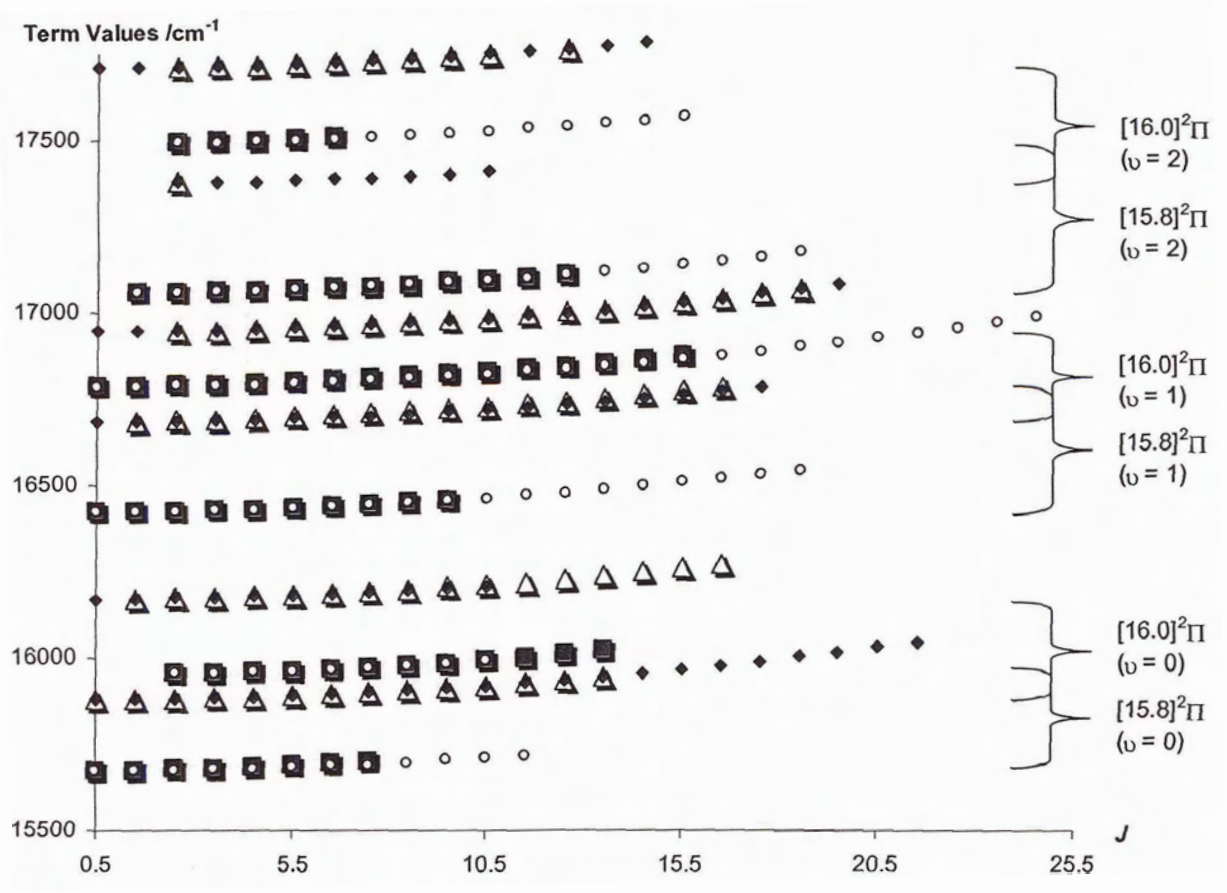

Figure 5.31 Term values for the upper states of the analyzed $Rh^{18}O$ bands. The [16.0] bands have e levels (small blue diamonds) and f levels (large white triangles). The [15.8] bands have e levels (small white circles) and f levels (large red squares).

5.8 Molecular Orbital Considerations

The 12σ orbital of RhO is considered to be basically a metallic 5*s* orbital and essentially non-bonding in character. Hyperfine results indicate the occupancy of the 12σ orbital in the …$6\pi^2 12\sigma$ leading electronic configuration of the $^4\Sigma^-$ ground state to be about 50%. A $\pi^2\sigma$ configuration also produces a $^2\Delta$ and two $^2\Sigma$ states however none are expected to be low lying in energy. The observed transitions in the RhO spectra are to

two $^2\Pi$ regular states indicating that the electronic sub-shell is less than half-filled. Since no hyperfine splitting is observed in the excited states, the electronic configurations must have no unpaired σ electrons. Electronic configurations with σ^0, σ^2 and π^1 occupancy are required. If a $\ldots 6\pi 12\sigma^2$ is chosen, this would imply that the 6π orbital is lower in energy than the 12σ orbital in RhO which is not how figure 5.32 depicts these orbitals. Since both orbitals are incomplete it is safe to assume they lie so close in energy that a transition (with an accompanying spin flip) would occur in the infrared and not the visible region of the spectrum, making the $\ldots 6\pi 12\sigma^2$ configuration an unlikely candidate.

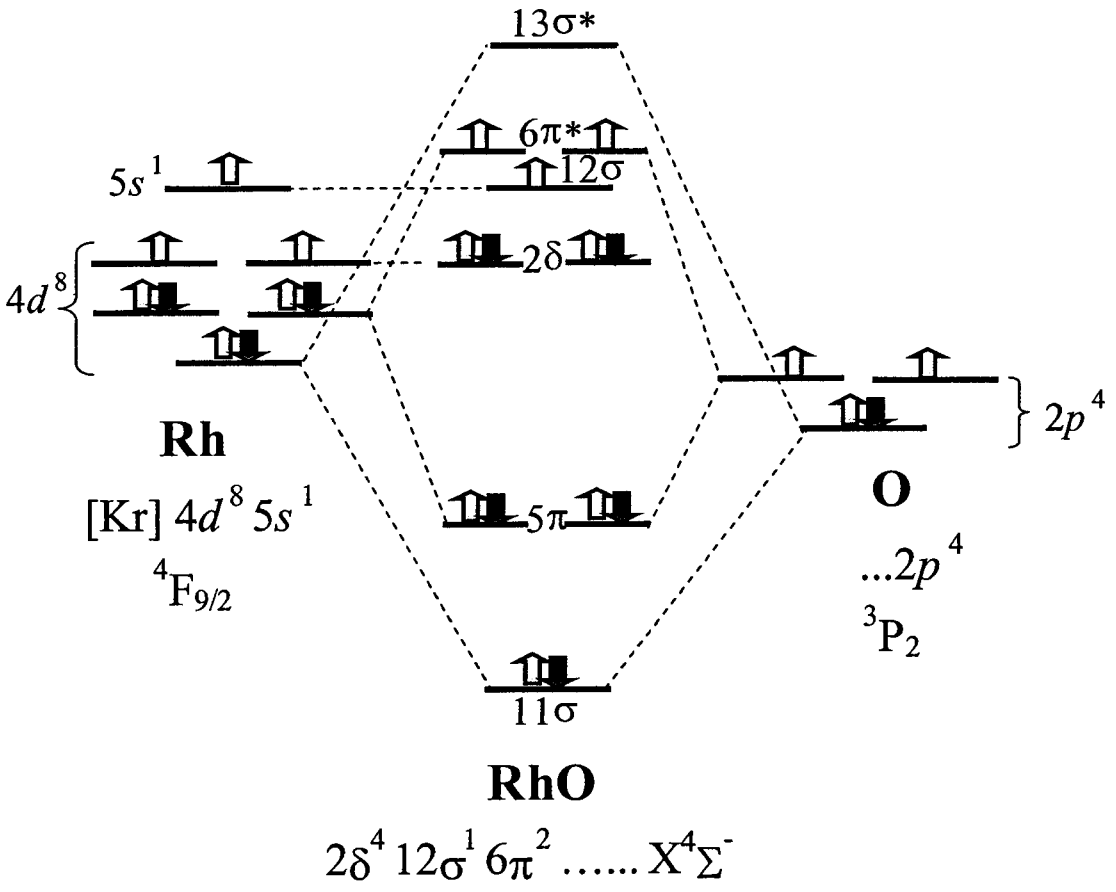

Figure 5.32 Single configuration analysis and molecular orbital/ valence diagram for RhO. There is no $^2\Pi_r$ state available from a $\pi^2\sigma$ electronic configuration. The energies of the 6π and 12σ are very close and their relative orderings unknown.*

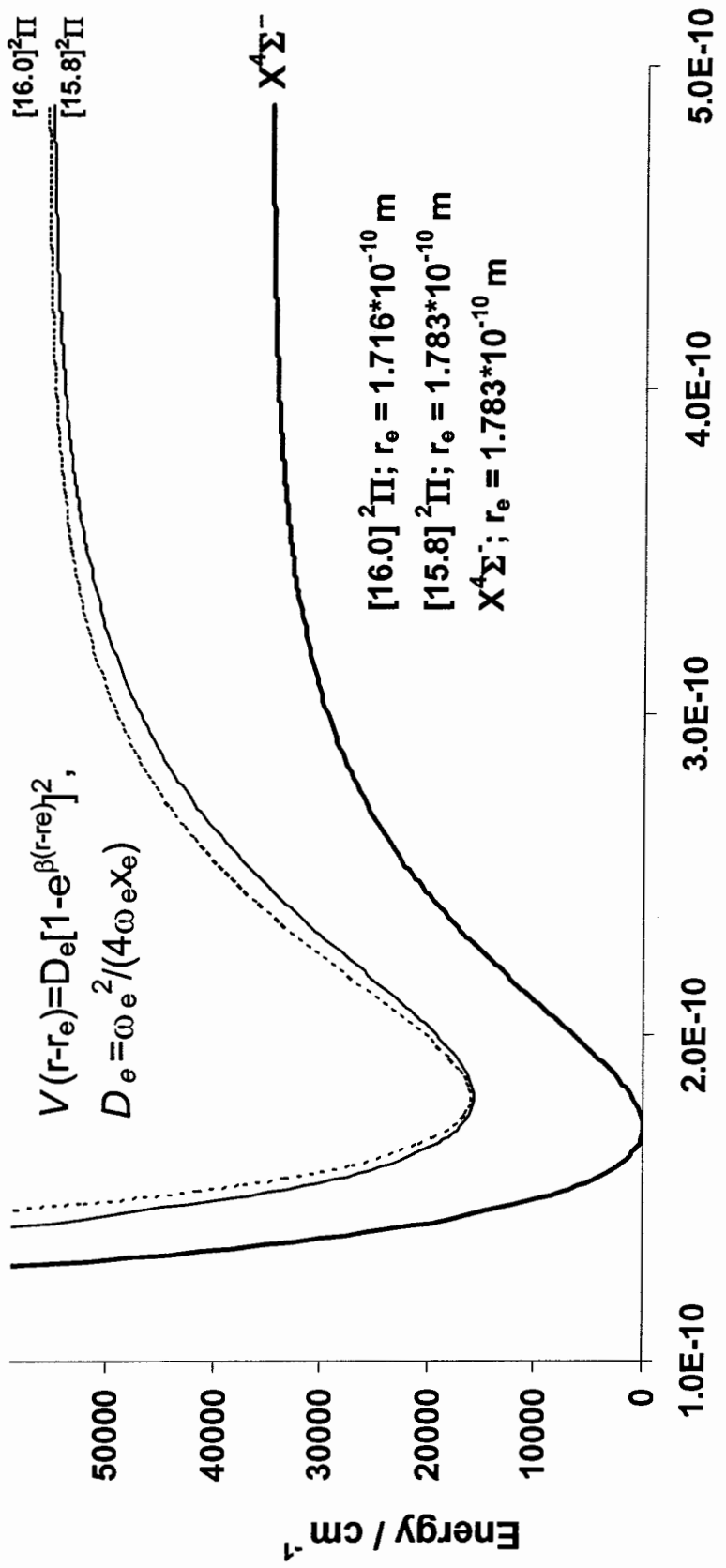

Figure 5.33 Potential curve approximations for the observed states of RhO.

The promotion of an electron from the 6π to the 12σ orbital, however, is possible-twice, and each configuration does give one state only, each of $^2\Pi_r$ symmetry. In such a case, one would expect the spin-orbit splitting to be approximately equal to the rhodium 4*d* atomic value of 1253 cm^{-1} (34). The observed splitting however is only ~300 cm^{-1}. In CoO (11) the ground state has been determined to be a $^4\Delta_i$ state arising from a $\ldots\sigma^2\delta^3\pi^2$ configuration which is lower in energy than the $\ldots\sigma\delta^4\pi^2$ configuration which leads to a $^4\Sigma^-$ state. The ground state of IrO is as yet undetermined (34). Morse potentials derived from ground and excited states molecular constants are shown in figure 5.33.

The molecular orbital diagrams for RhC through RhF are given in figure 5.34 with the electronic ground states and leading electron configurations. As the electro-negativity of the ligand atom increases, the energies of the ligand-sensitive σ and π orbitals decrease. The $\ldots6\pi^3 12\sigma$ ground state configuration of RhF recently determined in our laboratory (35) seems to indicate that the 6π orbital is now lower in energy than the 12σ orbital, a reversal from the results of RhO but in keeping with the stabilizing effect of the electro-negative ligand.

In a vibrational analysis performed by Jensen (31) a value for ω_e was determined which agrees well with the value of 799 cm^{-1} derived in the matrix isolation study (29). Extrapolation of the $Rh^{16}O$ vibrational constants gave the dissociation limit using the relation $D_e = \varpi_e^2/4\omega_e x_e$ of $D_e = 36000 cm^{-1}$ which is slightly higher than Chen and Armentrout's estimate (28) of 34000 cm^{-1} from thermo-chemistry data. Potential curves calculated using spectroscopic data for RhC, RhN and RhO (figures 5.33 and 5.35) show an increase in bond length and decrease in the dissociation limit of RhO due to the 6π* double occupancy. The potential curves of RhC and RhN are nearly identical confirming

the assumption that the 12σ orbital is metal centered and essentially non-bonding. The steepness of the potential curves is dependent upon the bond strength and hence, the vibrational constant ω_e (36). The curve is plotted as a function of the displacement of the nuclei from their equilibrium positions, but no correlation between the rotational constant and the vibrational constant (or dissociation limit) can be made.

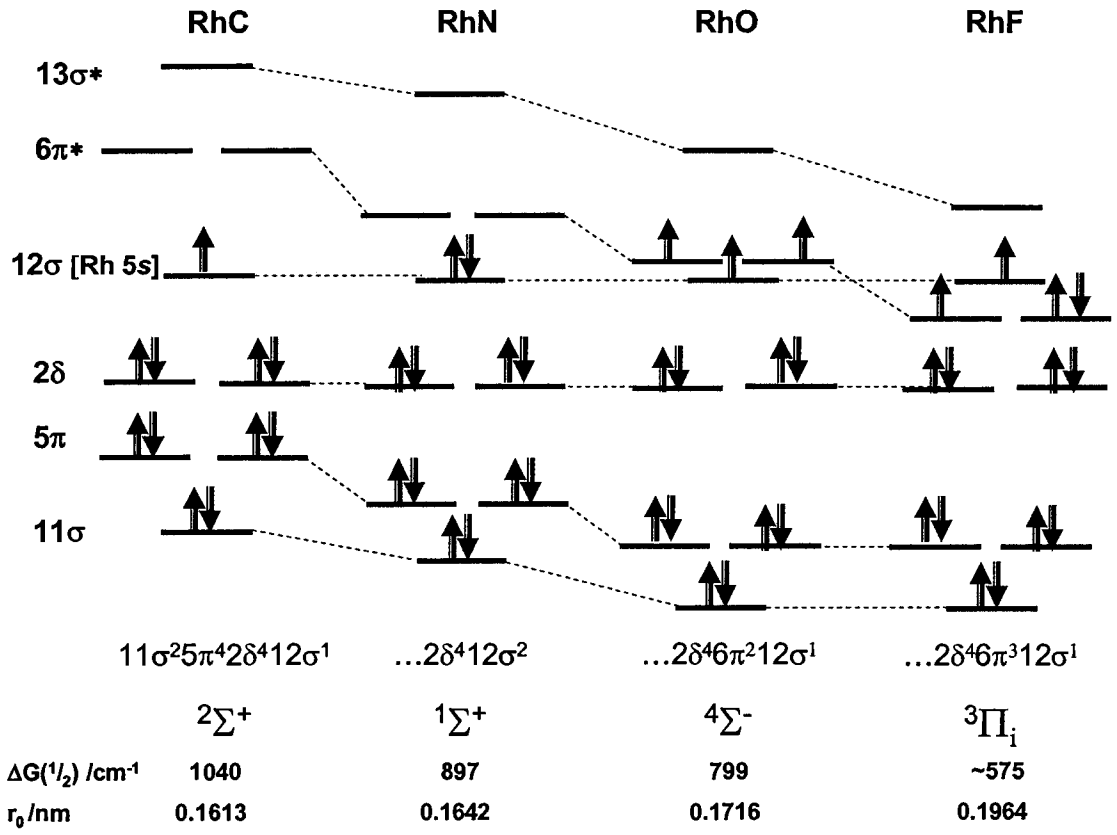

Figure 5.34 Molecular orbital diagrams for the ground states of RhC, RhN, RhO and RhF. The increase in electro-negativity going from left to right influences the relative energies of the molecular orbitals.

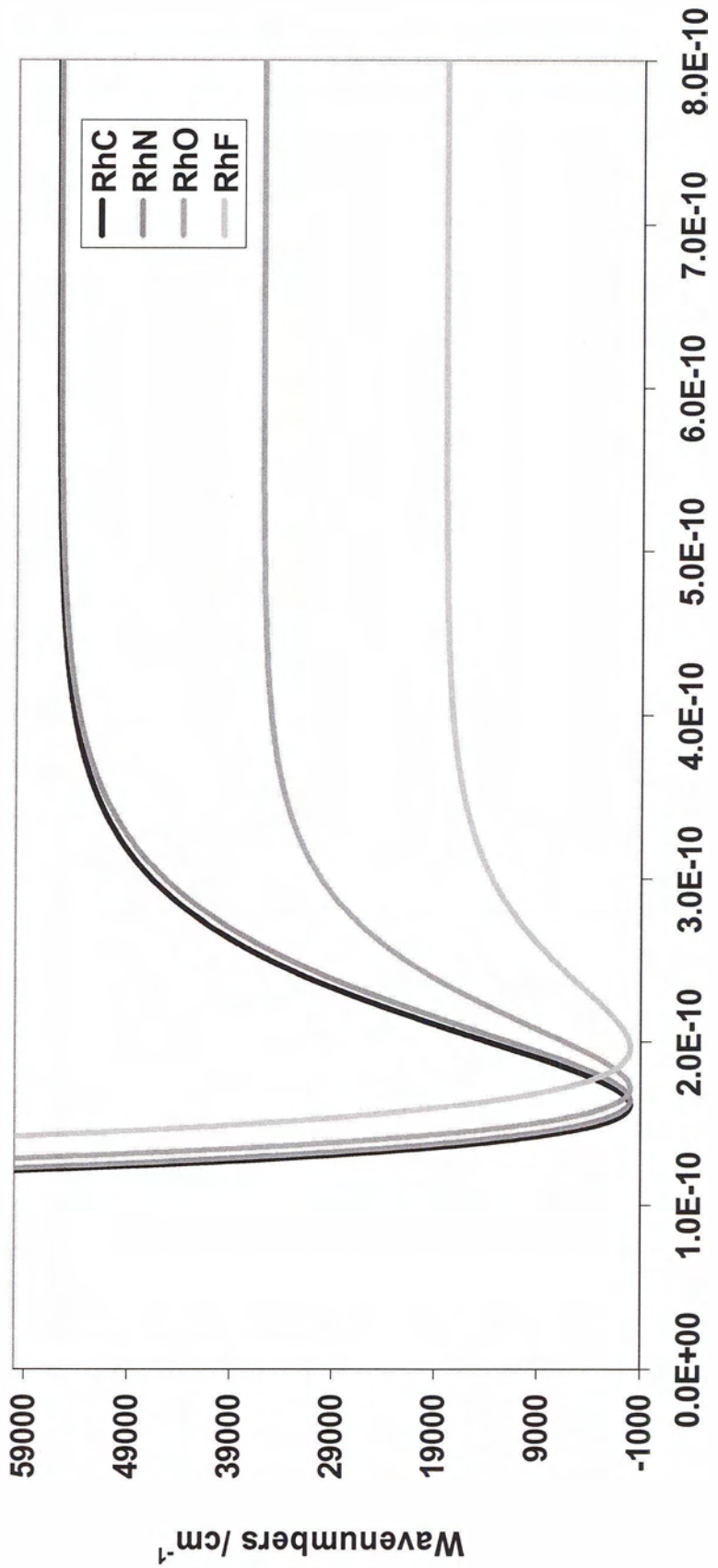

Figure 5.35 Potential curves (cm^{-1}) calculated from the spectroscopic data of RhC, RhN, RhO and RhF.

Chapter 6
Concluding Remarks

The relative energies of the n*s* and (n-1)*d* orbitals in transition metals are very close allowing for diversity in molecular bonding and giving rise to their well known reactivity. There are a few instances, however, in which the metal electrons do not occupy the predicted atomic orbitals, rhodium being one, with its [Kr] $5s^1\ 4d^8$ ground state electronic configuration. Cobalt and iridium, above and below rhodium in the periodic table, however, obey the normal occupancy rules of the *aufbau* principle, having electronic configurations of [Ar] $4s^2\ 3d^7$ and [Xe] $6s^2\ 5d^7$, respectively. Nevertheless, all three metal atoms have the same $^4F_{9/2}$ electronic ground state, despite this slight difference in their valence electron arrangement and the presence of 4*f* electrons in iridium.

The electronic ground state of rhodium carbide (RhC) was established by Lagerqvist and Scullman (14) to be of $^2\Sigma^+$ symmetry, arising from a $\ldots 11\sigma^2\ 5\pi^4\ 2\delta^4\ 12\sigma^1$ molecular orbital configuration. The 5π and 11σ electrons are bonding. The 4δ electrons, however, are essentially rhodium 4*d* orbitals and are generally considered to be non-bonding. The 12σ electron, thought to be predominantly a rhodium atomic 5*s* electron, is essentially non-bonding in character as well. The bond order for ground state RhC is, therefore, approximately $2^1/_2$, and the bond length is 0.1614 nm.

Iso-valent cobalt carbide (CoC) has a $\ldots 3\pi^4\ 1\delta^4\ 9\sigma^1$ ($^2\Sigma^+$) electronic ground state with a similar bond length to RhC, of 0.1612 nm. Iridium carbide (IrC), on the other hand has a $^2\Delta_i$ electronic ground state, arising from a $\ldots 8\pi^4\ 4\delta^3 16\sigma^2$ molecular orbital

configuration. This would indicate that the 16σ orbital, which is essentially the iridium 6*s* atomic orbital, is lower in energy than the non-bonding 4δ orbitals. This is different from CoC and RhC, where the metal centered (n)σ orbital is slightly higher in energy than the (n-1)δ orbital. Both RhC and CoC have only a single electron in the metal centered orbital, while IrC has this orbital filled. Either the energy of the 16σ orbital has decreased or the energy of the 4δ orbitals has increased. Since the 16σ orbital has a greater probability of being ligand sensitive than than the 4δ orbitals, the former situation is more likely. Therefore, the molecular orbital diagram of 5.33 should probably show the Rh 12σ orbital decreasing in energy somewhat, with increasing electro-negativity of the ligand.

The bond length of IrC is somewhat larger than RhC and CoC at 0.1683 nm. The atomic radius increases slightly from Co to Ir and may be responsible for the slight increase in the carbide bond length. Ruthenium carbide, [Kr] $5\pi^4\ 2\delta^4\ (^1\Sigma^+)$ has a bond length of 0.1608 nm while palladium carbide [Kr] $5\pi^4\ 2\delta^4\ 12\sigma^2\ (^1\Sigma^+)$ has a bond length of 0.1712 nm. The inclusion of two 12σ electrons from RuC to PdC increases the bond length, confirming that the metal centered atomic 5*s* / 12σ orbital is in fact slightly anti-bonding in nature.

The vibrational frequencies of CoC, RhC and IrC, are ~940 cm^{-1}, 1049 cm^{-1} and ~1060 cm^{-1}. This suggests that the bond strength is increasing from CoC to IrC, despite the increased occupancy of the supposedly anti-bonding metal centered orbital and slight increase in the bond length. The vibrational frequencies of Ru and Pd are 1100 cm^{-1} and 848 cm^{-1}. This time the increase in the occupancy of the 12σ orbital has decreased the bond strength. The fact that the observed vibrational frequencies cannot be interpreted by

a simple molecular orbital explanation of the slightly anti-bonding metal centered orbital is not surprising. Molecular orbital diagrams of the type found in figures 4.18, 5.32 and 5.33 are simplified models, giving the "leading" electronic configuration responsible for the observed state. In reality, many electronic configurations are required in *ab initio* calculation to correctly predict things like bond lengths and vibrational frequencies.

The large value for the vibrational constant of RhC suggests a dissociation energy of about 58 000 cm^{-1}(694 kJ/mol, or 166 kcal/mol). For comparison; carbon – carbon triple bonds have dissociation energies of 812 kJ/mol and carbon – carbon double bonds have bond energies of 619 kJ/mol (37).

Lagerqvist and Scullman observed transitions to two electronic states in the 400 – 500 nm region of the electromagnetic spectrum, assigning them as $B^2\Sigma^+$ and $C^2\Sigma^+$. The $B^2\Sigma^+$ state was reassigned as a $^2\Pi$ state based on the observation and analysis of new spectra recorded in our laboratory (9). Dispersed fluorescence of the $B^2\Pi$ ($\upsilon = 0$) level indicated a very long radiative lifetime which prompted us to search for new bands using a time delay on the integration window, enhancing the weak signals of the $^2\Pi_{3/2}$–$X\ ^2\Sigma^+$ transitions. A series of perturbations complicated the spectra and prevented a straightforward rotational analysis. Using a step-wise manner, the energy levels of the mixed states were unraveled, and to a good approximation the spectral lines have been simulated with effective rotational constants.

The spectra of RhO proved to be very complex due to the multiplicities of the states involved and the subsequent analysis difficult and time consuming. In the end, however, 28 bands were analyzed for $Rh^{16}O$ and $Rh^{18}O$, covering two spin –forbidden $^2\Pi_{reg} - X^4\Sigma^-$ transitions to two states labeled $[15.8]^2\Pi$ and $[16.0]^2\Pi$. Since atomic rhodium has many

low lying doublet and quartet electronic states which are linked through spin forbidden transitions, this is perhaps not so surprising. What is surprising is the lack of observation of a spin-allowed transition in the visible region.

Hyperfine coupling, in the ground state only, was observed leading to the conclusion that the ground state must arise from the [Kr] $2\delta^4\ 12\sigma^1\ 6\pi^2$ configuration. The ground state bond length and vibrational frequency for RhO has been determined as 0.1783 nm and 805 cm^{-1} respectively.

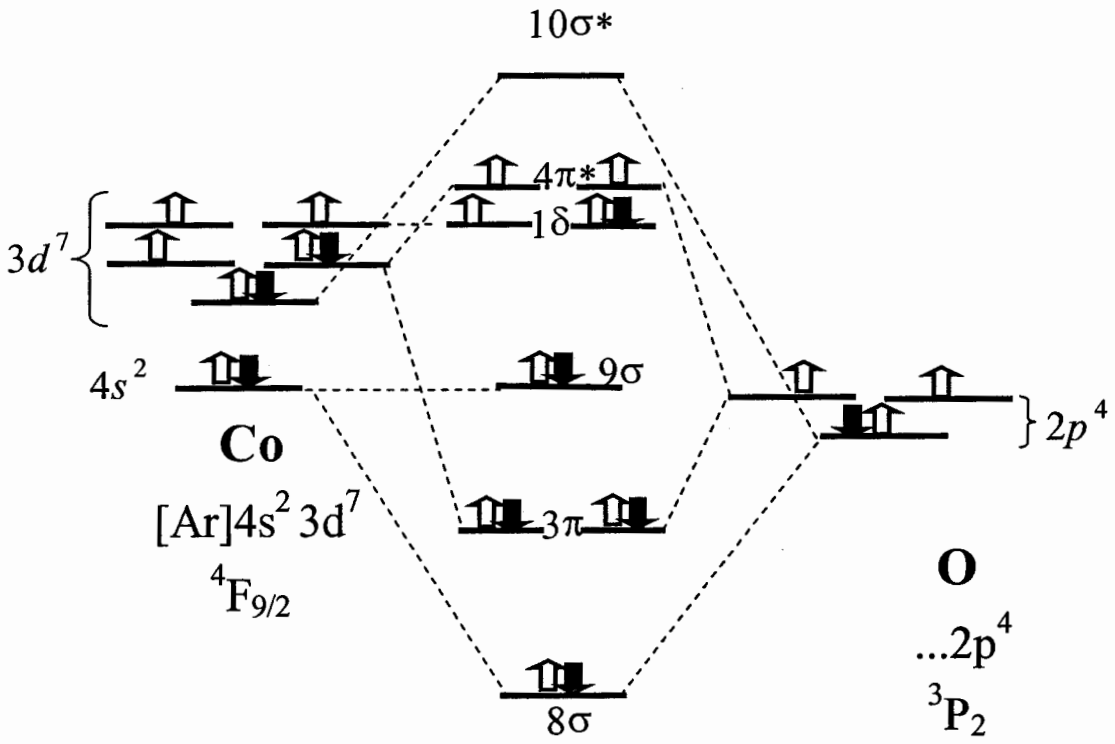

Figure 6.1 Molecular orbital diagram for cobalt oxide.

In CoO the ground state has been determined to be a $^4\Delta_i$ state arising from a $\ldots 9\sigma^2\, 1\delta^3\, 4\pi^2$ configuration, which is lower in energy than the $\ldots 9\sigma\, 1\delta^4\, 4\pi^2$ configuration which leads to a $^4\Sigma^-$ state (38). In RhO the 12σ (atomic $5s$) orbital is close in energy but above the non-bonding 2δ (atomic $4d$) orbital, which is consistent with the atomic orbital configuration of rhodium of $\ldots 5s^1\, 4d^8$. The atomic configuration of cobalt of $4s^2\, 3d^7$, however, suggests that the $4s$ orbital is well below the $3d$ orbital in energy. This is consistent with the CoO ground state configuration, where the metal based 9σ orbital is lower in energy than the 1δ orbital. The smaller size of the cobalt atom would allow for a closer approach of the oxygen atom, increasing the interaction effect of the 4π ligand sensitive orbital stabilizing it so that it is nearly degenerate with the 1δ orbital. The bond length of CoO is reported as 0.1631 nm (38) which is considerable shorter than the RhO bond length, further supporting this interpretation.

Further work investigating the effect of a more electronegative ligand on the molecular orbitals is already underway in our laboratory, with the spectral analysis of rhodium fluoride (RhF). Rhodium chloride (RhCl) is being studied under high resolution, in collaboration with spectroscopists at UNB. Other diatomics that have received little attention are the sulfides and phosphides, but these may prove difficult to observe experimentally. Nevertheless, RhP and RhS should be looked for, as a comparison of the RhP, RhS, and RhCl molecules with RhN, RhO, and RhF may shed further light on the role of the *d* electrons in the bonding of transition metals species.

References

1. CRC Handbook of Chemistry and Physics, 45 ed., pp B-131-132, (CRC Press: Clevland). 1964
2. Moore, C. E. *Atomic Energy Levels, Vol. III, Natl. Stand.*, USA, Circ. No 467 (U.S. GPO, Washington) (1971)
3. Hollas, J. M. *Modern Spectroscopy*, John Wiley & Sons, New York, (1987) p10
4. Graybeal, J. D. *Molecular Spectroscopy*, McGraw-Hill, Inc. 1988
5. Lefebvre-Brion, H.; Field, R. W. *Perturbations in the Spectra of Diatomic Molecules*, Academic Press, Inc. Harcourt Brace Jovanovich, Publishers, Orlando Florida, (1986) p. 15
6. Dunn, T. M. *Nuclear Hyperfine Structure in the Electronic Spectra of Diatomic Molecules* from *Molecular Spectroscopy, Modern Research*, Edited by Rao and Mathews, pp231-257 Academic Press, New York, (1972)
7. Townes, C. H.; Schawlow, A. L. *Microwave Spectroscopy*, Dover Publications, Inc. New York, (1975)
8. Zare, R. N.; Schmeltekopf, A. L. ; Harrop, W. J.; Albritton, D. L. , *J. Mol. Spec.* **46**, 37-66 (1973)
9. Herzberg, G. *Molecular Spectra and Molecular Structure, I. Spectra of Diatomic Molecules*, 2nd Edition, D. Van Nostrand, New York, (1950) p.258
10. Jensen, R. H. *Intramolecular Interactions in Rhodium Monoxide and Halogen Azides* Ph.D. Dissertation, Department of Chemistry, University of Victoria, (2003)

11. Fougère, S. G. *The Electronic Structure and Spectroscopy of Rhodium Diatomic Molecules* Ph.D. Dissertation, Department of Chemistry, University of Victoria, (2000)

12. Kovacs, I., *Rotational Structure in the Spectra of Diatomic Molecules*, Adam Hilger Ltd, London, (1969)

13. Scullman, R. *Personal Communication with W.J. Balfour* (1982)

14. Lagerqvist, A.; Scullman, R., *Arkiv för Fysik*, **32**, 479-508 (1966)

15. Pazyuk, E.A.; Moskvitina, E. N.; Kyzyakov, Y. Y., *Spectroscopy Letters*, **21**, 447-464 (1988)

16. Carlson, R.C.; Bates, J. K.; Dunn, T. M. *J. Mol. Spec.* **110**, 215-241 (1985)

17. Cheung, A. S. C.; Taylor, A. W.; Merer, A. J., *J. Mol. Spec.*, **92**, 391-409 (1982)

18. Balfour, W. J.; Qian, C. X. W.; Zhou, C., *J. Chem. Phys.*, **106**, 4383-4388 (1997)

19. Scullman, R.; Kaving, B., *J. Mol. Spec.* **32**, 475-500 (1969)

20. Brom, J. M.; Graham, W. R. M.; Weltner, W., *J. Chem. Phys.*, **57**, 4116 (1972)

21. Shim, I.; Gingerich, K. A., *J. Chem. Phys.* **81**, 5937-5944 (1984)

22. Tan, H.; Liao, M.; Balasubramanian, K., *Chem. Phys. Lett.* **280,** 423-429 (1997)

23. Balfour, W. J.; Fougère, S. G.; Heuff, R. F.; Qian, C. X. W. ; Zhou, C., *J. Mol. Spec.* **198**, 393-407 (1999)

24. Berg, L. E.; Klynning, L., *Physica Scripta.* **10**, 331-336 (1974)

25. Raziunas, V.; Macur, G.;Katz, J., *J. Chem. Phys.*, **43**, 1010-1015 (1965)

26. White, J.; Mains, G., *J. Phys. Chem.* **95,** 112 (1991)

27. Siegbahn, P. E. M. *Chem. Phys. Lett.* **201**, 15-23 (1993)

28. Chen, Y. M.; Armentrout, P. B.; *J. Chem. Phys.***103**, 618 (1995)

29. Li, X.; Wang, L-S. *J., Chem. Phys.* **109,** 5264-5268 (1998)

30. Citra, A.; Andrews, L., *J. Phys. Chem. A.*, **103,** 4845 (1999)

31. Jensen, R. H.; Fougère, S. G.; Balfour, W. J., *Chem. Phys. Lett.* **370**, 106 (2003)

32. Kleman, B.; Werhagen, E., *Arkiv for Fysik*, **6**,399-405, (1953)

33. Adam, A.G.; Azuma, Y.; Barry, J.A.; Merer, A.J.;Sassenberg, J.O.;Schroder, G.; Cheval, G. and Femenias, J.L., *J. Chem. Phys.* **100**, 6240-6262 (1994) *NbO*

34. Heuff F. R.; Balfour, W. J. Adam, A. G., *J. Mol. Spec.*, **216**, 136-150 (2002)

35. Balfour, W. J.; Li, R.; unpublished results

36. Bernath, P. F. *Spectra of Atoms and Molecules*, Oxford University Press, New York, (1995)

37. Mortimer, C. E., *Chemistry* 5^{th} *ed.*, Wadsworth Inc., pp67, (1983)

38. Adam, A.G.; Azuma, Y.; Barry, J.A.; Huang, G.; Lyne, M. P, J.; Merer, A, J. and Schroder, J.O., *J. Chem. Phys.* **86**, 5231 - 5238 (1987)

Appendix I

$Rh^{12}C$

Transition Lines /cm^{-1}

B $^2\Pi_{1/2}$ -$X^2\Sigma$ 0,0 LIF Transition Lines continued... (Lagerqvist and Scullman's data in bold type)

N	$^sR_{21}(N)$	$^QP_{21}(N)$	$^RR_{22}(N)$	$^PP_{22}(N)$
47	21170.43	21072.05	21132.62	21036.46
48	21163.80	21063.46	21124.80	21026.66
49	21156.96	21054.65	21116.82	21016.71
50	21149.95	21045.69	21108.61	21006.51
51	21142.71	21036.46	21100.13	20996.24
52	21135.27	21027.12	21091.54	20985.67
53	21127.65	21017.55	21082.71	20974.89
54	21119.81	21007.78	21073.67	20963.91
55	21111.79	20997.80	21064.42	20952.77
56	21103.53	20987.62	21054.98	20941.30
57	21095.09	20977.27	21045.33	20929.77
58	21086.46	20966.68	21035.46	20918.00
59	21077.60	20955.88	21025.41	20905.96
60	21068.50	20944.89	21015.11	20893.76
61	21059.28	20933.70	21004.61	20881.50
62	21049.83	20922.32	20993.91	20868.75
63	21040.16	20910.81	20983.16	20855.98
64	21030.24	20898.95	20971.85	20842.89
65	21020.18	20886.93	20960.50	20829.68
66	21009.90	20874.77	20948.94	20816.17
67	20999.38	20862.35	20937.14	20802.54
68	20988.64	20849.74	20925.19	20788.72
69	20977.68	20836.89	20913.05	20774.88
70	20966.46	20823.84	20900.64	20760.24
71	20955.14	20810.60	20888.08	20745.80
72	20943.59	20797.13	20875.20	20731.13
73	20931.99	20783.48	20862.25	20716.22
74	20919.80	20769.59	20849.03	20701.09
75	20907.68	20755.52	20835.61	20685.69
76	20895.13	20741.21	20821.93	20670.26
77	20882.55	20726.76	20808.07	20654.61
78	20869.70	20712.06	20794.02	20638.66
79	20856.58	20697.05		20622.57
80	20843.43	20681.92		20606.22
81		20666.55		
82		20651.00		

B $^2\Pi_{1/2}$ -$X^2\Sigma$ 1,0 LIF Transition Lines

N"	$^{s}R_{21}(N)$	$^{Q}P_{21}(N)$	$Q_2(N)$	$^{R}Q_{21}(N)$	$^{R}R_{22}(N)$	$^{P}P_{22}(N)$
0	22095.79					
1	22097.16	22093.15	22093.01			
2	22098.28	22092.28	22092.08	22094.72	22094.62	
3	22099.26	22091.15	22090.91	22094.91	22094.72	22088.47
4	22099.94	22089.88	22089.64	22094.72	22094.52	22086.13
5	22100.48	22088.47	22088.08	22094.42	22093.98	22083.83
6	22100.87	22086.81	22086.37	22093.69	22093.35	22081.25
7	22101.07	22085.00	22084.52	22092.91	22092.47	22078.32
8	22101.02	22082.91	22082.42	22091.98	22091.45	22075.25
9	22100.87	22080.66	22080.13	22090.91	22090.23	22072.18
10	22100.48	22078.32	22077.64	22089.49	22088.81	22068.67
11	22099.94	22075.64	22074.96	22088.05	22087.20	22065.07
12	22099.11	22072.86	22072.18	22086.27	22085.44	22061.22
13	22098.09	22069.94	22069.16	22084.27	22083.44	
14	22097.01	22066.82	22065.95	22082.13	22081.25	
15	22095.60	22063.41	22062.49	22079.78	22078.71	
16	22094.03	22059.91	22058.90	22077.30	22076.27	
17	22092.47	22056.11	22055.09	22074.62	22073.54	
18	22090.62	22052.17	22051.10	22071.64	22070.57	
19	22088.47	22048.11	22046.97	22068.57	22067.45	
20		22043.81	22042.49	22065.41	22064.14	
21		22039.29	22037.98	22061.90	22060.54	
22		22034.67	22033.26	22058.20	22056.84	
23		22029.85	22028.40	22054.45	22052.90	
24		22024.70	22023.20	22050.32	22048.81	
25		22019.50	22017.90	22045.99	22044.54	
26		22014.00	22012.35	22041.57	22040.06	
27				22036.96	22035.26	
28				22032.15	22030.40	
29				22027.15	22025.30	
30				22021.90	22021.10	
31				22016.50	22014.50	

B $^2\Pi_{1/2}$ -$X^2\Sigma$ 2,0 LIF Transition Lines

N"	$^{S}R_{21}(N)$	$^{Q}P_{21}(N)$	$Q_2(N)$	$^{R}Q_{21}(N)$	$^{R}R_{22}(N)$	$^{P}P_{22}(N)$
0						
1	22847.02		22842.96			
2	22848.17		22842.06		22844.49	22840.59
3	22849.12		22840.96	22844.49	22844.22	22838.28
4	22849.81		22839.65	22844.22	22843.86	22835.95
5	22850.33	22838.38	22838.07	22843.75	22843.33	22833.38
6	22850.70		22836.23	22842.96	22842.54	22830.65
7	22850.70	22834.75	22834.28	22842.06	22841.59	22827.65
8	22850.70	22832.70	22832.18	22840.96	22840.54	22824.55
9	22850.33	22830.33	22829.81	22839.66	22839.07	22821.18
10	22849.81	22827.75	22827.23	22838.17	22837.49	22817.56
11	22849.12	22825.18	22824.55	22836.33		22813.84
12	22848.17	22822.29	22821.51	22834.44	22833.70	22809.85
13	22847.02	22819.19	22818.35	22832.28	22831.54	22805.70
14		22815.83	22814.99	22829.97	22829.18	22801.19
15	22844.22	22812.37	22811.42	22827.50	22826.50	22796.63
16	22842.54	22808.64	22807.59	22824.76	22823.71	22791.81
17	22840.75	22804.70	22803.65	22821.77	22820.77	22786.78
18	22838.59	22800.61	22799.41	22818.62	22817.60	22781.59
19		22796.26	22795.00	22815.10	22813.90	22776.15
20	22833.70	22791.81	22790.44	22811.79	22810.40	22770.50
21	22830.91	22786.93	22785.62	22808.01	22806.55	22764.59
22			22780.54	22804.07	22802.70	22758.53
23	22824.87		22775.31	22799.83	22798.46	22752.26
24			22769.92	22795.37		22745.73
25			22764.22	22790.86		
26			22758.32	22785.99		
27			22752.26	22780.96		
28			22745.94	22775.83		
29				22770.50		
30				22764.63		

B $^2\Pi_{1/2}$ -$X^2\Sigma$ 3,0 LIF Transition Lines

N"	$^sR_{21}(N)$	$^QP_{21}(N)$	$^RR_{22}(N)$	$^PP_{22}(N)$
0	23581.47			
1	23582.72	23578.75		
2	23583.87	23577.82		23576.42
3	23584.74	23576.68	23580.22	23574.18
4	23585.39	23575.37	23579.89	23571.89
5	23585.88	23573.80	23579.35	23569.33
6	23586.04	23572.05	23578.58	23566.62
7	23586.04	23570.15	23577.66	23563.68
8	23585.88	23567.92	23576.42	23560.53
9	23585.55	23565.58	23575.16	23557.21
10	23584.96	23562.97	23573.52	23553.63
11	23584.19	23560.20	23571.80	23549.88
12	23583.16	23557.21	23569.77	23545.86
13	23581.91	23554.06	23567.59	23541.63
14	23580.49	23550.69	23565.09	23537.34
15	23578.86	23547.00	23562.54	23532.73
16	23577.06	23543.20	23559.71	23527.91
17	23575.16	23539.19	23556.67	23522.92
18	23572.76	23535.01	23553.52	23517.77
19	23570.26	23530.51	23549.99	23512.36
20	23567.59	23525.90	23546.40	23506.79
21	23564.71	23521.08	23542.50	23500.94
22	23561.61	23516.04	23538.48	23494.94
23	23558.30	23510.79	23534.25	23488.68
24	23554.88	23505.38	23529.69	
25	23551.13	23499.70	23525.03	
26	23547.16	23493.81	23520.16	
27		23487.70	23515.07	
28			23509.87	

B $^2\Pi_{1/2}$ -$X^2\Sigma$ 4,0 LIF Transition Lines

N"	$^sR_{21}(N)$	$^QP_{21}(N)$	$^RR_{22}(N)$	$^PP_{22}(N)$
0	24300.67			
1	24301.98	24298.05		
2	24303.00	24297.10	24299.53	24295.67
3	24303.86	24295.95	24299.42	24293.56
4	24304.42	24294.64	24299.08	24291.29
5	24304.82	24293.05	24298.51	24288.68
6	24304.99	24291.29	24297.71	24285.95
7	24304.99	24289.36	24296.69	24283.00
8	24304.82	24287.09	24295.50	24279.82
9	24304.31	24284.70	24294.08	24276.41
10	24303.63	24282.03	24292.43	24272.78
11	24302.72	24279.25	24290.55	24268.98
12	24301.64	24276.18	24288.51	24264.95
13	24300.33	24272.78	24286.18	24260.46
14	24298.79	24269.32	24283.68	24256.17
15	24297.03	24265.63	24280.95	24251.52
16	24295.04	24261.72	24278.06	24246.54
17	24292.88	24257.58	24274.85	24241.44
18	24290.45	24253.22	24271.48	24236.13
19	24287.82	24248.63	24267.84	24230.58
20	24285.04	24243.82	24264.10	24224.82
21	24282.03	24238.78	24260.08	24218.77
22	24278.74	24233.64	24255.83	24212.56
23	24275.28	24228.15	24251.43	24206.13
24	24271.65	24222.50	24246.77	
25	24267.67	24216.57	24241.84	
26	24263.54	24210.58	24236.69	
27	24259.17	24204.26	24231.43	
28	24254.63		24225.89	
29	24249.82		24220.07	
30	24244.90			

B $^2\Pi_{3/2}$ -$X^2\Sigma$ 1,0 Transition Lines

N	$[R_1(J)]$	$[Q_1(J)]$	$[P_1(J)]$	$[^QR_{12}(J)]$	$[^PQ_{12}(J)]$	$[^OP_{12}(J)]$
0	21698.70					
1	21700.02	21697.52		21697.52		
2	21701.15	21697.52	21694.87	21697.52	21694.98	
3	21702.05	21697.70	21693.94	21697.52	21693.85	21691.12
4	21702.71	21697.38	21692.72	21696.96	21692.72	21689.00
5	21703.18	21696.72	21691.12	21696.35	21691.12	21686.32
6	21703.46	21695.97	21689.38	21695.55	21689.00	21683.50
7	21703.46	21694.98	21687.40	21694.51	21686.98	21680.49
8	21703.27	21693.85	21685.29	21693.29	21685.05	21677.29
9	21702.94	21692.44	21682.89	21691.87	21682.32	21673.90
10	21702.33	21690.79	21680.49	21690.18	21679.64	21670.24
11	21701.53	21689.00	21677.53	21688.30	21676.78	21666.39
12	21700.49	21686.98	21674.57	21686.22	21673.77	21662.36
13	21699.27	21684.72	21671.33	21683.92	21670.48	21658.09
14	21697.52	21682.32	21667.90	21681.43	21667.01	21653.54
15	21695.97	21679.64	21664.24	21678.70	21663.30	21648.94
16	21694.15	21676.78	21660.39	21675.79	21659.35	21644.02
17	21692.10	21673.77	21656.35	21672.64	21655.27	21638.96
18	21689.90	21670.48	21652.09	21669.31	21650.91	21633.62
19	21687.40	21667.01	21647.63	21665.74	21646.36	21628.15
20	21684.54	21663.30	21642.94	21662.03	21641.63	
21	21681.67	21659.35	21638.02	21658.09	21636.71	
22	21678.60	21655.27	21632.92	21653.81	21631.61	
23	21675.18	21650.91	21627.63	21649.41	21626.23	
24	21671.64	21646.36		21644.86		
25	21667.90	21641.63		21639.99		
26	21663.86	21636.71		21635.03		
27	21659.35	21631.61		21629.78		
28	21655.27	21626.23				
29	21651.10					
30	21646.50					
31	21641.50					
32	21636.81					
33	21631.80					
34	21626.23					

B $^2\Pi_{3/2}$ -$X^2\Sigma$ 2,0 Transition Lines

N	$[R_1(J)]$	$[Q_1(J)]$	$[P_1(J)]$	$[^QR_{12}(J)]$	$[^PQ_{12}(J)]$	$[^OP_{12}(J)]$
0	22436.28					
1	22437.55	22435.06		22435.06		
2	22438.66	22435.06	22432.58	22435.06	22432.58	
3	22439.48	22435.06	22431.62	22435.06	22431.36	22428.68
4	22440.08	22434.81	22430.25	22434.41	22430.00	22426.50
5	22440.54	22434.15	22428.68	22433.80	22428.32	22423.97
6	22440.69	22433.34	22426.96	22432.94	22426.50	22421.13
7	22440.69	22432.33	22424.93	22431.82	22424.47	22418.20
8	22440.54	22431.11	22422.70	22430.55	22422.15	22414.81
9	22440.08	22429.64	22420.27	22429.03	22419.72	22411.37
10	22439.27	22427.97	22417.64	22427.31	22416.98	22407.57
11	22438.41	22426.04	22414.81	22425.39	22414.05	22403.73
12	22437.30	22423.97	22411.67	22423.16	22410.91	22399.59
13	22435.93	22421.64	22408.38	22420.83	22407.57	22395.24
14	22434.41	22419.11	22404.84	22418.20	22403.98	22390.70
15	22432.58	22416.37	22401.10	22415.41	22400.14	22385.90
16	22430.55	22413.34	22397.16	22412.38	22396.15	22380.90
17	22428.32	22410.15	22392.92	22409.09	22391.91	22375.66
18	22425.84	22406.71	22388.52	22405.65	22387.41	22370.26
19	22423.16	22403.12	22383.93	22401.90	22382.72	22364.62
20	22420.27	22399.23	22379.09	22397.97	22377.88	22358.68
21	22417.23	22395.24	22374.10	22393.83	22372.73	22352.59
22	22414.05	22390.80	22368.80	22389.48	22367.44	22346.30
23	22410.35	22386.25	22363.26	22384.89	22361.85	
24	22406.71	22381.61	22357.57	22380.10	22356.06	
25	22402.62	22376.67	22351.63	22375.10	22350.07	
26	22398.47	22371.52		22369.86	22343.94	
27	22393.98	22366.08		22364.42		
28	22389.48	22360.49		22358.68		
29	22384.54	22354.65		22352.84		
30	22379.44	22348.61		22346.75		

B $^2\Pi_{3/2}$ -$X^2\Sigma$ 4,0 Transition Lines

N	$[R_1(J)]$	$[Q_1(J)]$	$[P_1(J)]$	$[^QR_{12}(J)]$	$[^PQ_{12}(J)]$	$[^OP_{12}(J)]$
0	23898.38					
1	23899.70	23897.35		23897.35		
2	23900.68	23897.17	23894.81	23897.17	23894.81	
3	23901.49	23896.94	23893.66	23896.90	23893.53	23891.25
4	23902.01	23896.77	23892.28	23896.46	23892.11	23888.60
5	23902.35	23896.08	23890.73	23895.72	23890.44	23886.08
6	23902.47	23895.22	23888.95	23894.81	23888.55	23883.15
7	23902.35	23894.12	23886.88	23893.66	23886.36	23880.04
8	23902.15	23892.74	23884.52	23892.28	23884.01	23876.65
9	23901.49	23891.25	23882.00	23890.73	23881.36	23873.15
10	23900.57	23889.49	23879.24	23888.95	23878.55	23869.36
11	23899.53	23887.40	23876.20	23886.71	23875.51	23865.29
12	23898.27	23885.21	23872.98	23884.35	23872.79	23861.05
13	23896.77	23882.63	23869.54	23881.82	23868.73	23856.69
14	23894.93	23880.04	23865.86	23879.07	23865.00	23851.99
15	23893.14	23876.94	23861.96	23876.02	23861.05	23847.06
16	23890.73	23873.84	23857.83	23872.81	23856.86	23841.85
17	23888.49	23870.40	23853.48	23869.26	23852.45	23836.47
18	23885.73	23866.78	23848.95	23865.58	23847.81	23830.86
19	23882.84	23862.94	23844.14	23861.79	23842.88	23824.97
20	23880.10	23858.98	23839.10	23857.66	23837.84	23818.85
21	23876.54	23854.62	23833.78	23853.31	23832.52	23812.57
22	23872.98	23850.15	23828.29	23848.84	23826.91	23806.00
23	23869.36	23845.40	23822.63	23844.14	23821.14	
24	23865.58	23840.53	23816.86	23839.10	23815.20	
25	23861.39	23835.44		23833.78	23808.97	
26	23857.15		23804.06			
27	23852.62					
28	23847.81					

B $^2\Pi_{3/2}$ -$X^2\Sigma$ 4,0 Transition Lines

N	$[R_1(J)]$	$[Q_1(J)]$	$[P_1(J)]$	$[^QR_{12}(J)]$	$[^PQ_{12}(J)]$	$[^OP_{12}(J)]$
0	23898.38					
1	23899.70	23897.35		23897.35		
2	23900.68	23897.17	23894.81	23897.17	23894.81	
3	23901.49	23896.94	23893.66	23896.90	23893.53	23891.25
4	23902.01	23896.77	23892.28	23896.46	23892.11	23888.60
5	23902.35	23896.08	23890.73	23895.72	23890.44	23886.08
6	23902.47	23895.22	23888.95	23894.81	23888.55	23883.15
7	23902.35	23894.12	23886.88	23893.66	23886.36	23880.04
8	23902.15	23892.74	23884.52	23892.28	23884.01	23876.65
9	23901.49	23891.25	23882.00	23890.73	23881.36	23873.15
10	23900.57	23889.49	23879.24	23888.95	23878.55	23869.36
11	23899.53	23887.40	23876.20	23886.71	23875.51	23865.29
12	23898.27	23885.21	23872.98	23884.35	23872.79	23861.05
13	23896.77	23882.63	23869.54	23881.82	23868.73	23856.69
14	23894.93	23880.04	23865.86	23879.07	23865.00	23851.99
15	23893.14	23876.94	23861.96	23876.02	23861.05	23847.06
16	23890.73	23873.84	23857.83	23872.81	23856.86	23841.85
17	23888.49	23870.40	23853.48	23869.26	23852.45	23836.47
18	23885.73	23866.78	23848.95	23865.58	23847.81	23830.86
19	23882.84	23862.94	23844.14	23861.79	23842.88	23824.97
20	23880.10	23858.98	23839.10	23857.66	23837.84	23818.85
21	23876.54	23854.62	23833.78	23853.31	23832.52	23812.57
22	23872.98	23850.15	23828.29	23848.84	23826.91	23806.00
23	23869.36	23845.40	23822.63	23844.14	23821.14	
24	23865.58	23840.53	23816.86	23839.10	23815.20	
25	23861.39	23835.44		23833.78	23808.97	
26	23857.15		23804.06			
27	23852.62					
28	23847.81					

B $^2\Pi_{3/2}$ -X$^2\Sigma$ 0,0 Transition Lines

N	[R_1(J)]	[Q_1(J)]	[P_1(J)]	[$^QR_{12}$(J)]	[$^PQ_{12}$(J)]	[$^OP_{12}$(J)]
0	20938.68					
1	20940.04	20937.53		20937.53		
2	20941.13	20937.53	20935.24	20937.46	20935.02	
3	20942.04	20937.46	20934.15	20937.29	20933.84	20931.53
4	20942.79	20937.29	20932.85	20936.98	20932.53	20929.22
5	20943.31	20936.81	20931.36	20936.46	20930.96	20926.69
6	20943.62	20936.11	20929.65	20935.72	20929.22	20923.94
7	20943.70	20935.24	20927.73	20934.76	20927.26	20920.48
8	20943.62	20934.15	20925.64	20933.62	20925.08	20917.84
9	20943.31	20932.79	20923.29	20932.27	20922.72	20914.40
10	20942.79	20931.31	20920.80	20930.70	20920.19	20910.92
11	20942.13	20929.65	20918.10	20928.96	20917.41	20907.22
12	20941.22	20927.73	20915.19	20926.95	20914.40	20903.26
13	20940.17	20925.64	20912.09	20924.81	20911.27	20899.17
14	20938.81	20923.29	20908.70	20922.42	20907.87	20894.74
15	20937.29	20920.81	20905.31	20919.85	20904.35	
16	20935.64	20918.10	20901.56	20917.06	20900.56	
17	20933.71	20915.19	20897.61	20914.12	20896.56	
18	20931.36	20912.09	20893.52	20910.92	20892.35	
19	20928.96	20908.75	20889.18	20907.52	20887.96	
20	20926.43	20905.18	20884.70	20903.91	20883.36	
21	20923.68	20901.43	20880.02	20900.20	20878.58	
22	20920.80	20897.52	20874.98	20896.13	20873.55	
23	20917.58	20893.39	20869.82	20891.91	20868.39	
24	20914.18	20889.05	20864.40	20887.48	20862.93	
25	20910.66	20884.49	20858.90	20882.92	20857.30	
26	20906.87	20879.67	20853.06	20878.06	20851.50	
27	20902.91	20874.85	20847.21	20873.16	20845.48	
28	20898.74	20869.65		20867.70		
29	20894.39	20864.10		20862.37		
30	20889.79	20858.65		20856.71		
31	20885.01	20852.80				
32	20880.02	20846.83				
33	20874.85					

$C^2\Sigma^+ - X^2\Sigma^+$ 0,0 transition lines Lagerqvist and Scullman's (bold type) combined with the low *J* LIF data (normal type)

N	$R_1(N)$	$P_1(N)$	$R_2(N)$	$P_2(N)$
0	21453.29			
1	21454.76	21450.90	21453.29	
2	21455.87	21449.98	21453.75	21449.06
3	21456.79	21448.78	21454.08	21447.22
4	21457.62	21447.50	21454.40	21445.29
5	21458.26	21446.02	21454.40	21443.27
6	21458.72	21444.37	**21454.27**	**21441.03**
7	21459.09	21442.62	**21454.06**	**21438.72**
8	21459.37	**21440.78**	**21453.75**	**21436.19**
9	21459.37	**21438.72**	**21453.22**	**21433.59**
10	**21459.41**	**21436.57**	**21452.60**	**21430.84**
11	**21459.10**	**21434.20**	**21451.80**	**21427.93**
12	**21458.73**	**21431.74**	**21450.90**	**21424.88**
13	**21458.22**	**21429.15**	**21449.89**	**21421.72**
14	**21457.58**	**21426.39**	**21448.72**	**21418.40**
15	**21456.83**	**21423.49**	**21447.45**	**21415.00**
16	**21455.88**	**21420.46**	**21446.07**	**21411.44**
17	**21454.81**	**21417.29**	**21444.53**	**21407.72**
18	**21453.66**	**21413.97**	**21442.87**	**21403.92**
19	**21452.32**	**21410.50**	**21441.03**	**21400.00**
20	**21450.79**	**21406.90**	**21439.08**	**21395.92**
21	**21449.14**	**21403.15**	**21437.03**	**21391.72**
22	**21447.40**	**21399.28**	**21434.88**	**21387.38**
23	**21445.55**	**21395.27**	**21432.60**	**21382.97**
24	**21443.53**	**21391.12**	**21430.21**	**21378.44**
25	**21441.35**	**21386.83**	**21427.69**	**21373.76**
26	**21439.06**	**21382.42**	**21425.04**	**21368.96**
27	**21436.70**	**21377.94**	**21422.30**	**21364.05**
28	**21434.14**	**21373.24**	**21419.45**	**21359.05**
29	**21431.45**	**21368.40**	**21416.46**	**21353.95**
30	**21428.63**	**21363.49**	**21413.39**	**21348.69**
31	**21425.69**	**21358.44**	**21410.21**	**21343.34**
32	**21422.63**	**21353.25**	**21406.93**	**21337.88**
33	**21419.45**	**21347.93**	**21403.50**	**21332.29**
34	**21416.12**	**21342.45**	**21399.99**	**21326.65**
35	**21412.68**	**21336.90**	**21396.37**	**21320.84**
36	**21409.12**	**21331.21**	**21392.65**	**21314.97**
37	**21405.45**	**21325.38**	**21388.84**	**21308.93**
38	**21401.64**	**21319.44**	**21384.94**	**21302.87**
39	**21397.70**	**21313.39**	**21380.98**	**21296.70**
40	**21393.67**	**21307.20**	**21376.87**	**21290.40**
41	**21389.51**	**21300.92**	**21372.65**	**21284.00**
42	**21385.26**	**21294.49**	**21368.35**	**21277.51**
43	**21380.90**	**21288.00**	**21363.93**	**21270.92**
44	**21376.45**	**21281.38**	**21359.44**	**21264.25**
45	**21371.86**	**21274.65**	**21354.85**	**21257.50**

Lagerqvist and Scullman's C-X 0,0 transition lines continued

N	$R_1(N)$	$P_1(N)$	$R_2(N)$	$P_2(N)$
46	21367.13	21267.78	21350.16	21250.63
47	21362.36	21260.80	21345.37	21243.67
48	21357.45	21253.75	21340.46	21236.62
49	21352.42	21246.40	21335.51	21229.49
50	21347.29	21239.28	21330.41	21222.25
51	21342.03	21231.95	21325.23	21214.92
52	21336.65	21224.44	21319.97	21207.47
53	21331.21	21216.86	21314.64	21199.93
54	21325.68	21209.17	21309.15	21192.31
55	21320.05	21201.37	21303.59	21184.61
56	21314.27	21193.47	21297.96	21176.82
57	21308.42	21185.52	21292.21	21168.97
58	21302.47	21177.44	21286.38	21161.00
59	21296.42	21169.23	21280.45	21152.90
60	21290.26	21160.90	21274.39	21144.70
61	21284.02	21152.50	21268.20	21136.40
62	21277.68	21144.07	21261.93	21128.03
63	21271.19	21135.49	21255.53	21119.51
64	21264.65	21126.80	21249.02	21110.91
65	21258.00	21117.90	21242.30	21102.19
66	21251.22	21109.12	21235.47	21093.33
67	21244.35	21100.13	21228.25	21084.30
68	21237.33	21091.03		21075.08
69	21230.24	21081.89		21065.53
70	21223.03	21072.55	21213.70	
71	21215.74	21063.16	21205.14	
72	21208.26	21053.66	21197.20	21044.22
73	21200.70	21044.00	21189.57	21033.31
74	21192.87	21034.27	21181.95	21023.08
75	21184.74	21024.32	21174.26	21013.09
76	21176.20	21014.21	21166.55	21003.15
77			21158.79	20993.20
78			21150.95	20983.21
79			21142.96	20973.15
80			21134.90	20962.99
81			21126.72	20952.77
82			21118.46	20942.40
83			21110.11	20931.99
84			21101.63	20921.46
85			21093.03	20910.81
86			21084.33	20900.10
87			21075.54	20889.28
88			21066.61	20878.32
89			21057.58	20867.27
90			21048.41	20856.13
91			21039.15	20844.80
92			21029.73	20833.39

Lagerqvist and Scullman's C-X 0,0 transition lines continued

N	$R_1(N)$	$P_1(N)$	$R_2(N)$	$P_2(N)$
95			21000.69	20798.43
96			20990.71	20786.54
97			20980.59	20774.48
98			20970.35	20762.32
99			20959.90	20749.97
100			20949.31	20737.48
101			20938.52	20724.84
102			20927.56	20712.04
103			20916.37	20699.05
104			20904.99	20685.89
105			20893.40	20672.52
106			20881.54	20658.93
107			20869.38	20645.12
108			20856.85	20631.07
109			20844.01	20616.76
110			20830.75	20602.05
111			20817.12	20587.01
112			20802.91	20571.62
113			20788.11	20555.76
114			20772.74	20539.43
115				20522.50
116				20505.00
117				20486.76

$C^2\Sigma^+$ -$X^2\Sigma^+$ 0,1 transition lines Lagerqvist and Scullman's (bold type) combined with the low *J* LIF data (normal type)

N	$R_1(N)$	$P_1(N)$	$R_2(N)$	$P_2(N)$
0	20413.51			
1	20414.76	20410.76	20413.44	
2	20415.92	20409.76	20413.90	20408.77
3	20416.84	20408.76	20414.35	20407.10
4	20417.67	20407.43	20414.35	**20405.33**
5	20418.34	20405.93	20414.35	**20403.33**
6	20418.92	20404.35	20414.35	**20401.13**
7	**20418.88**	20402.68	20414.35	**20398.84**
8	**20419.33**	20400.93	**20413.78**	**20396.47**
9	**20419.74**	**20398.84**	**20413.47**	**20393.91**
10	**20419.74**	**20396.89**	**20412.97**	**20391.21**
11	**20419.60**	**20394.79**	**20412.29**	**20388.42**
12	**20419.33**	**20392.29**	**20411.49**	**20385.48**
13	**20418.92**	**20389.84**	**20410.55**	**20382.42**
14	**20418.40**	**20387.21**	**20409.51**	**20379.24**
15	**20417.76**	**20384.43**	**20408.33**	**20375.92**
16	**20416.97**	**20381.52**	**20407.04**	**20372.49**
17	**20416.04**	**20378.48**	**20405.64**	**20368.93**
18	**20414.98**	**20375.29**	**20404.09**	**20365.24**
19	**20413.78**	**20371.99**	**20402.45**	**20361.45**
20	**20412.48**	**20368.54**	**20400.69**	**20357.56**
21	**20411.02**	**20364.95**	**20398.84**	**20353.53**
22	**20409.46**	**20361.29**	**20396.84**	**20349.41**
23	**20407.73**	**20357.51**	**20394.74**	**20345.18**
24	**20405.88**	**20353.53**	**20392.53**	**20340.81**
25	**20403.93**	**20349.41**	**20390.22**	**20336.33**
26	**20401.85**	**20345.18**	**20387.80**	**20331.76**
27	**20399.65**	**20340.85**	**20385.25**	**20327.09**
28	**20397.29**	**20336.41**	**20382.62**	**20322.32**
29	**20394.84**	**20331.79**	**20379.87**	**20317.37**
30	**20392.29**	**20327.09**	**20377.04**	**20312.35**
31	**20389.57**	**20322.32**	**20374.08**	**20307.24**
32	**20386.77**	**20317.39**	**20371.08**	**20302.05**
33	**20383.88**	**20312.35**	**20367.91**	**20296.73**
34	**20380.82**	**20307.15**	**20364.66**	**20291.35**
35	**20377.65**	**20301.88**	**20361.29**	**20285.85**
36	**20374.38**	**20296.48**	**20357.92**	**20280.23**
37	**20370.99**	**20290.95**	**20354.39**	**20274.53**
38	**20367.49**	**20285.33**	**20350.79**	**20268.75**
39	**20363.89**	**20279.59**	**20347.10**	**20262.87**
40	**20360.15**	**20273.73**	**20343.29**	**20256.89**
41	**20356.35**	**20267.76**	**20339.41**	**20250.85**
42	**20352.44**	**20261.68**	**20335.44**	**20244.71**
43	**20348.37**	**20255.51**	**20331.45**	**20238.45**
44	**20344.25**	**20249.25**	**20327.29**	**20232.13**

45	20340.02	20242.85	20323.04	20225.72

Lagerqvist and Scullman's C-X 0,1 transition lines continued

N	$R_1(N)$	$P_1(N)$	$R_2(N)$	$P_2(N)$
46	20335.69	20236.37	20318.69	20219.20
47	20331.28	20229.80	20314.28	20212.62
48	20326.74	20223.11	20309.79	20205.94
49	20322.07	20216.31	20305.19	20199.19
50	20317.31	20209.45	20300.51	20192.36
51	20312.55	20202.45	20295.73	20185.39
52	20307.61	20195.35	20290.87	20178.39
53	20302.57	20188.23	20285.97	20171.30
54	20297.46	20180.98	20280.92	20164.10
55	20292.25	20173.59	20275.80	20156.82
56	20286.93	20166.15	20270.60	20149.45
57	20281.54	20158.60	20265.29	20142.04
58	20276.07	20150.96	20259.92	20134.50
59	20270.44	20143.21	20254.44	20126.88
60	20264.78	20135.43	20248.90	20119.18
61	20259.03	20127.55	20243.18	20111.38
62	20253.14	20119.57	20237.41	20103.51
63	20247.16	20111.47	20231.50	20095.52
64	20241.10	20103.30	20225.46	20087.42
65	20235.00	20095.03		20079.22
66	20228.27	20086.69		20070.82
67	20222.41	20078.26		20062.40
68	20216.02	20069.69		
69	20209.55	20061.04		
70	20202.98	20052.32		
71	20196.20	20043.46		
72		20034.54		
73		20025.48		
74		20016.26		
75		20006.89		
76		19997.40		

$C^2\Sigma^+$ -$X^2\Sigma^+$ 1,0 transition lines Lagerqvist and Scullman's (bold type) combined with the low *J* LIF data (normal type)

N	$R_1(N)$	$P_1(N)$	$R_2(N)$	$P_2(N)$
0	22286.17			
1	22287.16	22283.86	22286.70	
2	22288.18	22282.47	22287.52	22282.46
3	22288.95	22281.18	22288.12	22280.77
4	22289.64	**22279.57**	22288.72	**22279.14**
5	22290.44	**22278.02**	22289.15	**22277.37**
6	22290.07	**22276.27**	22289.41	**22275.52**
7	**22290.79**	**22274.39**	**22289.62**	**22273.53**
8	**22290.90**	**22272.40**	**22289.79**	**22271.41**
9	**22290.86**	**22270.35**	**22289.68**	**22269.18**
10	**22290.79**	**22268.03**	**22289.44**	**22266.85**
11	**22290.62**	**22265.69**	**22289.21**	**22264.32**
12	**22290.28**	**22263.22**	**22288.75**	**22261.75**
13	**22289.83**	**22260.61**	**22288.17**	**22259.05**
14	**22289.21**	**22257.90**	**22287.48**	**22256.21**
15	**22288.58**	**22255.08**	**22286.67**	**22253.27**
16	**22287.78**	**22252.11**	**22285.75**	**22250.21**
17	**22286.84**	**22249.02**	**22284.71**	**22246.99**
18	**22285.77**	**22245.80**	**22283.59**	**22243.71**
19	**22284.58**	**22242.46**	**22282.32**	**22240.28**
20	**22283.30**	**22239.01**	**22280.94**	**22236.71**
21	**22281.89**	**22235.46**	**22279.41**	**22233.05**
22	**22280.37**	**22231.79**	**22277.80**	**22229.27**
23	**22278.70**	**22228.00**	**22276.04**	**22225.36**
24	**22276.91**	**22224.11**	**22274.19**	**22221.34**
25	**22275.01**	**22220.06**	**22272.18**	**22217.21**
26	**22272.98**	**22215.87**	**22270.06**	**22212.95**
27	**22270.83**	**22211.56**	**22267.87**	**22208.57**
28	**22268.57**	**22207.10**	**22265.52**	**22204.07**
29	**22266.18**	**22202.55**	**22263.08**	**22199.46**
30	**22263.66**	**22197.91**	**22260.48**	**22194.73**
31	**22261.03**	**22193.14**	**22257.78**	**22189.88**
32	**22258.28**	**22188.23**	**22254.98**	**22184.91**
33	**22255.40**	**22183.21**	**22252.05**	**22179.83**
34	**22252.40**	**22178.09**	**22249.02**	**22174.63**
35	**22249.29**	**22172.81**	**22245.82**	**22169.31**
36	**22246.06**	**22167.44**	**22242.46**	**22163.85**
37	**22242.72**	**22161.96**	**22239.01**	**22158.29**
38	**22239.19**	**22156.35**	**22235.44**	**22152.63**
39	**22235.55**	**22150.59**	**22231.77**	**22146.83**
40	**22231.82**	**22144.75**	**22228.00**	**22140.90**
41	**22228.00**	**22138.77**	**22224.11**	**22134.85**
42	**22224.02**	**22132.66**	**22220.06**	**22128.66**
43	**22219.91**	**22126.45**	**22215.86**	**22122.39**
44	**22215.69**	**22120.10**	**22211.56**	**22115.96**
45	**22211.34**	**22113.65**	**22207.10**	**22109.41**
46	**22206.93**	**22107.05**	**22202.34**	**22102.77**

Lagerqvist and Scullman's C-X 1,0 transition lines continued

N	$R_1(N)$	$P_1(N)$	$R_2(N)$	$P_2(N)$
47	22202.34	22100.36	22197.58	22095.90
48	22197.58	22093.50	22192.36	22088.87
49	22192.71	22086.53	22186.63	22081.64
50	22187.79	22079.46		22074.17
51	22182.67	22072.29		22066.04
52	22177.44	22064.97	22175.61	
53	22172.04	22057.71	22169.77	
54	22166.46	22049.91	22164.06	22047.97
55	22160.75	22042.17	22158.29	22039.78
56	22154.79	22034.26	22152.45	22031.72
57	22148.56	22026.20	22146.58	22023.64
58	22141.90	22017.93	22140.56	22015.48
59		22009.34	22134.44	22007.21
60		22000.33	22128.22	21998.87
61	22129.18		22121.87	21990.42
62	22121.87		22115.42	21981.86
63	22114.79	21980.61	22108.63	21973.18
64	22107.78	21970.96	22102.11	21964.40
65	22100.82	21961.58	22095.28	21955.48
66	22093.77	21952.25	22088.30	21946.44
67	22086.63	21942.99	22081.23	21937.33
68	22079.40	21933.63	22074.03	21928.05
69	22072.08	21924.18	22066.67	21918.64
70	22064.58	21914.62	22059.18	21909.11
71	22057.03	21904.96	22051.59	21899.45
72	22049.30	21895.22	22043.83	21889.65
73	22041.48	21885.29	22035.96	21879.74
74	22033.51	21875.28	22027.94	21869.69
75	22025.42	21865.14	22019.78	21859.50
76	22017.22	21854.89	22011.49	21849.18
77	22008.90	21844.51	22003.06	21838.75
78	22000.44	21834.01	21994.47	21828.18
79	21991.81	21823.41	21985.74	21817.47
80	21983.04	21812.65	21976.87	21806.60
81	21974.15	21801.78	21967.87	21795.59
82	21965.17	21790.82	21958.66	21784.40
83	21956.01	21779.62	21949.31	
84	21946.72	21768.28	21939.82	21761.63
85	21937.28	21756.86	21930.13	21750.51
86	21927.67	21745.30	21920.25	21738.25
87	21917.97	21733.59	21910.23	21726.31
88	21908.10	21721.77	21899.98	21714.21
89	21898.04	21709.78	21889.55	21701.91
90	21887.86	21697.65	21878.89	21689.43
91	21877.51	21685.38	21868.05	21676.77
92	21866.99	21672.96	21856.91	21663.88
93	21856.31	21660.36	21845.53	21650.74

Lagerqvist and Scullman's C-X 1,0 transition lines continued

N	$R_1(N)$	$P_1(N)$	$R_2(N)$	$P_2(N)$
94	21845.48	21647.62	21833.94	21637.41
95	21834.48	21634.71	21822.06	21623.83
96	21823.28	21621.60	21809.83	21609.96
97	21811.92	21608.36	21797.29	21595.80
98	21800.32	21594.92	21784.33	21581.33
99	21788.54	21581.33	21770.96	21566.56
100	21776.53	21567.51	21757.13	21551.41
101	21764.30	21553.53	21742.87	21535.83
102	21751.82	21539.33	21728.08	21519.77
103	21739.14	21524.90	21712.70	21503.27
104	21726.20	21510.25	21696.79	21486.33
105	21712.95	21495.34	21680.20	21468.79
106	21699.41	21480.21	21663.00	21450.79
107	21685.56	21464.80	21645.13	21431.74
108	21671.34	21449.09	21626.67	
109	21656.76	21433.07	216.07.47	
110	21641.75	21416.65		
111	21626.30	21399.92		
112	21610.37	21382.72		
113		21365.13		

$C^2\Sigma^+$ -$X^2\Sigma^+$ 1,2 transition lines Lagerqvist and Scullman's (bold type) combined with the low *J* LIF data (normal type)

N	$R_1(N)$	$P_1(N)$	$R_2(N)$	$P_2(N)$
0	20216.27			
1	20217.17	20213.74	20216.79	
2	20218.07	20212.44	20217.69	20212.39
3	20218.97	20210.41	20218.59	20210.79
4	20219.79	20209.66	20219.41	20209.28
5	20220.67	20208.19	20219.98	20207.57
6	20221.39	20206.56	20219.98	20205.77
7	20221.59	20204.84	20219.98	20203.81
8	20221.59	20202.88	20219.98	20201.77
9	20221.59	20200.84	20219.98	20199.81
10	20221.59	20198.80	**20220.21**	20197.45
11	**20221.52**	**20196.57**	**20220.07**	**20195.21**
12	**20221.42**	**20194.38**	**20219.83**	**20192.87**
13	**20221.18**	**20191.95**	**20219.51**	**20190.38**
14	**20220.80**	**20189.43**	**20219.11**	**20187.82**
15	**20220.37**	**20186.88**	**20218.50**	**20185.09**
16	**20219.83**	**20184.17**	**20217.83**	**20182.25**
17	**20219.14**	**20181.34**	**20217.07**	**20179.30**
18	**20218.36**	**20178.39**	**20216.31**	**20176.31**
19	**20217.53**	**20175.40**	**20215.26**	**20173.21**
20	**20216.57**	**20172.27**	**20214.16**	**20169.93**
21	**20215.47**	**20169.04**	**20212.98**	**20166.58**
22	**20214.27**	**20165.69**	**20211.70**	**20163.18**
23	**20212.98**	**20162.23**	**20210.32**	**20159.63**
24	**20211.55**	**20158.67**	**20208.81**	**20155.96**
25	**20210.11**	**20155.01**	**20207.22**	**20152.23**
26	**20208.47**	**20151.29**	**20205.50**	**20148.39**
27	**20206.74**	**20147.39**	**20203.74**	**20144.45**
28	**20204.90**	**20143.45**	**20201.86**	**20140.39**
29	**20202.98**	**20139.35**	**20199.81**	**20136.26**
30	**20200.95**	**20135.23**	**20197.68**	**20131.97**
31	**20198.83**	**20130.90**	**20195.45**	**20127.55**
32	**20196.57**	**20126.49**	**20193.16**	**20123.15**
33	**20194.16**	**20122.00**	**20190.74**	**20118.59**
34	**20191.73**	**20117.42**	**20188.23**	**20113.93**
35	**20189.14**	**20112.73**	**20185.64**	**20109.13**
36	**20186.50**	**20107.92**	**20182.90**	**20104.29**
37	**20183.72**	**20103.00**	**20180.05**	**20099.32**
38	**20180.83**	**20098.00**	**20177.08**	**20094.19**
39	**20177.85**	**20092.89**	**20174.01**	**20089.06**
40	**20174.79**	**20087.66**	**20170.91**	**20083.85**
41	**20171.55**	**20082.34**	**20167.60**	**20078.42**
42	**20168.25**	**20076.91**	**20164.20**	**20072.85**
43	**20164.86**	**20071.35**	**20160.70**	**20067.25**
44	**20161.32**	**20065.69**	**20157.06**	**20061.54**
45	**20157.68**	**20059.95**	**20153.29**	**20055.69**
46	**20153.95**	**20054.12**	**20149.34**	**20049.73**

Lagerqvist and Scullman's C-X 1,2 transition lines continued

N	$R_1(N)$	$P_1(N)$	$R_2(N)$	$P_2(N)$
47	20150.09	20048.16	20145.24	20043.66
48	20146.12	20042.07	20140.85	20037.39
49	20142.04	20035.89	20135.88	20030.94
50	20137.88	20029.62		20024.15
51	20133.59	20023.17		20016.92
52	20129.18	20016.72	20127.28	
53	20124.61	20010.11	20122.30	
54	20119.87	20003.35	20117.42	20001.36
55	20115.05	19996.47	20112.56	19994.05
56	20110.00		20107.62	
57	20104.67		20102.66	
58	20099.00		20097.54	
59			20092.37	

$C^2\Sigma^+$ -$X^2\Sigma^+$ 2,0 transition lines Lagerqvist and Scullman's (bold type) combined with the low *J* LIF data (normal type)

N	$R_1(N)$	$P_1(N)$	$R_2(N)$	$P_2(N)$
0	23150.23			
1	23151.19	23147.71	23151.18	
2	23151.94	23146.43	23151.93	23146.45
3	23152.59	23145.03	23152.58	23145.05
4	23153.23	23143.43	23153.22	23143.45
5	23153.66	23141.71	23153.65	23141.52
6	23153.87	**23139.79**	23153.86	23139.68
7	23154.15	**23138.08**	23153.86	**23137.80**
8	23154.15	**23136.07**	23153.86	**23135.66**
9	**23154.21**	**23133.85**	23153.86	**23133.42**
10	**23153.92**	**23131.46**	**23153.59**	**23131.03**
11	**23153.58**	**23129.01**	**23153.17**	**23128.47**
12	**23153.17**	**23126.41**	**23152.60**	**23125.82**
13	**23152.60**	**23123.69**	**23151.97**	**23123.04**
14	**23151.85**	**23120.81**	**23151.21**	**23120.14**
15	**23151.00**	**23117.79**	**23150.17**	**23117.04**
16	**23149.98**	**23114.64**	**23148.82**	**23113.90**
17	**23148.82**	**23111.41**		**23110.48**
18	**23147.58**	**23108.01**	**23148.05**	**23106.81**
19	**23146.20**	**23104.49**	**23146.20**	
20	**23144.66**	**23100.81**	**23144.51**	**23101.21**
21	**23143.00**	**23097.00**	**23142.74**	**23097.00**
22	**23141.20**	**23093.08**	**23140.87**	**23092.83**
23	**23139.20**	**23089.04**	**23138.94**	**23088.63**
24	**23137.05**	**23084.84**	**23136.82**	**23084.42**
25	**23134.67**	**23080.48**	**23134.67**	**23080.07**
26	**23132.17**	**23075.94**	**23132.31**	**23075.61**
27		**23071.21**	**23129.83**	**23070.98**
28		**23066.25**	**23127.23**	**23066.25**
29			**23124.50**	**23061.39**
30	**23123.69**		**23121.64**	**23056.44**
31	**23120.53**		**23118.66**	**23051.32**
32	**23117.32**	**23048.24**	**23115.52**	**23046.09**
33	**23114.04**	**23042.73**	**23112.32**	**23040.71**
34	**23110.67**	**23037.12**	**23108.92**	**23035.23**
35	**23107.11**	**23031.44**	**23105.41**	**23029.60**
36	**23103.45**	**23025.67**	**23101.77**	**23023.83**
37	**23099.73**	**23019.77**	**23097.97**	**23017.96**
38	**23095.82**	**23013.78**	**23094.08**	**23011.93**
39	**23091.81**	**23007.63**	**23090.06**	**23005.79**
40	**23087.66**	**23001.37**	**23085.88**	**22999.52**
41	**23083.38**	**22995.00**	**23081.54**	**22993.11**
42	**23078.98**	**22988.49**	**23077.13**	**22986.55**
43	**23074.44**	**22981.83**	**23072.57**	**22979.89**
44	**23069.73**	**22975.05**	**23067.81**	**22973.06**
45	**23064.94**	**22968.16**	**23062.92**	**22966.15**
46	**23059.99**	**22961.09**	**23057.99**	**22959.10**

Lagerqvist and Scullman's C-X 2,0 transition lines continued

N	$R_1(N)$	$P_1(N)$	$R_2(N)$	$P_2(N)$
47	23054.91	22953.94	23052.85	22951.86
48	23049.68	22946.62	23047.59	22944.49
49	23044.34	22939.17	23042.22	22937.01
50	23038.85	22931.55	23036.65	22929.34
51	23033.25		23030.97	
52	23027.45		23025.17	
53	23021.56		23019.22	
54	23015.53		23013.10	
55	23009.36		23006.86	
56	23003.03		23000.49	
57	22996.58		22993.95	
58	22990.00		22987.28	
59	22983.27		22980.45	
60	22976.40		22973.44	
61	22969.39		22966.39	
62	22962.20		22959.14	
63	22954.89		22951.68	
64	22947.44		22944.09	
65	22939.86		22936.35	
66	22932.09		22928.38	

$C^2\Sigma^+$ -$X^2\Sigma^+$ 2,1 transition lines Lagerqvist and Scullman's (bold type) combined with the low *J* LIF data (normal type)

N	$R_1(N)$	$P_1(N)$	$R_2(N)$	$P_2(N)$
0	22110.07			
1	22111.04	22107.91	22110.74	
2	22111.92	22106.54	22111.62	22106.50
3	22112.61	22105.17	22112.31	22105.16
4	22113.20	22103.61	22112.90	22103.32
5	22113.78	22101.95	22113.48	22101.61
6	22114.07	22100.19	22113.77	22099.86
7	22114.47	22098.33	22113.77	22097.90
8	**22114.40**	22096.28	22113.77	22095.85
9	**22114.48**	**22094.15**	22113.77	22093.71
10	**22114.40**	**22091.95**	22113.77	22091.36
11	**22114.14**	**22089.49**	**22113.60**	22088.92
12	**22113.71**	**22087.00**	**22113.23**	22086.39
13	**22113.23**	**22084.42**	**22112.64**	**22083.72**
14	**22112.64**	**22081.64**	**22111.95**	**22080.97**
15	**22111.95**	**22078.72**	**22111.07**	**22077.98**
16	**22111.07**	**22075.76**	**22110.04**	**22074.93**
17	**22110.04**	**22072.59**	**22108.48**	**22071.65**
18	**22108.03**	**22069.35**	**22109.41**	**22068.20**
19	**22107.70**	**22065.99**	**22107.70**	
20	**22106.33**	**22062.48**	**22106.13**	**22062.85**
21	**22104.80**	**22058.84**	**22104.50**	**22058.79**
22	**22103.16**	**22055.14**	**22102.77**	**22054.81**
23	**22101.38**	**22051.23**	**22101.07**	**22050.85**
24	**22099.43**	**22047.23**	**22099.16**	**22046.80**
25	**22097.23**	**22043.06**	**22097.23**	**22042.62**
26	**22094.87**	**22038.72**	**22095.02**	**22038.35**
27		**22034.21**	**22092.77**	**22033.95**
28		**22029.44**	**22090.43**	**22029.44**
29	**22090.29**		**22087.95**	**22024.85**
30	**22087.34**		**22085.31**	**22020.11**
31	**22084.42**	**22017.81**	**22082.59**	**22015.23**
32	**22081.54**	**22012.43**	**22079.69**	**22010.25**
33	**22078.46**	**22007.21**	**22076.71**	**22005.13**
34	**22075.30**	**22001.84**	**22073.62**	**21999.91**
35	**22072.08**	**21996.43**	**22070.38**	**21994.59**
36	**22068.76**	**21990.95**	**22067.00**	**21989.10**
37	**22065.31**	**21985.36**	**22063.56**	**21983.48**
38	**22061.68**	**21979.62**	**22059.93**	**21977.79**
39	**22057.97**	**21973.79**	**22056.21**	**21971.94**
40	**22054.18**	**21967.87**	**22052.36**	**21965.96**
41	**22050.22**	**21961.80**	**22048.36**	**21959.88**
42	**22046.12**	**21955.61**	**22044.25**	**21953.71**
43	**22041.91**	**21949.31**	**22040.06**	**21947.33**
44	**22037.58**	**21942.91**	**22035.64**	**21940.87**
45	**22033.14**	**21936.33**	**22031.15**	**21934.28**
46	**22028.54**	**21929.64**	**22026.25**	**21927.55**

Lagerqvist and Scullman's C-X 2,1 transition lines continued

N	$R_1(N)$	$P_1(N)$	$R_2(N)$	$P_2(N)$
47	22023.88	21922.85	22021.77	21920.73
48	22018.99	21915.96	22016.87	21913.77
49	22014.05	21908.88	22011.86	21906.70
50	22008.90	21901.70	22006.71	21899.45
51	22003.72	21894.39	22001.43	21892.07
52	21998.35	21886.96	21996.03	21884.61
53	21992.88	21879.38	21990.48	21876.98
54	21987.29	21871.73	21984.82	21869.26
55	21981.52	21863.89	21979.00	21861.36
56	21975.65	21855.94	21973.06	21853.36
57	21969.65	21847.88	21967.01	21845.21
58	21963.54	21839.70	21960.77	21836.94
59	21957.24	21831.37	21954.43	21828.57
60	21950.87	21822.94	21947.94	21820.40
61	21944.34	21814.33	21941.30	21811.37
62	21937.67	21805.62	21934.50	21802.60
63	21930.87	21796.80	21927.57	21793.62
64	21923.92	21787.97	21920.54	21784.52
65	21916.83	21778.70	21913.29	21775.28
66	21909.62	21769.40	21905.95	21765.85
67	21902.28	21760.01	21898.41	21756.32
68	21894.78	21750.50	21890.70	21746.70
69	21887.13	21740.85	21882.91	21736.86
70	21879.35	21731.08	21874.87	21726.87
71	21871.38	21721.14	21866.66	21716.73
72	21863.34	21711.08	21858.28	21706.44
73	21855.11	21700.84	21849.75	21695.99
74	21846.75	21690.49	21841.08	21685.38
75	21838.25	21680.00	21832.15	21674.54
76	21829.60	21669.36	21822.94	21663.53
77	21820.73	21658.54	21813.75	21652.35
78	21811.78	21647.62	21804.20	21640.97
79	21802.60	21636.51	21794.44	21629.35
80	21793.38	21625.26	21784.56	21617.62
81	21783.87	21613.85	21774.22	21605.49
82	21774.22	21602.25	21763.51	21593.23
83	21764.30	21590.53	21752.64	21580.67
84	21753.34	21578.63	21741.47	21567.85
85	21744.15	21566.56	21729.97	21554.72
86	21733.82	21554.31	21718.06	21541.30
87	21723.25	21541.89	21705.75	21527.50
88	21712.45	21529.24	21693.02	21513.36
89	21701.47	21516.42		21498.80
90	21690.30	21503.40		21483.87
91	21678.96	21490.19		
92	21667.39	21476.77		
93	21655.66	21463.23		

$C^2\Sigma^+ - X^2\Sigma^+$ 3,0 transition lines Lagerqvist and Scullman's (bold type) combined with the low *J* LIF data (normal type)

N	$R_1(N)$	$P_1(N)$	$R_2(N)$	$P_2(N)$
0	23996.32			
1	23997.25	23993.57	23997.18	
2	23997.97	23992.29	23997.90	23991.40
3	23998.56	23990.89	23998.49	23989.97
4	23999.23	23989.28	23999.16	23988.64
5	23999.51	23987.32	23999.01	23986.52
6	23999.43	23985.37	23998.93	23984.64
7	23999.31	23983.52	23998.93	23982.72
8	23999.38	23981.32	23998.93	23980.63
9	23999.36	23978.95	23998.93	23978.32
10	**23998.49**	23976.34	23998.66	23975.86
11	**23997.98**	**23973.60**	**23997.63**	23973.22
12	**23997.35**	**23970.82**	**23997.01**	**23970.50**
13	**23996.58**	**23968.00**	**23996.18**	**23967.53**
14	**23995.62**	**23965.03**	**23995.17**	**23964.44**
15	**23994.53**	**23961.80**	**23994.09**	**23961.27**
16	**23993.33**	**23958.50**	**23992.85**	**23957.84**
17	**23992.02**	**23954.93**	**23991.50**	**23954.39**
18	**23990.52**	**23951.30**	**23989.95**	**23950.77**
19	**23988.88**	**23947.59**	**23988.31**	**23947.00**
20	**23987.08**	**23943.73**	**23986.46**	**23943.01**
21	**23985.10**	**23939.70**	**23984.48**	**23938.95**
22	**23983.01**	**23935.53**	**23982.38**	**23934.74**
23	**23980.80**	**23931.17**	**23980.05**	**23930.29**
24	**23978.43**	**23926.71**	**23977.65**	**23925.87**
25	**23975.93**	**23922.08**	**23975.12**	**23921.21**
26	**23973.27**	**23917.32**	**23972.34**	**23916.40**
27	**23970.50**	**23912.40**	**23969.48**	**23911.44**
28	**23967.53**	**23907.35**	**23966.50**	**23906.37**
29	**23964.44**	**23902.17**	**23963.40**	**23901.10**
30	**23961.27**	**23896.87**	**23960.16**	**23895.73**
31	**23957.84**	**23891.37**	**23956.61**	**23890.24**
32	**23954.30**	**23885.75**	**23953.05**	**23884.55**
33	**23950.60**	**23879.97**	**23949.28**	**23878.71**
34	**23946.68**	**23873.99**	**23945.38**	**23872.61**
35	**23942.70**	**23867.88**	**23941.34**	**23866.51**
36	**23938.58**	**23861.67**	**23937.15**	**23860.25**
37	**23934.28**	**23855.32**	**23932.75**	**23853.82**
38	**23929.21**	**23848.81**	**23928.27**	**23847.27**
39	**23925.31**	**23842.19**	**23923.63**	**23840.55**
40	**23920.56**	**23835.51**	**23918.81**	**23833.69**
41	**23915.68**	**23828.45**	**23913.77**	**23826.67**
42	**23910.63**	**23821.37**	**23908.64**	**23819.40**
43	**23905.45**	**23814.13**	**23903.43**	**23812.09**
44	**23900.11**	**23806.68**	**23897.94**	**23804.54**
45	**23894.64**	**23799.14**	**23892.30**	**23796.94**
46	**23888.99**	**23791.39**	**23886.50**	**23789.11**

Lagerqvist and Scullman's C-X 3,0 transition lines continued

N	$R_1(N)$	$P_1(N)$	$R_2(N)$	$P_2(N)$
47	23883.17	23783.55	23880.45	23781.10
48	23877.18	23775.57	23874.38	23772.96
49	23871.08	23767.42	23868.10	23764.63
50	23864.83	23759.12	23861.67	23756.15
51	23858.38	23750.63	23854.95	23747.48
52	23851.74	23741.92	23848.13	
53	23845.09		23841.17	
54	23838.17		23833.98	
55	23831.11		23826.55	
56	23823.88		23818.93	
57	23816.43		23811.07	
58	23808.93		23803.08	
59	23801.21		23794.80	
60	23793.31		23786.32	
61	23785.21		23777.56	
62	23776.94		23768.55	
63	23768.55		23759.26	
64	23759.95		23749.73	
65	23751.15		23739.95	
66	23741.92			

$C^2\Sigma^+ - X^2\Sigma^+$ 3,1 transition lines Lagerqvist and Scullman's (bold type) combined with the low *J* LIF data (normal type)

N	$R_1(N)$	$P_1(N)$	$R_2(N)$	$P_2(N)$
0	22956.16			
1	22957.10	22953.77	22956.74	
2	22957.95	22952.40	22957.59	22951.45
3	22958.58	22951.03	22958.22	22950.08
4	22959.20	22949.46	22958.84	22948.51
5	22959.63	22947.56	22958.84	22946.61
6	22959.63	22945.77	22958.84	22944.82
7	22959.63	22943.77	22958.84	22942.82
8	22959.63	22941.53	22958.84	22940.82
9	22959.63	22939.25	22958.84	22938.61
10	**22958.82**	22936.83	22958.84	22936.19
11	**22958.48**	**22934.19**	**22958.12**	22933.67
12	**22957.95**	**22931.37**	**22957.60**	**22931.10**
13	**22957.28**	**22928.69**	**22956.84**	**22928.23**
14	**22956.44**	**22925.85**	**22955.96**	**22925.28**
15	**22955.46**	**22922.74**	**22954.97**	**22922.19**
16	**22954.42**	**22919.56**	**22953.82**	**22918.89**
17	**22953.25**	**22916.12**	**22952.61**	**22915.60**
18	**22951.84**	**22912.62**	**22951.17**	**22912.09**
19	**22950.34**	**22909.08**	**22949.73**	**22908.45**
20	**22948.77**	**22905.37**	**22948.07**	**22904.65**
21	**22946.98**	**22901.50**	**22946.29**	**22900.76**
22	**22945.07**	**22897.54**	**22944.34**	**22896.77**
23	**22942.98**	**22893.41**	**22942.19**	**22892.50**
24	**22940.78**	**22889.12**	**22939.97**	**22888.24**
25	**22938.51**	**22884.66**	**22937.65**	**22883.78**
26	**22936.06**	**22880.08**	**22935.10**	**22879.20**
27	**22933.45**	**22875.31**	**22932.43**	**22874.48**
28	**22930.68**	**22870.52**	**22929.67**	**22869.64**
29	**22927.83**	**22865.56**	**22926.81**	**22864.52**
30	**22924.93**	**22860.47**	**22923.81**	**22859.39**
31	**22921.72**	**22855.25**	**22920.48**	**22854.14**
32	**22918.44**	**22849.89**	**22917.20**	**22848.72**
33	**22915.03**	**22844.39**	**22913.69**	**22843.15**
34	**22911.38**	**22838.69**	**22910.05**	**22837.31**
35	**22907.67**	**22832.86**	**22906.26**	**22831.52**
36	**22903.84**	**22826.94**	**22902.42**	**22825.51**
37	**22899.82**	**22820.89**	**22898.30**	**22819.42**
38	**22895.06**	**22814.70**	**22894.12**	**22813.15**
39	**22891.50**	**22808.39**	**22889.75**	**22806.72**
40	**22887.04**	**22802.04**	**22885.23**	**22800.18**
41	**22882.52**	**22795.29**	**22880.53**	**22793.52**
42	**22877.81**	**22788.56**	**22875.73**	**22786.60**
43	**22872.92**	**22781.64**	**22870.95**	**22779.62**
44	**22867.91**	**22774.55**	**22865.79**	**22772.42**
45	**22862.80**	**22767.34**	**22860.49**	**22765.16**
46	**22857.55**	**22759.98**	**22855.03**	**22757.68**

Lagerqvist and Scullman's C-X 3,1 transition lines continued

N	$R_1(N)$	$P_1(N)$	$R_2(N)$	$P_2(N)$
47	22852.09	22752.55	22849.36	22750.05
48	22846.47	22744.93	22843.71	22742.28
49	22840.73	22737.33	22837.78	22734.33
50	22834.85	22729.29	22831.77	22726.26
51	22828.90	22721.13	22825.45	22717.95
52	22822.70	22712.83	22819.03	
53	22816.45		22812.50	
54	22809.95		22805.75	
55	22803.31		22798.76	
56	22796.54		22791.57	
57	22789.55		22784.15	
58	22782.53		22776.62	
59	22775.23		22768.79	
60	22767.83		22760.83	
61	22760.22		22752.54	
62	22752.40		22744.03	
63	22744.52		22735.23	
64	22736.40		22726.17	
65	22728.15			
66	22718.97			

$C^2\Sigma^+ - X^2\Sigma^+$ 3,2 transition lines Lagerqvist and Scullman's (bold type) combined with the low *J* LIF data (normal type)

N	$R_1(N)$	$P_1(N)$	$R_2(N)$	$P_2(N)$
0	21925.43			
1	21926.40	21923.34	21926.65	
2	21927.16	21922.09	21927.41	21921.90
3	21927.93	21920.65	21928.18	21920.46
4	21928.41	21919.11	21928.66	21918.92
5	21928.90	21917.38	21929.15	21917.19
6	21929.28	21915.65	21929.15	21915.22
7	21929.28	21913.73	21929.15	21913.25
8	21929.28	21911.72	21929.15	21911.24
9	21929.28	21909.51	21929.15	21909.03
10	21929.28	21907.20	21929.15	21906.63
11	**21928.88**	**21904.48**	**21928.49**	**21904.11**
12	**21928.49**	**21901.98**	**21928.09**	**21901.62**
13	**21927.93**	**21899.34**	**21927.52**	**21898.86**
14	**21927.21**	**21896.56**	**21926.80**	**21896.05**
15	**21926.32**	**21893.60**	**21925.92**	**21893.09**
16	**21925.38**	**21890.56**	**21924.93**	**21889.88**
17	**21924.32**	**21887.25**	**21923.86**	**21886.70**
18	**21923.11**	**21883.89**	**21922.67**	**21883.37**
19	**21921.83**	**21880.53**	**21921.25**	**21879.93**
20	**21920.35**	**21876.99**	**21919.68**	**21876.23**
21	**21918.68**	**21873.28**	**21918.05**	**21872.48**
22	**21916.91**	**21869.43**	**21916.28**	**21868.65**
23	**21915.08**	**21865.40**	**21914.33**	**21864.56**
24	**21913.07**	**21861.27**	**21912.27**	**21860.49**
25	**21911.03**	**21857.03**	**21910.16**	**21856.23**
26	**21908.76**	**21852.74**	**21907.78**	**21851.84**
27	**21906.41**	**21848.23**	**21905.35**	**21847.32**
28	**21903.86**	**21843.70**	**21902.84**	**21842.69**
29	**21901.24**	**21838.97**	**21900.13**	**21837.90**
30	**21898.56**	**21834.19**	**21897.36**	**21832.97**
31	**21895.64**	**21829.13**	**21894.28**	**21827.91**
32	**21892.59**	**21824.01**	**21891.23**	**21822.79**
33	**21889.36**	**21818.76**	**21887.97**	**21817.47**
34	**21886.01**	**21813.32**	**21884.59**	**21811.91**
35	**21882.55**	**21807.80**	**21881.16**	**21806.33**
36	**21879.02**	**21802.15**	**21877.59**	**21800.69**
37	**21875.28**	**21796.36**	**21873.79**	**21794.85**
38	**21870.85**	**21790.46**	**21869.91**	**21788.83**
39	**21867.61**	**21784.49**	**21865.87**	**21782.78**
40	**21863.53**	**21778.42**	**21861.72**	**21776.64**
41	**21859.23**	**21772.02**	**21857.26**	**21770.24**
42	**21854.86**	**21765.62**	**21852.78**	**21763.59**
43	**21850.40**	**21759.03**	**21848.27**	**21756.95**
44	**21845.74**	**21752.27**	**21843.44**	**21750.12**
45	**21840.98**	**21745.44**	**21838.49**	**21743.22**
46	**21836.01**	**21738.46**	**21833.50**	**21736.07**

Lagerqvist and Scullman's C-X 3,2 transition lines continnued

N	$R_1(N)$	$P_1(N)$	$R_2(N)$	$P_2(N)$
47	21830.92	21731.35	21828.11	21728.86
48	21825.72	21724.14	21822.87	21721.48
49	21820.41	21716.78	21817.35	21713.93
50	21814.92	21709.28		21706.13
51	21809.30	21701.51		21698.36
52	21803.48	21693.67	21799.80	
53	21797.66		21793.70	
54	21791.58		21787.34	
55	21785.41		21780.82	
56	21779.09		21774.10	
57	21772.54		21767.15	
58	21766.03		21760.06	
59			21752.73	

Appendix II

$^4\Pi - {}^4\Sigma^-$

Simulation Program

```
DECLARE SUB result (T, j)
DECLARE SUB spec (T, j)
DECLARE SUB freque ()
DECLARE SUB lstrength ()
COMMON SHARED Bv1, nair#, 10

'THIS PROGRAM SIMULATES A 4Pi(5/2) regular <- 4Sigma TRANSITION

'4Pi(5/2) J=K-3/2,The splitting parameter A is +ve (ie. regular) so the
' 4Pi(5/2) lies higher in energy, hence the F4 designation (Herzberg
page 234)

'This program was created on Aug.8,1996, to simulate CrN 4pi(5/2)<-
4sigma
'transition near 646 nm,by Charles Qian and Chi Zhou.
'The program was subsequentially modified by Romey in order to
'simulate RhO 4Pi5/2(reg) <- 4Sigma

       SCREEN 0
      CLS
      PRINT "You are running a RhO(F4 4pi(5/2)regular <- X 4sigma-)
simulation"

       CALL lstrength

10       CALL freque

       CALL result(T, j)

       CALL spec(T, j)


      INPUT "New start (Y/n)? ", a$
      IF a$ = "n" GOTO 11 ELSE GOTO 10

11 END

  SUB freque

'*^^^^^^^^^^^^^^^^^^^^^^^^^^^^^^^^^^^^^^^^^^^^^^^^^^^^^^^^^^^^^^^^^^^*
'*       branches are labled as follows:                               *
'*   uR41=1, tQ41=2, sP41=3;   tR42=4, sQ42=5, rP42=6;     *
'*   sR43=7, rQ43=8, qP43=9;   R44=10, Q44=11, P44=12      *
'^^^^^^^^^^^^^^^^^^^^^^^^^^^^^^^^^^^^^^^^^^^^^^^^^^^^^^^^^^^^^^^^^^^^

      DIM frqncy(13, 105), engr(105), enex(105)
DIM sigma1(105), sigma2(105), sigma3(105), sigma4(105), PiF4(105)
'In frqncy(i,k),i=branch #, k=N" for the ground state. engr(N") is the
ground
'state energy. enex(N'=J'+1.5) or (J=N-1.5) is the excited state
energy.

'Note:the 4Sigma energy levels are calculated using Merer's matrix
elements (ref 2)
'however,the 4Pi energy levels are calculated using Nevin's case (ab)
formulae (ref 1)
```

```
        l0 = 618.2     'nm,

        Bv1 = .45112: dv1 = -.0000005: lamda = -.43: gama = -.001
        gS = 0!: gD = 0!
        a = 190: Bv2 = .4091: dv2 = -.0000005#

        sg = 1.5: s = 1.5: om = 2.5
        e0 = 10 ^ 7 / 10 - 1.5 * a
'Note that e0 needs to be shifted since case ab formula was used for
4pi(5/2) states

        nair# = 1 + 10 ^ (-7) * (2726.43 + 12.288 * 10 ^ 6 / 10 ^ 2 +
.3555 * 10 ^ 12 / 10 ^ 4)
'nair# formula is from CRC Handbook of Chemistry and Physics

       ' INPUT "Bv1=", Bv1
       ' INPUT "Bv2=", Bv2
       ' INPUT "lamda=", lamda
       ' INPUT "gama=", gama
       ' INPUT "A=", a

       FOR i = 0 TO 100
       x = i * (i + 1!)
       engr(i) = Bv1 * x - dv1 * x * x
       NEXT i
                     'Note the designation of the 4Pi energy levels has
                     'been done with the branch selection process
                     'in mind, which occurs after these calculations.
       FOR i = 3 TO 100
       aj = i - .5              'J=N'-.5 for N'= 3, 4, 5... is the same
as below
       x = aj * (aj + 1!)       'actually, J=N'-1.5 for N'= 4, 5, 6...

    'Hund's case (a) formulae for 4Pi is
    '    enex(i) = A * sg + bv2 * (s * (s + 1!) - om * om - sg * sg) +
bv2 * (i ^ 2 - 1 / 4) - dv2 * (i ^ 2 - 1 / 4) * (i ^ 2 - 1 / 4)

    'Hund's case (ab) formula as given by Nevin for 4Pi 5/2 (F4) is
       y = a / Bv2
       y1 = y * (y - 4!)
       y2 = y * (y - 1!)
       dl = 6! * y * (y + 4!) / (2! * y1 + 8! * (i ^ 2 - 1! / 4!) + 56!)
       enex(i) = Bv2 * (x + (3! / 2!) * SQR(y1 + 4! * x + (23! / 9!) +
(2! * dl / 9!)) - 2! * (y2 - 2! * x) / (y1 + 4! * x)) + dv2 * (aj + 3!
/ 2!) * (aj + 3! / 2!) * (aj + 5! / 2!) * (aj + 5! / 2!)

'4pi(5/2) energy level enec(N'=J'+1.5) is calculated using Nevin's
formula for F4,
'Phil.Trans.Roy.Soc.London 237,471,1938(Ref.1)

       PiF4(i) = enex(i)

       NEXT i
       OPEN "c:\temp\PiF4.dat" FOR OUTPUT AS #1
        FOR i = 3 TO 100
             WRITE #1, PiF4(i)'remember that enex(3) is actually enex(4)
and so on.
```

```
        NEXT i
      CLOSE #1

'Energy level calculation for case (a')and (b) 4sigma- state. Matrix
elements are
'taken from Merer JMSpec 92, 391-409 (1982) (Ref.2). This program was
tested
'on VO and Fig. 2 in Merer's review on oxides (Annu. Rev. Phys. Chem.
1989,
'40, 407-38) (Ref.3) was reproduced.

      FOR i = 0 TO 100
b = Bv1: d = dv1: n = i

j = n + 1.5 ' for 4Sigma-(F1)
z = (j + .5) ^ 2 - 1 ' another way to write J(J+1)
h33 = 2 * lamda + b * z - d * (z ^ 2 + 3 * z) - 1.5 * gama - 3 * gD * z
h11e = -2 * lamda + b * (z + 4!) - d * ((z + 4!) ^ 2 + 7! * z + 4!) -
3.5 * gama - gD * (7 * z + 16!) - 2 * (b - .5 * gama - .5 * gD * (z +
11!) + 1.5 * gS - 2! * d * (z + 4!)) * (j + .5)
h31e = -SQR(3 * z) * (b - .5 * gama - gS - .5 * gD * (z + 7! - (2 * j +
1)) - 2! * d * ((z + 2!) - (j + .5)))
e0e = .5 * (h33 + h11e)
f1 = e0e - SQR((h33 - e0e) ^ 2 + h31e ^ 2)
f1 = f1 - b * n * (n + 1) + d * (n * (n + 1)) ^ 2

'note n=N the case b quantum number, j=J the rotation without nuclear
spin
'h33=<3/2|H|3/2>, etc, see ref2.
'note that the sign before sqrt must be carefully selected to get the
case
'b limit correctly.
'The sign in terms h31 and h11 gave the e/f states h31e,h31f,h11e,and
h11f.

j = n + .5 'for 4Sigma-(F2)
z = (j + .5) ^ 2 - 1
h33 = 2 * lamda + b * z - d * (z ^ 2 + 3 * z) - 1.5 * gama - 3 * gD * z
h11f = -2 * lamda + b * (z + 4) - d * ((z + 4) ^ 2 + 7 * z + 4) - 3.5 *
gama - gD * (7 * z + 16!) + 2 * (b - .5 * gama - .5 * gD * (z + 11) +
1.5 * gS - 2 * d * (z + 4)) * (j + .5)
h31f = -SQR(3 * z) * (b - .5 * gama - gS - .5 * gD * (z + 7 + (2 * j +
1)) - 2 * d * ((z + 2) + (j + .5)))
e0f = .5 * (h33 + h11f)
f2 = e0f - SQR((h33 - e0f) ^ 2 + h31f ^ 2)
f2 = f2 - b * n * (n + 1) + d * (n * (n + 1)) ^ 2

j = n - .5  'for 4Sigma-(F3)
z = (j + .5) ^ 2 - 1
h33 = 2 * lamda + b * z - d * (z ^ 2 + 3 * z) - 1.5 * gama - 3 * gD * z
h11e = -2 * lamda + b * (z + 4) - d * ((z + 4) ^ 2 + 7 * z + 4) - 3.5 *
gama - gD * (7 * z + 16!) - 2 * (b - .5 * gama - .5 * gD * (z + 11) +
1.5 * gS - 2 * d * (z + 4)) * (j + .5)
h31e = -SQR(3 * ABS(z)) * (b - .5 * gama - gS - .5 * gD * (z + 7 - (2 *
j + 1)) - 2 * d * ((z + 2) - (j + .5)))
e0e = .5 * (h33 + h11e)
f3 = e0e + SQR((h33 - e0e) ^ 2 + h31e ^ 2)
```

```
f3 = f3 - b * n * (n + 1) + d * (n * (n + 1)) ^ 2

j = n - 1.5   'for 4Sigma-(F4)
z = (j + .5) ^ 2 - 1
h33 = 2 * lamda + b * z - d * (z ^ 2 + 3 * z) - 1.5 * gama - 3 * gD * z
h11f = -2 * lamda + b * (z + 4) - d * ((z + 4) ^ 2 + 7 * z + 4) - 3.5 *
gama - gD * (7 * z + 16!) + 2 * (b - .5 * gama - .5 * gD * (z + 11) +
1.5 * gS - 2 * d * (z + 4)) * (j + .5)
h31f = -SQR(3 * ABS(z)) * (b - .5 * gama - gS - .5 * gD * (z + 7 + (2 *
j + 1)) - 2 * d * ((z + 2) + (j + .5)))
e0f = .5 * (h33 + h11f)
f4 = e0f + SQR((h33 - e0f) ^ 2 + h31f ^ 2)
f4 = f4 - b * n * (n + 1) + d * (n * (n + 1)) ^ 2

      e1 = f1
      e2 = f2
      e3 = f3
      e4 = f4

sigma1(n) = f1
sigma2(n) = f2
sigma3(n) = f3
sigma4(n) = f4

      IF i < 5 THEN
      frqncy(12, i) = 2000!
      ELSE
      frqncy(12, i) = enex(i - 2) - engr(i) - e4 + e0
      END IF

      IF i < 4 THEN
      frqncy(11, i) = 2000!
      ELSE
      frqncy(11, i) = enex(i - 1) - engr(i) - e4 + e0
      END IF

      IF i < 3 THEN
      frqncy(10, i) = 2000!
      ELSE
      frqncy(10, i) = enex(i) - engr(i) - e4 + e0
      END IF

      IF i < 4 THEN
      frqncy(9, i) = 2000!
      ELSE
      frqncy(9, i) = enex(i - 1) - engr(i) - e3 + e0
      END IF

      IF i < 3 THEN
      frqncy(8, i) = 2000!
      ELSE
      frqncy(8, i) = enex(i) - engr(i) - e3 + e0
      END IF

      IF i < 2 THEN
      frqncy(7, i) = 2000!
      ELSE
```

```
        frqncy(7, i) = enex(i + 1) - engr(i) - e3 + e0
        END IF

        IF i < 3 THEN
        frqncy(6, i) = 2000!
        ELSE
        frqncy(6, i) = enex(i) - engr(i) - e2 + e0
        END IF

        IF i < 2 THEN
        frqncy(5, i) = 2000!
        ELSE
        frqncy(5, i) = enex(i + 1) - engr(i) - e2 + e0
        END IF

        IF i < 1 THEN
        frqncy(4, i) = 2000!
        ELSE
        frqncy(4, i) = enex(i + 2) - engr(i) - e2 + e0
        END IF

        IF i < 2 THEN
        frqncy(3, i) = 2000!
        ELSE
        frqncy(3, i) = enex(i + 1) - engr(i) - e1 + e0
        END IF

        IF i < 1 THEN
        frqncy(2, i) = 2000!
        ELSE
        frqncy(2, i) = enex(i + 2) - engr(i) - e1 + e0
        END IF
        frqncy(1, i) = enex(i + 3) - engr(i) - e1 + e0
         NEXT i

   OPEN "c:\temp\sigma.dat" FOR OUTPUT AS #1
       PRINT #1, "  N  "; "      F1      "; "        F2      "; "
F3      "; "       F4      "
        FOR i = 0 TO 100
        PRINT #1, USING "### ######.####  ######.####  ######.####
######.#### "; i; sigma1(i); sigma2(i); sigma3(i); sigma4(i)
           NEXT i
        CLOSE #1

       OPEN "c:\temp\fcrn4.dat" FOR OUTPUT AS #1
       FOR i = 1 TO 12
       FOR j = 0 TO 100
       WRITE #1, frqncy(i, j)
       NEXT j
       NEXT i
        CLOSE #1


' INPUT "Do you want to print out the wavelength ?
(y/N) ", a$
        OPEN "c:\temp\lcrn4.prt" FOR OUTPUT AS #6
 '       INPUT "Input J-max for print  ==> ", jm
```

```
       WRITE #6, "wavelengths for RhO4Pi(5/2)<-X(0,0) transition:"
      PRINT #6, " N"; "    uR41 "; "    tQ41 "; "    sP41 "; "    tR42
"; "    sQ42 "; "    rP42 "
      PRINT #6, ""
      r19# = 1E+07 / nair#
      FOR j = 0 TO 54
       PRINT #6, USING "###  ###.###  ###.###  ###.###  ###.###
###.###  ###.### "; j; r19# / frqncy(1, j); r19# / frqncy(2, j); r19# /
frqncy(3, j); r19# / frqncy(4, j); r19# / frqncy(5, j); r19# /
frqncy(6, j)
      NEXT j

      PRINT #6, " N"; "    sR43 "; "    rQ43 "; "    qP43 "; "     R44
"; "    Q44 "; "     P44 "
      PRINT #6, ""
      r19# = 1E+07 / nair#
      FOR j = 0 TO 54
       PRINT #6, USING "###  ###.###  ###.###  ###.###  ###.###
###.###  ###.### "; j; r19# / frqncy(7, j); r19# / frqncy(8, j); r19# /
frqncy(9, j); r19# / frqncy(10, j); r19# / frqncy(11, j); r19# /
frqncy(12, j)
      NEXT j

      CLOSE #6
       PRINT "The wavelengths for RhO 4Pi<-X(0,0) transition are saved
in "
       PRINT "File 'c:\temp\lcrn4.prt' "

1300
       ' INPUT "Do you want to print out the frequency ?
(y/N) ", a$
      PRINT
      IF UCASE$(a$) <> "Y" THEN GOTO 1400
       OPEN "c:\temp\fcrn4.prt" FOR OUTPUT AS #6
 '      INPUT "Input J-max for print  ==> ", jm
       PRINT
      WRITE #6, "Frequencies for RhO 4Pi5/2<-X(0,0) transition:"

      PRINT #6, " N"; "    uR41 "; "    tQ41 "; "    sP41 "; "    tR42
"; "    sQ42 "; "    rP42 "
      PRINT #6, ""
      FOR j = 0 TO 54
       PRINT #6, USING "### #####.## #####.## #####.## #####.##
#####.## #####.## "; j; frqncy(1, j); frqncy(2, j); frqncy(3, j);
frqncy(4, j); frqncy(5, j); frqncy(6, j)
      NEXT j

      PRINT #6, " N"; "    sR43 "; "    rQ43 "; "    qP43 "; "
R44"; "     Q44 "; "     P44"
      PRINT #6, ""
      FOR j = 0 TO 54
       PRINT #6, USING "### #####.## #####.## #####.## #####.##
#####.## #####.## "; j; frqncy(7, j); frqncy(8, j); frqncy(9, j);
frqncy(10, j); frqncy(11, j); frqncy(12, j)
      NEXT j

      CLOSE #6
```

```
       PRINT "The frequencies for RhO 4Pi5/2<-X(0,0) transitions are
saved in "
       PRINT "File 'c:\temp\fcrn4.prt' "

1400 END SUB

    SUB lstrength

'*   linestengths for 4 sigma->4 pi(-1/2) transition. Taken from Kovacs
*
'*   pg 147 assuming case a for the pi states.
*
'*
*
'*
*
'^^^^^^^^^^^^^^^^^^^^^^^^^^^^^^^^^^^^^^^^^^^^^^^^^^^^^^^^^^^^^^^^^^^^^^^*
'*       branches are labled as the following:                          *
'*   uR41=1, tQ41=2, sP41=3;   tR42=4, sQ42=5, rP42=6;     *
'*   sR43=7, rQ43=8, qP43=9;   R44=10, Q44=11, P44=12      *
'^^^^^^^^^^^^^^^^^^^^^^^^^^^^^^^^^^^^^^^^^^^^^^^^^^^^^^^^^^^^^^^^^^^^^^^
'*************************************************************************
**

      DIM s(13, 105)

    FOR i = 1 TO 12
    FOR j = 0 TO 100
    s(i, j) = 0
    NEXT j
    NEXT i

    FOR jl = 0 TO 100
      rj = jl + 2.5  'rj=J',jl=N"
       s(1, jl) = (2! * rj + 3!) * (2! * rj + 5!) * (2! * rj + 7!) /
(rj * (rj + 1!))
    NEXT jl

    FOR jl = 1 TO 100
      rj = jl + 1.5
        s(2, jl) = (2! * rj - 3!) * (2! * rj + 1!) * (2! * rj + 3!) *
(2 * rj + 5!) / (rj * rj * (rj + 1!))
        s(4, jl) = 3! * (2! * rj + 3!) * (2! * rj + 5!) * (2! * rj +
7!) / (rj + 1!) ^ 2
    NEXT jl

    FOR jl = 2 TO 100
      rj = jl + .5
        s(3, jl) = (2! * rj - 5!) * (2! * rj - 3!) * (2! * rj + 3!) /
rj ^ 2
        s(5, jl) = 3! * (2! * rj - 3!) * (2! * rj + 1!) * (2! * rj +
3!) * (2! * rj + 5!) / (rj * (rj + 1!) ^ 2)
        s(7, jl) = 3! * (2! * rj - 1!) * (2! * rj + 5!) * (2! * rj +
7!) / (rj * (rj + 1!))
    NEXT jl

    FOR jl = 3 TO 100
```

```
      rj = jl - .5
        s(6, jl) = 3! * (2! * rj - 5!) * (2! * rj - 3!) * (2! * rj +
3!) / (rj * (rj + 1!))
        s(8, jl) = 3! * (2! * rj - 3!) * (2! * rj - 1!) * (2! * rj +
1!) * (2! * rj + 5!) / (rj * rj * (rj + 1!))
        s(10, jl) = (2 * rj - 1!) * (2! * rj + 5!) * (2! * rj + 7!) /
(rj + 1!) ^ 2
    NEXT jl

    FOR jl = 4 TO 100
      rj = jl - 1.5
        s(9, jl) = 3! * (2! * rj - 5!) * (2! * rj - 3!) * (2! * rj -
1!) / rj ^ 2
        s(11, jl) = (2! * rj - 3!) * (2! * rj - 1!) * (2! * rj + 1!) *
(2! * rj + 5!) / (rj * (rj + 1!) ^ 2)
    NEXT jl

    FOR jl = 5 TO 100
      rj = jl - 2.5
      s(12, jl) = (2! * rj - 5!) * (2! * rj - 3!) * (2 * rj - 1!) / (rj
* (rj + 1!))
    NEXT jl

    FOR i = 1 TO 12
    FOR j = 0 TO 100
      s(i, j) = s(i, j) / 128!
      NEXT j
      NEXT i

'       INPUT ; "Do you want to save  the linestrengths ?
(y/N) ", answer$
'       PRINT
'       IF UCASE$(answer$) = "Y" THEN
    OPEN "c:\temp\lcrn4.dat" FOR OUTPUT AS #21
       FOR i = 1 TO 12
       FOR j = 0 TO 100
       WRITE #21, s(i, j)
       NEXT j
       NEXT i
   CLOSE #21

'     END IF

END SUB

SUB result (T, j)

      DIM pop(5, 103), enx(103), frqn(13, 103), s(13, 103), branch$(12)
       ak = .695

'=====================================================================
====
'==================== Calculate Boltzmann distribution
====================
'=====================================================================
====
```

```
        T = 30
      ' INPUT ; "Input temperature : ", T
        FOR kx = 0 TO 100
          x = kx * (kx + 1!)
          enx(kx) = Bv1 * x
        NEXT kx

       FOR i = 0 TO 100
          r1 = i + 1.5
         pop(1, i) = 2! * (r1 + .5) * EXP(-enx(i) / (ak * T))
          r1 = i + .5
          pop(2, i) = 2! * (r1 + .5) * EXP(-enx(i) / (ak * T))
          r1 = i - .5
          IF r1 < 0 GOTO 12
          pop(3, i) = 2! * (r1 + .5) * EXP(-enx(i) / (ak * T))
          r1 = i - 1.5
          IF r1 < 0 GOTO 12
          pop(4, i) = 2! * (r1 + .5) * EXP(-enx(i) / (ak * T))
12       NEXT i

'=============================================================================
====
'============== Read the frequencies and linestrengths from data files
===
'=============================================================================
====

      OPEN "c:\temp\fcrn4.dat" FOR INPUT AS #1
        FOR i = 1 TO 12
        FOR j = 0 TO 100
         INPUT #1, frqn(i, j)
        NEXT j
        NEXT i
       CLOSE #1

     OPEN "c:\temp\lcrn4.dat" FOR INPUT AS #21
       FOR i = 1 TO 12
       FOR j = 0 TO 100
        INPUT #21, s(i, j)
       NEXT j
       NEXT i
     CLOSE #21

       smax = 0!
       FOR j = 0 TO 100
        FOR i = 1 TO 3
        s(i, j) = pop(1, j) * s(i, j)
        IF s(i, j) > smax THEN smax = s(i, j)
        s(i + 3, j) = pop(2, j) * s(i + 3, j)
        IF s(i + 3, j) > smax THEN smax = s(i + 3, j)
        s(i + 6, j) = pop(3, j) * s(i + 6, j)
        IF s(i + 6, j) > smax THEN smax = s(i + 6, j)
        s(i + 9, j) = pop(4, j) * s(i + 9, j)
        IF s(i + 9, j) > smax THEN smax = s(i + 9, j)
        NEXT i
       NEXT j
```

```
'=========================================================================
'       save the intensities and frequencies in a file
'=========================================================================
=

       flname$ = "crn30"
    OPEN "c:\temp\crn30.dat" FOR OUTPUT AS #24
       PRINT #24, " Frequency                    Linestrength"
       FOR i = 1 TO 12
       FOR j = 0 TO 100
       PRINT #24, frqn(i, j), (s(i, j) / smax)
       NEXT j
       NEXT i
       CLOSE #24
'       GOTO 141

PRINT
PRINT "The frequencies and intensities were saved in file 'c:\temp\" +
flname$ + ".dat'"

branch$(1) = "uR41"
branch$(2) = "tQ41"
branch$(3) = "sP41"
branch$(4) = "tR42"
branch$(5) = "sQ42"
branch$(6) = "rP42"
branch$(7) = "sR43"
branch$(8) = "rQ43"
branch$(9) = "qP43"
branch$(10) = "rR44 "
branch$(11) = "qQ44 "
branch$(12) = "pP44 "
      ' INPUT "Branch asignment J max =", BN
    OPEN "c:\temp\" + flname$ + ".tab" FOR OUTPUT AS #25

       PRINT #25, "Boltzmann-distribution  ( T = "; T; " K)"

       PRINT #25, " N''  Wave#     Wavelength  intensity "
       PRINT #25, "     [cm-1]       [nm]        [-]"

       nair# = 1.0002798#
       x11 = 1E+07 / nair#
       FOR i = 1 TO 12
       PRINT #25,
       PRINT #25, "Branch " + branch$(i) + "(#"; i; ")"
       FOR j = 0 TO 30
       PRINT #25, USING "##    #####.##    ####.###    #.#### "; j;
frqn(i, j); x11 / frqn(i, j); (s(i, j) / smax)
       NEXT j
       NEXT i
       CLOSE #25
PRINT
PRINT "The frequency and linestrength were also saved in file
'c:\temp\" + flname$ + ".tab"
PRINT "for the assignment of the lines in the spectrum"
141
       END SUB
```

```
      SUB spec (T, j)
'
      DIM s(13, 105), wavel(13, 101), spe(-200 TO 5001), gauss(200),
ix(13, 105)
      imax = 5000

'        FILES "c:\temp\*.dat"
'        PRINT
'50      INPUT "Input filename of the results ==> ", flname$


OPEN "c:\temp\crn30.dat" FOR INPUT AS #20
 INPUT #20, a$
  FOR i = 1 TO 12
  FOR j = 0 TO 100
  INPUT #20, wavel(i, j), s(i, j)
  NEXT j
  NEXT i
CLOSE #20

    FOR i = 1 TO 12
     FOR j = 0 TO 100
     wavel(i, j) = 1E+07 / (wavel(i, j) * nair#)
     NEXT j
    NEXT i

60   FOR i = 1 TO imax
     spe(i) = 0!
     NEXT i
FOR i = 1 TO 12
FOR j = 0 TO 100
      ix(i, j) = 0
NEXT j
NEXT i

'=============================================================================
===
'================== Start of Convolution
================================
'=============================================================================
===

      INPUT "Input lower wavelength  [ 617 nm ] ", w1
      IF w1 = 0 THEN w1 = 617
      INPUT "Input higher wavelength [ 620 nm ] ", w0
      IF w0 = 0 THEN w0 = 620

      rt1# = (imax) / ABS(w1 - w0)
      PRINT " rt1 = ", rt1#
      INPUT "Input laser line width (in cm-1) [.13 cm-1 ]: ", wala

      IF wala = 0 THEN wala = .13
      wav = (w1 + w0) / 2!
      frav = 1E+07 / (wav * nair#)
      wala = wala * wav / frav
      wgauss = wala * rt1# * 4!
```

```
      ngauss = wgauss
      wlaser = wala * rt1#
      IF ngauss > 200 THEN ngauss = 200
      cst = 2 * SQR(LOG(2!))

     FOR i = 1 TO ngauss
     gauss(i) = EXP(-(cst * (i - 1!) / wlaser) ^ 2)
     NEXT i
      delt = 4! * wala * rt1#
      ldelt = delt
      FOR i = 1 TO 12
      FOR j = 0 TO 100
         s1 = s(i, j)

         ia = -(w1 - wavel(i, j)) * rt1#

         'ia = ABS(a)

         IF ia > (imax + ldelt) OR ia < (1 - ldelt) THEN GOTO 140
         IF ia < 1 OR ia > imax THEN GOTO 80
         spe(ia) = spe(ia) + gauss(1) * s1
         IF s(i, j) > .0001 THEN ix(i, j) = ia
80            FOR l = 2 TO ngauss
           iap = ia + l - 1
           IF iap > imax THEN GOTO 100
90           spe(iap) = spe(iap) + gauss(l) * s1
           NEXT l
100          FOR l = 2 TO ngauss
           iam = ia - l + 1
           IF iam < 1 OR iam > 5000 THEN GOTO 140
120          spe(iam) = spe(iam) + gauss(l) * s1
           NEXT l
140      NEXT j
         NEXT i

'=============================================================================
======
'========================== Normalization
================================
'=============================================================================
=====

    spmax = 0
    FOR i = 1 TO imax
    IF spe(i) > spmax THEN spmax = spe(i)
    NEXT i
    IF spmax = 0 THEN END
    FOR i = 1 TO imax
    spe(i) = spe(i) / spmax
    NEXT i

'INPUT "Do you want to save the spectral information ?
(y/N) ", a$

'IF a$ <> "y" THEN GOTO 160
       ' INPUT ; "File name for spectral information ==> ", flname$
```

```
        ' dw = (w1 - w0) / (imax - 1)
       ' OPEN flname$ + ".dat" FOR OUTPUT AS #21
       ' WRITE #21, imax, dw, w1, w0
        ' FOR i = 1 TO imax
        ' WRITE #21, spe(i)
        ' NEXT i
      '  CLOSE #21

       ' OPEN flname$ + ".lbl" FOR OUTPUT AS #22
       '   '  FOR i = 1 TO 12
        ' FOR j = 0 TO 100
        ' WRITE #22, ix(i, j)
        ' NEXT j
        ' NEXT i
       ' CLOSE #22

'================================================================================
====
'============================  graphics part
=================================
'================================================================================
====

160 scale = 1
    ybas = 0
'    INPUT "Do you want labels ?                    (y/N) ", A$
       a$ = "y"
      IF a$ = "y" THEN
      scale = .85
      ybas = .15
      END IF

'INPUT "Do you want to enlarge the Y-axis ?                    (y/N) ",
b$
'    b$ = "N"
'    IF b$ = "y" THEN
'    INPUT "Input scaling factor ==> ", scale
'    END IF

CLS
SCREEN 12

VIEW (1, 1)-(638, 450), 0, 15
WINDOW (5000, -.02)-(1, 1.02)

    FOR i! = 2 TO 5000
    LINE (i! - 1, (ybas + scale * spe(i! - 1)))-(i, (ybas + scale *
spe(i!))), 15
    NEXT i

xw = w1 - w0
n1 = FIX(xw)
rt2 = 1!
IF n1 <> 0 GOTO 13

DO
    xw = 10! * xw
```

```
    rt2 = 10! * rt2
    n1 = FIX(xw)
LOOP WHILE n1 = 0


13  i0 = rt1# * (w1 * rt2 - FIX(w1 * rt2)) / rt2
    ninc = rt1# / rt2

    FOR l = 1 TO n1 + 1
      iy = (l - 1) * ninc + i0
      i! = iy
      LINE (i!, -.02)-(i!, 0), 15
      IF FIX(FIX(w1 - i! / rt1# + .5) * 10) = FIX((w1 - i! / rt1#) *
10) THEN LINE (i!, -.02)-(i!, .06), 14
    NEXT l

    rt2 = rt2 * 10
    n1 = FIX(xw * 10!)
    i0 = rt1# * (w1 * rt2 - FIX(w1 * rt2)) / rt2
    ninc = rt1# / rt2

    FOR l = 1 TO n1 + 1
      iy = (l - 1) * ninc + i0
      i! = iy
      LINE (i!, -.02)-(i!, -.01), 7
    NEXT l


IF a$ <> "y" THEN GOTO 180
    FOR i = 1 TO 12
      FOR j = 0 TO 100
      IF (FIX(j / 5) = (j / 5)) THEN
          xtra = .02
          ELSE xtra = .01
      END IF
      LINE (ix(i, j), ((i - 1) * .0125))-(ix(i, j), ((i - 1) * .0125 +
xtra)), i
      NEXT j
    NEXT i

'=============================================================================
=====
'========================== Hardcopy for Genplot
==========================
'=============================================================================
=====
180  LOCATE 1, 2
PRINT "RhO 4Pi(5/2)<-4sigma- spectrum   range : "; w1; "nm to "; w0;
"nm"
LOCATE 2, 2

      INPUT "Do you want a hardcopy of this spectrum (e.g. for Genplot)
(y/N) ?", a$
    IF a$ = "y" THEN
      INPUT "File name ==> ", flname$
       OPEN "c:\temp\" + flname$ + ".prn" FOR OUTPUT AS #5
```

```
      'IF T <> 0 THEN
      ' PRINT #5, "Boltzmann-distribution  ( T = "; T; " K)"
      ' ELSE PRINT #5, "Gauss-distribution  ( J- average = "; jave; ")"

       PRINT #5, "VO-spectrum   range : "; wl; "nm to "; w0; "nm"

          FOR i! = 2 TO 5000 STEP 1
          PRINT #5, wl + i! / rt1#, (ybas + scale * spe(i! - 1))
          NEXT i
      CLOSE #5
       ' END IF
    PRINT "A file 'c:\temp\" + flname$ + ".prn' has been created"
     END IF


115 INPUT "Do you want a new window
(y/N) ?", a$
IF a$ = "y" GOTO 60


END SUB
```

Appendix III

$Rh^{16}O$ / $Rh^{18}O$

LIF Spectra /cm^{-1}
(Intensity in Arbitrary Units)

Band System /nm **Page**

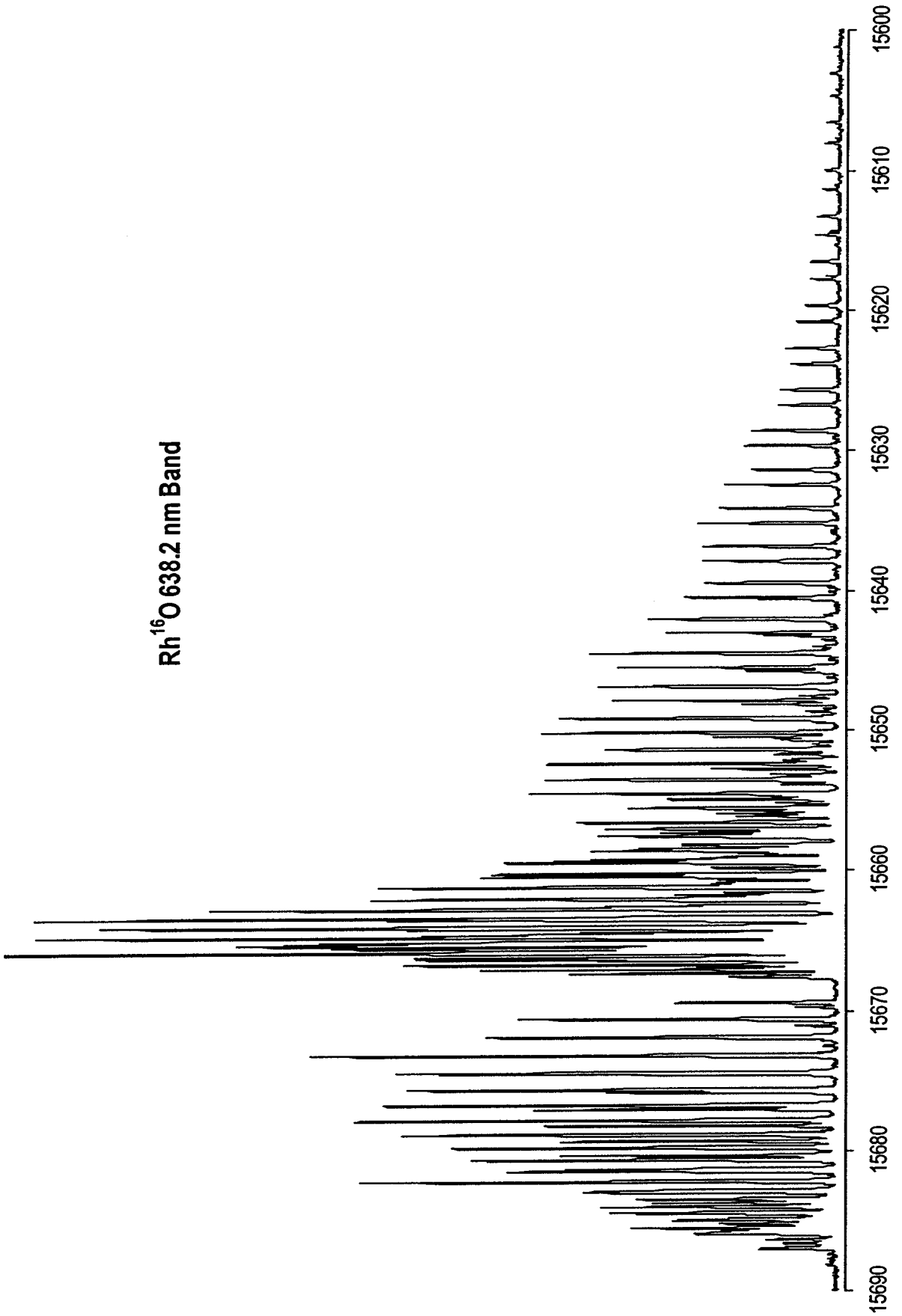
Rh16O 638.2 nm Band
15690
15680
15670
15660
15650
15640
15630
15620
15610
15600

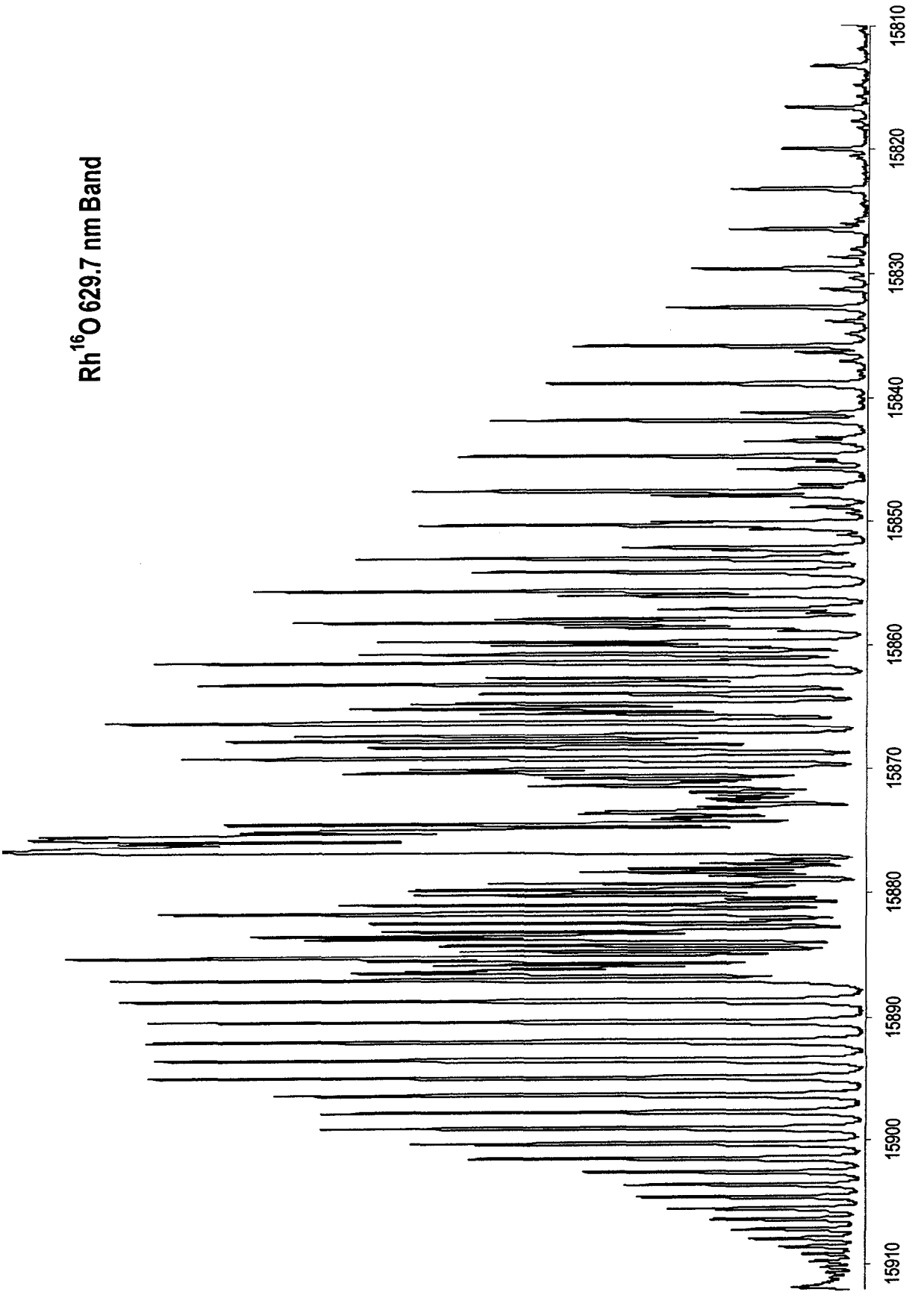
$Rh^{16}O$ 629.7 nm Band
15910
15900
15890
15880
15870
15860
15850
15840
15830
15820
15810

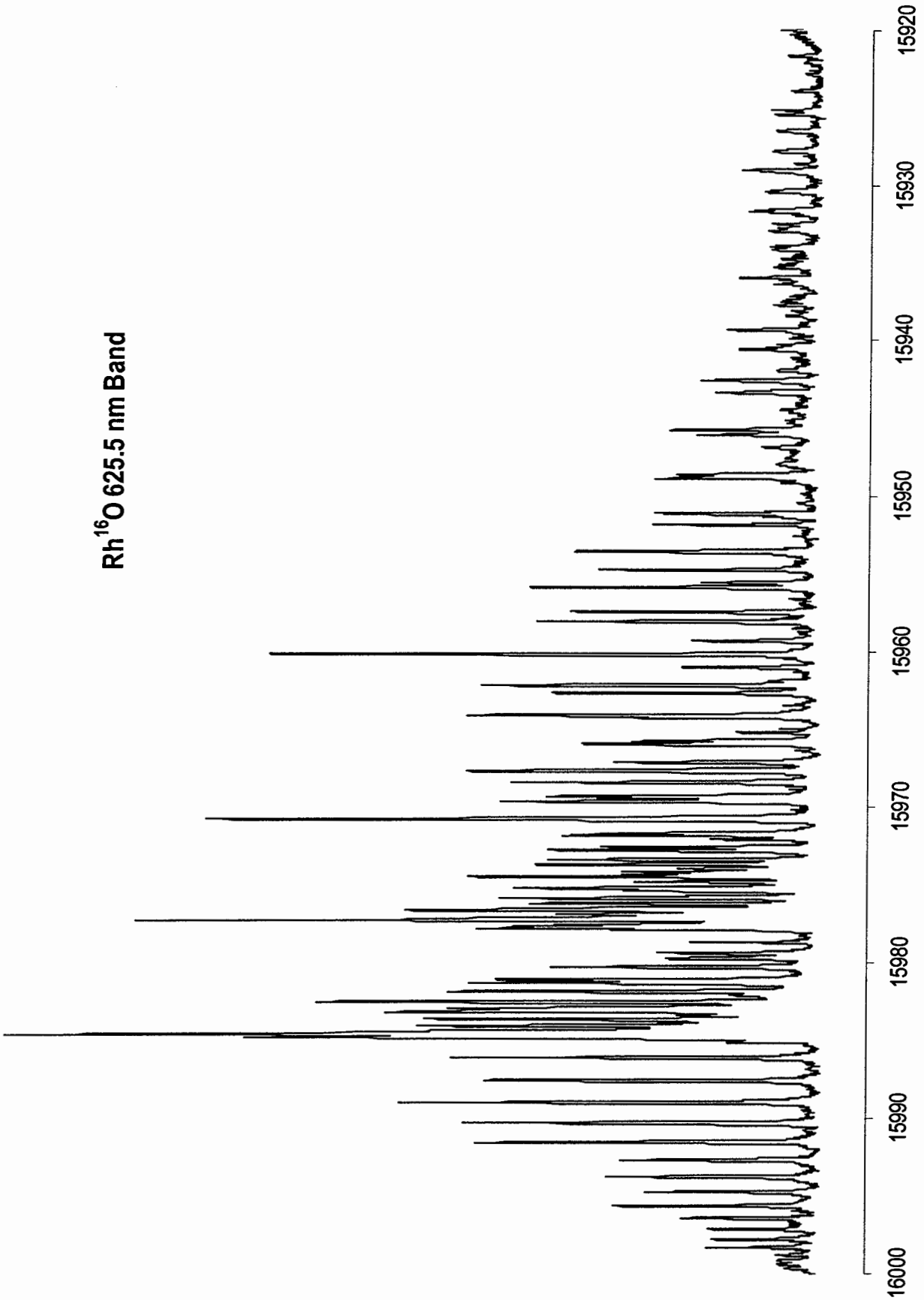
Rh16O 625.5 nm Band
16000
15990
15980
15970
15960
15950
15940
15930
15920

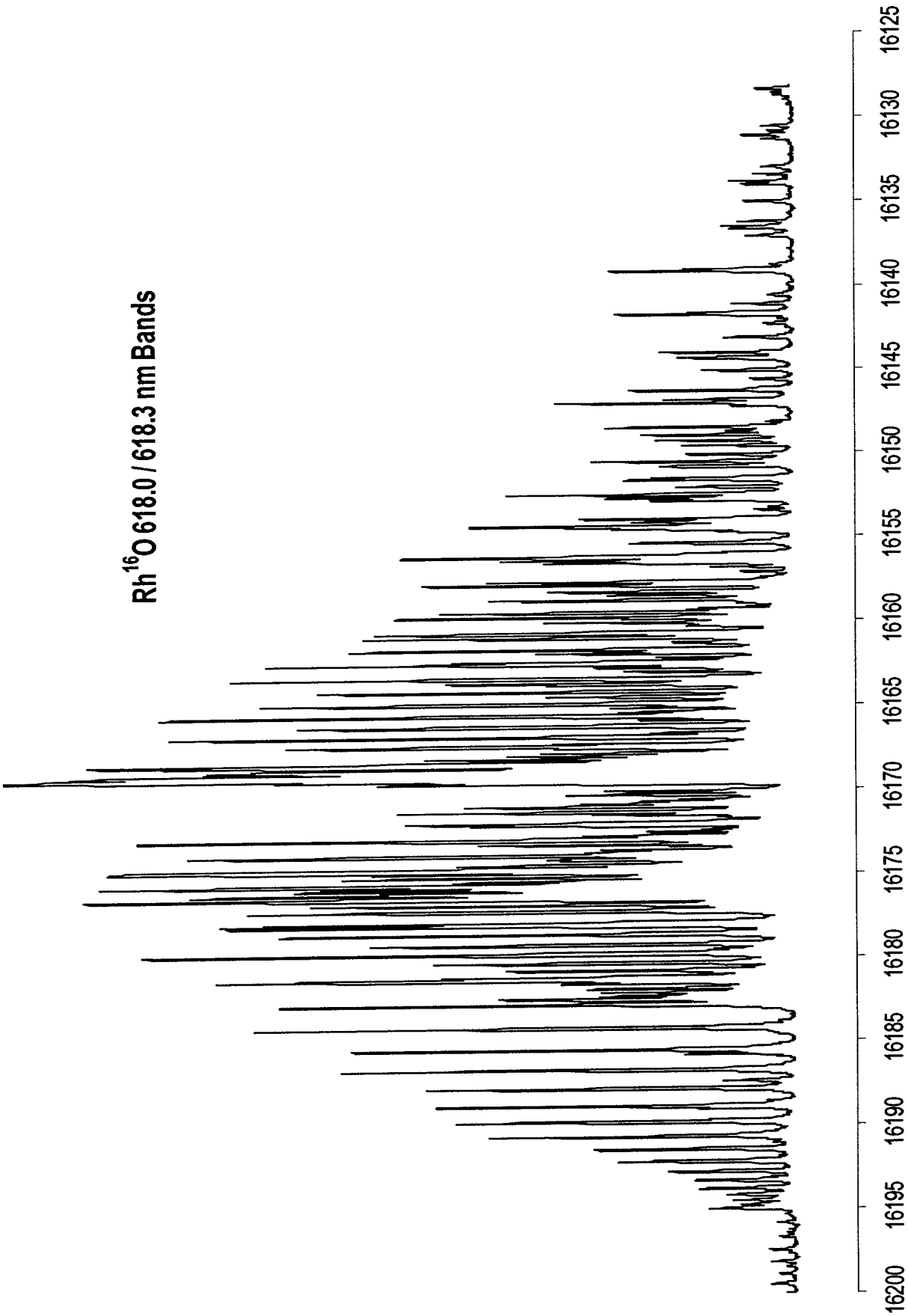
Rh 16O 618.0 / 618.3 nm Bands
16125
16130
16135
16140
16145
16150
16155
16160
16165
16170
16175
16180
16185
16190
16195
16200

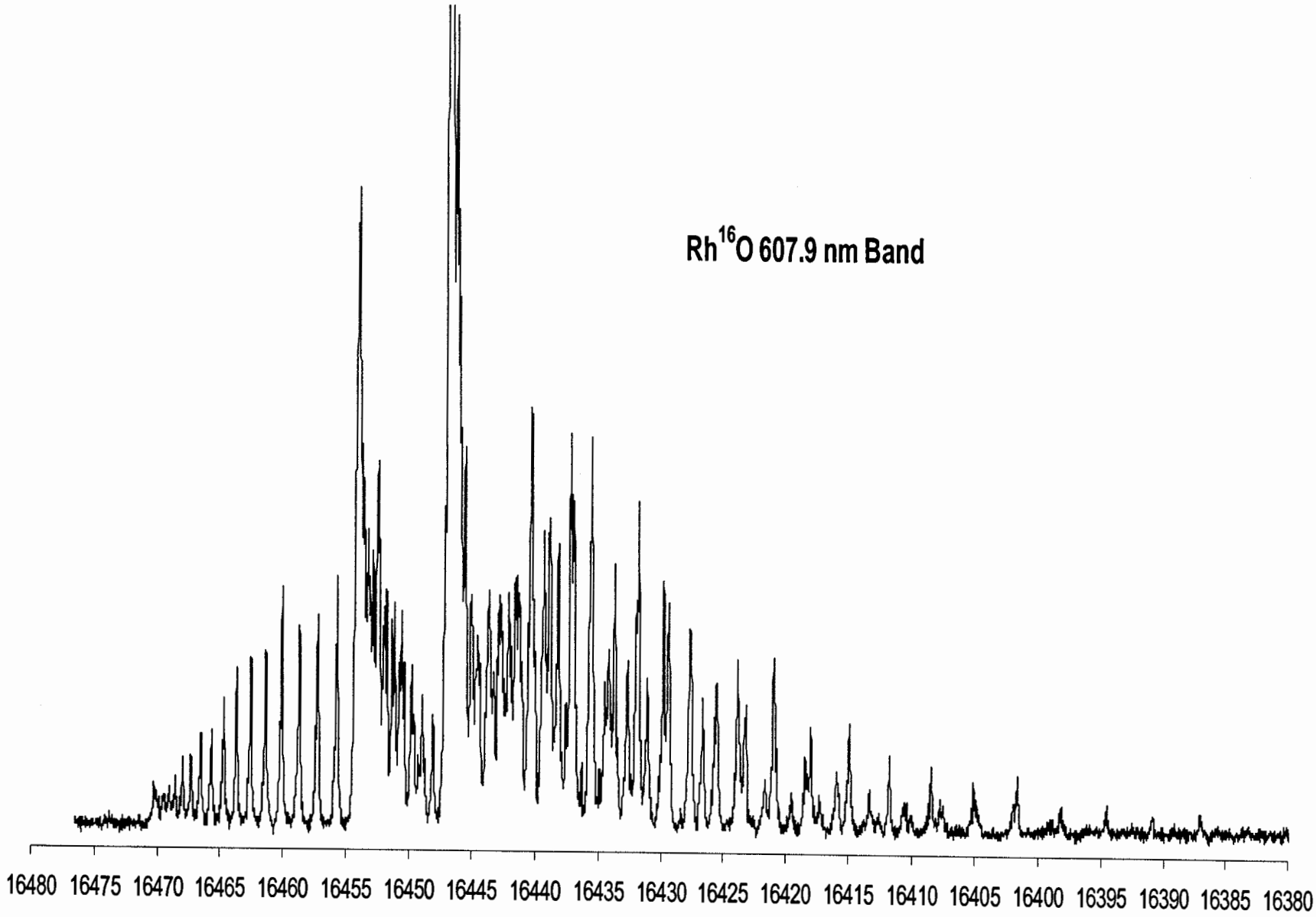
Rh16O 607.9 nm Band
16480 16475 16470 16465 16460 16455 16450 16445 16440 16435 16430 16425 16420 16415 16410 16405 16400 16395 16390 16385 16380

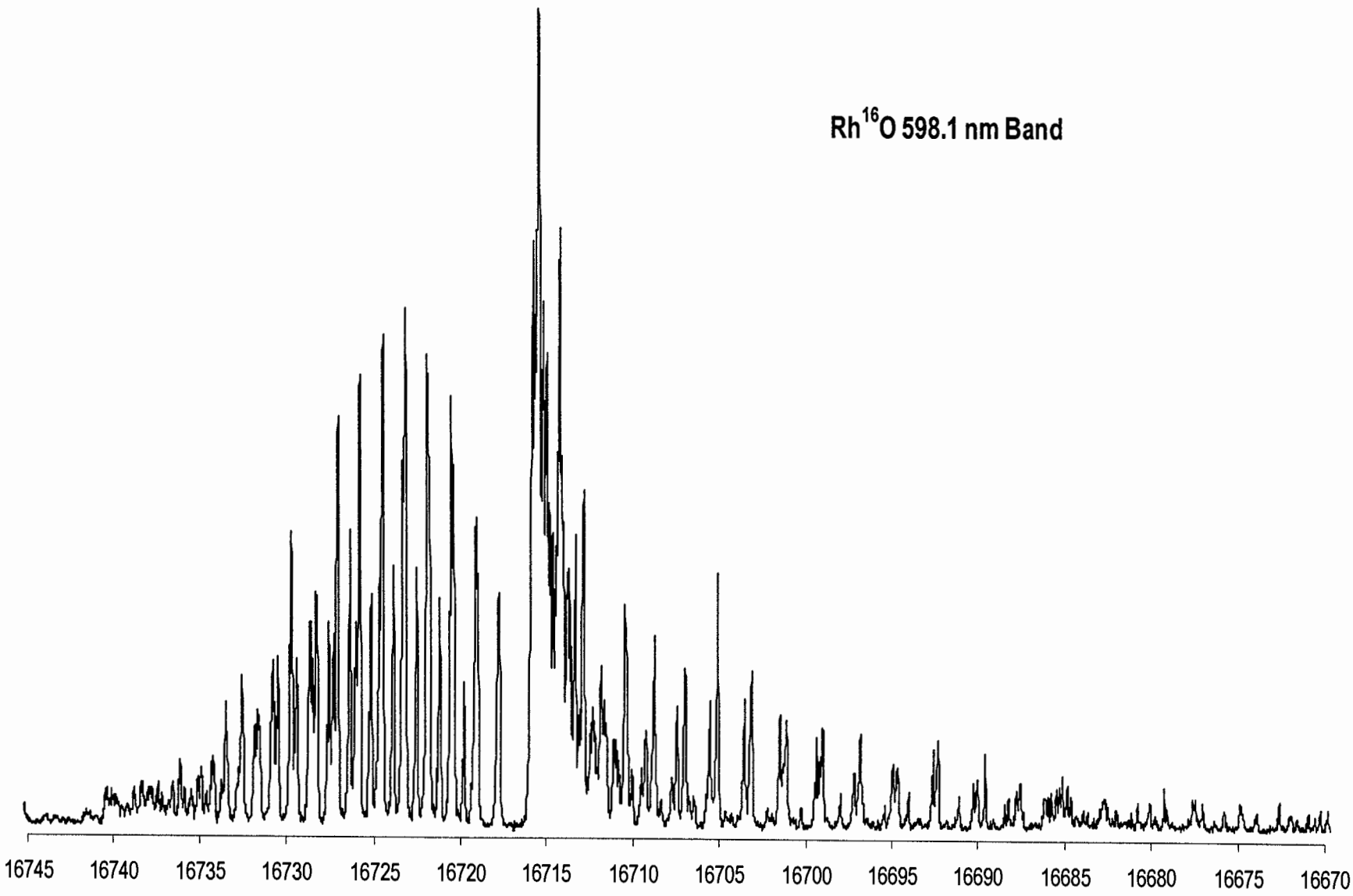
Rh16O 598.1 nm Band
16745
16740
16735
16730
16725
16720
16715
16710
16705
16700
16695
16690
16685
16680
16675
16670

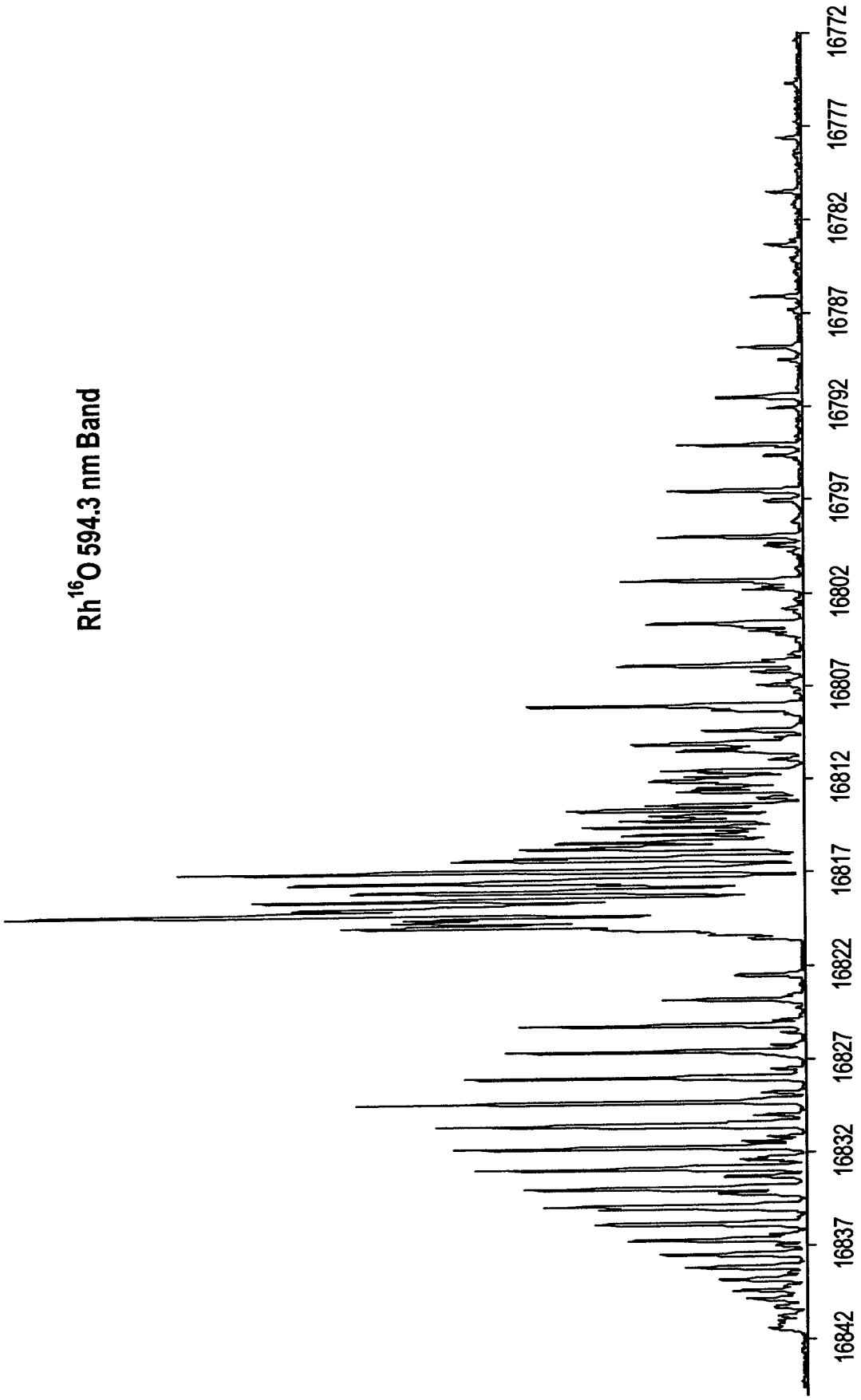
$Rh^{16}O$ 594.3 nm Band
16772
16777
16782
16787
16792
16797
16802
16807
16812
16817
16822
16827
16832
16837
16842

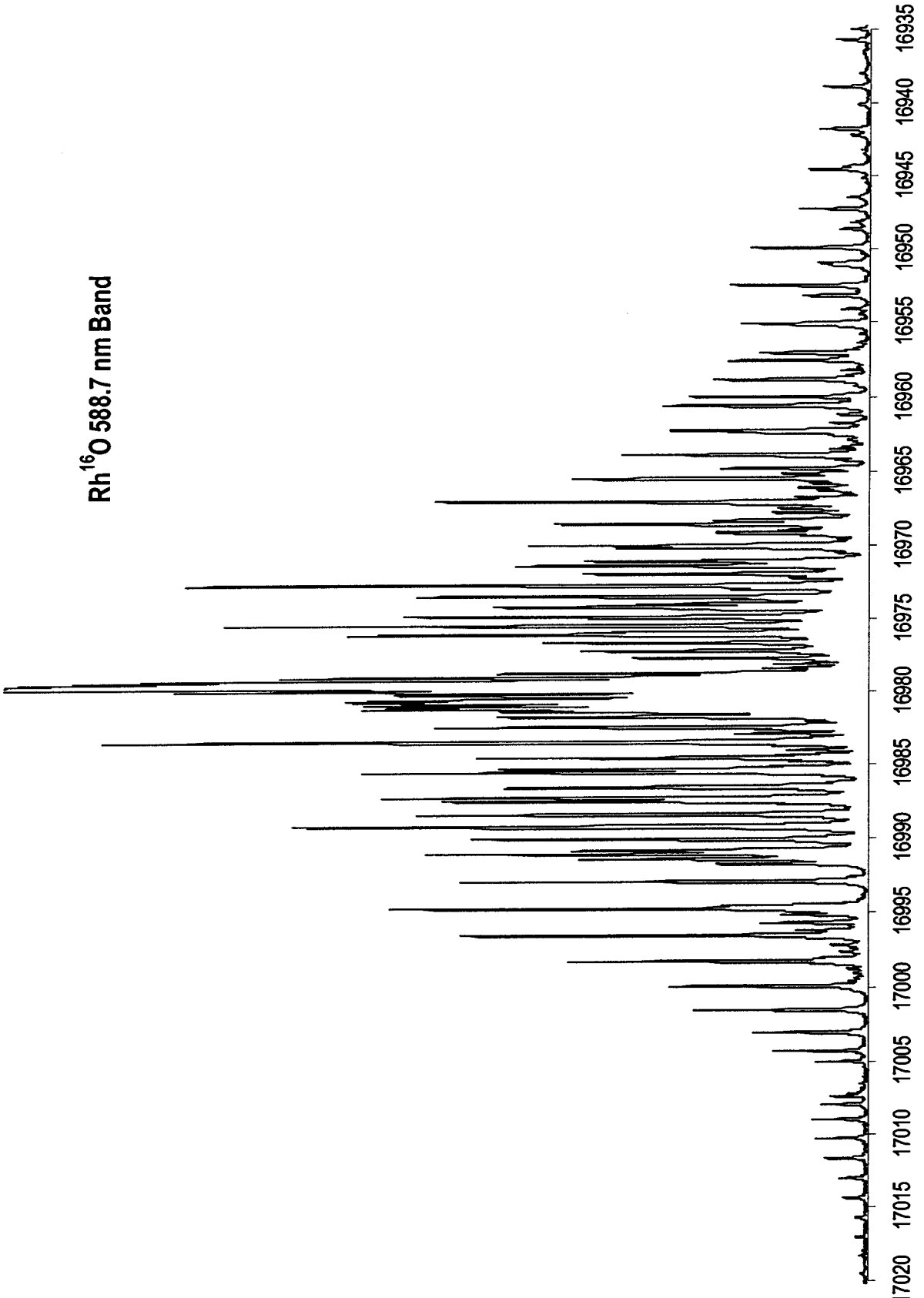
Rh16O 588.7 nm Band
17020
17015
17010
17005
17000
16995
16990
16985
16980
16975
16970
16965
16960
16955
16950
16945
16940
16935

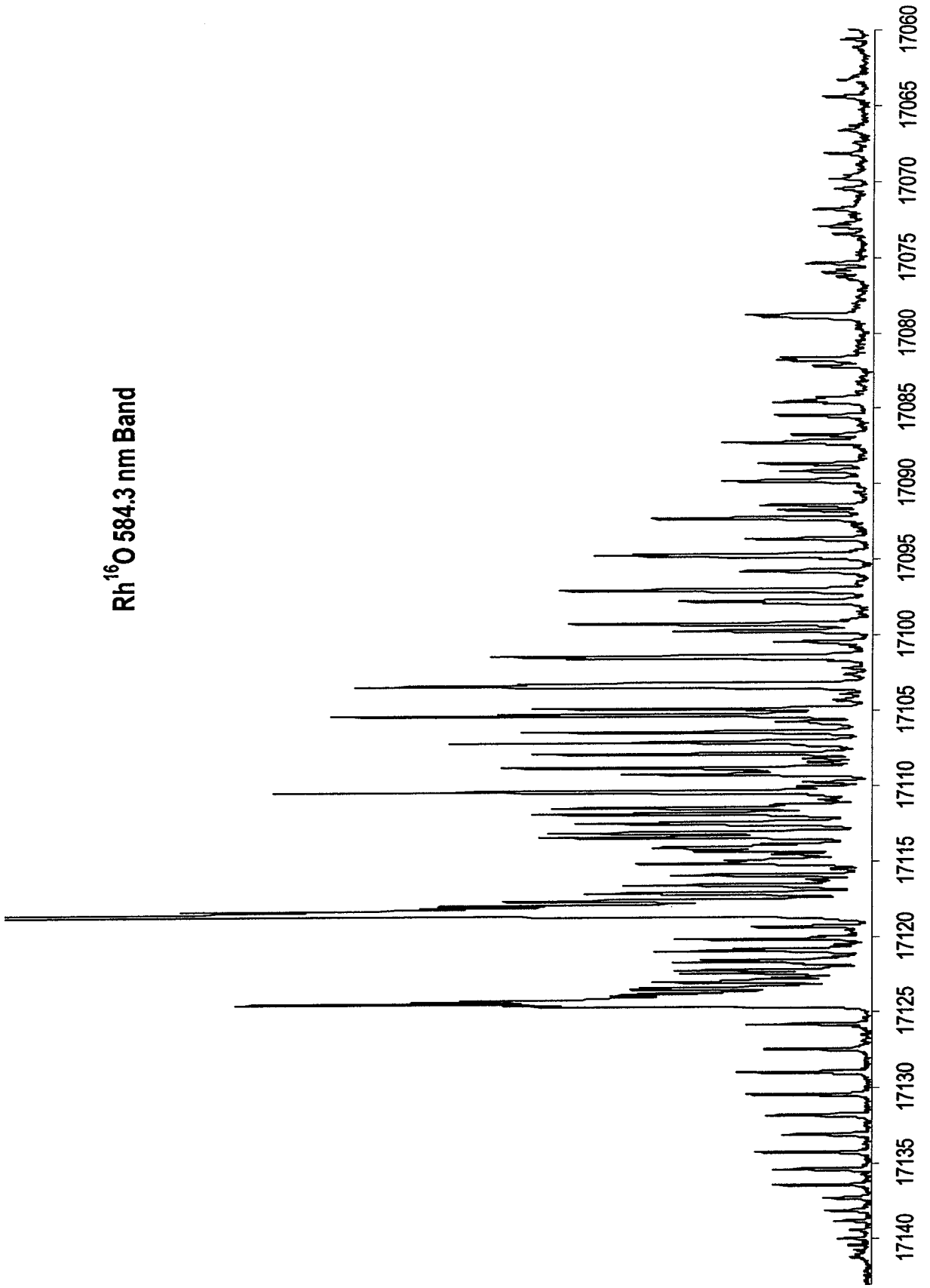
$Rh^{16}O$ 584.3 nm Band
17140
17135
17130
17125
17120
17115
17110
17105
17100
17095
17090
17085
17080
17075
17070
17065
17060

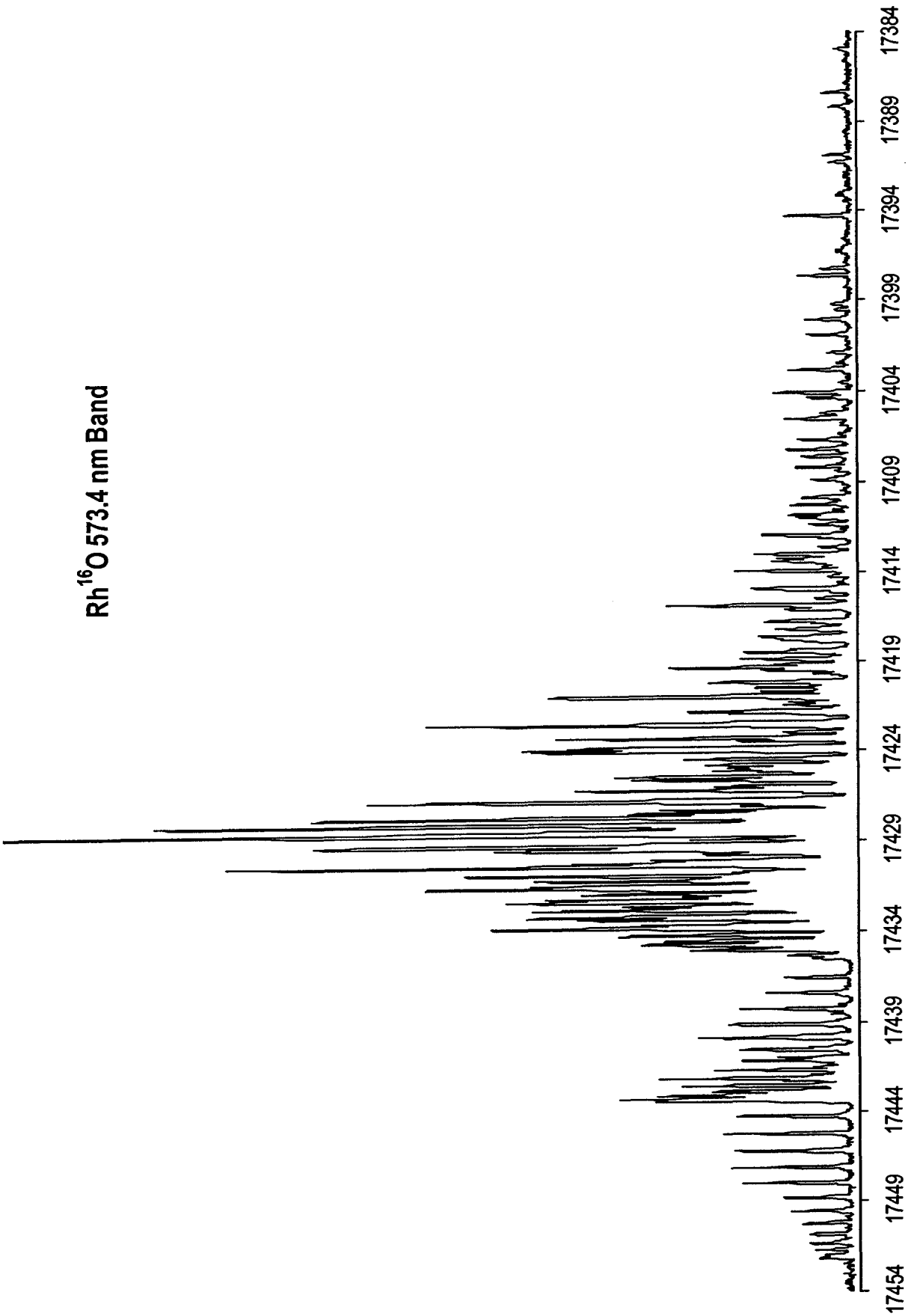
Rh16O 573.4 nm Band
17454
17449
17444
17439
17434
17429
17424
17419
17414
17409
17404
17399
17394
17389
17384

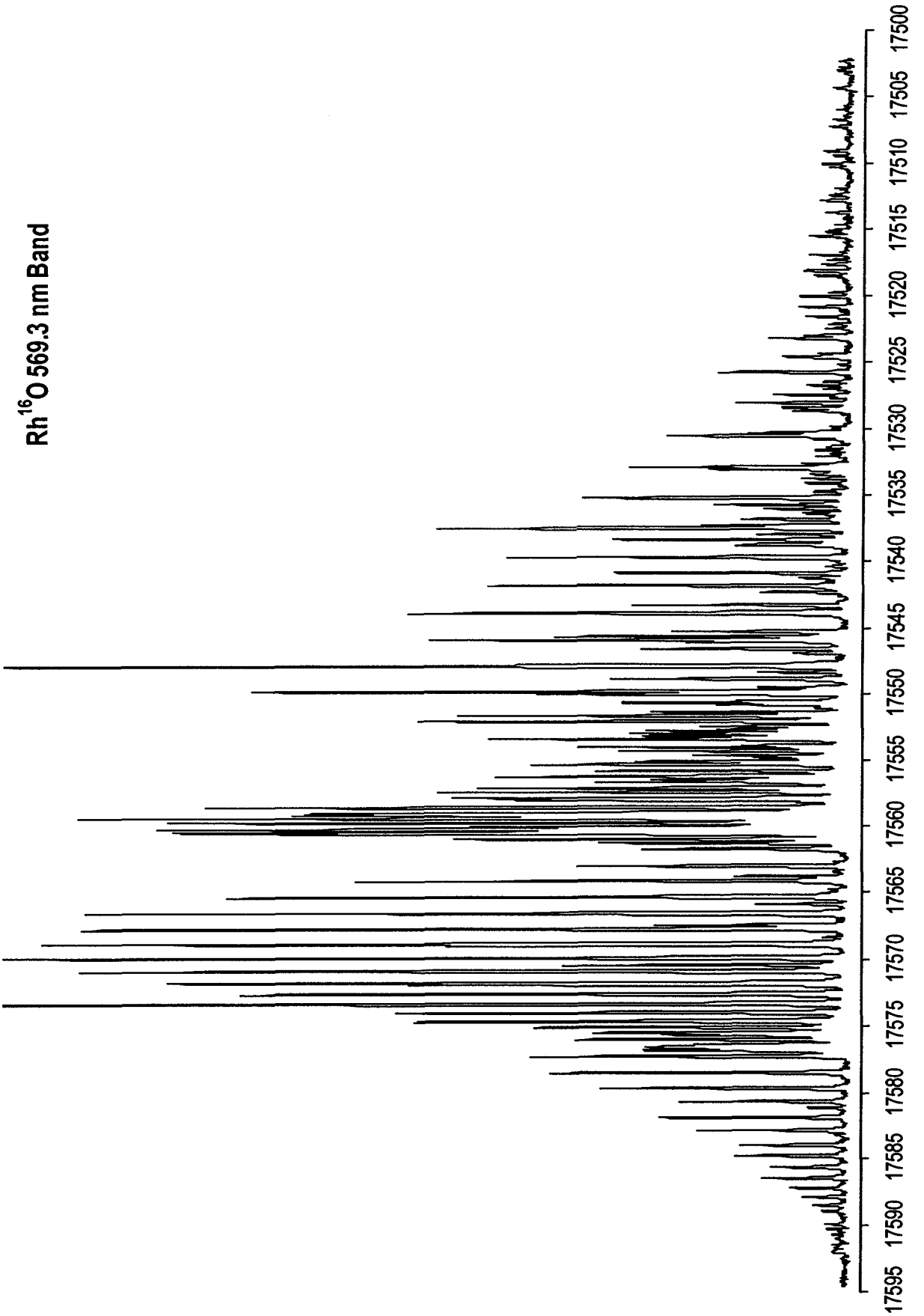
Rh 16O 569.3 nm Band
17595
17590
17585
17580
17575
17570
17565
17560
17555
17550
17545
17540
17535
17530
17525
17520
17515
17510
17505
17500

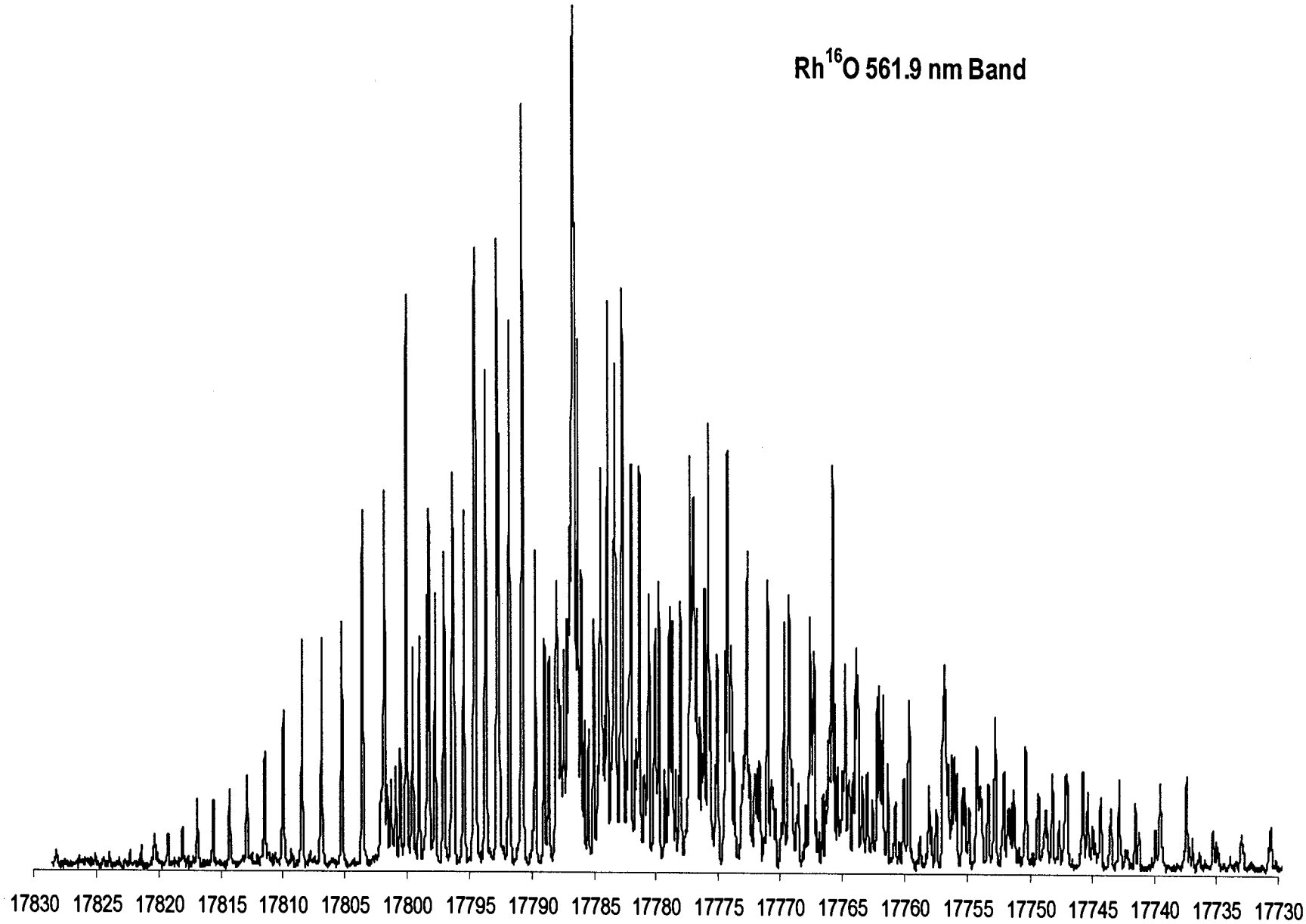
Rh16O 561.9 nm Band
17830 17825 17820 17815 17810 17805 17800 17795 17790 17785 17780 17775 17770 17765 17760 17755 17750 17745 17740 17735 17730

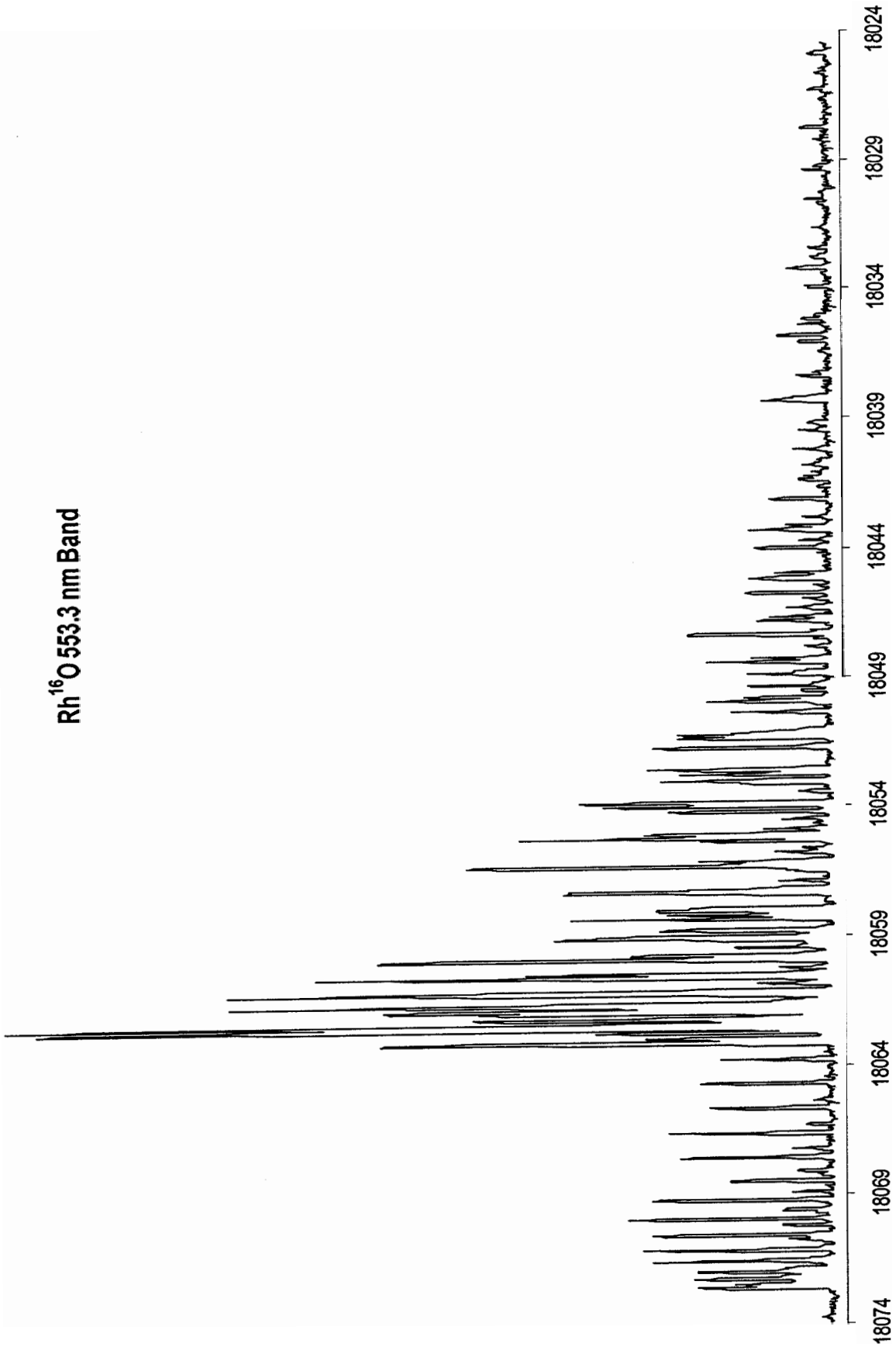
Rh16O 553.3 nm Band
18074
18069
18064
18059
18054
18049
18044
18039
18034
18029
18024

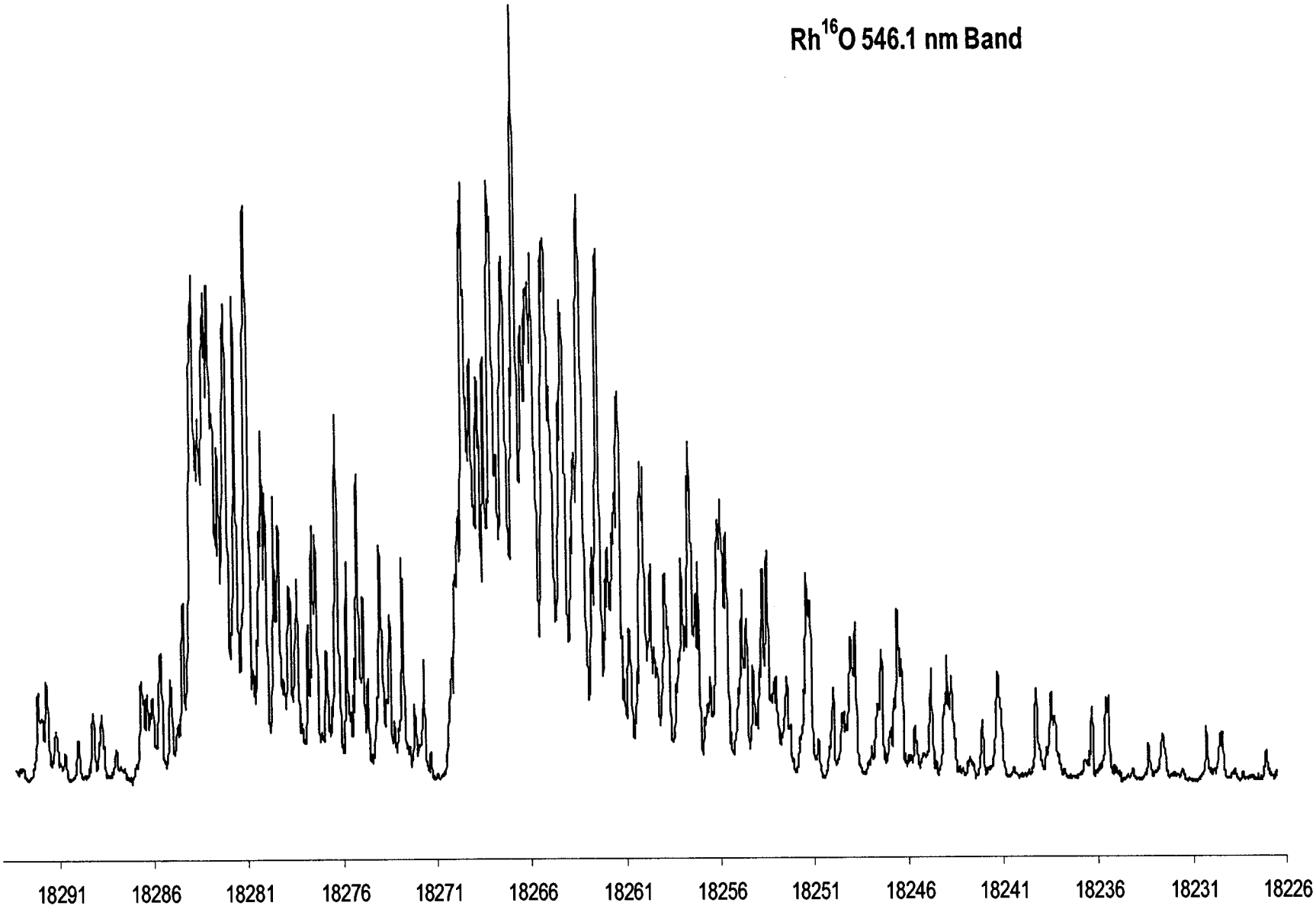
Rh16O 546.1 nm Band
18291
18286
18281
18276
18271
18266
18261
18256
18251
18246
18241
18236
18231
18226

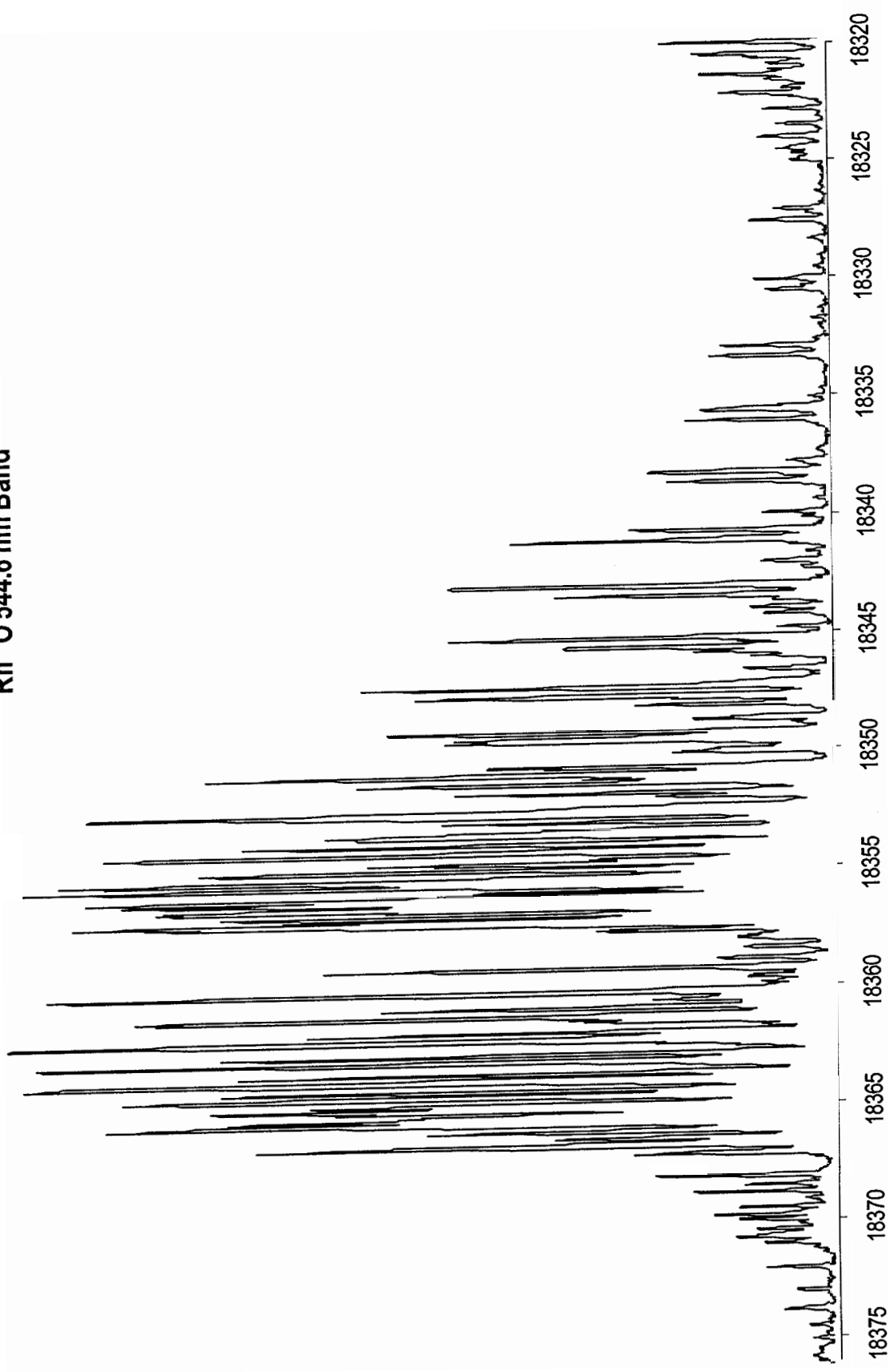
Rh16O 544.6 nm Band
18320
18325
18330
18335
18340
18345
18350
18355
18360
18365
18370
18375

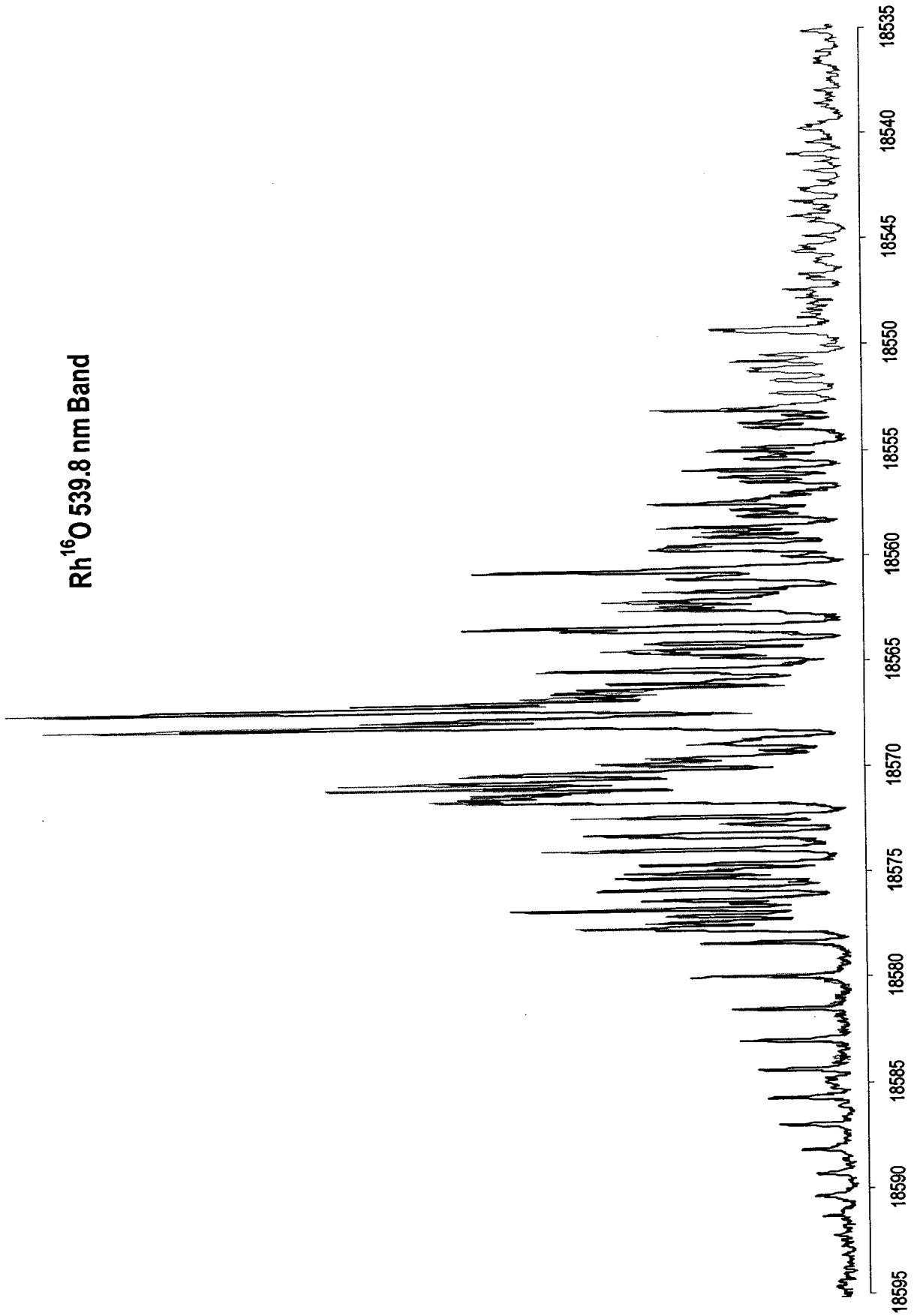
Rh 16O 539.8 nm Band
18595
18590
18585
18580
18575
18570
18565
18560
18555
18550
18545
18540
18535

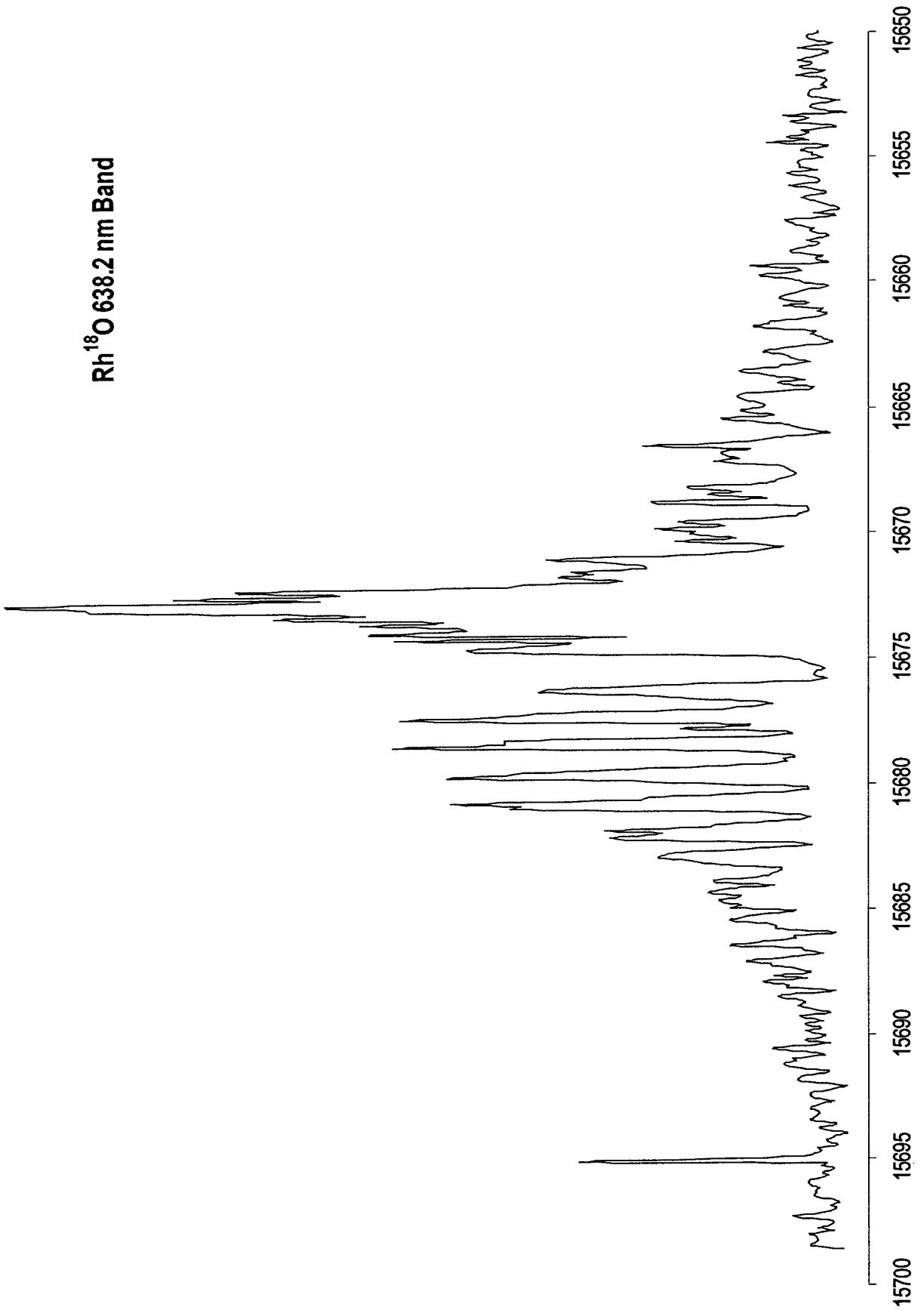
Rh18O 638.2 nm Band
15700
15695
15690
15685
15680
15675
15670
15665
15660
15655
15650

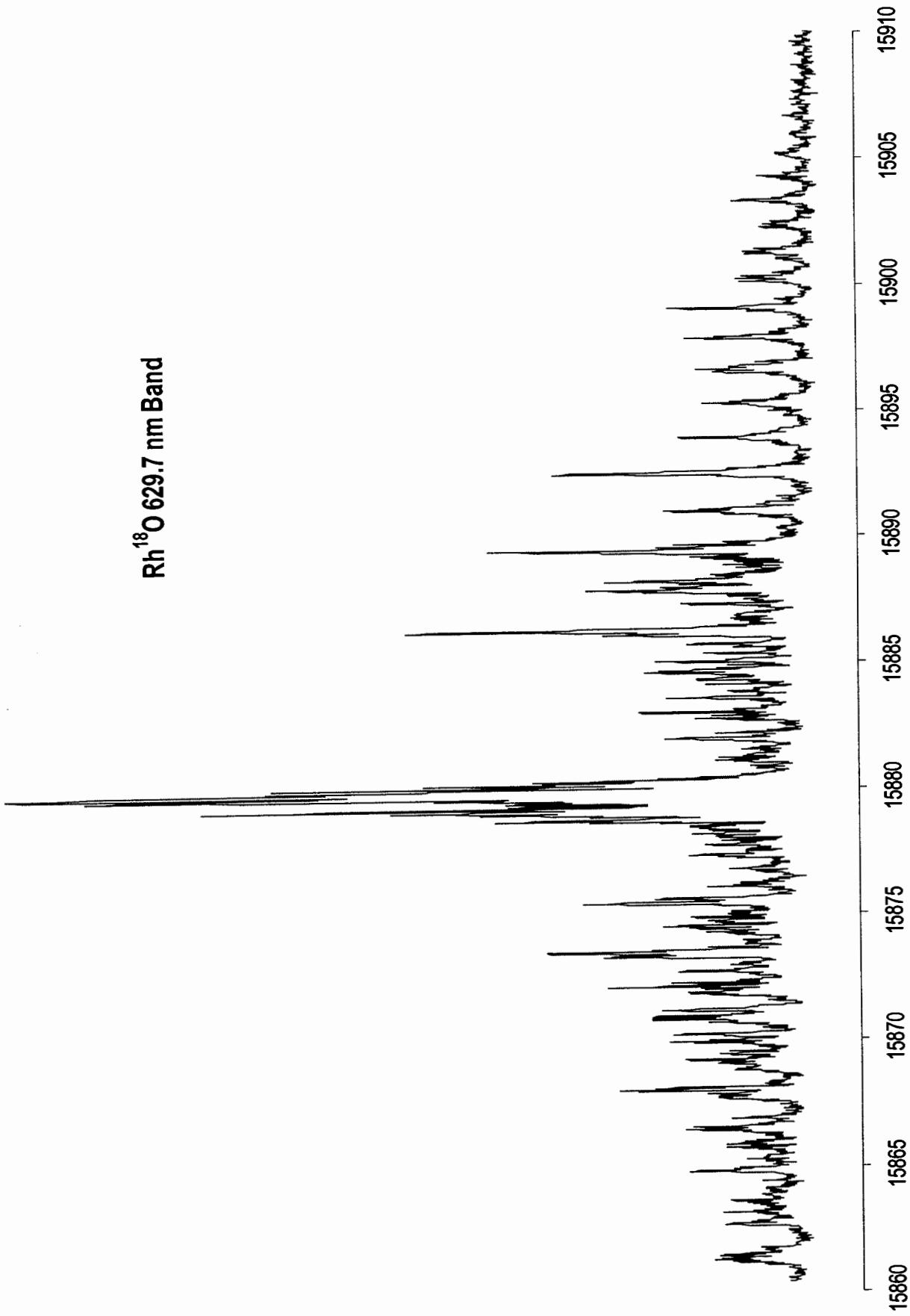
Rh18O 629.7 nm Band
15860
15865
15870
15875
15880
15885
15890
15895
15900
15905
15910

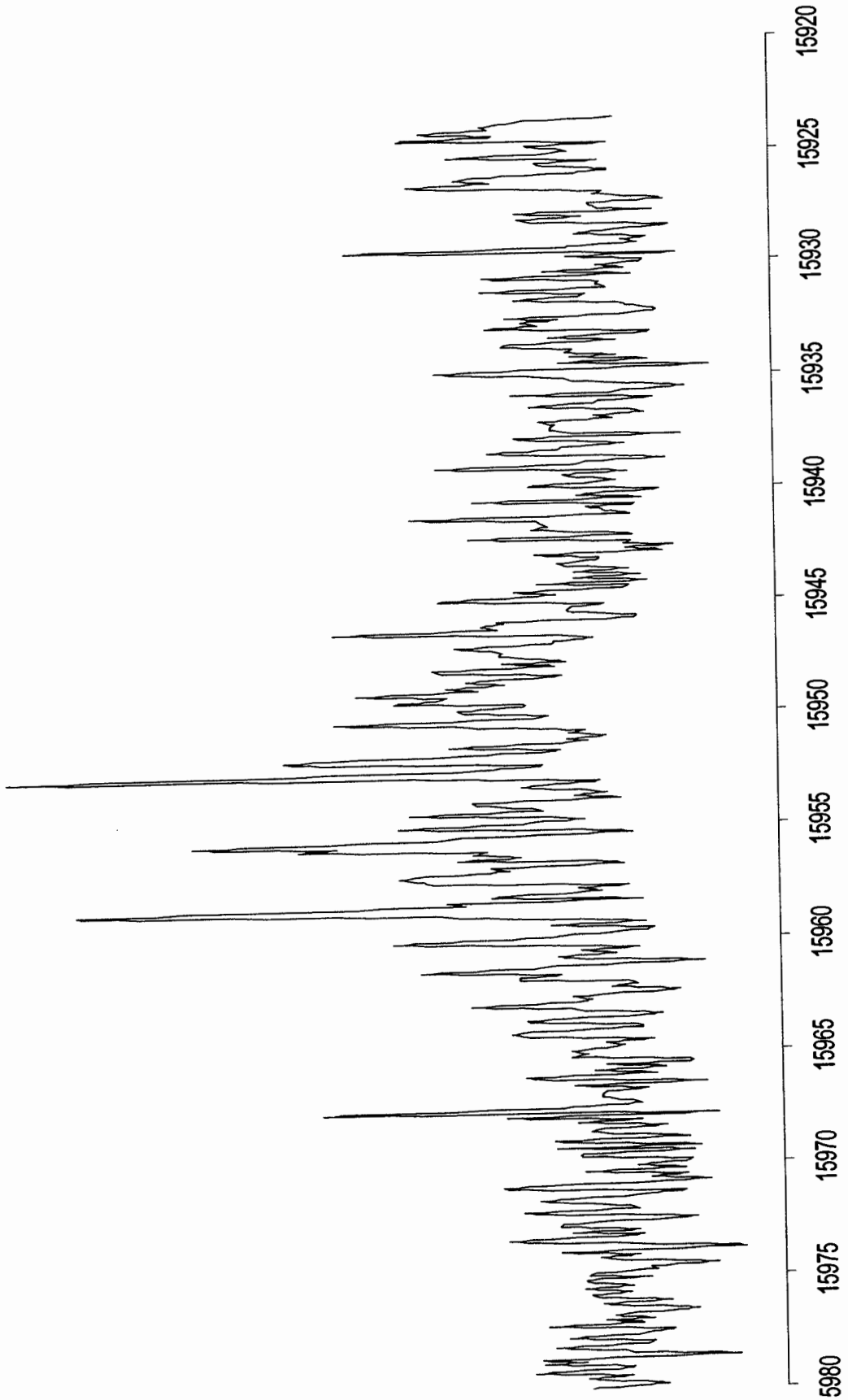
Rh18O 625.5 nm Band
15920
15925
15930
15935
15940
15945
15950
15955
15960
15965
15970
15975
15980

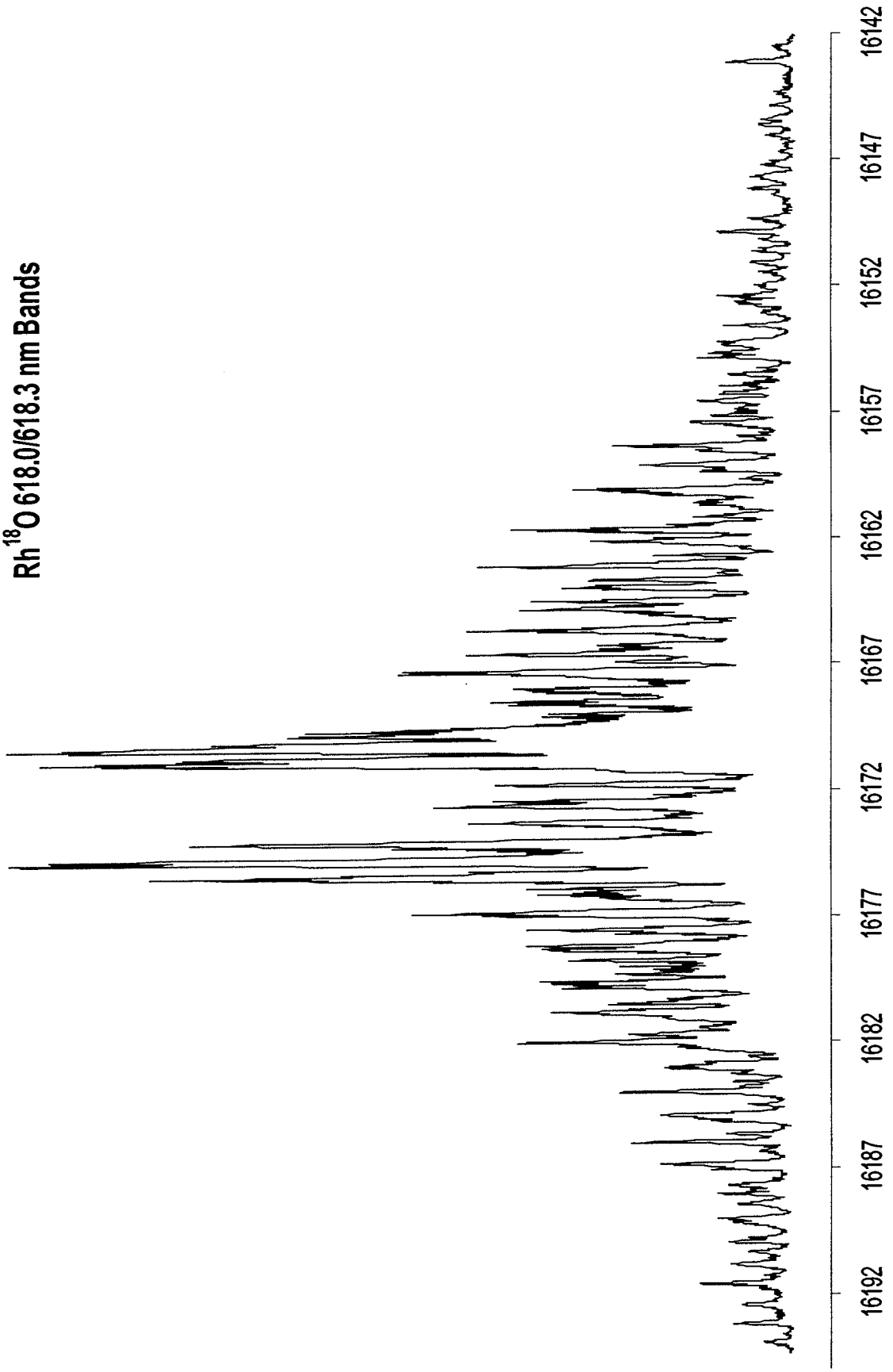
Rh 18O 618.0/618.3 nm Bands
16192
16187
16182
16177
16172
16167
16162
16157
16152
16147
16142

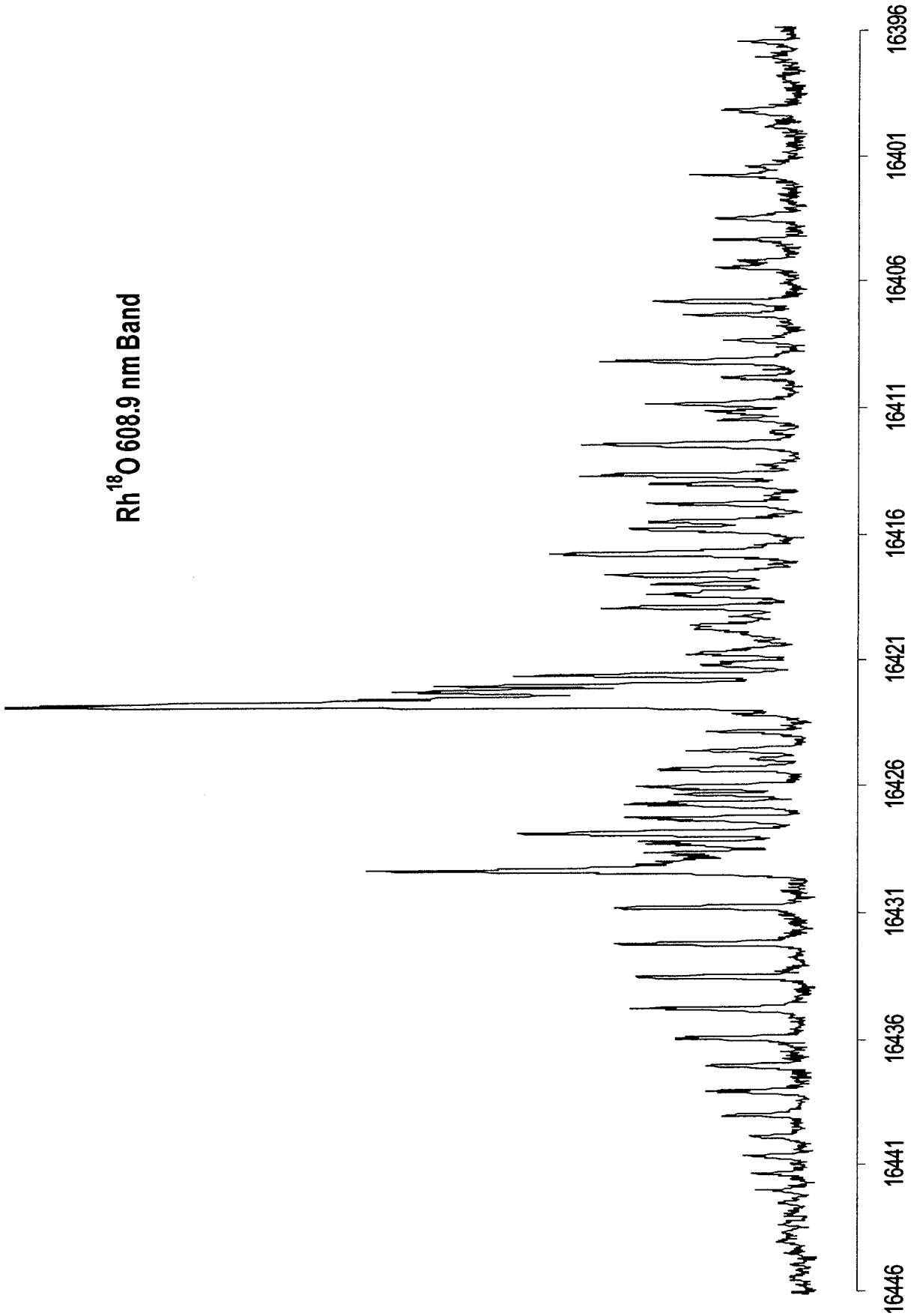
Rh18O 608.9 nm Band
16396
16401
16406
16411
16416
16421
16426
16431
16436
16441
16446

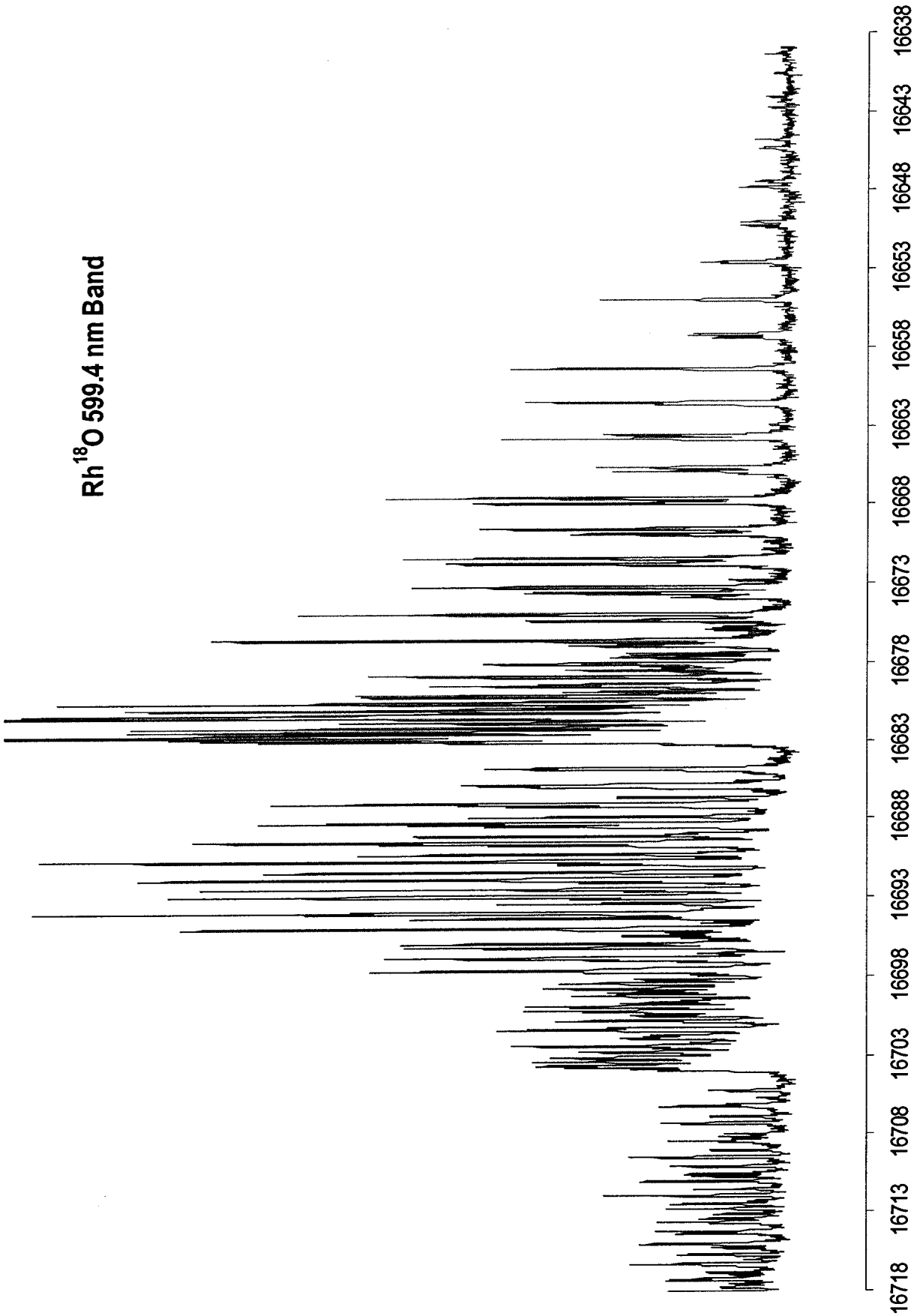
Rh18O 599.4 nm Band
16718
16713
16708
16703
16698
16693
16688
16683
16678
16673
16668
16663
16658
16653
16648
16643
16638

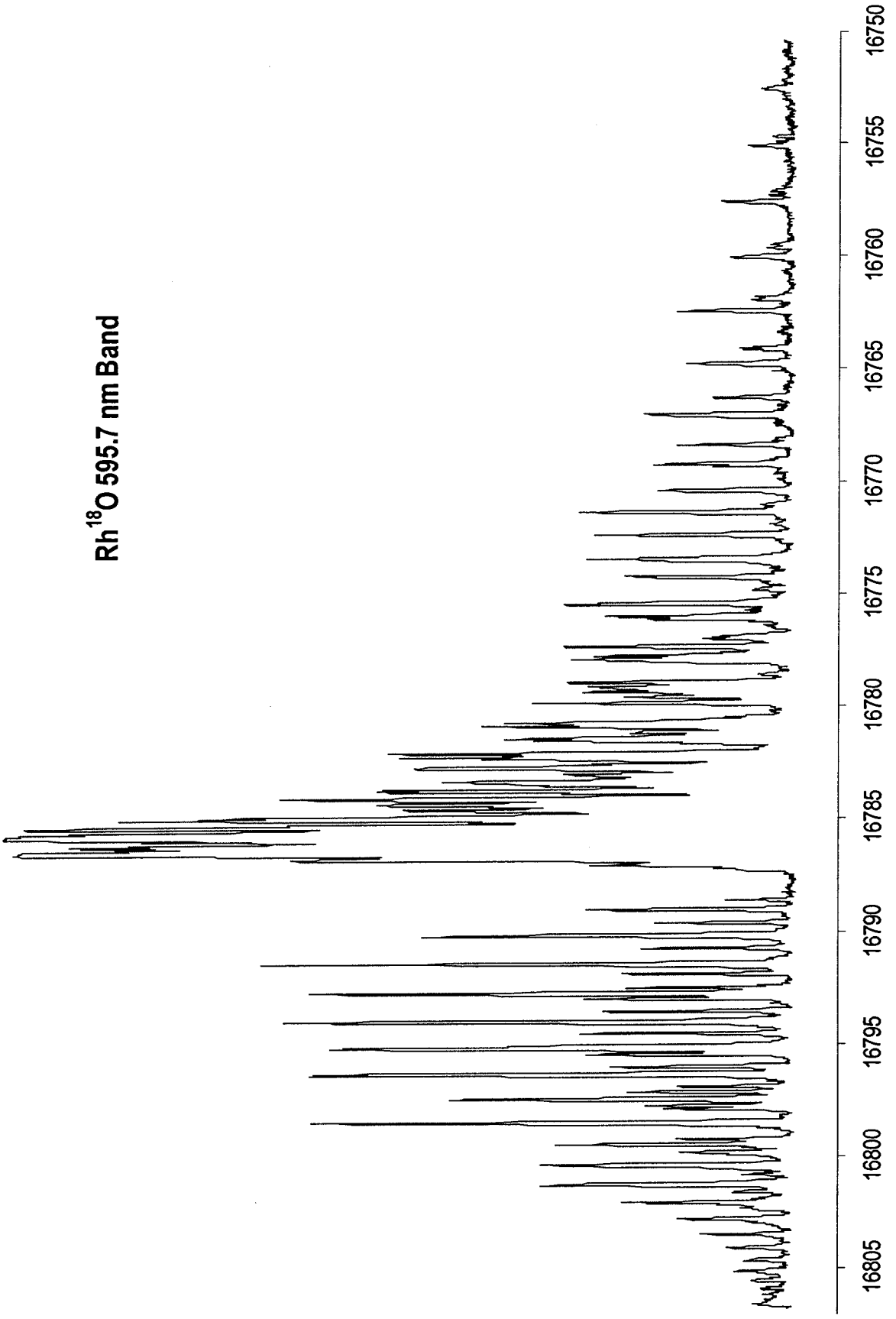
Rh18O 595.7 nm Band
16750
16755
16760
16765
16770
16775
16780
16785
16790
16795
16800
16805

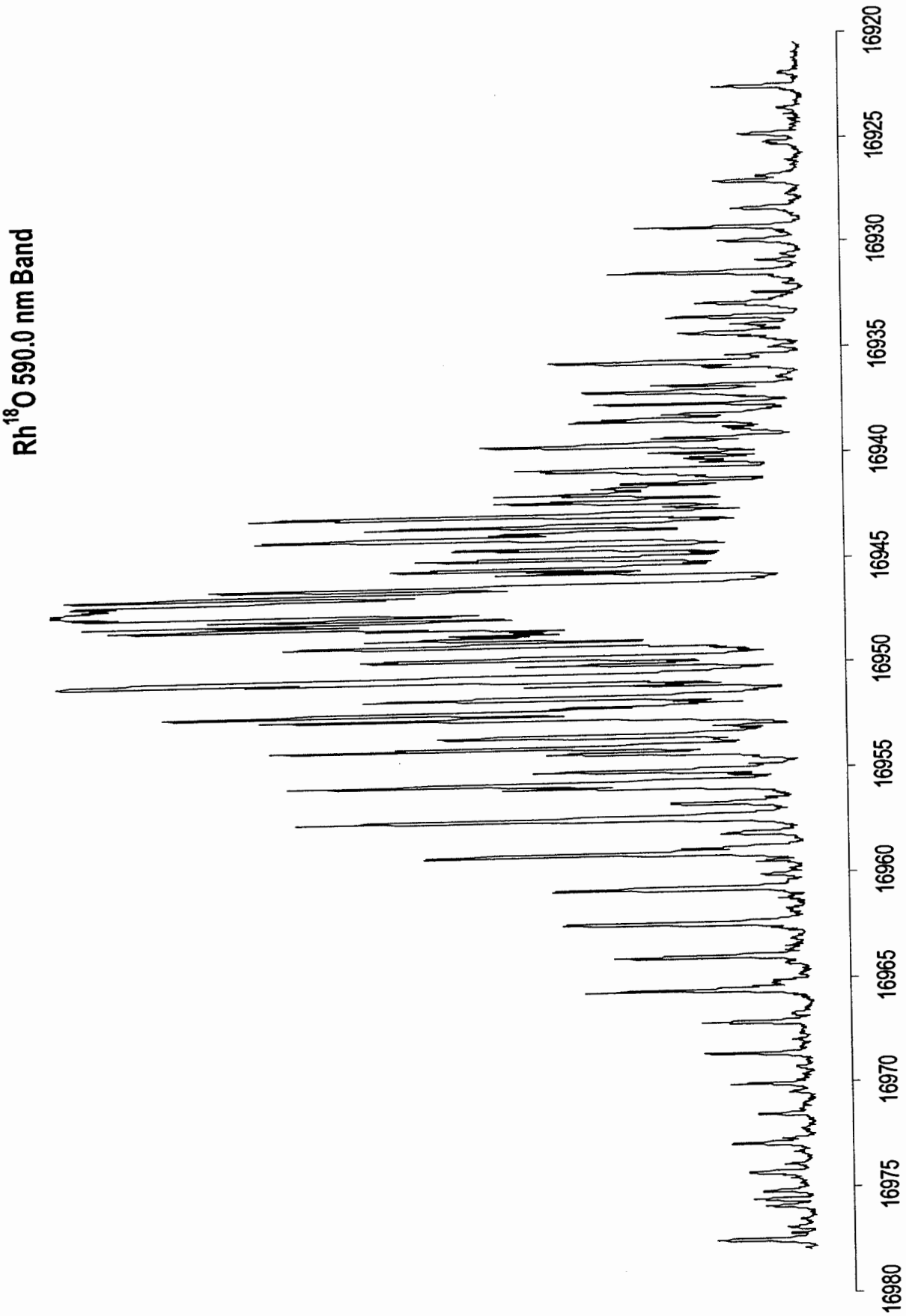
Rh18O 590.0 nm Band
16920
16925
16930
16935
16940
16945
16950
16955
16960
16965
16970
16975
16980

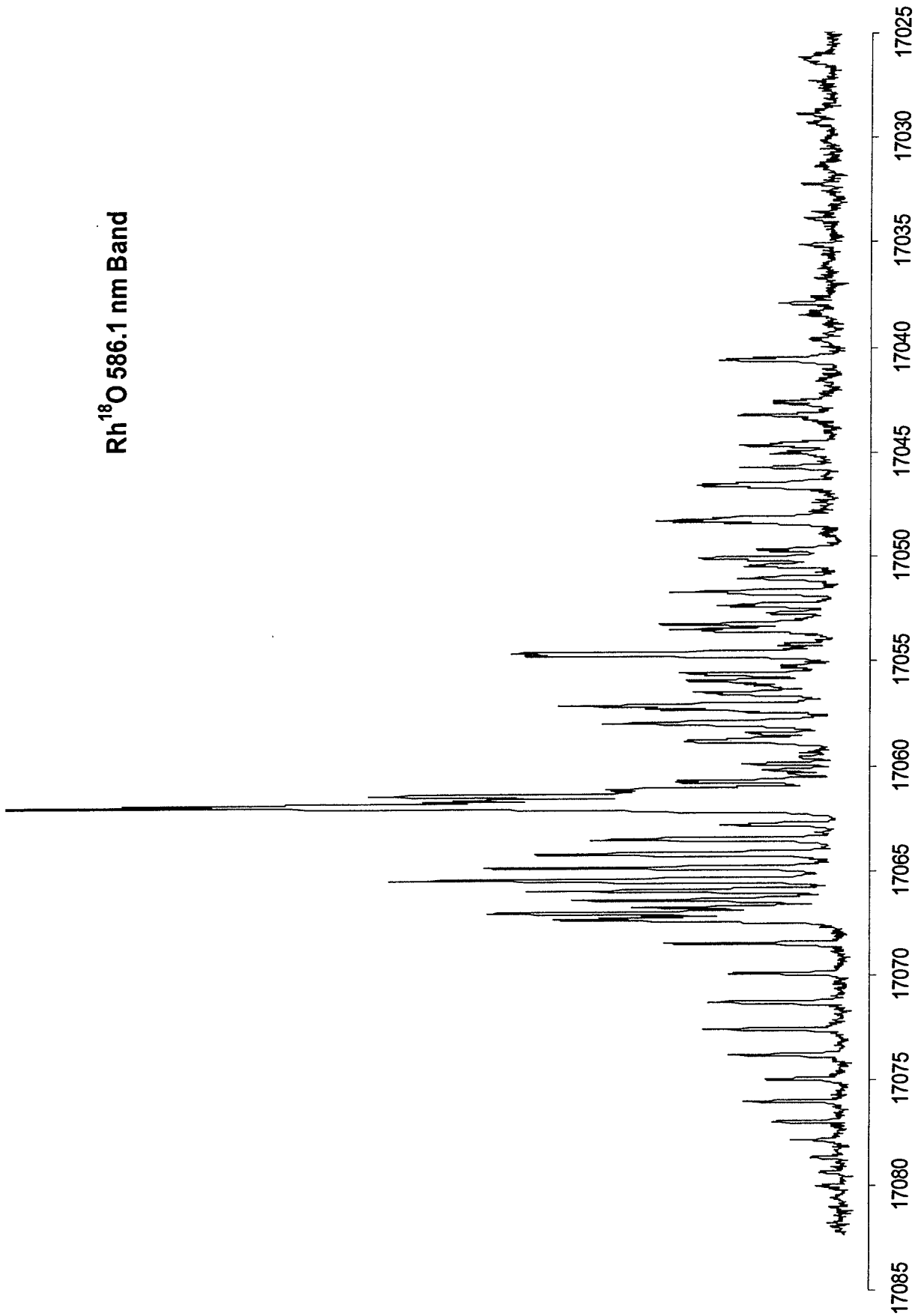
Rh18O 586.1 nm Band
17025
17030
17035
17040
17045
17050
17055
17060
17065
17070
17075
17080
17085

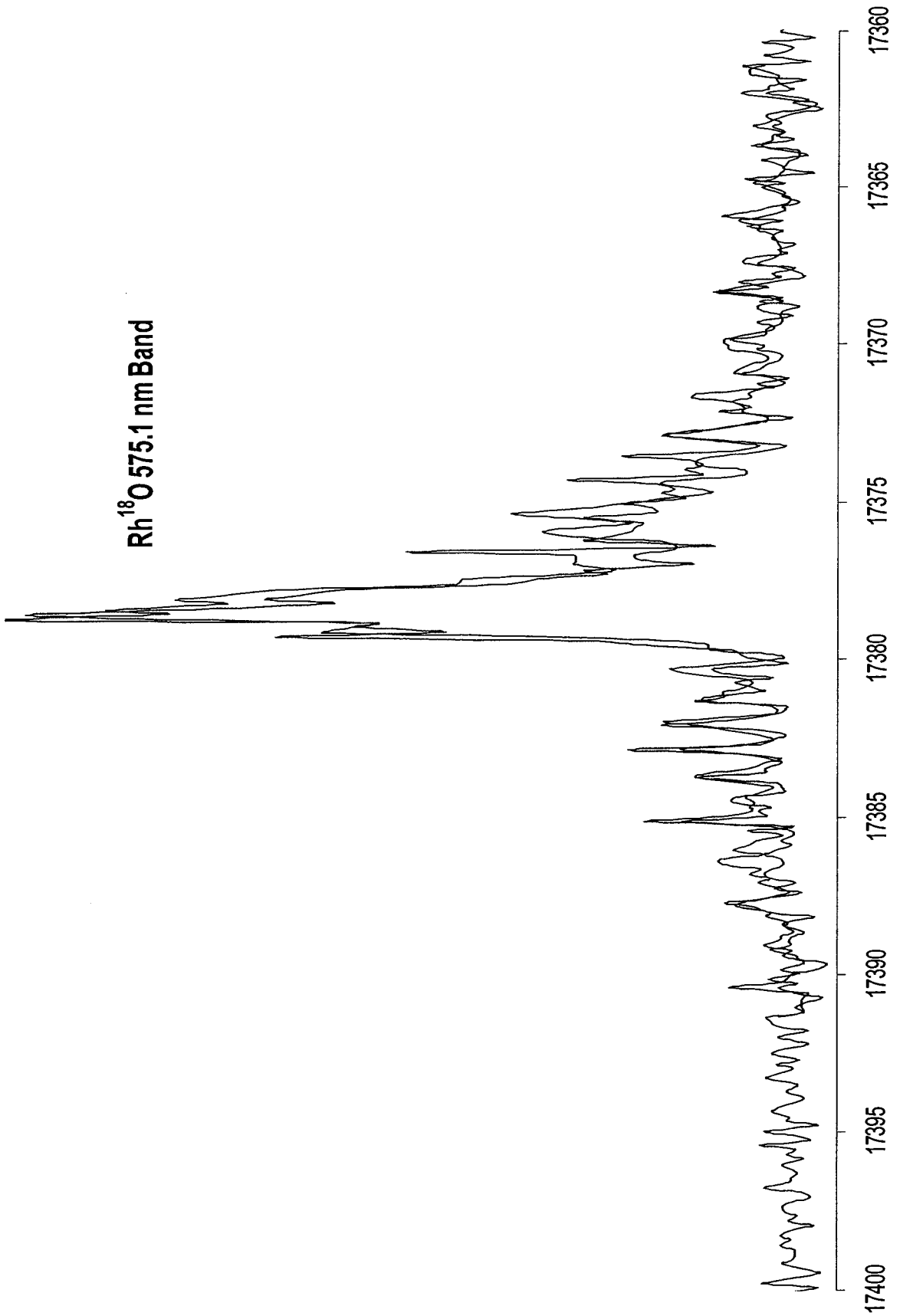
Rh 18O 575.1 nm Band
17400
17395
17390
17385
17380
17375
17370
17365
17360

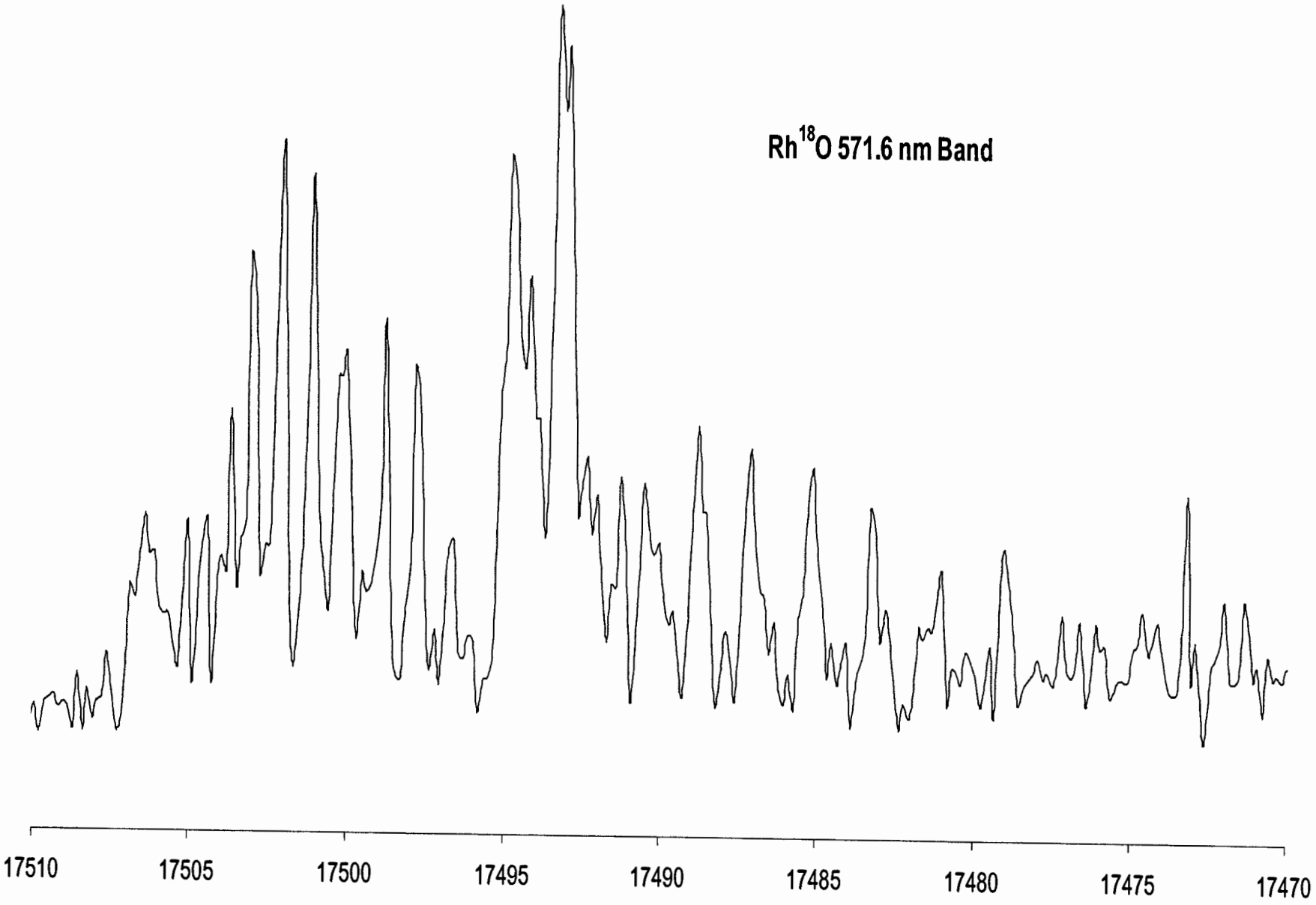
Rh18O 571.6 nm Band
17510
17505
17500
17495
17490
17485
17480
17475
17470

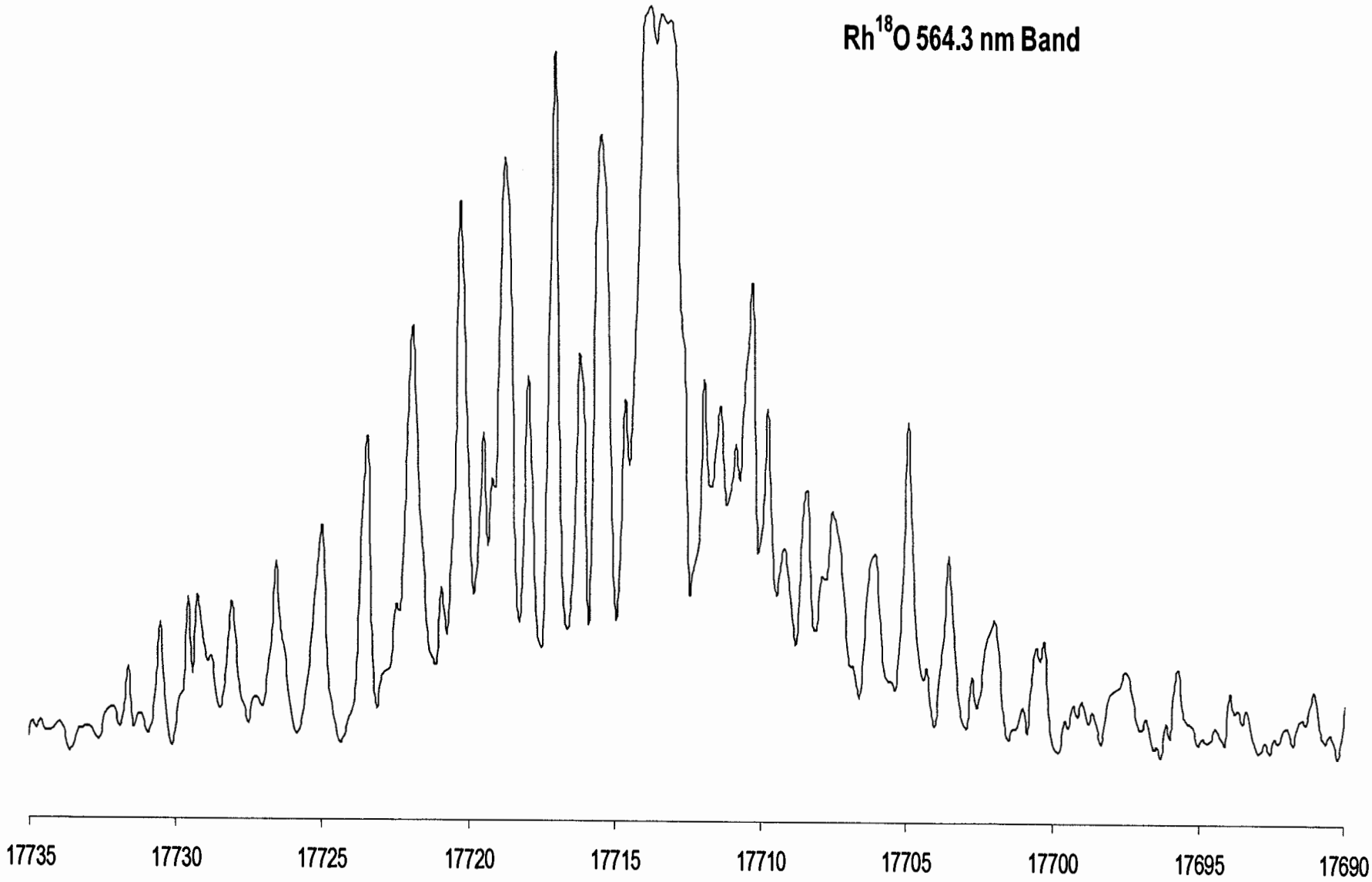
Rh18O 564.3 nm Band
17735
17730
17725
17720
17715
17710
17705
17700
17695
17690

Appendix IV

$Rh^{16}O$

High Resolution Spectra /cm^{-1}

(Overlaid by the corresponding section LIF spectrum
Intensity in arbitrary units)

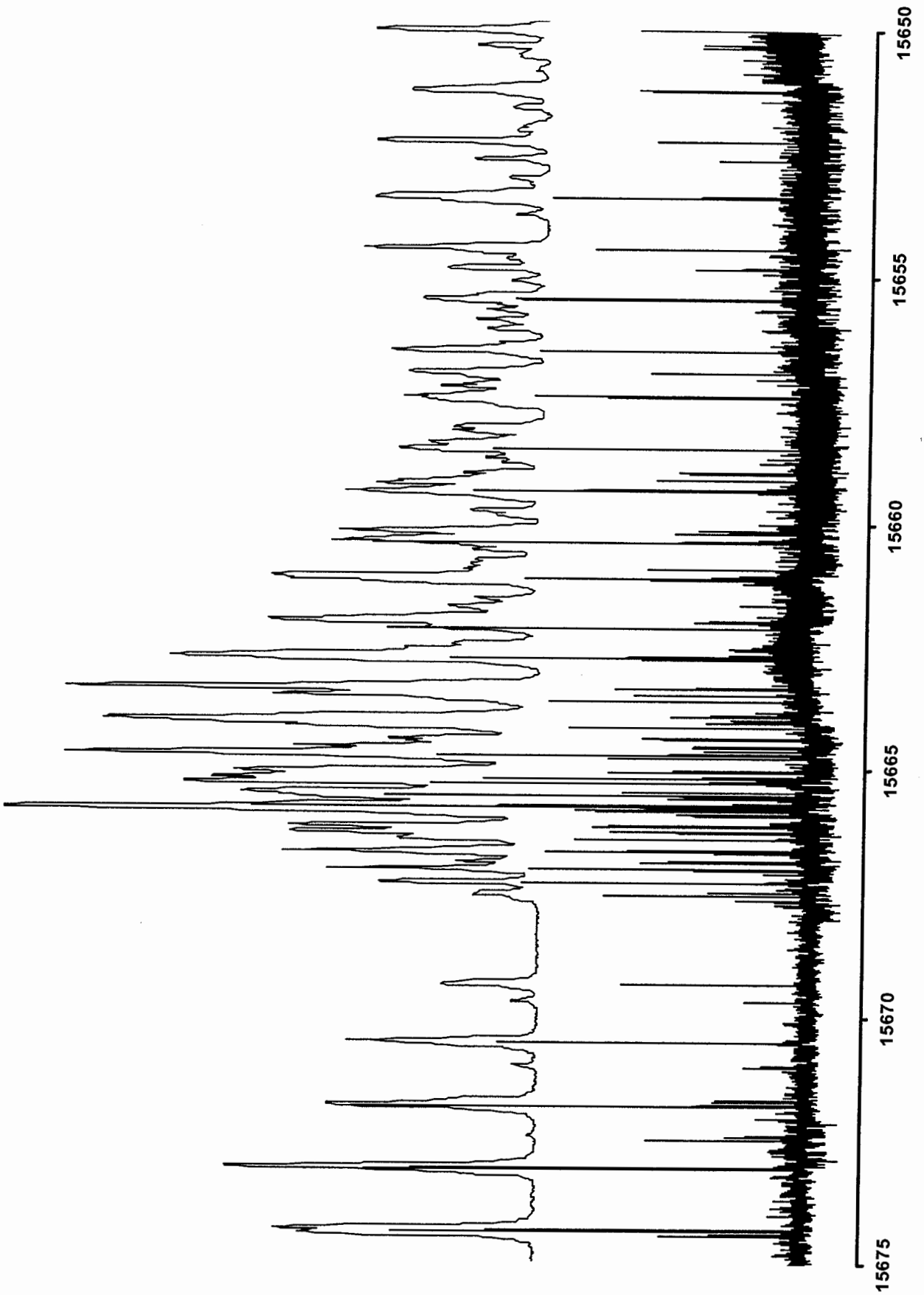
15650
15655
15660
15665
15670
15675

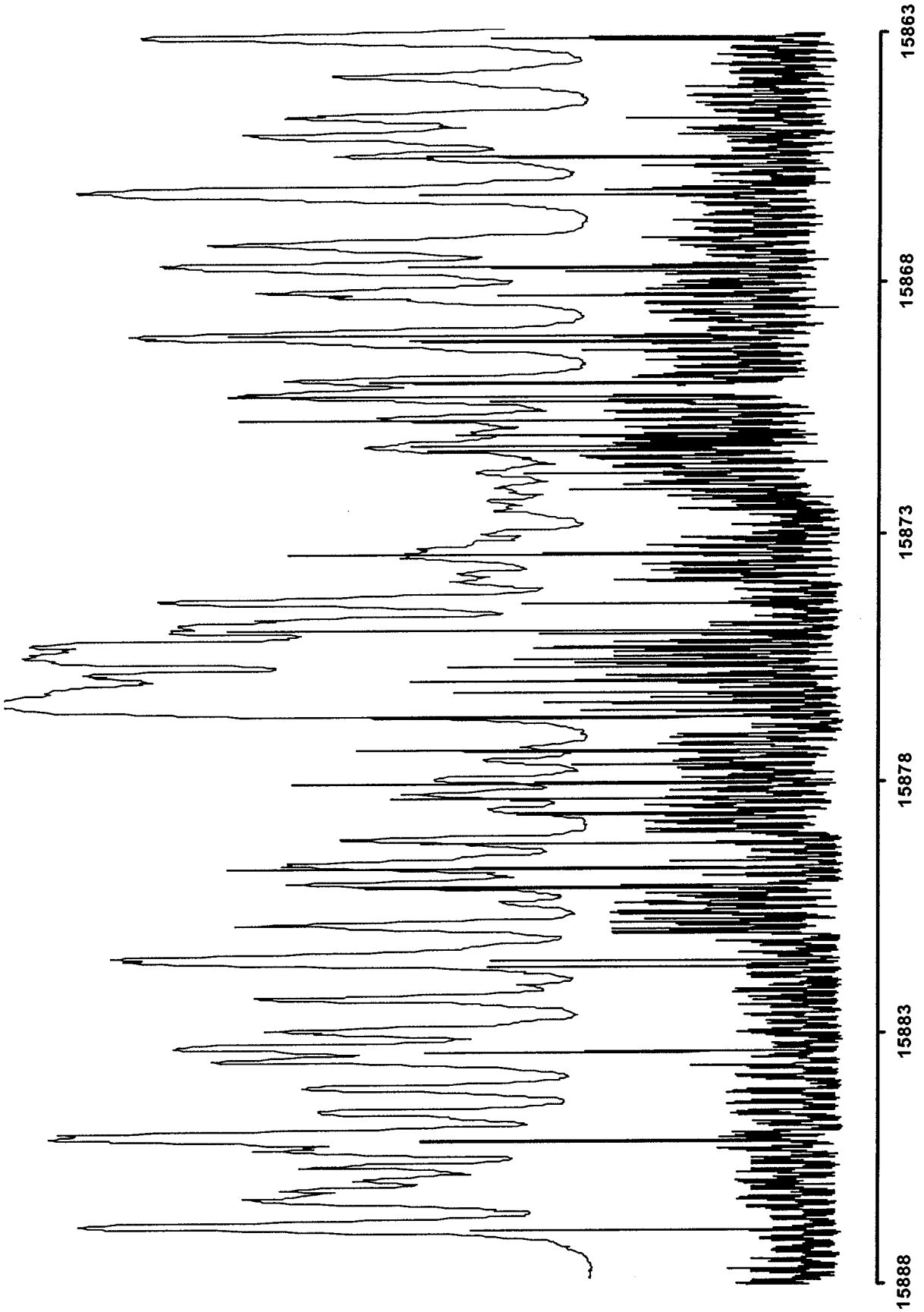
15863
15868
15873
15878
15883
15888

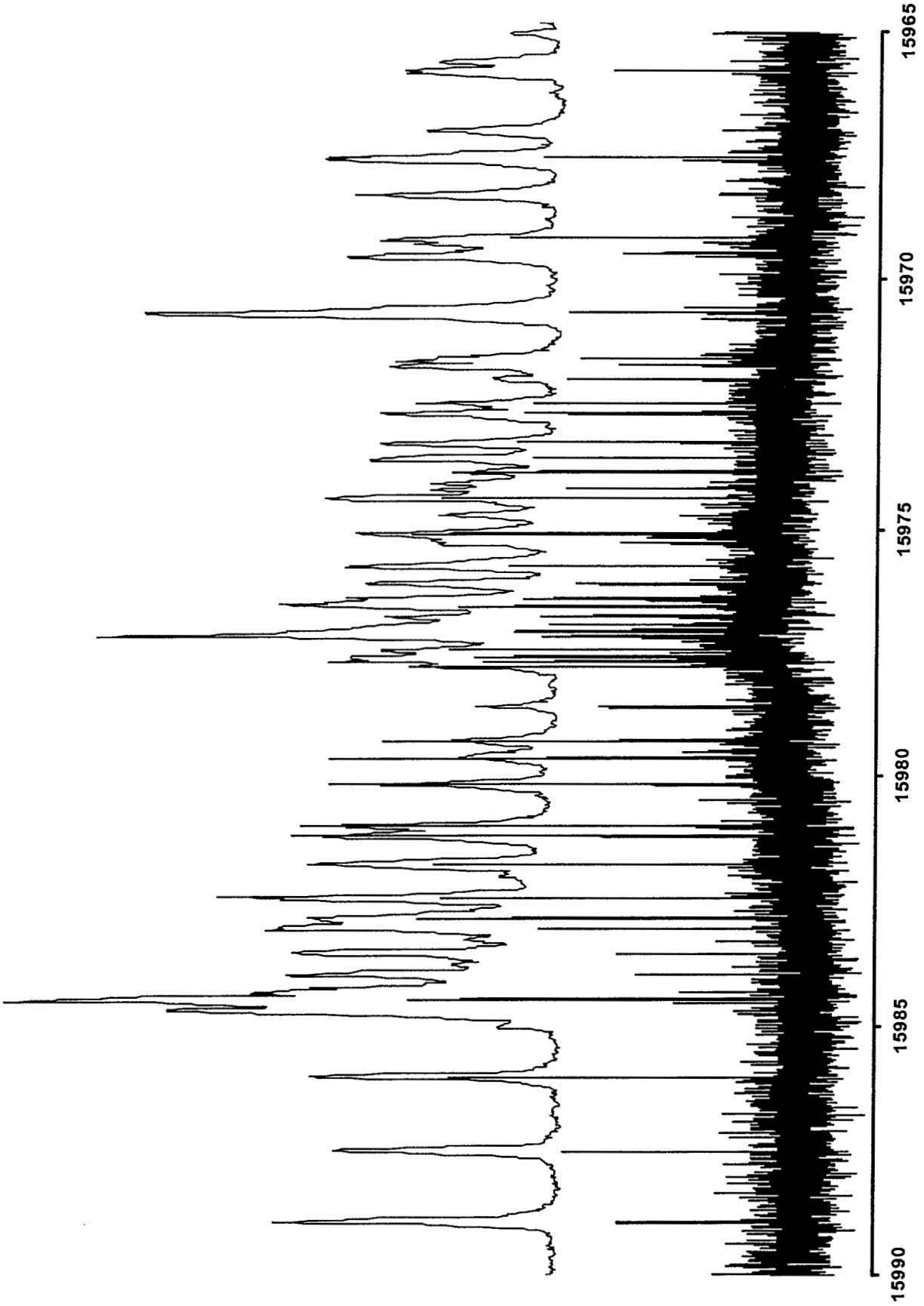
15965
15970
15975
15980
15985
15990

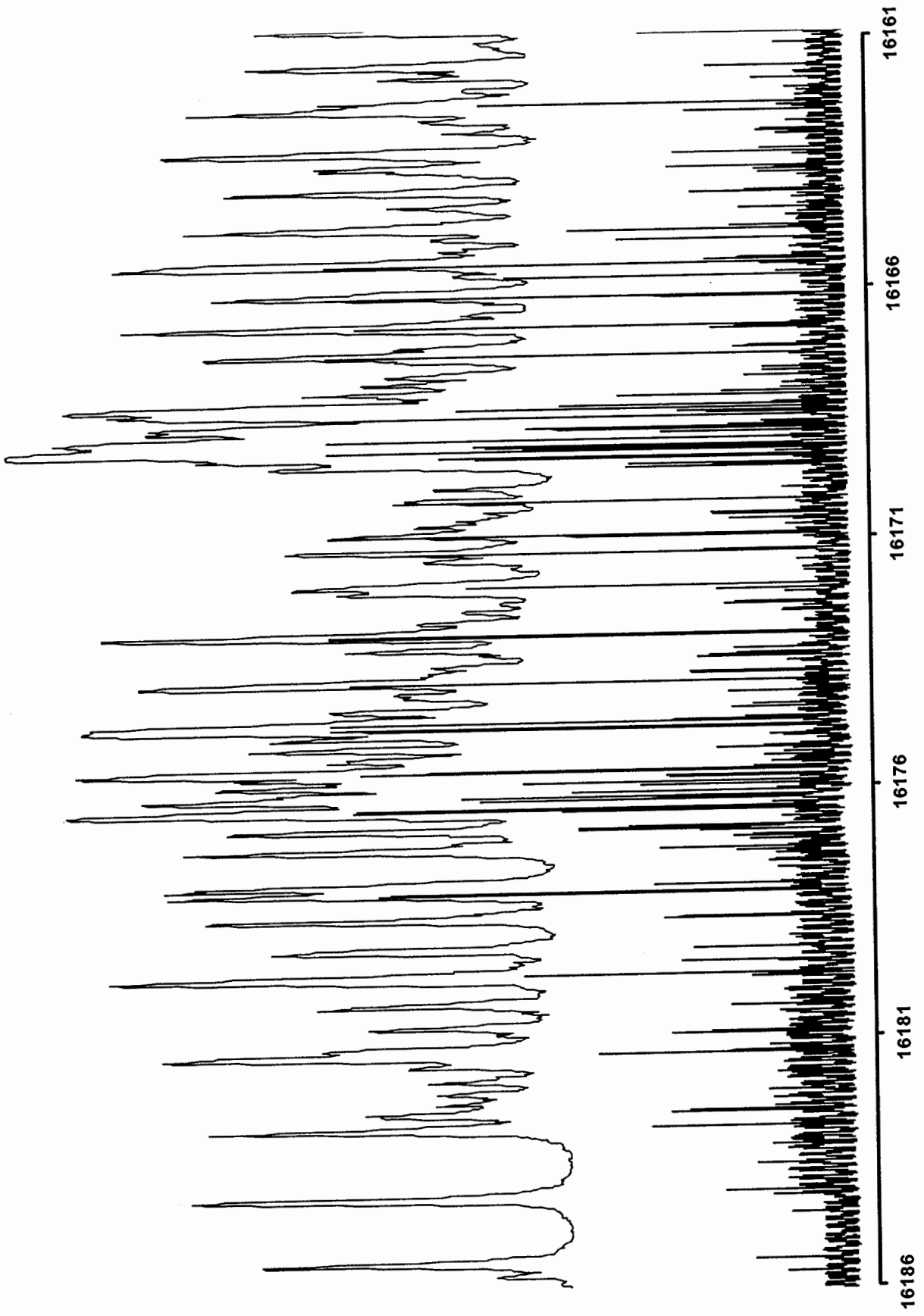
16161
16166
16171
16176
16181
16186

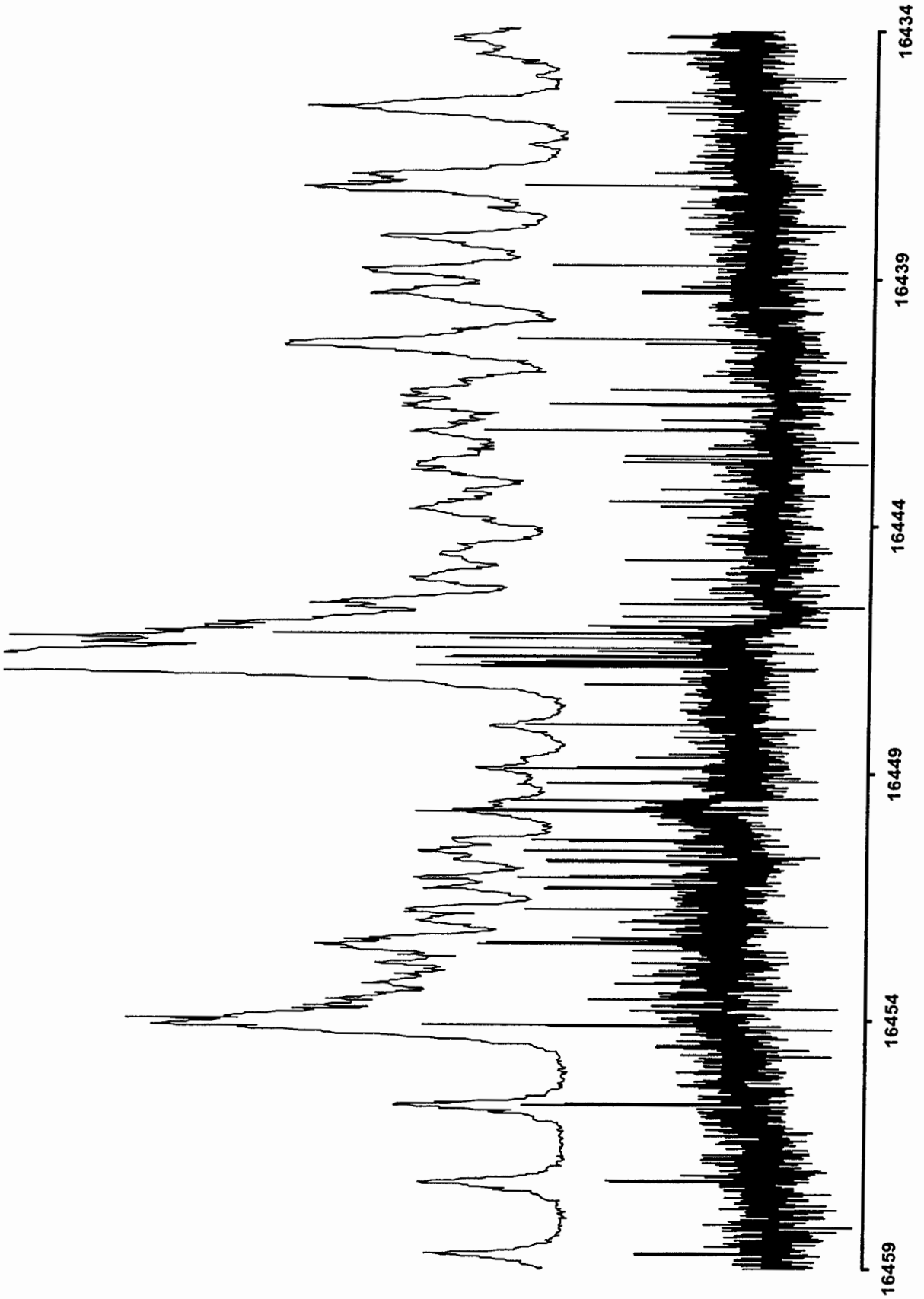
16459
16454
16449
16444
16439
16434

Appendix V

$Rh^{16}O$ / $Rh^{18}O$

Transition Lines /cm^{-1}

$Rh^{16}O$ / $Rh^{18}O$ Band Systems

$Rh^{16}O$ / $Rh^{18}O$ Band Systems

544.6 Band $Rh^{16}O$ Observed Transition Lines $[15.8]^2\Pi_{3/2}$ 3,0

N"	$^tR_{21}(0)$	$^sQ_{21}(0)$	$^rP_{21}(1)$	$^sR_{22}(1)$	$^rQ_{22}(1)$	$^qP_{22}(2)$	$^rR_{23}(1)$	$^qQ_{23}(2)$	$^pP_{23}(3)$	$^qR_{24}(2)$	$^pQ_{2p}(3)$	$^oP_{24}(4)$
0	18359.94	18359.27										
1	18361.26	18360.25	---	18360.92	---		---					
2	18362.61	18361.33	18357.31	18361.97	18357.92	18357.11	18356.40	18355.49		18354.65		
3	18363.92	18362.24	18357.21	18362.88	18357.92	18356.67	18356.61	18355.43	18352.66	18354.28	18351.45	
4	18365.14	18363.15	18356.91	18363.69	18357.42	18356.20	18356.20	18355.06	18351.05	18353.68	18349.63	---
5	18366.18	18363.99	18356.67	18364.39	18357.01	18355.49	18356.00	18354.35	18349.23	18352.77	18347.71	---
6	18367.19	18364.70	18356.34	18365.00	18356.61	18354.65	18355.49	18353.57	18347.31	18351.85	18345.59	18344.28
7	18368.07	18365.20	18355.66	18365.44	18355.83	18353.74	18354.79	18352.50	18345.26	18350.71	18343.44	18341.99
8	18368.85	18365.74	18355.19	18365.81	18355.19	18352.77	18353.98	18351.45	18343.00	18349.53	18341.12	
9	18369.49	18366.05	18354.35	18366.05	18354.35	18351.45	18353.07	18350.17	18340.72	18348.12	18338.63	
10	18369.99	18366.28	18353.57	18366.18	18353.41	18350.17	18352.02	18348.89	18338.26	18346.60	18336.07	
11	18370.43	18366.43	18352.50	18366.18	---	18348.89	18350.71	18347.31	18335.60	---	18333.39	
12	18370.67	18366.43	18351.45	18366.05	18351.05	18347.31	18349.53	18345.86	18332.95	18343.44	18330.60	
13	18370.77	18366.28	18350.10	18365.81	18349.63	18345.59	18348.12	18343.98	18330.13	18341.62	18327.64	
14	18370.77	18366.05	18348.72	18365.54	18348.12	18343.98		18342.23	18327.20	18339.40		
15		18365.74	18347.31	18365.14	18346.60	18341.99		18340.14		18337.35		
16			18345.59		18344.85	18340.14		18338.26				
17								18336.07				

546.1 Band $Rh^{16}O$ Observed Transition Lines $[16.0]^2\Pi_{1/2}$ 3,0

N"	$^{s}R_{11}(0)$	$^{r}Q_{11}(0)$	$^{q}P_{11}(0)$	$^{r}R_{12}(1)$	$^{q}Q_{12}(1)$	$^{p}P_{12}(1)$	$^{q}R_{13}(1)$	$^{p}Q_{13}(1)$	$^{o}P_{13}(2)$	$^{p}R_{14}(2)$	$^{o}Q_{14}(2)$	$^{n}P_{14}(3)$
0	18272.18	18270.15	18269.31									
1	18273.49	18270.91	18269.24	18271.68	18269.98	18268.38	18267.71	18266.14				
2	18274.89	18272.18	18269.38	18272.82	18270.15	18268.04	18268.38	18266.31	18265.81	18265.64	18264.87	
3	18276.36	18273.49	18269.38	18273.99	18269.98	18267.44	18268.78	18266.31	18264.40	18265.11	18263.30	18261.90
4	18277.56	18274.62	18269.24	18275.19	18269.75	18266.97	18268.64	18265.94	18263.17	18264.40	18261.90	18259.63
5	18278.76	18275.79	18269.08	18276.26	18269.51	18266.71	18268.38	18265.41	18261.50	18263.80	18260.00	18257.57
6	18280.03	---	18268.78	18277.39	18269.08	18266.04	18267.94	18265.11	18259.63	18263.30	18258.03	---
7	18280.97	---	18268.38	18278.40	18268.64	18265.64	18267.31	18264.40	18257.67	18262.74	18255.93	18253.00
8	18282.11	18279.10	18268.04	18279.33	18268.04	18265.11	18266.91	18263.80	18255.63	18261.90	18253.70	18250.73
9	18282.98	18280.20	18267.31	18280.20	18267.31	18264.40	18266.04	18263.17	18253.47	18261.27	18251.40	
10	18283.78	18281.10	18266.71	18280.97	18266.71	18263.80	18265.24	18262.37	18251.20	18260.17	18249.00	
11	18284.38	18281.61	18265.94	18281.61	18265.81	18262.90	18264.40	18261.50	18248.80	18259.30	18246.34	
12	18285.08	18282.51	18265.11	18282.24	18264.87	18262.00	18263.30	18260.67	18246.34	18258.30	18243.91	
13	18285.58	18283.18	---	18282.78	18263.64	18261.07	18262.00	18259.47	18243.71	18257.10	18241.28	
14	18285.99	18283.65	---	18283.18	18262.74	18260.00	18261.07	18258.30		18255.93	18238.45	
15	18286.29	18283.95	18261.90	18283.41	18261.37	18258.90	18259.63	18257.10		18254.57	18235.42	
16	18286.49	18284.08	18260.80	18283.51	18260.00	18257.67	18258.13	18255.93		18253.00	18232.59	
17	18286.59	18284.38	18259.30	18283.65	18258.67		18256.67	18254.37		18251.40	18229.40	
18			18257.80		18257.10		18254.97					

553.3 Band $Rh^{16}O$ Observed Transition Lines $[15.8]^2\Pi_{1/2}$ 3,0

N"	$^{s}R_{11}(0)$	$^{r}Q_{11}(0)$	$^{q}P_{11}(0)$	$^{r}R_{12}(1)$	$^{q}Q_{12}(1)$	$^{p}P_{12}(1)$	$^{q}R_{13}(1)$	$^{p}Q_{13}(1)$	$^{o}P_{13}(2)$	$^{p}R_{14}(2)$	$^{o}Q_{14}(2)$	$^{n}P_{14}(3)$
0	18063.81	---	18061.69									
1	18064.73	---	18061.20	18065.35	18061.99	18061.99	18059.70	18059.77				
2	18065.67	18065.67	18060.88	18066.33	18061.56	18061.66	18059.96	18059.96	18058.07	18059.05	---	
3	18066.65	18066.65	18060.62	18067.24	18061.20	18061.20	18059.96	18059.77	18056.38	18058.76	---	18055.27
4	18067.60	18067.60	18059.96	18068.12	18060.62	18060.48	18059.47	18059.47	18054.68	18058.07	---	18053.47
5	18068.48	18068.48	18059.47	18068.94	18059.96	18059.96	18058.82	18058.82	18052.59	18057.22	18051.06	18051.06
6	18069.26	18069.26	18058.82	18069.62	18059.15	18059.15	18057.97	18057.97	18050.41	18056.38	18048.76	18048.76
7	18069.98	18069.98	18058.07	18070.21	18058.23	18058.23	18057.22	18057.22		18055.40	18046.31	18046.31
8	18070.60	18070.60	18057.22	18070.77	18057.35	18057.32	18056.18	18056.18		18054.26	18043.73	18043.73
9	18071.19	18071.19	18056.18	18071.19	18056.38	18056.18	18055.14	18054.91		18053.05	18041.13	18041.13
10	18071.61	18071.61	18055.14	18071.61	18055.27	18055.14	18053.90	18053.90		18051.78	18038.23	18038.23
11	18072.01	18072.01	18054.06	18071.88	18054.06	18053.90	18052.59	18052.59		18050.41	18035.44	18035.44
12	18072.30	18072.30	18053.05	18072.20	18052.79	18052.79	18051.29	18051.23		18048.91	18032.48	18032.48
13	18072.50				18051.42	18051.42	18049.82	18049.82		18047.35	18029.42	18029.42
14	18072.63				18049.96	18049.96	18048.29	18048.29		18045.75	18026.30	18026.30
15					18048.46		18046.67	18046.67		18043.99		
16					18046.83		18044.97	18044.97		18042.14		
17					18045.17		18043.15	18043.15		18040.25		
18					18043.31		18041.29	18041.29		18038.23		
19					18041.39		18039.24	18039.24		18036.12		
20					18039.24			18037.29		18033.97		
21					18037.42			18035.08		18031.70		
22					18035.24					18029.29		
23					18032.83							

561.9 Band $Rh^{16}O$ Observed Transition Lines $[16.0]^2\Pi_{3/2}$ 2,0

N"	$^tR_{21}(0)$	$^sQ_{21}(0)$	$^rP_{21}(1)$	$^sR_{22}(1)$	$^rQ_{22}(1)$	$^qP_{22}(2)$	$^rR_{23}(1)$	$^qQ_{23}(2)$	$^pP_{23}(3)$	$^qR_{24}(2)$	$^pQ_{2p}(3)$	$^oP_{24}(4)$
0	17789.04	17787.07										
1	17790.77	17787.99	17786.06	17788.66	17786.73		17784.48					
2	17792.77	17789.04	17786.35	17789.73	17786.92	17785.02	17785.46	17783.47		17782.58		
3	17794.58	17790.14	17786.69	17790.77	17787.23	17784.48	17786.06	17783.28	17781.38	17782.04	17780.09	
4	17796.38	17791.19	17787.07	17791.79	17787.68	17783.94	17786.60	17782.80	17780.09	17781.38	17778.73	17776.73
5	17798.25	17792.23	17787.23	17792.61	17787.87	17783.37	17786.69	17782.24	17778.73	17780.75	17777.27	17774.43
6	17800.06	17793.37	17787.48	17793.72	17787.87	17782.74	17786.73	17781.60	17777.40	17779.99	17775.82	17772.09
7	17801.80		17787.68	17794.51	17787.99	17782.04	17786.73	17780.75	17775.82	17778.95	17774.05	17769.69
8	17803.57		17787.87	17795.43	17787.99	17781.38	17786.73	17780.09	17774.27	17778.19	17772.37	17767.26
9	17805.25		17787.99	17796.25	17787.99	17780.59	17786.73	17779.33	17772.69	17777.27	17770.70	17764.77
10	17806.87		17787.99	17797.01	17787.99	17779.80	17786.69	17778.44	17771.01	17776.29	17769.03	17762.21
11	17808.46		17787.99	17797.74	17787.99	17778.95	17786.60	17777.46	17769.31	17775.25	17767.16	17759.59
12	17809.95		17787.99	17798.38	17787.87	17778.06	17786.35	17776.48	17767.61	17774.27	17765.37	17756.94
13	17811.44		17787.99	17799.04	17787.68	17777.11	17786.06	17775.60	17765.78	17773.10	17763.38	17754.23
14	17812.89		17787.87	17799.55	17787.48	17776.10	17785.81	17774.43	17763.88	17771.90	17761.33	17751.49
15	17814.26		17787.68	17800.06	17787.07	17775.12	17785.46		17761.99	17770.70	17759.40	17748.81
16	17815.56		17787.48	17800.53	17786.92	17773.99	17785.02		17760.03	17769.41		17745.91
17	17816.86		17787.23	17800.91	17786.35	17772.82	17784.48		17758.02	17768.11		17743.14
18	17818.04		17786.92	17801.26	17786.06	17771.68	17783.94		17755.97	17766.60		17740.00
19	17819.18		17786.60	17801.58	17785.46	17770.39	17783.37		17753.85	17765.18		17737.16
20	17820.29		17786.06	17801.70	17785.02	17769.03	17782.74		17751.68	17763.76		
21	17821.34		17785.46	17801.80	17784.39		17782.04		17749.35	17762.21		
22	17822.29		17785.02		17783.63		17781.38		17747.05	17760.38		
23	17823.15		17784.48				17780.59		17744.81	17758.61		
24	17823.91		17783.63				17779.80		17742.36			

569.3 Band $Rh^{16}O$ Observed Transition Lines $[15.8]^2\Pi_{3/2}$ 2,0

N"	$^tR_{21}(0)$	$^sQ_{21}(0)$	$^rP_{21}(1)$	$^sR_{22}(1)$	$^rQ_{22}(1)$	$^qP_{22}(2)$	$^rR_{23}(1)$	$^qQ_{23}(2)$	$^pP_{23}(3)$	$^qR_{24}(2)$	$^pQ_{2p}(3)$	$^oP_{24}(4)$
0	17563.00	17563.77										
1	17564.11	17565.31	17560.56	17565.87	17561.27		17559.02					
2	17565.31	17566.70	17560.19	17567.41	17560.96	17561.73	17559.39	17560.19		17559.39		
3	17566.51	17568.30	17560.04	17568.92	17560.56	17561.73	17559.39	17560.44	17555.84	17559.39	17554.64	
4	17567.69	17569.85	17559.73	17570.38	17560.19	17561.63	17559.02	17560.56	17554.02	17559.02	17552.64	17553.41
5	17568.77		17559.14	17571.86	17559.77	17561.52	17558.55	17560.44	17552.05	17559.02	17550.54	17551.65
6	17569.85		17558.86	17573.28	17559.14	17561.27	17557.97	17560.19	17549.99	17558.56	17548.32	17549.80
7	17570.81		17558.22	17574.57	17558.55	17561.27	17557.41	17560.04	17547.86	17558.22	17546.01	17547.86
8	17571.70		17557.75	17575.96	17557.84	17560.96	17556.67	17559.73	17545.61	17557.88	17543.67	17545.86
9	17572.54		17557.11	17577.20	17557.10	17560.56	17555.84	17559.39	17543.27	17557.41	17541.21	17543.85
10	17573.28		17556.24	17578.44	17556.24	17560.44	17554.89	17559.02	17540.84	17556.77	17538.80	17541.79
11	17573.96		17555.32	17579.61	17555.32	17560.04	17553.87	17558.56	17538.35	17556.24		17539.67
12	17574.58		17554.64	17580.63	17554.30	17559.51	17552.79	17557.97	17535.76	17555.78		17537.49
13	17575.04		17553.50	17581.81	17553.22	17559.02	17551.65	17557.41	17533.09	17555.10		17535.21
14	17575.45		17552.64	17582.80	17552.05	17558.43	17550.31	17556.67	17530.32	17554.02		17532.93
15	17575.63		17551.37	17583.95	17550.79	17557.97	17549.00	17556.24	17527.49	17553.41		17530.56
16			17549.98	17584.75	17549.49	17557.20	17547.61	17555.32	17524.60			17528.22
17				17585.59	17547.86	17556.67	17545.86	17554.64	17521.59			17525.76
18				17586.42		17555.84		17553.87	17518.51			17523.21
19				17587.20		17555.10		17552.97				17520.88
20				17587.88		17554.30		17552.05				17518.15
21				17588.50		17553.41						17515.54
22				17588.93		17552.45						17512.81
23				17589.95		17551.37						17510.04
24				17590.29		17549.98						17507.22
25				17590.70		17549.49						17504.34
26				17591.05		17548.04						
27				17591.47		17546.87						
28				17591.66		17545.61						
29				17591.90								
30				17592.03								

573.5 Band $Rh^{16}O$ Observed Transition Lines $[16.0]^2\Pi_{1/2}$ 2,0

N"	$^{s}R_{11}(0)$	$^{r}Q_{11}(0)$	$^{q}P_{11}(0)$	$^{r}R_{12}(1)$	$^{q}Q_{12}(1)$	$^{p}P_{12}(1)$	$^{q}R_{13}(1)$	$^{p}Q_{13}(1)$	$^{o}P_{13}(2)$	$^{p}R_{14}(2)$	$^{o}Q_{14}(2)$	$^{n}P_{14}(3)$
0	17437.37	---	17435.30									
1	17438.52	---	17434.97	17436.49	---	17432.78	17433.29	17430.65				
2	17439.74	---	17434.66	17437.37	17435.30	17432.57	17433.75	17431.14	17431.56	17430.17	17430.83	
3	17440.96	---	17434.45	17438.25	17434.97	17432.29	17433.75	17430.83	17430.17	17429.71	17429.02	---
4	17442.11	17438.52	17434.18	17439.10	17434.66	17431.56	17433.57	17430.35	17428.53	17429.19	17427.25	---
5	17443.24	---	17433.75	17439.83	17434.18	17430.83	17433.14	17429.78	17426.76	17428.22	17425.09	---
6	17444.24	17440.38	17433.29	17440.53	17433.57	17430.04	17432.57	17428.89	17424.46	17427.46	17422.94	17419.84
7	17445.22	17440.96	17432.78	17441.11	17433.14	17429.19	17431.90	17428.04	17422.48	17426.31	17420.69	17417.33
8	17446.19	17441.51	17432.17	17441.66	17432.29	17428.22	17431.14	17427.01	17420.18	17425.25	17418.33	17414.90
9	17447.10	17442.11	17431.41	17442.11	17431.56	17427.25	17430.35	17425.94	17417.81	17424.00	17416.02	17412.05
10	17447.99	17442.51	17430.83	17442.51	17430.83	17426.16	17429.47	17424.76	17415.41	17422.67	17413.35	17409.35
11	17448.81		17430.17	17442.81	17430.04	17424.97	17428.53	17423.45	17412.99	17421.30	17410.80	17406.44
12	17449.54		17429.19	17443.06	17429.19	---	17427.68	17422.36	17410.53	17420.09	17408.16	17403.53
13	17450.24		17428.53	17443.24	17428.22	17422.36	17426.76	17420.69	---	17418.48	17405.53	
14	17450.84		17427.68	17443.36	17427.25	17420.97	17425.58	17419.33	17405.41	17416.75	17402.84	
15	17451.31		17426.76		17426.16	17419.48	17424.46	17417.81	17402.84	17415.14	17400.08	
16	17451.70		17425.58		17425.09	17417.81	17423.27	17416.02	17400.08	17413.35	17397.20	
17	17451.98		17424.46		17423.82		17421.78		17397.20			
18			17423.27		17422.48		17420.45		17394.27			
19			17421.78		17420.97		17418.84		17391.27			
20									17388.16			
21									17384.92			
22									17381.60			
23									17378.16			
24									17374.56			

584.1 Band $Rh^{16}O$ Observed Transition Lines $[15.8]^2\Pi_{1/2}$ 2,0

N"	$^{s}R_{11}(0)$	$^{r}Q_{11}(0)$	$^{q}P_{11}(0)$	$^{r}R_{12}(1)$	$^{q}Q_{12}(1)$	$^{p}P_{12}(1)$	$^{q}R_{13}(1)$	$^{p}Q_{13}(1)$	$^{o}P_{13}(2)$	$^{p}R_{14}(2)$	$^{o}Q_{14}(2)$	$^{n}P_{14}(3)$
0	17120.80	17118.42	---									
1	17122.41	17119.33	---	17119.98	---	---	---	17114.55				
2	17124.05	17120.15	17118.07	17120.80	17118.74	---	17117.10	17114.70	---	---	---	
3	17125.78	17120.91	17118.22	17121.53	17118.92	---	17117.69	17114.55	---	17113.38	---	17110.37
4	17127.36	17121.65	17118.33	17122.23	17118.92	17114.94	17117.89	17113.85	17111.86	17112.48	17110.37	---
5	17128.92	17122.41	17118.48	17122.85	17118.92	17114.09	17117.89	17113.15	17110.37	17111.45	17108.79	17105.71
6	17130.33	17122.99	17118.48	17123.38	17118.92	17113.15	17117.75	17111.98	17108.79	17110.37	17107.09	17103.14
7	17131.77	17123.58	17118.42	17123.84	17118.74	17112.07	17117.54	17110.92	17107.09	17109.20	17105.30	17100.45
8	17133.03	17124.05	17118.22	17124.17	17118.33	17110.92	17117.10	17109.75	17105.30	17107.85	17103.37	17097.76
9	17134.20	17124.23	17118.07	17124.37	17118.07	17109.75	17116.75	17108.41	17103.37	17106.42	17101.38	17094.78
10	17135.32	17124.49	17117.60	17124.49	17117.60	17108.41	17116.22	17107.09	17101.38	17104.98	17099.22	17091.74
11	17136.37	17124.61	17117.10	17124.55	17117.10	17107.09	17115.52	17105.71	17099.22	17103.37	17097.03	
12	17137.26	17124.75	17116.55	17124.55	17116.40	17105.45	17114.94		17097.03	17101.56	17094.72	
13	17138.11	17124.75	17115.93	17124.49	17115.53	17103.87	17114.09		17094.72		17092.29	
14	17138.78	17124.61	17115.14	17124.23	17114.82	17102.14	17113.15		17092.29		17089.78	
15	17139.40	17124.55	17114.32	17123.99	17113.85	17100.45	17111.98		17089.78		17087.27	
16	17139.99	17124.35	17113.38	17123.70	17112.77		17110.92		17087.27		17084.55	
17	17140.42	17123.99	17112.39	17123.20	17111.71		17109.75		17084.55		17081.78	
18	17140.74	17123.43	17111.25	17122.67	17110.51		17108.41		17081.78		17078.81	
19	17141.19	17122.91	17110.14	17122.03	17109.20		17107.09		17078.81		17075.98	
20	17141.37	17122.41	17108.79	17121.32	17107.85		17105.45		17075.98		17072.95	
21	17141.37			17120.53	17106.42				17072.95		17069.83	
22	17141.37			17119.98	17104.86				17069.83		17066.65	
23	17141.37				17103.14						17063.30	
24	17141.28				17101.50						17059.90	
25	17141.02				17099.72							
26					17097.76							
27					17095.77							
28					17093.61							
29					17091.39							
30					17089.14							

588.7 Band $Rh^{16}O$ Observed Transition Lines $[16.0]^2\Pi_{3/2}$ 1,0

N''	$^tR_{21}(0)$	$^sQ_{21}(0)$	$^rP_{21}(1)$	$^sR_{22}(1)$	$^rQ_{22}(1)$	$^qP_{22}(2)$	$^rR_{23}(1)$	$^qQ_{23}(2)$	$^pP_{23}(3)$	$^qR_{24}(2)$	$^pQ_{2p}(3)$	$^oP_{24}(4)$
0	16981.76	16979.76										
1	16983.49	16980.63	16978.72	16981.35	16979.42		---					
2	16985.34	16981.76	16979.04	16982.45	16979.68	16977.69	16978.13	16976.10		---		
3	16987.24	16982.88	16979.36	16983.49	16980.00	16977.17	16978.70	16975.96	16973.94	16974.72	16972.73	
4	16989.18	16984.01	16979.68	16984.53	16980.28	16976.63	16979.04	16975.47	16972.73	16973.94	16971.40	16969.33
5	16991.05	16985.14	16980.00	16985.57	16980.54	16976.11	16979.36	16974.90	16971.38	16973.48	16969.90	16967.09
6	16992.90	16986.23	16980.28	16986.52	16980.73	16975.47	16979.50	16974.38	16970.00	16972.71	16968.27	16964.79
7	16994.72	16987.24	16980.54	16987.49	16980.77	16974.87	16979.70	16973.69	16968.56	16971.90	16966.77	16962.42
8	16996.51		16980.73	16988.37	16980.92	16974.15	16979.70	16972.97	16967.09	16971.09	16965.16	16960.04
9	16998.25		16980.92	16989.24	16980.98	16973.46	16979.70	16972.19	16965.53	16970.14	16963.46	16957.56
10	16999.95		16981.09	16990.07	16981.03	16972.76	16979.65	16971.40	16963.89	16969.22	16961.79	16955.09
11	17001.57		16981.18	16990.79	16981.03	16971.90	16979.56	16970.48	16962.28	16968.27	16960.00	16952.50
12	17003.08		16981.18	16991.40	16980.98	16971.09	16979.42	16969.58	16960.58	16967.28	16958.20	16949.92
13	17004.32		16981.18	16991.69	16980.77	16970.14	16979.27	16968.52	16958.83	16966.10	16956.38	16947.27
14	17005.03		16981.03	16994.49	16980.54	16969.19	16979.01		16957.07	16964.80	16954.43	16944.60
15	17007.42		16980.63	16995.13	16979.97	16967.77	16978.35		16955.09	16963.33	16952.45	16941.80
16	17007.96		16979.65	16995.68	16979.04	16968.95	16977.17		16953.19	16964.28		16938.94
17	17008.99		16980.46	16996.17	16979.65		16977.69		16950.90			16935.67
18	17010.32		16979.27	16996.72	16978.35							16935.01
19	17011.66		16978.72	16997.15	16977.69							
20	17013.05		16978.35	16997.59								
21	17014.39		16978.12	16998.05								
22	17015.73		16977.69	16998.40								
23	17017.04			16999.03								
24	17018.31			16999.38								
25	17019.52			16999.64								
26	17020.73											
27	17021.91											
28	17022.98											

594.3 Band $Rh^{16}O$ Observed Transition Lines $[15.8]^2\Pi_{3/2}$ 1,0

N"	$^{t}R_{21}(0)$	$^{s}Q_{21}(0)$	$^{r}P_{21}(1)$	$^{s}R_{22}(1)$	$^{r}Q_{22}(1)$	$^{q}P_{22}(2)$	$^{r}R_{23}(1)$	$^{q}Q_{23}(2)$	$^{p}P_{23}(3)$	$^{q}R_{24}(2)$	$^{p}Q_{2p}(3)$	$^{o}P_{24}(4)$
0	16822.51	16822.30										
1	16823.78	16823.53	16819.97	16824.21	---		16818.35					
2	16825.17	16824.89	16819.80	16825.57	16820.52	16820.18	16818.82	16818.82	---	16817.93		
3	16826.59	16826.21	16819.67	16826.81	16820.18	16819.97	16819.03	16818.82	16815.30	16817.59	16814.07	
4	16827.92	16827.53	16819.54	16828.04	16819.97	16819.80	16818.82	16818.57	16813.46	16817.42	16812.07	16812.07
5	16829.22	16828.76	16819.37	16829.23	16819.80	16819.37	16818.82	16818.35	16811.86	16816.83	16810.29	16809.99
6	16830.47	16829.95	16819.03	16830.33	16819.44	16819.03	16818.35	16817.93	16809.91	16816.23	16808.30	16808.00
7	16831.66	16831.14	16818.82	16831.35	16819.03	16818.57	16817.93	16817.42	16808.00	16815.64	16806.22	16805.88
8	16832.82	16832.20	16818.35	16832.33	16818.56	16817.93	16817.42	16816.82	16805.88	16814.96	16804.02	16803.63
9	16833.81	16833.27	16817.92	16833.27	16817.93	16817.42	16816.83	16816.10	16803.64	16814.19	16801.77	16801.31
10	16834.83	16834.16	16817.41	16834.16	16817.42	16816.82	16816.10	16815.30	16801.60	16813.35	16799.44	16798.98
11	16835.74	16835.05	16816.82	16834.93		16816.10	16815.30	16814.47	16799.31	16812.42	16797.07	16796.52
12	16836.59	16835.73	16816.10	16835.73		16815.30	16814.49	16814.75	16797.07	16811.48	16794.57	16794.00
13	16837.38	16836.63	16815.29	16836.33		16814.49	16813.46	16812.67	16794.57	16810.46	16792.07	16791.44
14	16838.09	16837.39	16814.49	16836.97		16813.35	16812.42	16811.86	16792.07	16809.36	16789.45	16788.77
15	16838.75	16838.11	16813.60	16837.39		16812.41	16811.45		16789.45	16808.00	16786.79	16786.11
16	16839.31	16838.46	16812.67			16811.48	16810.29		16786.79	16806.90	16784.12	16783.36
17	16839.82	16839.18	16811.86			16810.29	16809.36		16784.12	16805.59		16780.53
18	16840.28						16808.00			16804.23		16777.61
19	16840.71									16802.83		16774.66
20	16841.07									16801.30		16771.66
21	16841.22									16799.78		16768.58
22	16841.39											16765.46
23												

598.1 Band $Rh^{16}O$ Observed Transition Lines $[16.0]^2\Pi_{1/2}$ 1,0

N"	$^{s}R_{11}(0)$	$^{r}Q_{11}(0)$	$^{q}P_{11}(0)$	$^{r}R_{12}(1)$	$^{q}Q_{12}(1)$	$^{p}P_{12}(1)$	$^{q}R_{13}(1)$	$^{p}Q_{13}(1)$	$^{o}P_{13}(2)$	$^{p}R_{14}(2)$	$^{o}Q_{14}(2)$	$^{n}P_{14}(3)$
0	16717.79	---	---									
1	16719.09	16719.18	---	16719.85	---	---	---	---				
2	16720.46	16720.55	16715.01	16721.24	16715.79	---	16714.06	---	16711.87		---	
3	16721.86	16721.97	16714.95	16722.59	16715.60	16715.71	16714.31	---	16710.48		---	---
4	16723.20	16723.37	16714.81	16723.93	16715.32	16715.49	16714.06	16714.31	16708.75		16707.47	---
5	16724.55	16724.74	16714.62	16725.22	16715.01	16715.21	16713.86	16714.06	16707.02		16705.54	16705.54
6	16725.86	16726.08	16714.31	16726.42	16714.70	16714.95	16713.56	16713.75	16705.12		16703.56	16703.56
7	16727.09	16727.32	16714.06	16727.62	16714.31	16714.51	16713.08	16713.30	16703.14		16701.38	16701.49
8	16728.32	16728.52	16713.67	16728.72	16713.86	16714.06		16712.86	16701.13		16699.21	16699.43
9	16729.47	16729.73		16729.78		16713.67		16712.33	16699.01		16697.00	16697.23
10	16730.52	16730.79		16730.79		16713.08		16711.82	16696.86		16694.75	16694.97
11	16731.54	16731.82		16731.71					16694.66		16692.40	16692.68
12	16732.52	16732.80		16732.61					16692.40		16690.03	16690.31
13	16733.48	16733.76		16733.48					16690.03			
14	16734.26	16734.60		16734.26								

607.9 Band $Rh^{16}O$ Observed Transition Lines $[15.8]^2\Pi_{1/2}$ 1,0

N"	$^{s}R_{11}(0)$	$^{r}Q_{11}(0)$	$^{q}P_{11}(0)$	$^{r}R_{12}(1)$	$^{q}Q_{12}(1)$	$^{p}P_{12}(1)$	$^{q}R_{13}(1)$	$^{p}Q_{13}(1)$	$^{o}P_{13}(2)$	$^{p}R_{14}(2)$	$^{o}Q_{14}(2)$	$^{n}P_{14}(3)$
0	16449.1639	16447.1952	16446.1599									
1	16450.7461	16447.9898	16446.2671	16448.6611	16446.9501	16445.74	16444.6703	16443.4871				
2	16452.4118	16448.8698	16446.4583	16449.5272	16447.12	16445.15	16445.5660	16443.5951	16442.5658	16442.7052	16441.73	
3	16454.0652	16449.7321	16446.6409	16450.3372	16447.31	16444.56	16445.9993	16443.2430	16441.5219	16442.0462	16440.27	16439.1431
4	16455.6708	16450.5483	16446.7664	16451.0733	16447.39	16443.64	16446.1663	16442.6211	16440.2117	16441.2329	16438.81	16436.8725
5	16457.2062	16451.2990	16446.8265	16451.7357	16447.20	16442.9365	16446.1663	16441.8365	16438.7399	16440.2979	16437.17	16434.4438
6	16458.6647	16451.9709	16446.8082	16452.3145	16447.12	16442.0383	16446.0427	16440.9230	16437.1401	16439.2561	16435.55	16431.95
7	16460.0404	16452.5550	16446.7090	16452.8064	16446.90	16441.02	16445.8122	16439.95	16435.4334	16438.1053	16433.67	16429.33
8	16461.3363	16453.0554	16446.5283	16453.2152	16446.71	16440.00	16445.4780	16438.68	16433.6269	16436.8725	16431.78	16426.70
9	16462.54	16453.43	16446.26	16453.5385	16446.26	16438.81	16445.0418	16437.52	16431.78	16435.55	16429.77	16423.85
10	16463.67	16453.76	16445.90	16453.7653	16445.85	16437.60	16444.5600	16436.34	16429.77	16434.15	16427.64	16420.91
11	16464.67	16454.05	16445.50	16453.89	16445.37	16436.31	16443.88	16434.91	16427.64	16432.62	16425.45	16417.96
12	16465.64	16454.19	16445.04	16453.95	16444.66	16434.91	16443.24	16433.45	16425.54	16431.00	16423.25	16414.81
13	16466.48	16454.38	16444.37	16453.95	16443.88	16433.45	16442.45	16431.78	16423.25	16429.33	16420.75	16411.67
14	16467.24	16454.19	16443.65	16453.86	16443.24	16431.78	16441.51	16430.09	16420.75	16427.56	16418.25	16408.42
15	16467.91	16454.13	16442.86	16453.68		16430.09	16440.49	16428.37	16418.41	16425.68	16415.70	16405.15
16	16468.54					16428.37			16415.90	16423.85		16401.66
17	16469.02								16413.23	16421.61		16398.15
18	16469.46								16410.44	16419.49		16394.50
19	16469.84								16407.75	16417.26		16390.80
20	16470.11								16404.88	16415.11		16387.03
21	16470.24								16401.93			16383.14
22												

618.0 Band $Rh^{16}O$ Observed Transition Lines $[16.0]^2\Pi_{1/2}$ 1,1

N"	$^{s}R_{11}(0)$	$^{r}Q_{11}(0)$	$^{q}P_{11}(0)$	$^{r}R_{12}(1)$	$^{q}Q_{12}(1)$	$^{p}P_{12}(1)$	$^{q}R_{13}(1)$	$^{p}Q_{13}(1)$	$^{o}P_{13}(2)$	$^{p}R_{14}(2)$	$^{o}Q_{14}(2)$	$^{n}P_{14}(3)$
0	16179.4439	16179.0666	16176.9355									
1	16180.8574	16180.3149	16176.7651	16181.01	16177.4431	---	16175.1576	16174.9358				
2	16182.4176	16181.6842	16176.7385	16182.27	16177.4019	16177.0216	16175.8430	16175.4652	16173.3366	16174.5766	16172.48	
3	16184.0289	16183.0893	16176.7522	16183.76	16177.3553	16176.8058	16176.1120	16175.5641	16172.0175	16174.3682	16170.76	16170.6028
4	16185.6575	16184.4807	16176.7760	16185.10	16177.2952	16176.5649	16176.1729	16175.4378	16170.4926	16174.0573	16169.01	16168.7210
5	16187.2896	16185.8392	16176.7875	16186.29	16177.2267	16176.2887	16176.1304	16175.1909	16168.8504	16173.6551	16167.36	16166.7684
6	16188.9106	16187.1663	16176.7974	16187.52	16177.19	16175.9630	16176.0296	16174.8511	16167.1465	16173.1840	16165.56	16164.7458
7	16190.47	16188.7930	16176.8023	16188.97	16177.09	16175.6200	16175.8885	16174.4200	16165.3938	16172.6651	16163.62	16162.6621
8	16192.07	16190.0020	16176.7760	16190.18	16176.88	16175.1800	16175.7234	16174.069	16163.6141	16172.0900	16161.77	16160.644
9	16193.67	16191.2980		16191.40	16176.80	16175.0890	16175.5373	16173.781	16161.7971	16171.7990	16159.81	16158.310
10		16192.6140		16192.40	16176.54	16174.5920	16175.3386	16173.258	16159.93	16171.1340	16157.78	16156.189
11		16193.7960		16193.72	16176.49	16174.1500	16175.1292	16172.611	16158.10	16170.5640	16155.87	16154.188
12		16195.1520		16194.82	16176.36	16173.4670	16174.9047	16172.015	16156.25	16169.7830	16153.86	16151.869
13		16196.0960		16195.80	16176.07	16173.1530	16174.6565	16171.572	16154.40	16169.1650	16151.95	
14		16197.145		16196.75	16175.94	16172.604		16170.894	16152.54	16168.425		
15		16198.404		16197.88	16175.75	16172.003		16170.198	16150.61	16167.646		
16		16199.390		16198.83		16171.192		16169.493	16148.76	16166.738		
17		16200.494		16199.93		16170.669		16168.707	16146.81	16166.032		
18		16201.752		16200.82		16170.042		16168.098	16144.87	16164.971		
19		16202.628		16201.71		16169.493		16167.358	16142.95	16164.344		
20		16203.623		16202.63		16168.734		16166.480	16140.97	16163.407		
21		16204.443		16203.29		16168.055		16165.703		16162.402		
22		16205.401		16204.26		16167.271		16164.762		16161.562		
23		16206.226		16204.92		16166.252		16163.691		16160.305		
24		16207.182		16205.73		16165.494		16162.881		16159.464		
25		16208.111		16206.60		16164.606		16161.784		16158.272		
26		16208.882		16207.18		16163.691		16160.897		16157.241		
27		16209.610		16207.82		16162.880		16159.998		16156.189		
28		16210.363		16208.46		16161.784		16158.964		16154.927		
29		16211.093		16209.06		16160.865		16157.790		16153.714		
30		16211.693		16209.61		16159.756		16156.605		16152.498		
31		16212.234		16210.20		16158.797				16151.313		

618.0 Band $Rh^{16}O$ Observed Transition Lines continued... $[16.0]^2\Pi_{1/2}$ 1,1

N"	$^{s}R_{11}(0)$	$^{r}Q_{11}(0)$	$^{q}P_{11}(0)$	$^{r}R_{12}(1)$	$^{q}Q_{12}(1)$	$^{p}P_{12}(1)$	$^{q}R_{13}(1)$	$^{p}Q_{13}(1)$	$^{o}P_{13}(2)$	$^{p}R_{14}(2)$	$^{o}Q_{14}(2)$	$^{n}P_{14}(3)$
32		16212.911		16210.71		16157.683				16149.949		
33		16213.590		16211.21		16156.605				16148.700		
34		16214.149		16211.69		16155.519				16147.434		
35		16214.631		16212.13		16154.345				16146.086		
36		16215.244		16212.54		16153.088				16144.694		
37				16212.91		16151.869				16143.291		
38				16213.24						16141.849		
39				16213.59						16140.269		
40				16213.90						16138.861		
				16214.15						16137.329		
										16135.748		
										16134.137		

618.3 Band $Rh^{16}O$ Observed Transition Lines $[16.0]^2\Pi_{3/2}$ 0,0

N"	$^{t}R_{21}(0)$	$^{s}Q_{21}(0)$	$^{r}P_{21}(1)$	$^{s}R_{22}(1)$	$^{r}Q_{22}(1)$	$^{q}P_{22}(2)$	$^{r}R_{23}(1)$	$^{q}Q_{23}(2)$	$^{p}P_{23}(3)$	$^{q}R_{24}(2)$	$^{p}Q_{2p}(3)$	$^{o}P_{24}(4)$
0	16171.2350	16169.3327										
1	16172.8767	16170.2250	16168.3023	16170.8995	16168.9806		16166.6997					
2	16174.6169	16171.2457	16168.5316	16171.9053	16169.1995	16167.2887	16167.6392	16165.7319		---		
3	16176.3595	16172.2862	16168.7652	16172.8856	16169.3683	16166.7208	16168.1238	16165.4805	16163.5516	---	---	
4	16178.0560	16173.3078	16168.9754	16173.8331	16169.4912	16166.1192	16168.3727	16165.0061	16162.2810	16163.6110	16160.8972	16158.9968
5	16179.6895	16174.3018	16169.1182	16174.7333	16169.5522	16165.4805	16168.4635	16164.3859	16160.8658	16162.8474	16159.3220	16156.6846
6	16181.2477	16175.2552	16169.1889	16175.5979	16169.5387	16164.7925	16168.4348	16163.6868	16159.3467	16162.0114	16157.6830	16154.3042
7	16182.7150	16176.1652	16169.1957	16176.4117	16169.4451	16164.0574	16168.3065	16162.9067	16157.7295	16161.1136	16155.9380	16151.8607
8	16184.1077	16177.0216	16169.1182	16177.180	16169.2712	16163.2741	16168.0575	16162.0683	16156.0142	16160.1617		16149.389
9	16185.4053	16177.89	16168.9392	16177.898	16169.010	16162.4429	16167.7331	16161.1698	16154.2051	16159.21		16146.807
10	16186.6095	16178.61	16168.720	16178.562	16168.720	16161.5602	16167.3114	16160.2160	16152.3134	16158.19		16144.227
11	16187.7281	16179.451	16168.380	16179.181	16168.120	16160.6342	16166.790	16159.21	16150.314	16157.02		16141.569
12	16188.77	16179.998	16167.930	16179.744	16167.646	16159.6548	16166.110	16158.19	16148.267	16155.87		16138.861
13	16189.71	16180.593	16167.360	16180.330	16166.984	16158.6198	16165.320	16157.02	16146.078	16154.62		16136.074
14	16190.60		16166.738	16180.750	16166.253	16157.502	16164.656	16155.87	16143.810	16153.36		16133.289
15	16191.36		16166.032	16181.170	16165.482	16156.370	16163.839	16154.62	16141.491	16151.96		16130.403
16	16192.07		16165.209	16181.510	16164.656	16155.170	16162.686	16153.36	16138.991	16150.59		16127.464

618.3 Band $Rh^{16}O$ Observed Transition Lines continued... $[16.0]^2\Pi_{3/2}$ 0,0

N"	$^tR_{21}(0)$	$^sQ_{21}(0)$	$^rP_{21}(1)$	$^sR_{22}(1)$	$^rQ_{22}(1)$	$^qP_{22}(2)$	$^rR_{23}(1)$	$^qQ_{23}(2)$	$^pP_{23}(3)$	$^qR_{24}(2)$	$^pQ_{2p}(3)$	$^oP_{24}(4)$
17	16192.70		16164.482	16181.830	16163.640	16153.950	16161.562		16136.491			16124.448
18	16193.22		16163.407	16182.060	16162.686	16152.660	16160.644		16133.888			16121.433
19	16193.72		16162.402	16182.270	16161.562	16151.310	16159.322		16131.110			16118.315
20	16194.06		16161.228	16182.454	16160.305	16149.940	16158.102		16128.314			16115.043
21	16194.43		16160.060	16182.454	16158.960	16148.490	16156.605		16125.380			16111.973
22	16194.64		16158.797	16182.454	16157.683	16146.970	16155.168		16122.392			16108.728
23	16194.80		16157.508	16182.454	16156.189	16145.390	16153.714		16119.408			16105.354
24	16194.80		16156.189	16182.454	16154.581	16143.730	16152.080		16116.230			
25	16194.64		16154.581	16182.270	16153.088	16142.120	16150.350		16113.142			
26	16194.43		16153.088	16181.997	16151.313	16140.370	16148.569		16109.728			
27	16194.28		16151.313	16181.745	16149.490	16138.560	16146.581		16106.400			
28	16193.92		16149.390	16181.416	16147.434	16136.730	16144.460		16102.973			
29	16193.53		16147.434	16181.089	16145.391	16134.800	16142.350		16099.379			
30	16192.92		16145.391	16180.593	16143.375	16132.780	16140.269					
31	16192.35		16143.375		16141.390	16130.840	16137.834					
32	16191.68		16141.150		16138.909	16128.720	16135.639					
33	16191.00						---					
34	16190.00						16130.624					
35	---						16128.066					
36	16188.18						16125.248					
37							16122.392					
38							16119.668					

625.5 Band $Rh^{16}O$ Observed Transition Lines $[15.8]^2\Pi_{3/2}$ 0,0

N"	$^tR_{21}(0)$	$^sQ_{21}(0)$	$^rP_{21}(1)$	$^sR_{22}(1)$	$^rQ_{22}(1)$	$^qP_{22}(2)$	$^rR_{23}(1)$	$^qQ_{23}(2)$	$^pP_{23}(3)$	$^qR_{24}(2)$	$^pQ_{2p}(3)$	$^oP_{24}(4)$
0	15979.6002	15977.7565										
1	15981.1500	15978.5715	15976.7303	15979.2467	15977.4057		15975.1329					
2	15982.7882	15979.4734	15976.8939	15980.1316	15977.5554	15975.7133	15976.0085	15974.1594		15973.2673		
3	15984.4124	15980.42	15977.0442	15980.9602	15977.6495	15975.0666	15976.4313	15973.8262	15971.9911	15972.6274	15970.79	
4	15985.9834	15981.16	15977.1426	15981.7186	15977.6741	15974.3517	15976.5424	15973.2272	15970.6486	15971.8427	15969.2630	15967.4193
5	15987.4846	15981.93	15977.1708	15982.3944	15977.6082	15973.5531	15976.5231	15972.4617	15969.1669	15970.93	15967.6106	15965.0276
6	15988.9070	15982.59	15977.1209	15982.9928	15977.4647	15972.6745	15976.3559	15971.5669	15967.5183	15969.95	15965.8469	15962.5287
7	15990.2471	15983.21	15976.9900	15983.4990	15977.2395	15971.7153	15976.0885	15970.5637	15965.7774	15968.83	15963.9849	15960.05
8	15991.4984	15983.85	15976.7696	15983.9202	15976.9373	15970.6665	15975.7204	15969.4571	15963.9386	15967.63	15962.04	15957.33
9	15992.6677	15984.23	15976.4774	15984.2575	15976.5131	15969.5257	15975.2569	15968.2557	15962.0012	15966.28	15960.05	15954.39
10	15993.7456	15984.61	15976.0733	15984.4983	15976.0140	15968.3042	15974.6924	15966.9491	15960.05	15964.90	15957.86	15951.67
11	15994.66	15984.77	15975.60	15984.6517	15975.4700	15966.9889	15974.0367	15965.5666	15957.96	15963.38	15955.62	15948.67
12	15995.53	15984.94	15975.09	15984.7004	15974.7500	15965.5887	15973.2673	15964.0500	15955.72	15961.77	15953.30	15945.65
13	15996.32	15984.94	15974.37	15984.7172	15974.0600	15964.15	15972.49	15962.5700	15953.37	15960.05	15950.86	15942.47
14	15997.04	15984.94	15973.61	15984.48	15973.2400	15962.57	15971.56	15960.7900	15950.94	15958.36	15948.32	15939.19
15	15997.70		15972.77	15984.28		15960.89	15970.54	15959.0300	15948.49	15956.47	15945.85	15935.84
16	15998.22					15959.18			15945.95	15954.43		15932.39
17	15998.68					15957.32			15943.26	15952.45		15929.01
18	15999.03					15955.39			15940.46	15950.31		15925.26
19	15999.27					15953.40			15937.59			15921.51
20	15999.50					15951.34			15934.69			15917.89
21						15948.93			15931.45			15913.89
22						15946.74			15928.45			
23						15944.32			15925.26			
24						15941.78			15921.86			
25						15939.17						
26						15936.55						
27												

629.9 Band $Rh^{16}O$ Observed Transition Lines $[16.0]^2\Pi_{1/2}$ 0,0

N"	$^{s}R_{11}(0)$	$^{r}Q_{11}(0)$	$^{q}P_{11}(0)$	$^{r}R_{12}(1)$	$^{q}Q_{12}(1)$	$^{p}P_{12}(1)$	$^{q}R_{13}(1)$	$^{p}Q_{13}(1)$	$^{o}P_{13}(2)$	$^{p}R_{14}(2)$	$^{o}Q_{14}(2)$	$^{n}P_{14}(3)$
0	15877.9861	15875.8218	15874.8243									
1	15879.6778	15876.6643	15874.9959	15877.3381	15875.6673	---	15873.3946	15872.1009				
2	15881.4973	15877.6154	15875.2815	15878.2745	15875.9383	---	15874.3851	15872.2264	15871.2264	15871.3367	15870.3249	
3	15883.3320	15878.5804	15875.5784	15879.1825	15876.1791	15873.1574	15874.9382	15871.8400	15870.2459	15870.7189	15869.0519	15867.7705
4	15885.1287	15879.5256	15875.8513	15880.0479	15876.3764	15872.4934	15875.2540	15871.3100	15869.0320	15869.9802	15867.6495	15865.4834
5	15886.8936	15880.4306	15876.0848	15880.8679	15876.5227	15871.7754	15875.4279	15870.7000	15867.6780	15869.1434	15866.1340	15863.1170
6	15888.6019	15881.34	15876.2714	15881.6352	15876.6253	15871.0090	15875.5045	15869.8200	15866.2256	15868.2314	15864.69	15860.6709
7	15890.1950	15882.06	15876.3977	15882.31	15876.6253	15870.1867	15875.5045	15869.03	15864.6926	15867.2483	15862.85	15858.250
8	15891.8120	15882.81	15876.43	15882.97	15876.6253	15869.3128	15875.4279	15868.18	15863.0841	15866.1936	15861.22	15855.514
9	15893.3540	15883.57	15876.43	15883.57	15876.5227	15868.33	15875.24	15867.19	15861.4086	15865.0774		15852.908
10	15894.8060	15884.13	15876.43	15884.13	15876.3764	15867.19	15875.03	15865.98	15859.61	15863.82		15850.214
11	15896.2330	15884.64	15876.33	15884.58	15876.1791	15866.21	15874.78	15864.82	15857.77	15862.68		15847.426
12	15897.6960	15885.31	15876.15	15885.04	15875.90	15865.15	15874.44	15863.69	15855.88	15861.32		15844.623
13	15898.9100	15885.64	15875.90	15885.37	15875.54	15863.94	15874.03	15862.41	15853.99	15859.94		15841.691
14	15900.1730	15886.17	15875.62	15885.72	15875.24	15862.76	15873.55	15861.12	15851.98	15858.48		15838.710
15	15901.5320	15886.55	15875.25	15886.00	15874.81	15861.38	15873.08	15859.61	15849.89	15857.04		15835.739
16	15902.425	15886.88	15874.91	15886.17	15874.31	15860.14	15872.42	15858.25	15847.78	15855.71		15832.592
17	15903.687		15874.44	15886.30	15873.65	15858.78	15871.84	15856.79	15845.59	15854.02		15829.503
18	15904.584		15873.88	15886.35	15873.08	15857.32	15871.09	15855.25	15843.33	15852.18		15826.320
19	15905.598		15873.28	15886.35	15872.24	15855.71	15870.25	15853.64	15841.10	15850.45		15823.078
20	15906.257		15872.55	15886.30	15871.59	15854.20	15869.22	15851.98	15838.68	15848.71		15819.680
21	15907.024		15871.84	15886.17	15870.78	15852.61	15868.34	15850.15	15836.22	15846.88		15816.380
22	15907.761		15871.00	15886.00		15850.95	15867.25		15833.71	15844.97		15812.957
23	15908.436		15870.17			15849.19	15866.30		15831.20	15843.03		15809.468
24	15909.049		15869.31			15847.38	15865.17		15828.54			15805.927
25	15909.602		15868.25				15864.04					15802.324
26	15910.057		15867.19				15862.68					15798.686
27	15910.554		15866.14				15861.42					15794.977
28	15910.864		15865.00				15860.04					15791.216
29	15911.23		15863.82				15858.80					15787.361
30	15911.43		15862.41				15857.14					15783.529

629.9 Band $Rh^{16}O$ Observed Transition Lines continued... $[16.0]^2\Pi_{1/2}$ 0,0

N"	$^{s}R_{11}(0)$	$^{r}Q_{11}(0)$	$^{q}P_{11}(0)$	$^{r}R_{12}(1)$	$^{q}Q_{12}(1)$	$^{p}P_{12}(1)$	$^{q}R_{13}(1)$	$^{p}Q_{13}(1)$	$^{o}P_{13}(2)$	$^{p}R_{14}(2)$	$^{o}Q_{14}(2)$	$^{n}P_{14}(3)$
31	15911.51		15861.12				15855.59					15779.607
32	15911.69		15859.61				15854.08					15775.640
33	15911.69		15858.15				15852.29					15771.595
34	15911.69		15856.79				15850.56					15767.504
35	15911.69						15848.83					15763.358
36	15911.55						15846.99					15759.195
37	15911.29						15845.09					15754.921
38	15911.025						15843.15					15750.616
39	15910.716						15841.02					15746.268
40	15910.304						15838.89					15741.849
41	15909.858						15836.70					15737.397
42	15909.328						15834.54					15732.891
43	15908.770											15728.329
44	15908.106											15723.706
45	15907.420											15719.040
46	15906.658											15714.300
47	15905.821											15709.561
48	15904.912											15704.719
49	15903.946											15699.836
50	15902.924											15694.907
51	15901.857											15689.909
52	15900.645											15684.865
53	15899.433											15679.747
54	15898.134											15674.639
55	15896.655											15669.400
56	15895.371		**N"**	$^{s}R_{11}(0)$								15663.977
57	15893.824		**62**	15885.021								
58	15892.255		**63**	15883.015								
59	15890.556		**64**	15880.984								
60	15888.732		**65**	15878.735								
61	15886.870											

638.2 Band $Rh^{16}O$ Observed Transition Lines $[15.8]^2\Pi_{1/2}$ 0,0

N"	$^{s}R_{11}(0)$	$^{r}Q_{11}(0)$	$^{q}P_{11}(0)$	$^{r}R_{12}(1)$	$^{q}Q_{12}(1)$	$^{p}P_{12}(1)$	$^{q}R_{13}(1)$	$^{p}Q_{13}(1)$	$^{o}P_{13}(2)$	$^{p}R_{14}(2)$	$^{o}Q_{14}(2)$	$^{n}P_{14}(3)$
0	15669.3126	15669.6550	15667.1829									
1	15670.4783	15670.9620	15666.8359	15671.6372	15667.5088		15665.2399	15665.4462				
2	15671.7565	15672.3746	15666.6040	15673.0413	15667.2547	15667.6099	15665.7062	15666.0496	15663.5795	15665.1560	15662.6791	
3	15673.0413	15673.73	15666.3690	15674.3934	15666.9834	15667.4562	15665.7307	15666.2134	15662.0902	15665.0099	15660.8905	15661.1041
4	15674.2970		15666.1055	15675.6966	15666.6389	15667.2547	15665.5103	15666.1264	15660.3544	15664.7388	15659.01	15659.3167
5	15675.4957		15665.7950	15676.9405	15666.2362	15666.9917	15665.1434	15665.8917	15658.4748	15664.3524	15656.98	15657.4202
6	15676.6430		15665.4363	15678.1193	15665.7761	15666.6628	15664.6684	15665.5495	15656.4848	15663.8821	15654.87	15655.4354
7	15677.7245		15665.0032	15679.2293	15665.2556	15666.2613	15664.1041	15665.1132	15654.4084	15663.3201	15652.66	15653.3671
8	15678.7436		15664.5008	15680.2716	15664.6684	15665.7992	15663.4586	15664.5900	15652.2504	15662.6791	15650.38	15651.2211
9	15679.6986		15663.9456	15681.2376	15664.0061	15665.2605	15662.7351	15663.9740	15650.0084	15661.9648	15648.03	15648.9998
10	15680.5848		15663.3171	15682.0900	15663.2838	15664.6700	15661.9383	15663.2838	15647.7025	15661.1666	15645.61	15646.6948
11	15681.4025		15662.6240	15682.9597	15662.5120	15663.9709	15661.0689	15662.5511	15645.3222	15660.35	15643.14	15644.3246
12	15682.1561		15661.95	15683.7087	15661.7280	15663.2218	15660.1287	15661.7280	15642.8628	15659.35	15640.55	15641.91
13	15682.8380		15661.06	15684.3843	15660.6640	15662.44	15659.149	15660.6640	15640.37	15658.37	15637.88	15639.42
14	15683.4553		15660.13	15684.89	15659.7830	15661.51	15658.16	15659.7830	15637.78	15657.24	15635.19	15636.75
15	15684.0020		15659.20	15685.43	15658.7010	15660.52	15656.87	15658.7010	15635.11	15656.09	15632.45	15634.09
16	15684.30		15658.15	15685.85	15657.4280	15659.376	15655.672	15657.4280	15632.37	15654.84	15629.60	15631.30
17	15684.82		15657.07	15686.24	15656.3450	15658.240	15654.41	15656.3450	15629.57	15653.44	15626.66	15628.49
18	15685.13		15655.78	15686.51	15654.930	15657.067		15655.076	15626.68	15652.07	15623.66	15625.58
19	15685.43		15654.64	15686.78	15653.754	15655.878		15653.49	15623.73	15650.53	15620.59	15622.58
20	15685.58			15686.78	15652.304	15654.514	15649.980	15652.14	15620.70	15649.01	15617.47	15619.51
21	15685.68			15686.78	15650.670	15653.031	15648.361		15617.66	15647.39	15614.27	15616.39
22	15685.75				15649.216	15651.350	15646.707		15614.49		15610.98	15613.14
23	15685.80				15647.480	15649.697			15611.27		15607.65	15609.83
24	15685.83				15645.850				15607.98		15604.26	15606.49
25					15644.106				15604.62		15600.92	15602.99
26									15601.17		15597.15	15599.44
27									15597.64			

564.3 Band $Rh^{18}O$ Observed Transition Lines $[16.0]^2\Pi_{3/2}$ 2,0

N"	$^tR_{21}(0)$	$^sQ_{21}(0)$	$^rP_{21}(1)$	$^sR_{22}(1)$	$^rQ_{22}(1)$	$^qP_{22}(2)$	$^rR_{23}(1)$	$^qQ_{23}(2)$	$^pP_{23}(3)$	$^qR_{24}(2)$	$^pQ_{2p}(3)$	$^oP_{24}(4)$
0	17715.42	---										
1	17716.99	---	17712.59	17714.64			---					
2	17718.72	---	17712.91	17715.42		---	17711.97					
3	17720.28	---	17713.23	17716.20		17710.87	17712.60		17708.36			
4	17721.86	---	17713.69	17716.99		17710.24	17712.91		---			
5	17723.43	---	17713.80	17717.93			17713.06		17706.01			
6	17725.00	---	17714.01	17718.72			17713.06		17704.92			
7	17726.57	17719.19	17714.01	17719.50			17713.06		17703.50			
8	17728.14	---		17720.28			17713.06		17701.94			
9	17729.24	17720.91					17712.92		17700.53			
10	17730.50	---					17712.91		17698.96			
11	17731.60	17722.48					17712.28		17697.39			
12							17711.97		17695.67			
13							17711.35					
14							17710.87					

571.6 Band $Rh^{18}O$ Observed Transition Lines $[15.8]^2\Pi_{3/2}$ 2,0

N"	$^tR_{21}(0)$	$^sQ_{21}(0)$	$^rP_{21}(1)$	$^sR_{22}(1)$	$^rQ_{22}(1)$	$^qP_{22}(2)$	$^rR_{23}(1)$	$^qQ_{23}(2)$	$^pP_{23}(3)$	$^qR_{24}(2)$	$^pQ_{2p}(3)$	$^oP_{24}(4)$
0	17496.59	---										
1	17497.81	---	---	17497.20	---		---					
2	17498.73	---	17494.14	17498.12	17494.75	---	17493.22					
3	17499.96	---	17494.14	17498.73	17494.75	---			---		---	
4	17501.03	---	---	17499.50	17494.14	17492.92			17488.48		17487.10	17486.34
5	17501.95	17499.50	---	17499.96	17493.83	17492.00			17486.80		17485.42	
6	17503.02		---	17500.26	---	17491.31			17485.12		17483.28	
7	17503.63		---		---	17490.47			17483.22		17481.45	
8	17504.40		17492.00		17492.30				17480.99		17479.20	
9	17505.01		17491.36		17491.23				17479.00			
10	17505.62				17490.47							
11	17506.08				17489.55							
12	17506.39				17488.48							
13	17506.85											

575.1 Band $Rh^{18}O$ Observed Transition Lines $[16.0]^2\Pi_{1/2}$ 2,0

N"	$^{s}R_{11}(0)$	$^{r}Q_{11}(0)$	$^{q}P_{11}(0)$	$^{r}R_{12}(1)$	$^{q}Q_{12}(1)$	$^{p}P_{12}(1)$	$^{q}R_{13}(1)$	$^{p}Q_{13}(1)$	$^{o}P_{13}(2)$	$^{p}R_{14}(2)$	$^{o}Q_{14}(2)$	$^{n}P_{14}(3)$
0	17380.27	---	---									
1	17381.18	17379.52	---		---		---					
2	17382.08		---		17378.31		17376.95		---			
3	17382.84		17377.40		17378.01		---		---			
4	17383.75		17376.95		17377.40		17376.50		17372.12			
5	17384.35		---		---		17375.74		17370.16			
6	17385.11		17375.74		17376.19		17374.99		17368.35			
7	17386.02		17374.99				17373.93		17366.09			
8	17386.77		17374.23				---					
9			---				---					
10			17372.87				17371.52					

586.1 Band $Rh^{18}O$ Observed Transition Lines $[15.8]^2\Pi_{1/2}$ 2,0

N"	$^{s}R_{11}(0)$	$^{r}Q_{11}(0)$	$^{q}P_{11}(0)$	$^{r}R_{12}(1)$	$^{q}Q_{12}(1)$	$^{p}P_{12}(1)$	$^{q}R_{13}(1)$	$^{p}Q_{13}(1)$	$^{o}P_{13}(2)$	$^{p}R_{14}(2)$	$^{o}Q_{14}(2)$	$^{n}P_{14}(3)$
0	17064.18		---									
1	17065.51		---	17063.48			---	---				
2	17066.97		17061.76	17064.18			17060.78	---	---	---		
3	17068.43		17061.87	17064.82			17061.09	17058.41	17057.22	17057.28		---
4	17069.89		17062.02	17065.40			17061.18	17057.86	17055.91	17056.49		17052.65
5	17071.26		17062.02	17065.92			17061.18	17057.13	17054.65	17055.56		17050.39
6	17072.54		17062.02	17066.36			17061.09	17056.06	17053.21	17054.37		17048.12
7	17073.76		17062.02	17066.71			17060.97	17055.21	17051.66	17053.21		17045.71
8	17074.90		17061.76	17066.97			17060.57	17054.11	17050.07			
9	17075.98		17061.47	17067.21					17048.26			
10	17076.91		17061.18	17067.29					17046.55			
11	17077.81		17060.74	17067.29					17044.54			
12	17078.60		17060.33						17042.54			
13	17079.30								17040.48			
14	17079.97											
15	17080.59											
16	17081.02											

590.0 Band $Rh^{18}O$ Observed Transition Lines $[16.0]^2\Pi_{3/2}$ 1,0

N"	$^tR_{21}(0)$	$^sQ_{21}(0)$	$^rP_{21}(1)$	$^sR_{22}(1)$	$^rQ_{22}(1)$	$^qP_{22}(2)$	$^rR_{23}(1)$	$^qQ_{23}(2)$	$^pP_{23}(3)$	$^qR_{24}(2)$	$^pQ_{2p}(3)$	$^oP_{24}(4)$
0	16948.95	16947.11	16946.14									
1	16950.53	16948.00	16946.19	16948.64	16946.91		---					
2	16952.17	16948.95	16946.45	16949.64	16947.11	---	16945.56	---		---		
3	16953.89	16949.96	16946.83	16950.53	16947.37	16944.87	16946.14	16943.64	---	16942.46	---	
4	16955.62	16950.96	16947.11	16951.54	16947.60	16944.41	16946.45	16943.29	16940.80	16941.86	---	---
5	16957.34	16952.00	16947.46	16952.43	16947.86	16943.84	16946.77	16942.78	16939.56	16941.37	16938.13	16935.63
6	16959.04	16952.97	16947.77	16953.35	16948.00	16943.29	16946.91	16942.20	16938.44	16940.65	16936.75	16933.54
7	16960.71		16947.95	16954.21	16948.15	16942.81	16946.97	16941.57	16937.04	16939.96	16935.35	16931.42
8	16962.32		16948.15	16955.07	16948.29	16942.25	16947.03	16941.08	16935.63	16939.25	16933.85	16929.24
9	16963.93		16948.38	16955.85	16948.38	16941.69	16947.11	16940.37	16934.28	16938.44	16932.36	16927.03
10	16965.49		16948.46	16956.62	16948.46	16941.08	16947.03		16932.88	16937.67	16930.84	16924.8
11	16967.04		16948.64	16957.34	16948.46	16940.37	16946.97		16931.42	16936.75	16929.24	16922.51
12	16968.54			16958.12	16948.46	16939.56	16946.91		16929.90	16935.86	16927.66	
13	16970.01			16958.81	16948.38		16946.77		16928.35		16926.03	
14	16971.45			16959.44	16948.29		16946.60		16926.80			
15	16972.86			16960.05	16948.15		16946.45		16925.14			
16	16974.21			16960.71	16948.00		16946.14		16923.54			
17	16975.54			16961.20	16947.86				16921.85			
18					16947.60							
19					16947.37							

595.7 Band $Rh^{18}O$ Observed Transition Lines $[15.8]^2\Pi_{3/2}$ 1,0

N''	$^tR_{21}(0)$	$^sQ_{21}(0)$	$^rP_{21}(1)$	$^sR_{22}(1)$	$^rQ_{22}(1)$	$^qP_{22}(2)$	$^rR_{23}(1)$	$^qQ_{23}(2)$	$^pP_{23}(3)$	$^qR_{24}(2)$	$^pQ_{2p}(3)$	$^oP_{24}(4)$
0	16789.03	16788.61										
1	16790.19	16789.59	16786.59	16790.25	16787.20		16785.03					
2	16791.43	16790.72	16786.55	16791.43	16787.20	16786.78	16785.59	16785.25		16784.35		
3	16792.72	16791.85	16786.47	16792.47	16787.03	16786.47	16785.85	16785.25	16782.30	16784.13	16781.20	
4	16793.96	16792.95	16786.35	16793.51	16786.78	16786.27	16785.73	16785.11	16780.83	16783.79	16779.59	16779.14
5	16795.21	16794.08	16786.27	16794.50	16786.69	16785.85	16785.59	16784.66	16779.40	16783.34	16777.90	16777.34
6	16796.31	16795.15	16786.13	16795.43	16786.35	16785.42	16785.25	16784.21	16777.76	16782.75	16776.13	16775.46
7	16797.43	16795.97	16785.85	16796.31	16785.93	16784.97	16784.89	16783.79	16775.99	16782.10	16774.19	16773.43
8	16798.51	16796.87	16785.42	16797.12	16785.59	16784.35	16784.35	16783.06	16774.19	16781.40	16772.33	16771.35
9	16799.47	16797.72	16785.03	16797.89	16785.03	16783.79	16783.79	16782.41	16772.33	16780.70	16770.39	16769.24
10	16800.37	16798.51	16784.61	16798.51	16784.61	16783.06	16783.34	16781.68	16770.39	16779.87	16768.37	16767.02
11	16801.27	16799.47	16784.13	16799.24	16784.13	16782.35	16782.58	16780.92	16768.37	16778.95	16766.26	16764.77
12	16802.04		16783.51	16799.83	16783.34	16781.48			16766.26	16777.90	16764.04	16762.46
13	16802.80	16800.79	16783.06	16800.37	16782.58	16780.75			16764.12	16777.00	16761.82	16760.05
14	16803.47	16801.27	16782.30	16800.79		16779.87			16761.85	16775.91	16759.51	16757.60
15	16804.07		16781.48			16778.95			16759.51	16774.68	16757.13	16755.13
16	16804.63		16780.75			16777.90			16757.13	16773.43		16752.52
17	16805.06		16779.87						16754.71			
18	16805.54		16778.95						16752.13			
19	16805.82		16777.90									
20	16806.10		16777.00									
21	16806.36		16775.68									
22	16806.50											

599.4 Band $Rh^{18}O$ Observed Transition Lines $[16.0]^2\Pi_{1/2}$ 1,0

N"	$^{s}R_{11}(0)$	$^{r}Q_{11}(0)$	$^{q}P_{11}(0)$	$^{r}R_{12}(1)$	$^{q}Q_{12}(1)$	$^{p}P_{12}(1)$	$^{q}R_{13}(1)$	$^{p}Q_{13}(1)$	$^{o}P_{13}(2)$	$^{p}R_{14}(2)$	$^{o}Q_{14}(2)$	$^{n}P_{14}(3)$
0	16684.80	16684.85	16682.77									
1	16685.91	16685.97	16682.46	16686.66	16683.10	16683.10	16680.90	16680.90				
2	16687.05	16687.25	16682.32	16687.94	16682.90	16683.04	16681.12	16681.43	16679.32			
3	16688.33	16688.53	16682.24	16689.11	16682.77	16682.90	16681.43	16681.54	16678.06			16676.98
4	16689.50	16689.75	16682.13	16690.28	16682.46	16682.77	16681.12	16681.43	16676.62			16675.37
5	16690.73	16690.92	16681.87	16691.43	16682.24	16682.49	16681.04	16681.37	16674.98			16673.67
6	16691.90	16692.09	16681.65	16692.48	16681.87	16682.24	16680.65	16680.90	16673.22			16671.78
7	16692.93		16681.37	16693.43	16681.54	16681.87	16680.21	16680.65	16671.45			16669.92
8	16694.02		16681.04	16694.35	16681.12	16681.43	16679.90	16680.12	16669.58			16667.94
9	16695.02		16680.65	16695.47	16680.65	16680.90	16679.32	16679.54	16667.64			16665.97
10	16695.97		16680.21	16696.19	16680.21			16678.98	16665.67			16663.86
11	16696.86				16679.54			16678.30	16663.64			16661.64
12	16697.72				16678.98			16677.67	16661.53			16659.39
13	16698.45				16678.20				16659.39			16657.23
14	16699.20											16654.95
15	16699.90											16652.65
16												16650.27
17												16647.83
18												16645.36
19												16642.76

608.9 Band $Rh^{18}O$ Observed Transition Lines $[15.8]^2\Pi_{1/2}$ 1,0

N"	$^{s}R_{11}(0)$	$^{r}Q_{11}(0)$	$^{q}P_{11}(0)$	$^{r}R_{12}(1)$	$^{q}Q_{12}(1)$	$^{p}P_{12}(1)$	$^{q}R_{13}(1)$	$^{p}Q_{13}(1)$	$^{o}P_{13}(2)$	$^{p}R_{14}(2)$	$^{o}Q_{14}(2)$	$^{n}P_{14}(3)$
0	16424.92	16423.11	16422.25					16419.61				
1	16426.35	16423.84	16422.30	16424.57	16422.92	16421.98	16420.74	16419.69	16418.82	16418.91	16417.93	
2	16427.83	16424.57	16422.49	16425.35	16423.11	16421.41	16421.57	16419.61	16417.93	16418.34	16416.72	16415.75
3	16429.29	16425.34	16422.64	16426.00		16420.74	16421.98	16418.91	16416.80	16417.58	16415.46	16413.65
4	16430.78	16426.09	16422.71	16426.70		16420.17	16422.19	16418.34	16415.46	16416.72	16414.00	16411.47
5	16432.18	16426.75	16422.84	16427.24			16422.19	16417.58	16414.00	16415.75		16409.15
6	16433.48		16422.84	16427.83			16422.19	16416.40	16412.46	16414.75		16406.78
7	16434.72		16422.84	16428.18			16421.87	16415.46	16410.82	16413.65		16404.31
8	16435.93		16422.64	16428.59			16421.49	16414.43	16409.15	16412.46		16401.75
9	16437.01		16422.49					16413.25	16407.32	16411.12		16399.17
10	16438.01		16422.19						16405.44			16396.43
11	16439.01								16403.47			16393.63
12	16439.82								16401.43			
13	16440.61								16399.28			
14	16441.34								16397.04			
15	16441.99								16394.81			
16	16442.50											
17	16442.96											

618.3 Band $Rh^{18}O$ Observed Transition Lines $[16.0]^2\Pi_{3/2}$ 0,0

N"	$^tR_{21}(0)$	$^sQ_{21}(0)$	$^rP_{21}(1)$	$^sR_{22}(1)$	$^rQ_{22}(1)$	$^qP_{22}(2)$	$^rR_{23}(1)$	$^qQ_{23}(2)$	$^pP_{23}(3)$	$^qR_{24}(2)$	$^pQ_{2p}(3)$	$^oP_{24}(4)$
0	16171.78											
1	16173.27		---	16171.78	---		16167.57					
2	16174.92		---	16172.62	16170.00	---	16168.54	---		---		
3	16176.15		16169.59	16173.27	16170.11	16168.07	16168.96	16166.66	16164.86	---	16163.71	16162.71
4	16177.56		---	16174.08	16170.37	16167.40	16168.96	16166.22	16163.63	16164.86	16162.16	16160.70
5	16178.77		16169.77	16174.74	16170.11	16166.65	16168.96	---	---	16163.99	---	16158.53
6	16179.78		16169.59	16175.47	16170.00		16168.62	16164.86	---	16163.13	16159.32	16156.52
7	16180.84		---	16175.89	16169.58		16168.40	16163.99	16159.27	16162.16	16157.41	
8			16168.96	16176.88	---			16163.13		16161.17		
9			16168.59	16177.56	16168.59			16162.16				
10				16178.32	16168.07			---				
11				16179.00				16160.57				
12				16179.66								
13				16180.47								
14				16181.02								
15				16181.70								

625.5 Band $Rh^{18}O$ Observed Transition Lines $[15.8]^2\Pi_{3/2}$ 0,0

N"	$^tR_{21}(0)$	$^sQ_{21}(0)$	$^rP_{21}(1)$	$^sR_{22}(1)$	$^rQ_{22}(1)$	$^qP_{22}(2)$	$^rR_{23}(1)$	$^qQ_{23}(2)$	$^pP_{23}(3)$	$^qR_{24}(2)$	$^pQ_{2p}(3)$	$^oP_{24}(4)$
0	15954.43	---	15951.51									
1	15955.71	---	---	15953.67	---		---					
2	15957.23	15953.67	---	15954.43	15952.65	---	---	---		---	---	
3	15958.64	15954.43	15952.02	15955.07	15952.65	15949.85	---	15948.58	---	---	---	
4	15960.16	---		15955.96	15952.65	---	15951.51	15948.07	15946.17	15946.81	15945.02	
5	15961.44	15956.22		15956.47	15952.65	15948.58	15951.51	15947.31	---	15945.91	15943.37	---
6	15962.97			15957.23	15952.65	15947.82	15951.51	---	15943.37	15945.02	15941.84	15938.41
7	15964.11			15958.13		15947.06		---	15941.84	15944.00	15940.32	15935.87
8	15965.00			15958.64		15946.17		15945.02	15940.32	15943.37	15938.41	15933.72
9				15959.40				15944.26	15938.41	15942.23	15936.76	
10				15960.16				15943.37	15936.76	15941.34	15934.86	
11				15960.80				15942.48	15934.86	15940.32		
12				15961.69				15941.59	15932.60			
13								15940.83				
14								15939.94				

629.7 Band $Rh^{18}O$ Observed Transition Lines $[16.0]^2\Pi_{1/2}$ 0,0

N"	$^{s}R_{11}(0)$	$^{r}Q_{11}(0)$	$^{q}P_{11}(0)$	$^{r}R_{12}(1)$	$^{q}Q_{12}(1)$	$^{p}P_{12}(1)$	$^{q}R_{13}(1)$	$^{p}Q_{13}(1)$	$^{o}P_{13}(2)$	$^{p}R_{14}(2)$	$^{o}Q_{14}(2)$	$^{n}P_{14}(3)$
0	15881.59	15879.72	15878.91									
1	15883.05	15880.43	15879.01	15881.13	15879.59	15878.49	15877.35	---				
2	15884.64	15881.36	15879.24	15881.99	15879.80	15877.96	15878.16	---	15875.46	15875.46	15874.50	
3	15886.28	15882.22	15879.47	15882.80	15880.07	15877.35	15878.76	15876.12	15874.50	15874.88	15873.34	15872.34
4	15887.90	15883.05	15879.72	15883.63	15880.20	15876.80	15879.12	15875.61	15873.52	15874.28	15872.16	15870.23
5	15889.46	15883.88	15879.87	15884.36	15880.20	15876.12	15879.24	15875.03	15872.34	15873.52	15870.72	15868.08
6	15891.03	15884.64	15880.07		15880.33	15875.46	15879.12	15874.28	15870.85	15872.61	15869.24	15865.91
7	15892.52	15885.40	15880.20		15880.33	15874.70	15879.01	15873.52	15869.49	15871.58	15867.63	15863.52
8	15893.96	15886.13			15880.20	15873.92	15878.91	15872.61	15868.03			15861.13
9	15895.32	15886.71			15880.07	15873.07	15878.76	15871.58	15866.37			
10	15896.66	15887.34			15879.97	15872.16						
11	15897.92	15887.90				15871.23						
12	15899.09	15888.43				15870.24						
13	15900.27					15869.24						
14	15901.31					15868.08						
15	15902.40					15866.95						
16	15903.36											
17	15904.29											
18	15905.10											
19	15905.86											

638.2 Band $Rh^{18}O$ Observed Transition Lines $[15.8]^2\Pi_{1/2}$ 0,0

N"	$^{s}R_{11}(0)$	$^{r}Q_{11}(0)$	$^{q}P_{11}(0)$	$^{r}R_{12}(1)$	$^{q}Q_{12}(1)$	$^{p}P_{12}(1)$	$^{q}R_{13}(1)$	$^{p}Q_{13}(1)$	$^{o}P_{13}(2)$	$^{p}R_{14}(2)$	$^{o}Q_{14}(2)$	$^{n}P_{14}(3)$
0	15676.32	15676.56	---									
1	15677.42	15677.79	15674.23	15678.28	15674.84	---	15672.51	15672.75				
2	15678.53	15679.03	15673.98	15679.76	15674.60	15674.84	15673.00	15673.37	15671.03	15672.26	---	
3	15679.76	15680.37	15673.61	15680.74	15674.23	15674.60	15673.00	15673.37	15669.81	15672.02	15668.46	15668.70
4	15680.74	15681.6	15673.37	15682.09	15673.98	15674.60	15672.88	15673.37	15668.09	15672.02	15666.74	15667.11
5	15681.85	15682.71	15673.37	15683.08	15673.61	15674.23	15672.51	15673.00	15666.49	15671.52	15665.14	15665.39
6	15682.71	15683.81	15672.75	15684.31	15673.00	15673.98	15672.02	15672.88	15664.72			15663.55
7	15683.81	15684.92	15672.51		15672.75	15673.37	15671.52	15672.26	15662.81			15661.58
8	15684.68		15672.02		15672.02	15673.00		15672.02	15660.73			15659.75
9	15685.41		15671.52		15671.52				15658.76			15657.54
10									15656.68			15655.70

Appendix VI

$Rh^{16}O$ / $Rh^{18}O$

Excited State Term Values /cm^{-1}

Averaged Term Values for $Rh^{16}O$

J	638.2 (e)	638.2 (f)	629.7(e)	629.7(f)	625.5(e)	625.5(f)	618.3(e)	618.3(f)
0.5	15666.78	15667.69	15874.42	15874.35				
1.5	15667.46	15669.25	15875.62	15875.43	15977.35	15977.35	16168.92	16168.92
2.5	15668.90	15671.57	15877.58	15877.27	15979.18	15979.18	16170.83	16170.84
3.5	15671.10	15674.66	15880.30	15879.90	15981.76	15981.75	16173.49	16173.54
4.5	15674.05	15678.49	15883.82	15883.32	15985.06	15985.08	16176.91	16177.00
5.5	15677.75	15683.09	15888.04	15887.44	15989.10	15989.10	16181.08	16181.25
6.5	15682.21	15688.43	15893.08	15892.39	15993.87	15993.85	16185.99	16186.25
7.5	15687.43	15694.52	15898.86	15898.11	15999.39	15999.38	16191.65	16192.05
8.5	15693.40	15701.37	15905.39	15904.54	16005.63	16005.62	16198.05	16198.62
9.5	15700.13	15708.98	15912.67	15911.71	16012.61	16012.62	16205.17	16205.97
10.5	15707.61	15717.35	15920.76	15919.73	16020.31	16020.31	16213.07	16214.08
11.5	15715.86	15726.42	15929.62	15928.49	16028.75	16028.75	16221.63	16222.98
12.5	15724.89	15736.28	15939.22	15937.99	16037.92	16037.92	16230.96	16232.64
13.5	15734.62	15746.88	15949.57	15948.31	16047.86	16047.82	16241.01	16243.06
14.5	15745.15	15758.24	15960.75	15959.32	16058.50	16058.48	16251.83	16254.25
15.5	15756.39	15770.27	15972.64	15971.24	16069.88	16069.81	16263.40	16266.24
16.5	15768.39	15783.14	15985.31	15983.84	16081.94	16081.93	16275.67	16279.00
17.5	15781.19	15796.75	15998.79	15997.14	16094.80	16094.84	16288.68	16292.48
18.5	15794.62	15811.07	16012.92	16011.26	16108.39	16108.39	16302.49	16306.83
19.5	15808.99	15826.18	16027.87	16026.17	16122.60	16122.87	16316.99	16321.91
20.5	15824.00	15842.03	16043.54	16041.82	16137.71	16137.71	16332.24	16337.73
21.5	15839.77	15858.53	16060.05	16058.26	16153.49	16153.60	16348.24	16354.40
22.5	15856.34	15875.84	16077.18	16075.45	16169.98	16170.08	16365.00	16371.74
23.5	15873.65	15893.92	16095.17	16093.44		16187.27	16382.56	16389.86
24.5	15891.67		16113.94	16112.15		16205.21	16400.78	16408.83
25.5	15910.54		16133.44	16131.66			16419.78	16428.56
26.5			16153.67	16151.89			16439.51	16448.99
27.5			16174.74	16172.97			16459.90	16470.19
28.5			16196.54	16194.79			16480.96	16492.18
29.5			16219.20	16217.38			16502.87	16514.92
30.5			16242.41	16240.72			16525.54	16538.52
31.5			16266.54	16264.84			16548.95	16562.77
32.5			16291.37	16289.72			16573.02	
33.5			16316.91	16315.41			16597.88	
34.5			16343.36	16341.81			16623.53	
35.5			16370.47	16369.00			16649.95	
36.5			16398.37	16396.97			16676.90	
37.5			16427.07	16425.68			16704.70	
38.5			16456.50	16455.19			16733.40	
39.5			16486.59	16485.46				
40.5			16517.51	16516.50				
41.5			16549.19	16548.30				
42.5			16581.66	16580.87				
43.5			16614.82	16614.19				
44.5			16648.77	16648.32				
45.5			16683.50	16683.18				

Averaged Term Values for $Rh^{16}O$
continued...

J	638.2 (e)	638.2 (f)	629.7(e)	629.7(f)	625.5(e)	625.5(f)	618.3(e)	618.3(f)
46.5			16718.95	16718.81				
47.5			16755.20	16755.21				
48.5			16792.19	16792.36				
49.5			16829.92	16830.29				
50.5			16868.40	16868.95				
51.5			16907.64	16908.44				
52.5			16947.65	16948.62				
53.5			16988.42	16989.43				
54.5			17029.87					
55.5			17072.14					
56.5			17115.13					

J	607.9(e)	607.9(f)	598.1(e)	598.1(f)	594.3(e)	594.3(f)	588.7(e)	588.7(f)
0.5	16445.78		16715.09					
1.5	16446.88	16446.79	16715.86		16820.62	16821.94	16979.33	16979.32
2.5	16448.75	16448.61	16717.35	16719.78	16822.06	16824.14	16981.33	16981.29
3.5	16451.36	16451.14	16719.70	16722.86	16824.40	16827.21	16984.09	16984.03
4.5	16454.72	16454.44	16722.73	16726.70	16827.45	16830.96	16987.62	16987.62
5.5	16458.76	16458.48	16726.55	16731.35	16831.36	16835.48	16992.00	16991.97
6.5	16463.59	16463.24	16731.14	16736.72	16835.89	16840.77	16997.13	16997.10
7.5	16469.14	16468.71	16736.51	16742.88	16841.23	16846.80	17003.04	17003.02
8.5	16475.43	16474.95	16742.65	16749.83	16847.34	16853.61	17009.73	17009.71
9.5	16482.43	16481.94	16749.57	16757.53	16854.19	16861.16	17017.22	17017.20
10.5	16490.23	16489.64	16757.27	16765.99	16861.83	16869.49	17025.50	17025.46
11.5	16498.71	16498.09	16765.72	16775.20	16870.16	16878.77	17034.56	17034.53
12.5	16507.92	16507.28	16774.92	16785.18	16879.28	16888.44	17044.38	17044.29
13.5	16517.89	16517.17	16784.89	16795.95	16889.10	16899.04	17054.95	17054.81
14.5	16528.62	16527.86	16795.65	16807.52	16899.74	16910.38	17066.28	17065.81
15.5	16540.03	16539.24	16807.21	16819.81	16911.14	16922.58	17078.11	17080.17
16.5	16552.18	16551.33	16819.42		16923.26	16935.45	17090.27	17093.17
17.5	16565.15	16564.18			16936.32	16949.08	17104.93	17106.92
18.5	16578.83	16577.77			16949.86	16963.59	17118.52	17121.43
19.5	16593.22	16592.27			16964.28	16978.75	17133.52	17136.84
20.5	16608.27				16979.48	16994.74	17149.59	17152.94
21.5	16624.18				16995.47		17166.55	17169.89
22.5	16640.80				17012.22		17184.26	17187.69
23.5	16658.11				17029.59		17202.86	17206.20
24.5					17047.80		17222.26	17225.82
25.5							17242.46	17245.98
26.5							17263.44	
27.5							17285.19	
28.5							17307.77	
29.5							17331.15	

Averaged Term Values for $Rh^{16}O$

J	584.1(e)	584.1(f)	573.5(e)	573.5(f)	569.3(e)	569.3(f)	561.9(e)	561.9(f)
0.5			17434.84	17432.79				
1.5		17117.96	17435.54	17434.25	17561.22	17563.40		17786.67
2.5	17120.38	17119.95	17436.99	17436.31	17562.58	17565.87	17788.64	17788.62
3.5	17123.04	17122.44	17439.16	17438.96	17564.74	17569.05	17791.41	17791.35
4.5	17126.40	17125.71	17442.04	17442.33	17567.62	17573.09	17795.08	17794.90
5.5	17130.55	17129.69	17445.69	17446.49	17571.23	17577.81	17799.29	17799.21
6.5	17135.42	17134.43	17450.03	17451.30	17575.65	17583.45	17804.33	17804.21
7.5	17141.02	17139.89	17455.18	17456.92	17580.78	17589.80	17810.21	17810.18
8.5	17147.30	17146.12	17460.98	17463.26	17586.72	17596.89	17816.87	17816.81
9.5	17154.42	17153.10	17467.59	17470.33	17593.37	17604.84	17824.30	17824.26
10.5	17162.20	17160.77	17475.03	17478.15	17600.72	17613.51	17832.54	17832.46
11.5	17170.72	17169.10	17483.22	17486.81	17608.85	17622.98	17841.54	17841.48
12.5	17179.99	17178.26	17492.18	17496.05	17617.78	17633.21	17851.29	17851.31
13.5	17189.99	17188.17	17501.96	17506.13	17627.39	17644.11	17861.86	17861.82
14.5	17200.74	17198.85	17512.42	17516.97	17637.81	17656.03	17873.19	17873.22
15.5	17212.17	17210.19	17523.67	17528.47	17648.90	17668.51	17885.27	17885.26
16.5	17224.34	17222.39	17535.63		17660.76	17682.02	17898.19	17898.19
17.5	17237.30	17235.32	17548.29			17696.07	17911.80	17911.83
18.5	17250.98	17248.89	17561.73			17710.98	17926.25	17926.25
19.5	17265.41	17263.16	17575.80			17726.67	17941.43	17941.47
20.5	17280.51	17278.23	17590.57			17743.10	17957.40	17957.49
21.5	17296.48		17606.10			17760.31	17974.13	17974.07
22.5	17313.08		17622.30			17778.27	17991.66	17991.51
23.5							18010.00	

Averaged Term Values for $Rh^{16}O$
continued...

J	553.3(e)	553.3(f)	546.1(e)	546.1(f)	544.6(e)	544.6(f)
0.5	18061.27	18061.92	18268.96	18268.38		
1.5	18061.85	18063.25	18269.87	18269.64	18358.03	18358.76
2.5	18063.22	18065.25	18271.72	18271.62	18359.57	18360.83
3.5	18065.28	18067.95	18274.11	18274.41	18361.91	18363.59
4.5	18067.96	18071.39	18277.18	18278.09	18364.82	18366.98
5.5	18071.42	18075.54	18281.01	18282.55	18368.57	18371.07
6.5	18075.56	18080.47	18285.51	18287.76	18373.00	18375.85
7.5	18080.48	18086.06	18290.75	18293.77	18378.04	18381.40
8.5	18086.08	18092.37	18296.82	18300.56	18383.89	18387.53
9.5	18092.45	18099.52	18303.42	18308.01	18390.39	18394.46
10.5	18099.53	18107.34	18310.97	18316.28	18397.64	18402.09
11.5	18107.36	18115.94	18319.14	18325.29	18405.51	18410.44
12.5	18115.98	18125.27	18328.02	18334.91	18414.16	18419.42
13.5	18125.29	18135.36	18337.50	18345.41		
14.5	18135.34	18146.13	18348.05	18356.62		
15.5	18146.15	18157.65	18359.04	18368.52		
16.5	18157.68	18169.91	18370.86	18381.06		
17.5	18169.99	18182.92	18383.40	18394.28		
18.5	18182.98	18196.61	18396.61	18408.41		
19.5	18196.67	18211.16	18410.61			
20.5	18210.98	18226.34				
21.5	18226.44	18242.15				
22.5	18242.36					
23.5	18258.88					

Averaged Term Values for $Rh^{18}O$

J	638.2 (e)	638.2 (f)	629.7(e)	629.7(f)	625.5(e)	625.5(f)	618.3(e)	618.3(f)
0.5	15674.01	15674.84	15878.43	15878.40				
1.5	15674.67	15676.21	15879.46	15879.33			16169.78	16169.85
2.5	15675.93	15678.23	15881.21	15880.99	15954.00	15953.49	16171.39	16171.60
3.5	15677.91	15681.12	15883.66	15883.38	15956.25	15955.81	16173.77	16174.00
4.5	15680.54	15684.43	15886.74	15886.40	15959.25	15958.73	16176.85	16176.91
5.5	15683.93	15688.69	15890.50	15890.11	15962.94	15962.53	16180.32	16180.67
6.5	15687.78	15693.32	15894.97	15894.51	15967.32	15966.87	16184.54	16185.01
7.5	15692.56	15698.96	15900.09	15899.59	15972.25	15972.05	16189.39	16190.11
8.5	15697.82		15905.91	15905.33	15978.04	15977.98	16194.67	16195.76
9.5	15703.91		15912.43	15911.86	15984.29	15984.54	16200.82	16202.55
10.5	15710.55		15919.68	15918.99	15991.00	15991.89	16207.72	16209.87
11.5	15717.82		15927.58	15926.86		16000.01		16217.97
12.5			15936.18	15935.41		16008.88		16226.75
13.5			15945.43	15944.68		16018.55		16236.25
14.5			15955.34					16246.64
15.5			15965.99					16257.51
16.5			15977.24					16269.24
17.5			15989.28					
18.5			16001.93					
19.5			16015.30					
20.5			16029.28					
21.5			16043.95					

J	608.9(e)	608.9(f)	599.4(e)	599.4(f)	595.7(e)	595.7(f)	590.0(e)	590.0(f)
0.5	16421.79	16421.80	16682.32		16786.34	16786.91		
1.5	16422.82	16422.72	16682.99	16684.44	16787.13	16788.16	16946.75	
2.5	16424.53	16424.41	16684.29	16686.51	16788.58	16790.12	16948.52	16948.51
3.5	16426.89	16426.69	16686.38	16689.27	16790.71	16792.82	16951.02	16951.00
4.5	16429.89	16429.65	16689.02	16692.73	16793.46	16796.10	16954.21	16954.18
5.5	16433.58	16433.30	16692.47	16696.81	16796.94	16800.08	16958.13	16958.07
6.5	16437.98	16437.55	16696.52	16701.64	16801.08	16804.79	16962.72	16962.70
7.5	16443.00	16442.57	16701.30	16707.09	16805.90	16810.11	16968.03	16968.06
8.5	16448.65	16448.20	16706.80	16713.20	16811.37	16816.14	16974.07	16974.10
9.5	16455.05	16454.50	16712.93	16720.03	16817.52	16822.85	16980.82	16980.90
10.5	16462.08		16719.77	16727.65	16824.41	16830.24	16988.25	16988.31
11.5	16469.70		16727.28	16735.86	16831.95	16838.28	16996.41	16996.44
12.5	16478.04		16735.53	16744.83	16840.12	16847.15	17005.27	17005.31
13.5	16487.07		16744.37	16754.46	16849.02	16856.56	17014.82	17014.96
14.5	16496.76		16753.95	16764.77	16858.54	16866.72	17025.11	17025.26
15.5	16507.07		16764.15	16775.79	16868.76	16877.47	17036.10	17036.25

Averaged Term Values for $Rh^{18}O$
continued...

J	608.9(e)	608.9(f)	599.4(e)	599.4(f)	595.7(e)	595.7(f)	590.0(e)	590.0(f)
16.5	16518.10		16775.11	16787.42	16879.66		17047.76	17047.96
17.5	16529.81		16786.76		16891.31		17060.19	17060.46
18.5	16542.11				16903.59		17073.26	17073.53
19.5					16916.48		17087.09	
20.5					16930.22			
21.5					16944.39			
22.5					16959.37			
23.5					16975.05			
24.5					16991.36			

J	586.1(e)	586.1(f)	575.1(e)	575.1(f)	571.6(e)	571.6(f)	564.3(e)	564.3(f)
0.5								
1.5	17062.11	17061.77					17713.17	
2.5	17063.72	17063.33	17379.83	17380.03	17496.18	17497.09	17714.95	17714.47
3.5	17065.99	17065.57	17381.62		17498.34	17499.53	17717.44	17716.78
4.5	17068.95	17068.45	17384.11		17500.74	17502.33	17720.70	17719.79
5.5	17072.56	17071.85	17387.09		17504.17	17506.10	17724.45	17723.53
6.5	17076.87	17076.06	17390.83		17508.08	17510.25	17728.90	17728.15
7.5	17081.83	17080.93	17395.03		17512.63		17734.07	17733.35
8.5	17087.40	17086.39	17400.13		17518.05		17739.98	17739.23
9.5	17093.58	17092.50	17406.11		17523.67		17746.57	17745.94
10.5	17100.48	17099.33	17412.64		17530.27		17753.90	17753.22
11.5	17108.03	17106.73			17537.45		17761.53	
12.5	17116.23	17114.79			17545.29		17770.09	17770.04
13.5	17125.05				17553.79		17779.16	
14.5	17134.53				17562.86		17789.10	
15.5	17144.65				17572.82			
16.5	17155.47							
17.5	17166.98							
18.5	17179.04							

Appendix VII

$Rh^{16}O$

Hyperfine Transition Lines /cm^{-1}

Band System
nm /cm^{-1} (υ',υ") **Page**

607.9 nm Band RhO Observed Transition Lines $[16.0]^2\Pi_{3/2}$ **1,0**

	$^sR_{11}(0)$		$^rQ_{11}(0)$		$^qP_{11}(0)$		$^rR_{12}(1)$		$^qQ_{12}(1)$		$^pP_{22}(1)$	
N"	upper	lower	upper	lower	upper	lower	upper	lower	upper	lower	upper	lower
0	16449.1715	16449.1562	16447.2023	16447.1881	16446.1663	16446.1534	---	---	---	---		
1	16450.7525	16450.7397	16447.9965	16447.9831	16446.2736	16446.2605	16448.6665	16448.6557	16446.9501		---	---
2	16452.4181	16452.4054	16448.8761	16448.8635	16446.4648	16446.4518	16449.5314	16449.5230			---	---
3	16454.0714	16454.0589	16449.7382	16449.7259	16446.6475	16446.6342	16450.3372				---	---
4	16455.6750	16455.6666	16450.5541	16450.5425	16446.7727	16446.7600	16451.0757	16451.0708			---	---
5	16457.2130	16457.1994	16451.3046	16451.2933	16446.8322	16446.8207	16451.7357				16442.9398	16442.9332
6	16458.6715	16458.6578	16451.9755	16451.9662	16446.8140	16446.8023	16452.3145				16442.0420	16442.0345
7	16460.0463	16460.0344	16452.5629	16452.5470	16446.7148	16446.7032	16452.8064					
8	16461.3413	16461.3313	16453.0607	16453.0500	16446.5340	16446.5225	16453.2152					
9			16453.4740	16453.4630	16446.2736	16446.2605	16453.5420	16453.5350				
10			16453.8052	16453.7953	16445.9151	16445.9061	16453.7707	16453.7599				

	$^qR_{13}(1)$		$^pQ_{13}(1)$		$^oP_{13}(2)$		$^pR_{14}(2)$		$^oQ_{14}(2)$		$^nP_{14}(3)$	
N"	upper	lower	upper	lower	upper	lower	upper	lower	upper	lower	upper	lower
0												
1	16444.6703		16443.4871									
2	16445.5660		16443.5951		16442.5658		16442.7079	16442.7024				
3	16445.9993		16443.2430		16441.5219		16442.0503	16442.0420			16439.1462	16439.1399
4	16446.1663		16442.6211		16440.2117		16441.2368	16441.2290			16436.8772	16436.8677
5	16446.1663		16441.8365		16438.7399		16440.3030	16440.2927			16434.4478	16434.4397
6	16446.0427		16440.9230		16437.1401		16439.2607	16439.2514				
7	16445.8122				16435.4334		16438.1107	16438.0999				
8	16445.4780				16433.6269		16436.8772	16436.8677				
9	16445.0418						16435.5452	16435.5356				

618.0 nm Band RhO Observed Transition Lines $[16.0]^2\Pi_{1/2}$ 1,1

	$^{s}R_{11}(0)$		$^{r}Q_{11}(0)$		$^{q}P_{11}(0)$		$^{r}R_{12}(1)$		$^{q}Q_{12}(1)$		$^{p}P_{22}(1)$	
N"	upper	lower	upper	lower	upper	lower	upper	lower	upper	lower	upper	lower
0	16179.4497	16179.4380	16179.0666	---	16176.9413	16176.9297	---	---				
1	16180.8629	16180.8519	16180.3214	16180.3083	16176.7709	16176.7593	---	---	16177.4466	16177.4396	---	---
2	16182.4231	16182.4121	16181.6906	16181.6777	16176.7450	16176.7320			16177.4019		16177.0260	16177.0172
3	16184.0349	16184.0229	16183.0953	16183.0833	16176.7593	16176.7450			16177.3553		16176.8106	16176.8009
4	16185.6622	16185.6528	16184.4867	16184.4747	16176.7811	16176.7709			16177.2952		16176.5649	
5	16187.2958	16187.2833	16185.8446	16185.8337	16176.7939	16176.7811			16177.2267		16176.2887	
6	16188.9158	16188.9053	16187.1740	16187.1586	16176.8009	16176.7939					16175.9630	
7			16188.4404	16188.4309	16176.8106	16176.7939						
8					16176.7811	16176.7709						

	$^{q}R_{13}(1)$		$^{p}Q_{13}(1)$		$^{o}P_{13}(2)$		$^{p}R_{14}(2)$		$^{o}Q_{14}(2)$		$^{n}P_{14}(3)$	
N"	upper	lower	upper	lower	upper	lower	upper	lower	upper	lower	upper	lower
0												
1	16175.1576		16174.9358									
2	16175.8430		16175.4652		16173.3366		16174.5805	16174.5726	16172.4394			
3	16176.1120		16175.5641		16172.0175		16174.3717	16174.3646	16170.8318	16170.8193	16170.6078	16170.5978
4	16176.1729		16175.4378		16170.4926		16174.0614	16174.0531	16169.0974		16168.7255	16168.7164
5	16176.1304		16175.1909		16168.8504		16173.6590	16173.6511	16167.3114		16166.7730	16166.7637
6	16176.0296		16174.8511		16167.1465		16173.1883	16173.1797	---	---	16164.7505	16164.7411
7	16175.8885				16165.3938		16172.6684	16172.6617	16163.6141		16162.6648	16162.6593
8	16175.7234				16163.6141						16160.5261	16160.5173
9	16175.5373				16161.7971							
10	16175.3386											
11	16175.1292											
12	16174.9047											
13	16174.6565											

618.3 nm Band RhO Observed Transition Lines

$[16.0]^2\Pi_{3/2}$ 0,0

N"	$^tR_{21}(0)$ upper	$^tR_{21}(0)$ lower	$^sQ_{21}(0)$ upper	$^sQ_{21}(0)$ lower	$^rP_{21}(0)$ upper	$^rP_{21}(0)$ lower	$^sR_{22}(1)$ upper	$^sR_{22}(1)$ lower	$^rQ_{22}(1)$ upper	$^rQ_{22}(1)$ lower	$^qP_{22}(2)$ upper	$^qP_{22}(2)$ lower
0	16171.2406	16171.2293	16169.3383	16169.3270	---	---	16170.9039	16170.8951	---	---		
1	16172.8832	16172.8701	16170.2304	16170.2196	16168.3065	16168.2981	16171.9086	16171.9020	16168.9806		---	---
2	16174.6223	16174.6114	16171.2507	16171.2406	16168.5367	16168.5265	16172.8879	16172.8832	16169.1995		16167.2887	
3	16176.3648	16176.3541	16172.2923	16172.2800	16168.7703	16168.7601	16173.8352	16173.8309	16169.3683		16166.7208	
4	16178.0614	16178.0505	16173.3135	16173.3021	16168.9806	16168.9702	16174.7333		16169.4912		16166.1192	
5	16179.6951	16179.6839	16174.3074	16174.2961	16169.1229	16169.1134	16175.5979		16169.5522		16165.4805	
6	16181.2525	16181.2428	16175.2599	16175.2504	16169.1918	16169.1859	16176.4129	16176.4104	16169.5387		16164.7925	
7	16182.7200	16182.7101	16176.1729	16176.1574	16169.1995	16169.1918	16177.1800		16169.4451		16164.0574	
8	16184.1137	16184.1016	16177.0260	16177.0172	16169.1229	16169.1134	16177.8980		16169.2712		16163.2741	
9	16185.4104	16185.4002			16168.9418	16168.9365	16178.5620				16162.4429	
10	16186.6139	16186.6050					16179.1811				16161.5602	
11	16187.7326	16187.7235					16179.7440				16160.6342	
12											16159.6548	
13											16158.6198	

N"	$^rR_{23}(1)$ upper	$^rR_{23}(1)$ lower	$^qQ_{23}(2)$ upper	$^qQ_{23}(2)$ lower	$^pP_{23}(3)$ upper	$^pP_{23}(3)$ lower	$^qR_{24}(2)$ upper	$^qR_{24}(2)$ lower	$^pQ_{24}(3)$ upper	$^pQ_{24}(3)$ lower	$^oP_{24}(4)$ upper	$^oP_{24}(4)$ lower
0												
1	16166.6997											
2	16167.6392		16165.7319									
3	16168.1238		16165.4805		16163.5516		---	---	16162.3627	16162.3510		
4	16168.3727		16165.0061		16162.2810		16163.6141	16163.6079	16160.9028	16160.8915	16159.0032	16158.9903
5	16168.4635		16164.3859		16160.8658		16162.8529	16162.8419			16156.6895	16156.6796
6	16168.4348		16163.6868		16159.3467		16162.0164	16162.0063			16154.3102	16154.2982
7	16168.3065		16162.9067		16157.7295		16161.1176	16161.1095			16151.8663	16151.8551
8	16168.0575		16162.0683		16156.0142		16160.1677	16160.1556				
9	16167.7331		16161.1698		16154.2051							
10	16167.3114		16160.2160		16152.3134							
11					16150.3140							

625.5 nm Band RhO Observed Transition Lines $[15.8]^2\Pi_{3/2}$ **0,0**

	$^tR_{21}(0)$		$^sQ_{21}(0)$		$^rP_{21}(0)$		$^sR_{22}(1)$		$^rQ_{22}(1)$		$^qP_{22}(2)$	
N"	upper	lower	upper	lower	upper	lower	upper	lower	upper	lower	upper	lower
0	15979.6065	15979.5939	15977.7628	15977.7502			---	---	---	---		
1	15981.1557	15981.1442	15978.5773	15978.5656	15976.7355	15976.7251	15979.2517	15979.2417	15977.4104	15977.4009	---	---
2	15982.7938	15982.7826	15979.4788	15979.4680	15976.8993	15976.8884	15980.1347	15980.1284	15977.5587	15977.5521	15975.7158	15975.7108
3	15984.4178	15984.4070			15977.0494	15977.0389	15980.9627	15980.9576	15977.6523	15977.6466	15975.0688	15975.0643
4	15985.9890	15985.9777			15977.1481	15977.1370	15981.7206	15981.7165	15977.6769	15977.6713	15974.3517	
5	15987.4901	15987.4790			15977.1767	15977.1649	15982.3944		15977.6101	15977.6062	15973.5531	
6	15988.9127	15988.9013			15977.1269	15977.1148	15982.9928		15977.4647		15972.6745	
7	15990.2529	15990.2412			15976.9954	15976.9846	15983.4990		15977.2395		15971.7153	
8	15991.5038	15991.4930			15976.7753	15976.7638	15983.9221	15983.9183	15976.9373		15970.6665	
9	15992.6734	15992.6619			15976.4871	15976.4676	15984.2585	15984.2565	15976.5131		15969.5257	
10	15993.7504	15993.7408			15976.0775	15976.0690	15984.4983		15976.0140		15968.3042	
11					15975.6023	15975.5905	15984.6517				15966.9889	
12							15984.7004				15965.5887	
13							15984.7172					

	$^rR_{23}(1)$		$^qQ_{23}(2)$		$^pP_{23}(3)$		$^qR_{24}(2)$		$^pQ_{24}(3)$		$^oP_{24}(4)$	
N"	upper	lower	upper	lower	upper	lower	upper	lower	upper	lower	upper	lower
0											upper	lower
1	15975.1329											
2	15976.0085		15974.1594		15973.2272		15973.2673					
3	15976.4313		15973.8262		15971.9911		15972.6274		15970.7941	15970.7859		
4	15976.5424		15973.2272		15970.6486		15971.8427		15969.2675	15969.2584		
5	15976.5231		15972.4617		15969.1669				15967.6151	15967.6060	15967.4243	15967.4142
6	15976.3559		15971.5669		15967.5183				15965.8515	15965.8422	15965.0328	15965.0224
7	15976.0885		15970.5637		15965.7774				15963.9892	15963.9806	15962.5323	15962.5250
8	15975.7204		15969.4571		15963.9386							
9	15975.2569		15968.2557		15962.0012							
10	15974.6924		15966.9491									
11	15974.0367		15965.5666									
12	15973.2673											

629.7 nm Band RhO Observed Transition Lines $[16.0]^2\Pi_{1/2}$ **0,0**

	$^{s}R_{11}(0)$		$^{r}Q_{11}(0)$		$^{q}P_{11}(0)$		$^{r}R_{12}(1)$		$^{q}Q_{12}(1)$		$^{p}P_{22}(1)$	
N"	upper	lower	upper	lower	upper	lower	upper	lower	upper	lower	upper	lower
0	15877.9941	15877.9780	15875.8271	15875.8164	15874.8301	15874.8185			---	---		
1	15879.6850	15879.6706	15876.6701	15876.6584	15875.0030	15874.9887	15877.3381		15875.6707	15875.6639	---	---
2	15881.5037	15881.4908	15877.6202	15877.6105	15875.2888	15875.2741	15878.2772	15878.2718	15875.9421	15875.9345	---	---
3	15883.3385	15883.3254	15878.5851	15878.5757	15875.5849	15875.5719	15879.1825		15876.1829	15876.1753	15873.1574	
4	15885.1352	15885.1222	15879.5304	15879.5208	15875.8580	15875.8445	15880.0479		15876.3789	15876.3738	15872.4934	
5	15886.9001	15886.8871	15880.4359	15880.4252	15876.0916	15876.0780	15880.8679		15876.5246	15876.5208	15871.7754	
6	15888.6091	15888.5946			15876.2782	15876.2645	15881.6352		15876.6302	15876.6204	15871.0090	
7					15876.4036	15876.3918					15870.1867	
8											15869.3128	

	$^{q}R_{13}(1)$		$^{p}Q_{13}(1)$		$^{o}P_{13}(2)$		$^{p}R_{14}(2)$		$^{o}Q_{14}(2)$		$^{n}P_{14}(3)$	
N"	upper	lower	upper	lower	upper	lower	upper	lower	upper	lower	upper	lower
0												
1	15873.3946		15872.1009									
2	15874.3851		15872.2264		15871.2264		15871.3367		15870.3309	15870.3188		
3	15874.9382				15870.2459		15870.7235	15870.7142	15869.0554	15869.0483	15867.7767	15867.7642
4	15875.2540				15869.0320		15869.9864	15869.9740	15867.6542	15867.6447	15865.4891	15865.4776
5	15875.4279				15867.6780		15869.1491	15869.1376	15866.1340		15863.1230	15863.1110
6	15875.5045				15866.2256		15868.2375	15868.2252			15860.6729	15860.6689
7	15875.5045				15864.6926		15867.2545	15867.2420				
8	15875.4279				15863.0841		15866.1979	15866.1892				
9					15861.4086		15865.0830	15865.0717				

638.2 nm Band RhO Observed Transition Lines $[15.8]^2\Pi_{1/2}$ **0,0**

	$^sR_{11}(0)$		$^rQ_{11}(0)$		$^qP_{11}(0)$		$^rR_{12}(1)$		$^qQ_{12}(1)$		$^pP_{22}(1)$	
N"	upper	lower	upper	lower	upper	lower	upper	lower	upper	lower	upper	lower
0	15669.3186	15669.3066	15669.6625	15669.6474	15667.1829	---	---	---	---	---		
1	15670.4834	15670.4731	15670.9696	15670.9543	15666.8412	15666.8305	15671.6441	15671.6302	15667.5140	15667.5035	---	---
2	15671.7615	15671.7515	15672.3826	15672.3666	15666.6091	15666.5989	15673.0458	15673.0367	15667.2593	15667.2501	15667.6152	15667.6045
3	15673.0458	15673.0367				15666.3690	15674.3981	15674.3887	15666.9876	15666.9791	15667.4609	15667.4515
4	15674.3019	15674.2920				15666.1055	15675.7013	15675.6919	15666.6389		15667.2593	15667.2501
5	15675.5003	15675.4911				15665.7950	15676.9446	15676.9364	15666.2362		15666.9957	15666.9876
6	15676.6476	15676.6383				15665.4363	15678.1232	15678.1153	15665.7761		15666.6665	15666.6590
7	15677.7289	15677.7200				15665.0032	15679.2334	15679.2252	15665.2556		15666.2652	15666.2573
8	15678.7480	15678.7391				15664.5008	15680.2759	15680.2673	15664.6684		15665.8033	15665.7950
9	15679.7032	15679.6939				15663.9456	15681.2412	15681.2339	15664.0061		15665.2653	15665.2556
10	15680.5883	15680.5813				15663.3171	---	---	15663.2838		---	---
11	15681.4068	15681.3981				15662.6240	15682.9631	15682.9563			15663.9740	15663.9677
12	15682.1605	15682.1516					15683.7112	15683.7062			15663.2250	15663.2185
13	15682.8421	15682.8339					15684.3871	15684.3814				
14	15683.4596	15683.4509										
15	15684.0020											

	$^qR_{13}(1)$		$^pQ_{13}(1)$		$^oP_{13}(2)$		$^pR_{14}(2)$		$^oQ_{14}(2)$		$^nP_{14}(3)$	
N"	upper	lower	upper	lower	upper	lower	upper	lower	upper	lower	upper	lower
0												
1	15665.2399		15665.4462									
2	15665.7062		15666.0496		15663.5795		15665.1621	15665.1498	15662.6840	15662.6742		
3	15665.7307		15666.2134		15662.0902		15665.0165	15665.0032	15660.8948	15660.8861	15661.1070	15661.1012
4	15665.5103		15666.1264		15660.3544		15664.7415	15664.7360			15659.3200	15659.3134
5	15665.1434		15665.8917		15658.4748		15664.3559	15664.3488			15657.4233	15657.4170
6	15664.6684		15665.5495		15656.4848		15663.8851	15663.8791			15655.4378	15655.4330
7	15664.1041		15665.1132		15654.4084		15663.3231	15663.3171			15653.3703	15653.3639
8	15663.4586		15664.5900		15652.2504		15662.6840	15662.6742			15651.2242	15651.2179
9	15662.7351		15663.9740		15650.0084		15661.9685	15661.9611			15649.0035	15648.9960
10	15661.9383		15663.2838		15647.7025		15661.1725	15661.1607			15646.6970	15646.6925
11	15661.0689		15662.5511		15645.3222						15644.3282	15644.3209
12	15660.1287				15642.8628							